

**Membrane Based on Crystalline Porous Materials:
Preparation and Investigation for Gas and Niche
Liquid Separations**

by

Shebeeb K. H.

10CC19J26027

A thesis submitted to the
Academy of Scientific & Innovative Research
For the Award of the Degree of
DOCTOR OF PHILOSOPHY
in
SCIENCE

Under the supervision of
Dr. Ulhas K. Kharul



CSIR-National Chemical Laboratory, Pune




Academy of Scientific and Innovative Research
AcSIR Headquarters, CSIR-HRDC campus
Sector 19, Kamla Nehru Nagar,
Ghaziabad, U.P.–201002, India

December-2022

Certificate

This is to certify that the work incorporated in this Ph.D. thesis entitled, '*Membrane Based on Crystalline Porous Materials: Preparation and Investigation for Gas and Niche Liquid Separations*', submitted by *Shebeeb K. H.* to the Academy of Scientific and Innovative Research (AcSIR), in partial fulfillment of the requirements for the award of the Degree of *Doctor of Philosophy in Science*, embodies original research work carried out by the student. We, further certify that this work has not been submitted to any other University or Institution in part or full for the award of any degree or diploma. Research material(s) obtained from other source(s) and used in this research work has/have been duly acknowledged in the thesis. Image(s), illustration(s), figure(s), table(s) etc., used in the thesis from other source(s), have also been duly cited and acknowledged.



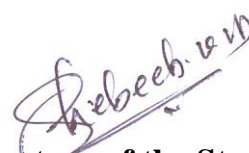
(Signature of Student)
Shebeeb K. H.
Date: 06-12-2022



(Signature of Supervisor)
Dr. Ulhas K. Kharul
Date: 06-12-2022

STATEMENTS OF ACADEMIC INTEGRITY

I, Shebeeb K. H. a Ph.D. student of the Academy of Scientific and Innovative Research (AcSIR) with Registration No. 10CC19J26027 hereby undertake that, the thesis entitled “Membrane Based on Crystalline Porous Materials: Preparation and Investigation for Gas and Niche Liquid Separations” has been prepared by me and that the document reports original work carried out by me and is free of any plagiarism in compliance with the UGC Regulations on [“Promotion of Academic Integrity and Prevention of Plagiarism in Higher Educational Institutions \(2018\)”](#) and the CSIR Guidelines for *“Ethics in Research and in Governance (2020)”*.



Signature of the Student

Date : 06-12-2022

Place : CSIR-NCL, Pune

It is hereby certified that the work done by the student, under my/our supervision, is plagiarism-free in accordance with the UGC Regulations on [“Promotion of Academic Integrity and Prevention of Plagiarism in Higher Educational Institutions \(2018\)”](#) and the CSIR Guidelines for *“Ethics in Research and in Governance (2020)”*.

NA

Signature of the Co-supervisor (if any)

Name :

Date :

Place :



Signature of the Supervisor

Name : Dr. Ulhas K. Kharul

Date : 06-12-2022

Place : CSIR-NCL, Pune

ACKNOWLEDGEMENT

I would like to express my sincere gratitude to my supervisor Dr. Ulhas K. Kharul. It was impossible for me to complete the expedition without your support. My heartfelt thanks go to him for introducing me to the wonders of scientific research and for his persistent guidance, encouragement, inspiration and support during every stage of my doctoral research work. Again I warmly thank him for his precious advice, analysis, criticism and discussions on my research work. I am very much thankful to him for his pursuit of improving me as a person and my scientific skills. I want to thank Dr. Rahul Banerjee, who introduced me to CSIR-NCL and provided a field to enrich my scientific knowledge. The initial lessons I learned from you helped me to resolve the hurdles in my journey. I would also like to sincerely thank my DAC committee members, Dr. H. Thulsiram, Dr. K. Krishnamoorthy and Dr. Ashootosh Ambade, for their constructive, innovative suggestions and comments throughout my Ph.D. work at CSIR-NCL, Pune. I would like to thank Dr. Kiran V. Pandhare for his support and for helping me resolve critical issues faced in my PhD work.

I sincerely thank the Director of CSIR-NCL Dr. Ashish K. Lele, former Directors Dr. Ashwini Kumar Nangia, Dr. Vijayamohanan K. Pillai and Dr. Sourav Pal, Head of Polymer Science and Engineering division for their kind help and encouragement during the course of this work.

I am very grateful to CSIR, New Delhi, for fellowship support to carry out my research work. I want to thank the non-academic staff of CSIR-NCL, especially the SAC, AcSIR, Bills, F&A, C&P, and E2 sessions. Also, special thanks to Mr. Gati Nayak and the staff of the CSIR-NCL library for their timely help whenever I needed it. I would like to thank my seniors Dr. Sharath and Dr. Bishnu for teaching me experimental skills and guiding me in my PhD's initial stage. I wish to thank my seniors all my friendly and cooperative lab mates Varsha Ashok, Nishina A. S, Anand Bhaskar, Anita Rewar, Sayali Saligram, Harshal Chaudhary, Vijay Patl, Harsha Bonde, Vrushali, Runali, Nitin Thorat, Vipin Sherwal, Mukesh Valvi, Suresh Vali, Keerthana, Harshala, Shreetham, Lavaanya Alladi, Saroj Gawas, Nitin Somuvunkar, Kiran Bansode, Rohith, Vikas Mahule, Santhosh, Rohit Ghanda, Karan Kubadikar, Yadha Sharma, Prachiti Bendhadur, Chetna Oge, Supriya Gigrm, Supriya Jadhav, Jayashri Thote, Prakash Narude, Ramendra Pande, and Chinmay Behara, for creating a cheerful and enjoyable working atmosphere in the lab. They were highly supportive as well as helpful during my tenure. I also thank project students Fahad, Tushar, and Sruthy who helped in various projects. I would like to thank Mr. Swaraj Sing for his support, Mr Mahesh and Havildar Senior uncle for keeping my lab clean and neat without any hesitation. In addition, I thank my lab mates in Dr. Rahul Banrjee's lab Bikas, Showvik, Kaushik, Himadri, Mohitosh, Arjun, Suman, Supadeep, Saibal, Suvendu, Manas, Harshitha, Tany, Neethu, Resha, Arjith, Sushil, Amith, and Digambar.

My stay on this campus has been pleasant with the association of all the research scholar and friendss at CSIR-NCL. I am thankful to Renjish, Vidyaa, Meena, Shailaja Mangesh, Pranav, Rajith, Munavar, Vedi, Shubin, Vidya Sanoop Haris, Rashid, Fayis, Santosh, Munavar, Anumon, Unnichetan, Zenoy, Ashwathy, Betsy, Ashwini, Geethu, Priyanka, Anurag, Amarnath, Pinka,

Sharath, Sreejith, Manu, Christy, Arun Torus, Vyshak, Sunil, Kiran Jadavedan, Aneesh, Bihag, Anumon, Rajesh, Giggil, Sreekuttan, Prajitha, Amrutha, Lavanya K, Kavya, Chaithanya, Minal, Ashis, Amith, Praveen, Emmanuel, Niveditha, Alaka, Pawan, Sheethal, Sairam, Nagaraj, Seema, and Apparav for their support, guidance, and advice. I would like to thank Kandekar uncle and Prameela anti for there support and love.

I would also like to thank to all my juniors, Smruthy, Amrutha, Annmarie, Midhun, Arun, Subramaniam, Jugnu, Richa, Linto and Ajmal. I would also like to thank my football mates Subhrashsi, Narugopal, Kailash, Ajith, Basudeb, Abdul Motelib, and Arindam. I would like to express my gratitude to my trekking groups, Fayis, Santhosh, Sharath, and Kiran, who helped me to keep physically well. Special thanks to Chotu and Surajith for making delicious meals for me. I would like to extend my sincere gratitude to Vipin Raj, who has supported me throughout my tenure as a good friend and brother.

I am grateful to all my teachers, and I expressed gratitude for their encouragement in a different part of my life. I thank the entire members of my family for their constant care and wishes. Last but not least, I would like to pay high regard to my parents for their continuous encouragement and inspiration throughout my research work and for lifting me uphill this phase of life. I owe everything to them. Dedicating this thesis to them is a minor recognition of their valuable support and encouragement.

Shebeeb K. H.

List of figures	ix
List of Tables	xiii
Chapter 1 Importance of Crystalline Porous Materials in Separation Application	
1.1 Preamble	1
1.2 Separation technologies	1
1.3 Membrane: An emerging separation technology	2
1.3.1 Structure and materials of synthetic membranes	3
1.3.2 Membrane separation processes	3
1.4 Crystalline porous materials (CPMs)	5
1.5 Metal-Organic Framework (MOFs)	6
1.5.1 Synthesis of MOFs	8
1.5.2 Metal Organic framework for separation	8
1.5.3 Basic criteria of MOFs for membrane-based gas separation	9
1.5.4 MOF membrane fabrication techniques	9
1.5.4.1 MOF membrane on porous support	10
1.5.4.2 In-situ growth method	11
1.5.4.3 Secondary seed growth	12
1.5.4.4 Counter diffusion method	14
1.5.4.5 Interfacial microfluid processing	15
1.5.4.6 Vapor phase synthesis	16
1.5.4.7 Current-driven synthesis	17
1.5.4.8 MOF films on polymer support	18
1.5.4.9 Mixed matrix membrane	19
1.5.5 MOF-based membranes: Gas separation performance	19
1.5.5.1 Hydrogen purification	20
1.5.5.2 CO ₂ Separation	22
1.5.5.3 Hydrocarbon separation	22
1.6 Covalent Organic Framework(COF)	24
1.6.1 Synthesis of COFs	25
1.6.1.1 Solvothermal synthesis	25
1.6.1.2 Microwave synthesis	25
1.6.1.3 Ionothermal synthesis	25
1.6.1.4 Synthesis of monolayers on a surface	25
1.6.1.5 Mechano-chemical synthesis	26
1.6.1.6 Organic terracotta process	26
1.6.2 Application of COFs	26
1.6.3 COFs for membrane application	27
1.6.4 Fabrication of COF membranes	28
1.6.4.1 In-situ growth	29
1.6.4.2 Layer-by-layer method	30

1.6.4.3	Interfacial synthesis	30
1.6.4.4	Langmuir-Blodgett (LB) Method	31
1.6.5	Various separations of COF membranes	31
1.6.5.1	Gas separation	31
1.6.5.2	Liquid separation	32
1.6.5.3	Water separation	33
1.6.5.4	Organic solvent nanofiltration	33
1.7	Reference	34
Chapter 2 Investigations of PPO-ZIF Mixed Matrix Membranes (MMMs) for Olefin/Paraffin Separation		49
2.1	Introduction	50
2.1.1	Scop and objectives	52
2.2	Results and discussion	53
2.2.1	Physical characterizations	53
2.2.1.1	Formation of MMMs	53
2.2.1.2	Thermo gravimetric analysis (TGA)	54
2.2.1.3	Structural integrity of ZIF particles in resulting MMMs	55
2.2.1.4	Interaction between ZIF particles and host PPO	57
2.2.2	Gas permeation properties	59
2.2.2.1	Pure gas analysis	59
2.2.2.2	Sorption analysis	62
2.2.2.3	Mixed gas performance	64
2.3	Conclusions	65
2.4	Experimental	66
2.4.1	Materials	66
2.4.2	Synthesis of polymer and ZIF nanoparticles	66
2.4.2.1	Synthesis of polyphenylenoxide (poly(2,6-dimethyl-1,4-phenylene oxide), PPO)	66
2.4.2.2	Synthesis of ZIF-8	66
2.4.2.3	Synthesis of ZIF-67	66
2.4.3	Membrane fabrication	66
2.4.4	Gas permeation and sorption analysis	68
2.4.5	Characterization methods	70
2.5	Reference	71
Chapter 3 In-situ, Interfacially synthesized, Scalable Covalent Organic Framework (COF) Hollow Fibre Membranes for Organic Solvent Nano-filtration		
3.1	Introduction	77
3.1.1	Scope and objectives	78
3.2	Results and Discussion	79
3.2.1	Membrane fabrication and characterizations	79

3.2.2	Nanofiltration performance analysis	88
3.3	Conclusions	94
3.4	Experimental section	95
3.4.1	Materials and Method s	95
3.4.2	Polyacrylonitrile (PAN) hollow fibre membrane (HFM) spinning	95
3.4.3	COF thin-film HF membrane fabrication	95
3.4.4	Hollow fibre member module making	96
3.4.5	Solvent permeation analysis	96
3.4.6	Rejection analysis	97
3.4.7	Adsorption Study	97
3.4.8	Characterisation method	98
3.5	Reference	99
Chapter 4 Ionic COFs: Thin Film Membrane Preparation and Analysis		102
4.1	Introduction	103
4.1.1	Scope and objective	104
4.2	Interfacial synthesis of cationic COFs and anion exchange	104
4.3	Results and discussion	105
4.3.1	FTIR and C ¹³ NMR analyses	105
4.3.2	Wide-angle X-ray diffraction	106
4.3.3	Scanning electron microscopy	107
4.3.4	Contact angle analysis	108
4.3.5	X-ray photoelectron spectroscopy	108
4.3.6	Molecular rejection performance	109
4.4	Conclusions	112
4.5	Experimental procedures	112
4.5.1	Materials	112
4.5.2	Spinning of polyacrylonitrile (PAN) based HFM and their analysis	112
4.5.3	TpEt-based membrane preparation	113
4.5.4	Characterization methods	114
4.5.5	Preparation of HFM modules	115
4.4.6	Solvent permeation analysis	115
4.5.7	Rejection analysis	116
4.6	Reference	116
Chapter 5 Conclusion		
5.1	Conclusion	119
ABSTRACT		121
Details of publications emanating from the thesis work		122

List of figures

Figure 1.1	US national energy consumption	1
Figure 1.2	schematic representations of various structures of synthetic membranes	4
Figure 1.3	Features and composition of CPMs	6
Figure 1.4	Model representation of MOF fabricated from a metal node and organic linker	7
Figure 1.6	Schematic of (a) MOF-based mixed matrix membrane and (b) supported, thin film MOF membrane	10
Figure 1.7	Schematics of methods developed for MOF membrane on porous support	11
Figure 1.8	Schematic representation of (a) ZIF-90 and (b) ZIF-8 membrane by substrate modification by APTES and dopamine, respectively	12
Figure 1.9	Fabrication of (a) HKUST-1 and MIL-53 membrane by seeded growth method	13
Figure 1.10	(a) Diffusion cell for ZIF-8 film preparation and the schematic of ZIF-8 film formation on nylon support, (b) schematic illustration of the membrane synthesis using the counter-diffusion-based in situ method	14
Figure 1.11	(a) Photographic image of hollow fibre module (b) Schematics of interfacial synthesis of CuBTCMOF membrane on PBI HF substrate (c) microscopic image of fabricated membrane	16
Figure 1.12	Schematic of the (a) ZIF-8 membrane formation by gel vapour deposition and (b) all-vapour phase LIPS membrane fabrication process	17
Figure 1.13	(a) The electrochemical cell for membrane growth by FCDS. The substrate served as a cathode in the electrochemical system, (b) schematic illustration of the ZIF-8 membrane growth via FCDS in comparison with solvothermal growth	18
Figure 1.14	Schematic representation of different organic symmetric combination used in COF framework construction	24
Figure 1.15	Synthesis scheme of stable COF by Schiff base reaction	28
Figure 1.16	(a) Synthesis of tubular COF-LZU1 membranes. First, the surface of the alumina tubes is modified by APTES, followed by a grafting reaction with TFB. Finally, the COF layers are grown on to the support by imine condensation of TFB and PDA (b) Schematic representation of the preparation of a COF-1 membrane via the assembly of exfoliated COF-1 nanosheets	29
Figure 1.17	Synthesis scheme of COF thin films. (a) Schematic representation of the interfacial crystallization process used to synthesize the Tp-Bpy thin film. (b, c) SEM and AFM images respectively, of the Tp-Bpy thin film	31
Figure 2.1	Designing MMM by incorporating ZIF into PPO polymer matrix	52
Figure 2.2	TEM images of ZIF-8 (a) and ZIF-67 (b) particles	53
Figure 2.3	SEM images of ZIF-8 (a) and ZIF-67 (b) particles	54

Figure 2.4	The DLS spectra of (a) ZIF-8 and (b) ZIF-67	54
Figure 2.5	The WAXD patterns of (a) ZIF-8 and (b) ZIF-67 based MMMs	55
Figure 2.6	Cross-sectional SEM images of ZIF-8 and ZIF-67-based MMMs	56
Figure 2.7	The WAXD patterns of (a) ZIF-8 and (b) ZIF-67 based MMMs	56
Figure 2.8	DSC thermograms of (a) ZIF-8@PPO and (b) ZIF-67@PPO MMMs	57
Figure 2.9	High resolutions ‘O1s’ XPS spectra of (a) PPO, ZIF-8@PPO (b-e) and ZIF-67@PPO (f-i) MMMs with ZIF loading 10, 20, 30 and 40%, respectively	58
Figure 2.10	(a) Zn 2p and (b) Co 2p XPS spectra of ZIF-8@PPO and ZIF-67@PPO MMMs, respectively	59
Figure 2.11	Schematic representation of the metal-oxygen interaction present in the MMMs	59
Figure 2.12	Variation of gas permeability with kinetic diameter of penetrants in (a) ZIF-8@ PPO and (b) ZIF-67@ PPO MMM; pure gas permeability of C ₂ H ₄ , C ₂ H ₆ , C ₃ H ₆ and C ₃ H ₈ , and selectivity of C ₂ H ₄ /C ₂ H ₆ and C ₃ H ₆ /C ₃ H ₈ in (c) ZIF-8@PPO and (d) ZIF-67@PPO MMMs	60
Figure 2.13	Variation in C ₃ H ₆ permeability of ZIF-8@PPO-30 MMM with (a) upstream gas pressure (a) long-term exposure at 60 psi upstream	62
Figure 2.14	(a) Sorption isotherm, and (b) diffusion and sorption selectivity of PPO, ZIF-8@PPO-40 and ZIF-67@PPO MMMs	63
Figure 2.15	Mixed gas permeability and selectivity of ZIF-8@PPO-40 and ZIF-67@PPO-40 membranes at the different composition of C ₃ H ₆ in feed	64
Figure 2.16	Appearance of present and reported membranes on empirical C ₃ H ₆ /C ₃ H ₈ Robeson’s upper bound; ★: ZIF-8@PPO, ★: ZIF-67@PPO and reported membranes	65
Scheme 2.1	Solution casting of ZIF@PPO MMMs	68
Figure 2.17	Variable pressure gas separation set-up	69
Figure 2.18	Digital photographic images of MMMs	70
Figure 3.1	Structures of COFs: Tp-Tta and Tp-Azo	79
Figure 3.2	Schematics of interfacially synthesized COF thin film layer on HFM	80
Figure 3.3	IR spectra showing the PAN-amine interactions	80
Figure 3.4	Surface SEM images of COF thin-film HFM	81
Figure 3.5	SEM images of Tp-Tta-120 and Tp-Ttaa-240 showing rod like morphology	81
Figure 3.6	Stereomicroscopic images and SEM images of COF thin-film HFM	82
Figure 3.7	a) photographic images of COF thin-film HFM before and after removing the PAN substrate, b) SEM images, c) AFM images of COF thin films after removing the PAN substrate, d) height profile of COF thin films	82
Figure 3.8	PXRD pattern of COF thin film HF membrane	83
Figure 3.9	PXRD pattern of Tp-Azo (a) and Tp-Tta (b) thin-film membrane	83

Figure 3.10	FTIR spectra of Tp-Tta thin-film HF membrane	84
Figure 3.11	FTIR spectra of Tp-Azo thin-film HF membrane	84
Figure 3.12	C^{13} NMR spectra of thin-film membrane	85
Figure 3.13	XPS survey of (a) Tp-Tta and (b) Tp-Azo thin film HF membrane	85
Figure 3.14	High-resolution C1s XPS pattern of COF thin-film HF membrane	86
Figure 3.15	TGA thermogram of Tp-Tta (a) and Tp-Azo (b) thin film HF membrane	86
Figure 3.16	IR spectroscopy of Tp-Azo-400 (a) and Tp-Tta-30 (b) membranes after keeping them in the corresponding solvent for seven days.	87
Figure 3.17	Contact angle of Tp-Tta thin film HFM by a) sessile drop method and b) wilhelmy plate method	87
Figure 3.18	Contact angle of Tp-Azo thin film HF membrane by a) sessile drop method and b) wilhelmy plate method	88
Figure 3.19	a) Photograph of HF module, b) pure solvent permeance of COF thin film HFMs	88
Figure 3.20	Acetone and methanol presence and direct-80 rejection of Tp-Tta thin film HFM as a function of the concentration of precursor solution. Inset: photograph showing the color intensity variation with precursor concentration	89
Figure 3.21	Organic solvent nanofiltration performance of COF thin film HFM	90
Figure 3.22	UV-visible spectra showing the concentration of dye molecule a)BB b) CR c) DR-23 and d) DR-80 in the feed and permeate after passing through Tp-Tta-120 membrane	91
Figure 3.23	UV-visible spectra showing the concentration of dye molecule a)BB b) Congo red c) DR-23 and d) DR-80 in the feed and permeate after passing through Tp-Tta-60 membran	91
Figure 3.24	UV-visible spectra showing the concentration of dye molecule, a) BB, b) Congo red c) DR-23 and d) DR-80 in the feed and permeate after passing through	92
Figure 3.25	Structure of dye molecule used for OSN study	92
Figure 3.26	Adsorption study: a) Rejection performance of Tp-Tta-15 carried out using 100mg/l direct red-80 in methanol solution, b) photographic images of permeate and retentate collected in each interval c,d) UV-absorption spectra of retentate and permeate respectively	93
Figure 3.27	Durability study of Tp-Tta-15 membrane (b) Pressure v/s flux of COF thin film HF membrane	94
Figure 3.28	Schematic representation of permeation setup	97
Figure 4.1	The (a) structure of TpEt-COF and photographic images of TpEt-PTSA-1, and (c) TpEt-TFA-1 membranes	105
Figure 4.2	FTIR spectra of TpEt-PTSA (a) and TpEt-TFA (b) membrane in comparison to the PAN substrate	106

Figure 4.3 C ¹³ NMR spectra of TpEt-PTSA membrane	106
Figure 4.4 Comparison WAXD patterns of as-synthesized TpEt membranes with that of a simulated one	107
Figure 4.5 Microscope images showing cross-sectional view of (a,d) COF thin film HFM and SEM images showing cross-sectional (b,e) and surface (c,f) view of COF thin film HFM	108
Figure 4.6 Comparison of contact angle of PAN substrate with COF thin film HFM	108
Figure 4.7 The XPS spectra of COF thin film HFM: (a) high-resolution XPS spectra of Br 3d in TpEt-PTSA-1, (b) TpEt-TFA-1 membrane; (d) high-resolution XPS spectra of S 2p in TpEt-PTSA-1, and (e) high-resolution XPS spectra of F 1s in TpEt-TFA-1	109
Figure 4.8 Rejection performance of various dyes in methanol through TpEt-PTSA-0.5 (a), and TpEt-TFA-0.5 thin film HF membrane, (b) Molecular structure of methylene blue (MB), brilliant blue (BB), cibacron blue (CB), direct red-23 (DR-80), and direct red-80 dye	110
Figure 4.9 Ultra-violet absorption spectra of mixed dye (MB, DR-23, and DR-80) in feed and permeate of TpEt-PTS-0.5 membrane	111
Figure 4.10 Methanol permeance of TpEt-PTSA-0.5 and TpEt-TFA-0.5 membrane before and after dye rejection analysis	112

List of tables

Table1.1 Industrial mass transfer separation technologies	2
Table1.2 Membrane processes, their principles and applications	4
Table 1.3 Summary of H ₂ separation performance of some of the reported MOF-based membranes	20
Table 1.4 Propylene/propane separation performance of some of the ZIF-8 based membranes	23
Table 2.1 Comparison of experimental ZIF loading with that of TGA analysis	55
Table 2.2 Pure gas permeability of MMMs and pristine PPO	61
Table 2.3 Langmuir sorption parameter, sorption and diffusion coefficient of ZIF membrane	63
Table 3.1 Pure solvent permeance (Lm ⁻² h ⁻¹ bar ⁻¹) of Tp-Tta and Tp-Azo thin film HFM	89
Table 3.2 Nanofiltration performance of Tp-Tta and Tp-Azo thin film HFM in comparison to the PAN substrate	90
Table 3.3 Dimension of dye molecule obtained from DFT study	93
Table 3.4 Spinning parameters for making PAN-based HFMs	95
Table 3.5 Concentration of precursor solution used for thin film HF fabrication	96
Table 4.1 Dope solution composition and spinning parameters used for making PAN-based HFMs	113
Table 4.2 Concentration of precursor solution used for membrane fabrication	114

Importance of Crystalline Porous Materials in Separation Application

1.1 Preamble

A substantial portion of the energy consumed in industry accounts for separating chemicals into pure form by processes such as distillation, evaporation, etc. [1]. It is reported that separation processes consume 10-15% of the world's energy consumption for separating chemicals [1,2]. This situation will persist because of the high demand for chemicals in the modern world. For example, approximately two litres of crude oil and 30 kilograms of ethylene and propylene are processed annually for each individual in the world [1]. It requires a tremendous amount of energy. In the United States, 32% of their total energy consumption is accounted for the industry [1]. In industry, 45-55% of energy is used for separations (Figure 1.1) [2]. It is also said that more than 80% of the energy is associated with thermally driven, phase change-based separations. The major thermals separation widely used in industries is distillation, evaporation and drying. Further, thermally driven separations emit CO₂ into the atmosphere. For example, the US petroleum industry and paper industry itself accounts for 100 million tons of CO₂ emission.

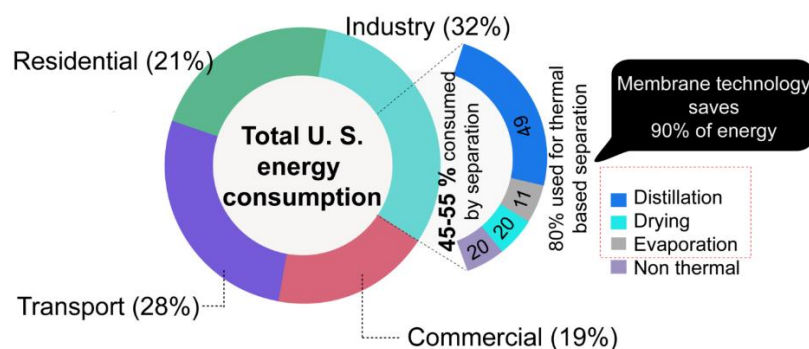


Figure 1.1 US national energy consumption [2]

1.1 Separation technologies

Separation technologies can be classified into a) physical operation and b) mass transfer operation. The former includes processes like screening, cyclones, and floatation, which deals with separating larger particles or objects. The latter comprises separation methods such as

distillation, drying, etc. The mass transfer operations are energy-intensive in comparison to physical separations [3]. Among the mass transfer separations, evaporation, distillation, and drying account for 80% of energy consumption [1]. Membrane-based separation is recognized as an efficient technology that assures high selectivity, low energy consumption, and a small footprint, fulfilling the need for new sustainable industrial separation processes [4,5].

Table 1.1 Industrial mass transfer separation technologies

Separation Technologies	Material's primary role	Energy intensity	Technical Status
Distillation: A thermally driven separation based on the boiling point difference in the miscible constituent.	Structural member	High	Established
Evaporation: A thermally driven process that separates volatile solvents from a solution containing nonvolatile solute.	Structural member	High	Established
Drying: It differs from evaporation in that the residue is typically solid.	Structural member	High	Established
Extraction: The separation of a constituent is based on its solubility in another solvent. Further, a thermally driven process recovers the components from the reclaimable solvent.	Separation agent	Medium	Established
Absorption: The components enter into the bulk of solid or liquid, and the absorbed components are recovered by a thermally or chemically driven processes.	Separation agent	Medium	Established
Adsorption: Adhesion of a constituent on the surface of a solid or a liquid. The components are recovered using a second chemical or thermally driven process.	Separation agent	Medium	Established
Crystallization: Thermally driven, but based on the heat of fusion, instead of the more energy-intensive vaporization. A substance is concentrated by the precipitation of crystals from a solution.	Structural member	Low	Established
Membranes: Use diversified mechanisms, including size exclusion to solution/diffusion. The driving force is the chemical/electrical potential gradient.	Separation agent	Low	Emerging

1.3 Membrane: An emerging separation technology

A membrane is a barrier that allows one or more constituents to pass through faster than others, resulting in the separation of components. The membrane process does not involve any

phase change [6]. These characteristics of membranes make this process superior in terms of energy, compact design, environmentally friendly and cost-effectiveness. Therefore, membrane separation can perform better in terms of energy consumption than other heat-based separations. Membranes have been widely used in various industries such as water (surface, sea, and brackish water desalination, wastewater treatment), dairy, N₂/O₂ enrichment of air, industrial waste treatment, food and beverages, hemodialysis, gas and vapour separation, separation of microorganisms, chemical industries, etc. Synthetic membranes can be classified on a different basis such as membrane material, morphology, geometry, preparation methods, separation regime and processes, etc. [7]. Based on the membrane material, they can be classified into organic, inorganic, metallic, solid, or liquid, and electrically charged or neutral. Membrane geometrical classification can be plate and frame, tubular, flat sheet, and hollow fibre. To achieve acceptable membrane performance, the membrane module should have characteristics such as high packing density, low operating and maintenance costs, good control of concentration polarization and fouling, and cost-efficient production [7].

The flux and selectivity are the two intrinsic characteristics of the membrane. They are controlled by the membrane material and its morphology [3]. However, in industrial applications, the membrane performance not only depends on the intrinsic characteristics but also on the process parameters (e.g. temperature, feed velocity, etc.), pretreatment of stream, and provision to clean membrane to attain better membrane performance [3].

1.3.1 Structure and materials of synthetic membranes

Synthetic membranes can be differed greatly based on the structure and the material used for the fabrication. Based on the structure, membranes can be classified as porous membranes, homogeneous membranes, membranes carrying electrical charges, and liquids or solid films containing selective carriers. In addition, according to the structural variation, membranes are further classified into asymmetric and symmetric membranes (Figure 1.2). In symmetric membranes, the entire cross-section of the membranes has an identical structure; however, in asymmetric membranes, the structure of the membrane varies throughout the cross-section.

1.3.2 Membrane separation processes

The membrane separation process can be classified based on the driving force (pressure, concentration gradient, or electrochemical potential gradient), which leads to the transport of a specific component through membrane material. The major pressure-driven membrane process

are ultrafiltration, microfiltration, nanofiltration, reverse osmosis and gas separation. Dialysis and electrodialysis are membrane processes driven by concentration and electrochemical potential, respectively. Following Table 1.2 summarizes the commercially significant membrane separation process [7–9].

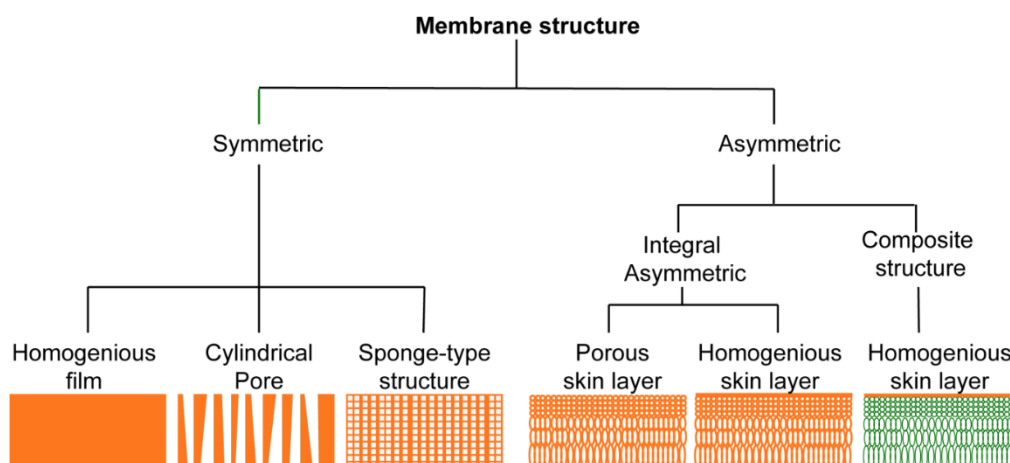


Figure 1.2 schematic representations of various structures of synthetic membranes

Table 1.2 Membrane processes, their principles and applications

Separation process	Driving force	Mode of separation	Major applications
Microfiltration (MF)	Hydrostatic pressure, 0.05-0.2 MPa	Filtration (size exclusion)	Water purification, sterilization, etc.
Ultrafiltration (UF)	Hydrostatic pressure, 0-0.5 MPa	Filtration (size exclusion)	Separation of molecular mixtures
Nanofiltration (NF)	Pressure, 1-10 MPa	Filtration (steric and electrostatic)	Organic molecules, mono and multivalent ion separation
Reverse osmosis	pressure, 1-10 MPa	Solution and diffusion	Sea- and brackish water desalination, effluent treatment, etc.
Gas and vapor separation	Concentration gradient	Solution-diffusion	Gases, vapors
Pervaporation	Vapor pressure	Solution and diffusion	Separation of solvents, azeotropic mixtures
Dialysis	Conc. gradient	Diffusion	Artificial kidney
Electrodialysis	Electrical potential	Charge based exclusion	Water desalination
Donnan dialysis	Concentration of ions	Donnan exclusion	Water softening
Membrane distillation	Vapor pressure	Diffusion	Liquid-nonvolatile solute separation
Membrane contactors	Chemical potential	Diffusion and solution	Solvent extraction

Polymeric materials are widely used as membrane materials for separation applications due to their excellent processability and cost-effectiveness [10,11]. Membrane pore size varies from micrometres to nanometers. They have been prepared using amorphous polymers such as polyether sulfone (PES), polyvinylidene fluoride (PVDF), polysulfone (PSF), polyimide (PI), polyacrylonitrile (PAN), polyamide (PA) and cross-linked poly(amide-imide)-based polymers, etc. [11]. However, the absence of ordered identical pores and pore connectivity in amorphous polymers lacks a trade-off between permeability and selectivity [12]. Membrane barriers comprised of uniform pore channels with identical pore sizes can offer less resistance to the permeant and guarantee selectivity. Crystalline porous materials (CPMs) can be an alternative material for membrane fabrication due to their long-range order and porosity [13]. The uniform pore channel will offer better selectivity, and a large pore volume imparts a better permeation rate, which brings remarkable advancement to the membrane performance. CPMs have attracted wide attention as membrane materials. They include zeolites [14], metal-organic frameworks [15,16], covalent organic frameworks [17,18], and porous organic cages [12,19] (Figure 1.3). This thesis is mainly focused on scalable and industrially viable membrane fabrication methods using porous, crystalline organic materials, with special attention to MOFs and COFs.

1.4 Crystalline porous materials (CPMs)

Porous materials are substances comprising voids through which gases or liquids can pass through. There are several natural examples of porous materials, e.g., hollow bamboo, diatomaceous earth, honeycombs, bones, etc. [20–22]. The ones with a pore size in the micrometre and nanometer range have unique properties and, thus, applications. Some of the widely used examples of crystalline porous materials (CPMs) are porous carbons, mesoporous silica, zeolites, metal-organic frameworks (MOFs) and covalent organic frameworks (COFs) (Figure 1.3) [23–28]. Many academic and industrial groups showcased these materials for several applications, including adsorbents, purification, chemical sensing, catalysis, optoelectronics, etc. [29–31] A tuneable pore size, ultrahigh surface area, outstanding surface properties, and adjustable framework cavity are the important characteristics of CPMs [32].

Inorganic porous materials called zeolites are a class of ‘tectosilicate’ minerals that are made from corner-sharing aluminate and silicate tetrahedral units, connected together to generate three-dimensional frameworks [33,34]. Even though zeolites have good crystallinity and porosity, predesigning the structure and functionality is difficult. This made researchers think

about other porous materials [26,35]. In 1998, Omer M. Yaghi and coworkers developed a new inorganic-organic hybrid porous material called Metal-Organic Frameworks (MOFs) [35,36]. MOFs have excellent crystallinity, porosity, and the possibility to do pore modification for the desired separation. Nonetheless, the coordination bond made this material less stable. Replacing the covalent bond with the weak coordination bond was the only alternative method to tackle the stability issue. In 2005, Yagi and coworkers introduced a new porous material consisting of only covalent bonds called the covalent organic framework (COFs) [37]. Generally, porous materials are classified based on the porosity and the nature of the material. Based on porosity, the international union of pure and applied chemistry (IUPAC), porous materials can be classified into three general classes i) microporous materials (pore size 0.2-2 nm), ii) mesoporous materials (pore size 2-50 nm) and iii) macroporous materials (pore size 50-1000 nm) [38]. Based on the framework materials, they can be classified into i) inorganic porous frameworks, ii) inorganic-organic hybrid porous frameworks, and iii) organic porous frameworks.

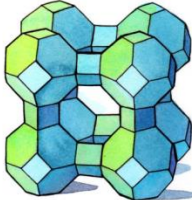
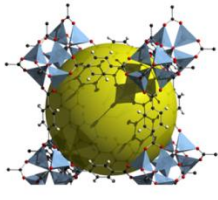
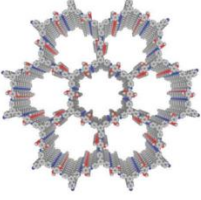
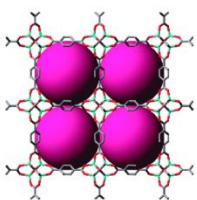
PCMs				
	Zeolites	MOFs	COFs	POCs
Nodes	Inorganic	Inorganic-organic hybrid	Organic	Organic
Bonds	Covalent bonds	Co-ordination bonds	Covalent bonds	Covalent bonds and intermolecular forces
Structural dimension	2D and 3D	2D and 3D	2D and 3D	0D
Stability	High	Low to medium	Medium to high	Low to medium

Figure 1.3 Features and composition of CPMs

1.5 Metal-Organic Framework (MOFs)

Metal-organic frameworks are crystalline porous materials composed of ordered structures resulting from metal atom nodes and organic electron pair donor linkers (Figure 1.4) [36,39]. As compared to common porous materials (zeolites, porous carbon, porous polymers

etc.), MOFs exhibit excellent surface area (up to $10,000 \text{ m}^2\text{g}^{-1}$), and pore volume ($4.40 \text{ cm}^3\text{g}^{-1}$). Their exceptional compositional and structural diversity, permanent porosity, and well-defined pore channel make them suitable for several applications [40,41]. The accurate information about the pore size/shape of the MOFs can be well determined using X-ray crystallography, which will give a better understanding of the structural parameter. The porosity of MOFs can be tuned as required by an application. This can be achieved by varying the organic linkers. Besides that, organic moieties with different functional groups can be incorporated into the MOF, which enables functionalization and post-synthetic modification. The advantage of uniform porosity of MOFs is utilized in different applications such as chemical sensing, magnetism, gas storage and adsorption, catalysis, proton conductivity, etc. [23,25–28,42–54]. In the recent past, these materials have been widely studied for renewable energy applications such as gas separation, oxygen reduction catalysts, light harvesting and lithium-ion battery [40,41,55,56].

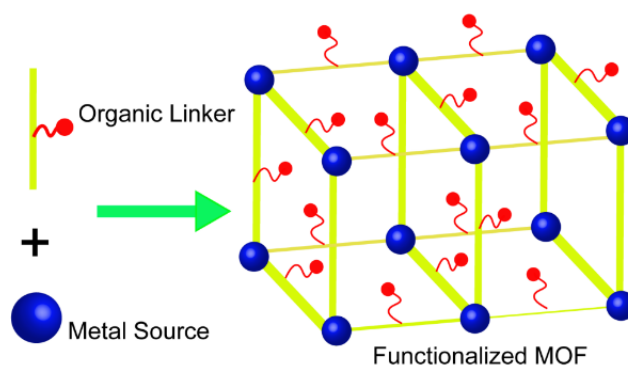


Figure 1.4 Model representation of MOF fabricated from a metal node and organic linker

Zeolitic imidazolate frameworks (ZIFs) are a sub-family of metal-organic frameworks consisting of imidazole (Im) based ligands [57,58]. The metal centres are coordinated through the ‘N’ atom in the imidazole ligand. The five-membered ring serves as a bridge between two metal atoms (such as Co, Ni, Zn, etc.), resulting in a metal-Im-metal angle of 145° throughout the framework [57,59,60]. The structure of ZIFs is similar to zeolites. The metal atom plays the role of Si and the imidazolate anion forms the bridge that mimics the oxygen atom in zeolites. This leads to a similar topology structure to those observed in Zeolites. The ZIFs possess the combined advantage of both MOFs and zeolites, such as high surface area, porosity, crystallinity, functionality, and thermo-chemical stability [60,61]. So far, more than 150 ZIFs have been reported. Among the ZIFs, ZIF-8 is one of the widely studied ones, which is comprised of Zn^{2+}

metal atoms interconnected with 2-methylimidazole as an organic ligand [62]. The superior properties of ZIFs make them a potential candidate for large applications, including gas uptake, separation, catalysis, and drug delivery [63].

1.5.1 Synthesis of MOFs

Most of the metal atom present in the periodic table (S- block metals, d-block metals and lanthanides) has been tried for the synthesis of metal-organic frameworks with different organic linkers. The framework structure is decided by the characteristics (ligand length, bond angles, chirality, bulkiness, etc.) of the linker molecule [40]. Multidentate ligands, including aromatic polycarboxylate and functional groups such as $-\text{SO}_3\text{H}$, $-\text{CN}$, $-\text{SH}$, $-\text{OH}$, $-\text{NH}_2$, $-\text{N}_3$, $-\text{H}_3\text{PO}_4$ are suitable for MOF synthesis. In addition, heterocyclic compounds, e.g., imidazole, tetrazole, pyridine, pyrazin triazole, and their derivatives, can also be used as organic linkers. Generally, MOFs are synthesized using different liquid phase methods in which both the ligand and metal ions are dissolved and kept for crystallization at a particular temperature and pressure. Solvothermal synthesis is one of the widely used methods for MOF synthesis. A large proportion (~70%) of MOFs are synthesized following this method [64]. The reactants are dissolved in high-boiling solvents such as dimethyl sulfoxide, water, dialkyl formamide or acetonitrile. The concentration and solubility of the precursors, pH of the solution, and temperature are the important factors of solvothermal MOF synthesis. In addition to the solvothermal method, several other methods are also reported, including sonochemical synthesis [65], mechanochemical synthesis [66], electrochemical synthesis [67], microwave synthesis [68]; and the mixture of non-miscible solvents [69].

1.5.2 Metal Organic framework for separation

Among the applications of MOFs, separation has a special weightage not only due to its importance but also the special characteristics of MOFs which make them ideal for some challenging separations [70,71]. One of the main advantages of MOFs, while used for separation is their precise control over pore apertures and functionality by deliberately changing the metal and the ligand. The modular nature of synthesis and enormous choice of building blocks (metal and ligand) make MOFs superior to porous material for separation application. For example, zeolites are crystalline porous materials like MOFs and are widely studied for separation applications [72]. Nonetheless, the pore size of the zeolites is limited by the small size of inorganic anions, which restricts them for a wide range of separation applications. The pore size

of MOFs ranges from a few angstroms to nanometers. This range is broad over that of zeolites. Besides that, pore engineering is easily possible in MOFs, which opens a window for a broad range of separation applications. Among the different separation applications, MOF membrane is proven as a promising candidate for gas separation. The following section discusses the different MOF membrane fabrication methodologies and their performance in gas separation applications.

1.5.3 Basic criteria of MOFs for membrane-based gas separation

Solubility and diffusivity are the two factors governing gas separation through the membrane. Solubility is governed by the thermodynamic affinity/interaction of the gas permeant and the membrane material, while the relative size of the gas molecule governs diffusivity. If the gas molecule has high affinity, it will adsorb into the pore and diffuse through the membrane faster if the pore aperture and size are larger than the dimension of the gas molecule. This leads to the fast permeation of the specific gas molecule through the membrane. Further, good selectivity could be attained if the other gas components have opposite behaviour. The sorption-based separation can be achieved in MOFs either by modifying the pore surface by ligand modification or by post-synthetic methodology [71]. These modifications result in change in pore aperture, pore volume and the properties of pores, such as hydrophilicity, polarity and hydrophobicity. This leads to a change in the separation performance. In the case of size-based separation, the kinetic diameter of the gas molecule and the pore aperture decide the membrane performance. There are cases in which gas molecules having higher dimensions than the aperture also pass through the membrane. It is due to the framework flexibility of the MOFs and the swing effects of a linker molecule. Other important factors that need to be considered while choosing MOFs for gas separation application are i) ease of fabrication, ii) ease of activation (MOFs synthesized in water and alcohol do not require activation, which further saves time and energy), iii) active metal centre (unsaturated metal centre create electro static metal-guest molecule interaction), iv) gate opening or breathing effect (several MOFs shows breathing effect due to the interaction between the incoming gas molecule and MOF). The breathing effects depend upon the threshold pressure, which varies with gas molecules [70].

1.5.4 MOF membrane fabrication techniques

The major challenge that persists in MOF-based membranes is their successful fabrication without any defect with sufficient scalability. The fragile and brittle nature of MOFs restricts the formation of self-supported films or membranes. Therefore MOF based membranes

are generally prepared on a highly porous, mechanically stable support or mixed matrix membrane, in which pre-synthesized particles are incorporated in host polymers (Figure 1.6). Both methods have their own advantages and disadvantages. For example, supported membranes have scalability issues and mixed matrix membranes lack selectivity and permeability, like pristine MOF membranes.

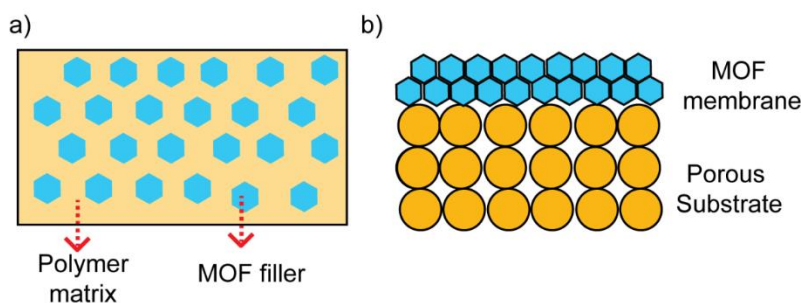


Figure 1.6 Schematic of (a) MOF-based MMMs and (b) supported, thin film MOF membrane

1.5.4.1 MOF membrane on porous support

There are several factors that need to be considered while making a pristine MOF-membrane on support. These include eliminating cracks or defect formation while making or activating adhesion between the support and MOF layer, MOF film stability, and enhancing the intergrowth of MOF particles [14,16,73,74]. As compared to zeolites, MOFs have an advantage that their formation is possible in milder conditions. This aspect enables a large spectrum of fabrication methodologies for pristine MOF membranes on support.

In 2009, Lai and Geong et al. reported the first MOF-5-based thin film membrane made by solvothermal method on alumina support [75]. This report showcased the practicability of MOF membranes for gas separation. Later several membranes are reported using different fabrication methods (Figure 1.7). Generally, the fabrication of MOF thin film on substrate follows two methods i) in-situ growth and ii) secondary or seeded growth. In situ method, the substrate without any premodified surface with crystals is immersed in a reactant solution and the nucleation growth and intergrowth of crystals happen in the fabrication step. In the seeded growth method, a premodified substrate with crystals is used for the fabrication. The following section describes diverse approaches implemented for the fabrication of MOF-based gas separation membranes.

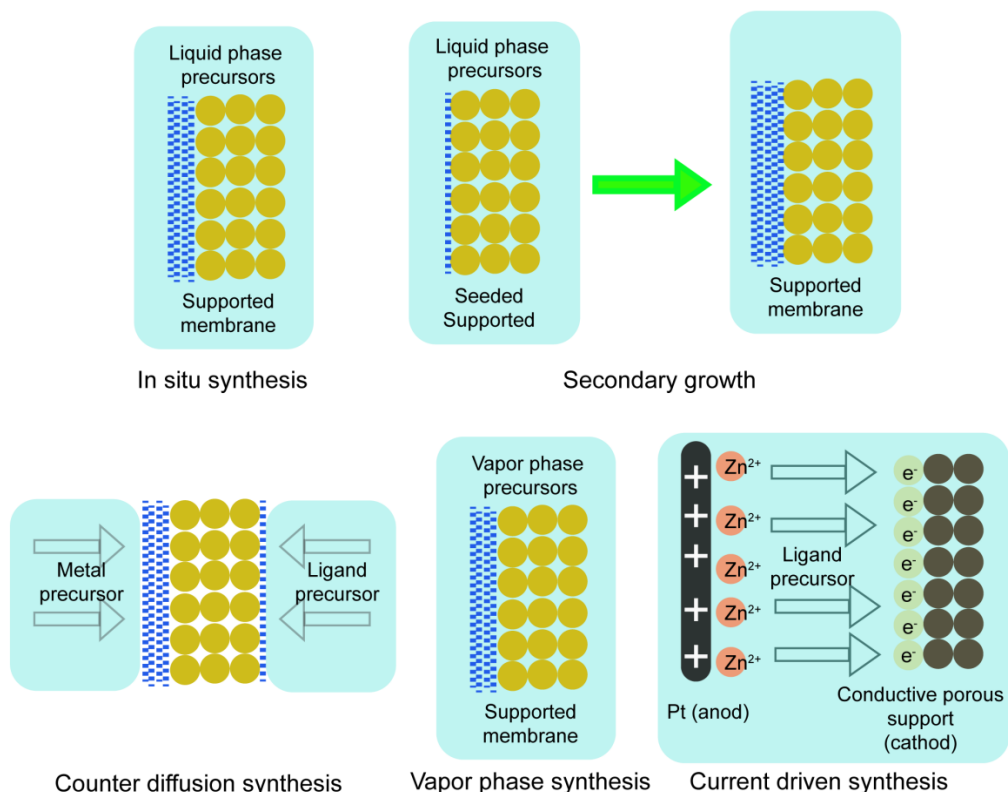


Figure 1.7 Schematics of methods developed for MOF membrane on porous support

1.5.4.2 In-situ growth method

This is a direct approach to MOF film fabrication. The substrate used in this method may or may not be chemically functionalized or modified before the growth of MOFs. Different MOF membranes, such as HKAUST-1, UiO-66, ZIF-8, ZIF-67, MOF-77, etc., were reported by a solvothermal method using an unmodified substrate [75–77]. The unmodified substrate lacks the strong interfacial interaction between the MOF and the support. As a result, this method is limited only to a few reports. To overcome this issue, modified substrates are used for the MOF membrane fabrication, which can improve the heterogeneous nucleation and helps to retain the MOF crystals on the surface without their detaching from the surface. Caro and coworkers reported MOF membrane on a modified alumina substrate with 3-aminopropyltriethoxysilane (APTES). The APTES acted as a covalent linker between MOF particles and the substrate surface [78,79]. The ethoxy functional group of APTES reacted with the OH functionality of alumina. This resulted in NH_2 functionality on the surface of the alumina, thereby providing nucleation sites for the MOFs by imine bond formation with the aldehyde functionality in the organic linker (Figure 1.8a).

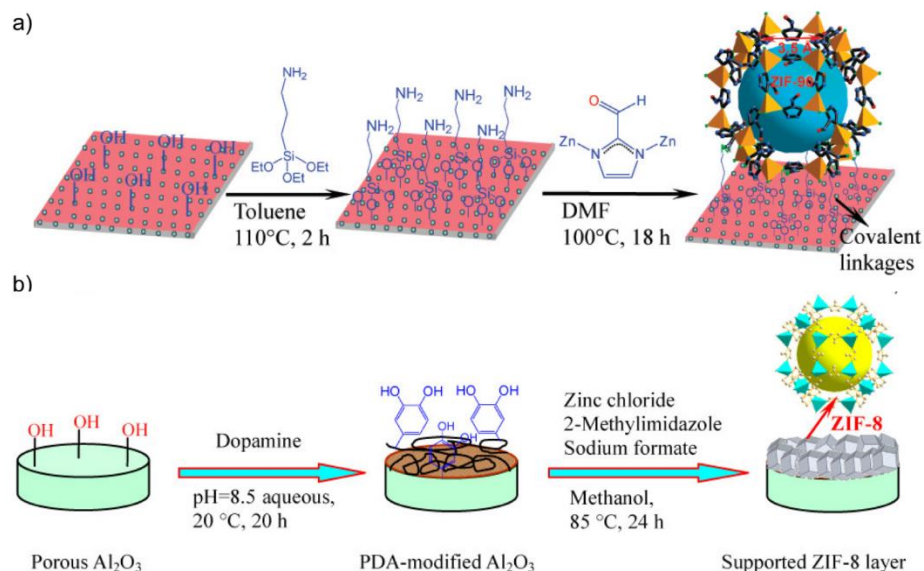


Figure 1.8 Schematic representation of (a) ZIF-90 and (b) ZIF-8 membrane by substrate modification by APTES and dopamine, respectively (*Reprinted with permission from Ref 78, copyright@2010 American Chemical Society and 81 copyright@2013 American Chemical Society*)

Jeong's group reported another strategy to modify the substrate and they could achieve a well-attached polycrystalline MOF membrane. They fabricated ZIF-8 and ZIF-67 membranes by covalently linking the imidazole ligand to the substrate surface through Al-N bond. The covalent linkage is achieved by evaporation of the ligand solution on the hot surface (200°C) of the alumina. They confirmed the covalent bond formation using N1s XPS analysis. [80]. In another report, Caro et al. used a polydopamine-modified Al₂O₃ for the ZIF-8 membrane fabrication. The thin layer of polydopamine is generated on the substrate surface by dipping in dopamine solution at pH 8.5 (Figure 1.8b) [81]. Later, they reported the use of stainless steel nets as a substrate [82]. Another approach is the metal atom present on the substrate surface as a source of anchor group for MOF nucleation. Guo et al. have demonstrated the MOF membrane based on HKUST-1 on an oxidized copper mesh [83].

1.5.4.3 Secondary seed growth

This alternative approach is adopted from the zeolites membrane [84,85]. In this method, the hydrothermal or solvothermal synthesis of MOF crystals was carried out on a support that was seeded with the same crystals. This method allowed attaining a better control of microstructure such as orientation, film thickness, and density of grain boundary by controlling

the properties of the seed crystal layer [86]. In zeolites, the seeding was relatively easy because the calcination of the support with crystals led to the covalent bond formation by condensation reaction between the support and the crystals. The low thermal stability of MOFs as compared to zeolites, makes this method impractical for MOF membranes. Many alternative seeding techniques were followed for membrane making. These include dip coating, support rubbing, layer-by-layer, and heat methods.

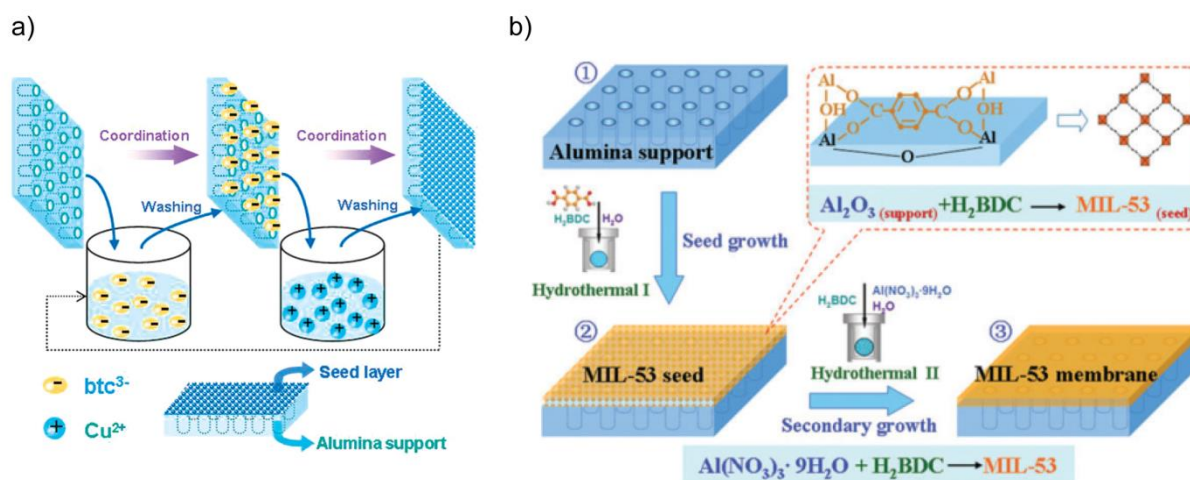


Figure 1.9 Fabrication of (a) HKUST-1 and MIL-53 membrane by seeded growth method (Reprinted with permission from ref 90 and 91 Copyright 2011 Royal Society of Chemistry, Copyright 2011, and American Chemical Society)

Tsapatsis et al. fabricated MOF membrane by manually rubbed seeding on PEI functionalized alumina substrate followed by solvothermal method [87]. Venna et al. also used the same approach for the fabrication of a ZIF-8-based tubular membrane. [88]. Jeong's group demonstrated a thermal-based seeding for the fabrication of HKUST-1 based membrane. They achieved the seeding by dropping the HKUST-1 crystals seed solution into hot (200°C) alumina support, followed by rinsing with gentle sonication. Further, the solvothermal synthesis resulted in a crack-free, continuous, well-intergrown membrane [89]. Nan and coworkers reported a stepwise growth on alumina support for fabricating HKUST-1 membrane (Figure 1.9a) [90]. Lee and coworkers used reactive seeding for the fabrication of MIL-53 films. They have attained the seeding by in situ growth of MIL-53 on alumina support without the presence of metal atoms. This seeded substrate was used further for the membrane fabrication [91] (Figure 1.9b). Jin et al.

demonstrated a layer-by-layer method to attain a thin coating of the seeded layer. Later the HKUST-1 membrane was fabricated on the seeded support by in situ solvothermal method [90].

1.5.4.4 Counter diffusion method

In this method, two different precursors (ligand and metal solution) are separated by a porous substrate. The crystallization takes place when the precursors diffuse through the substrate from each side and meet together. Yao et al. [92] for the first time reported counter diffusion method for the fabrication of ZIF-8 on the macroporous substrate. In their method, the zinc nitrate solution and imidazole solution were separated by a Nylon substrate (Figure 10a). The crossover of the two solutions happened through the nylon support. After 72 h, a 16 μm thick film was formed on the zinc side of the support.

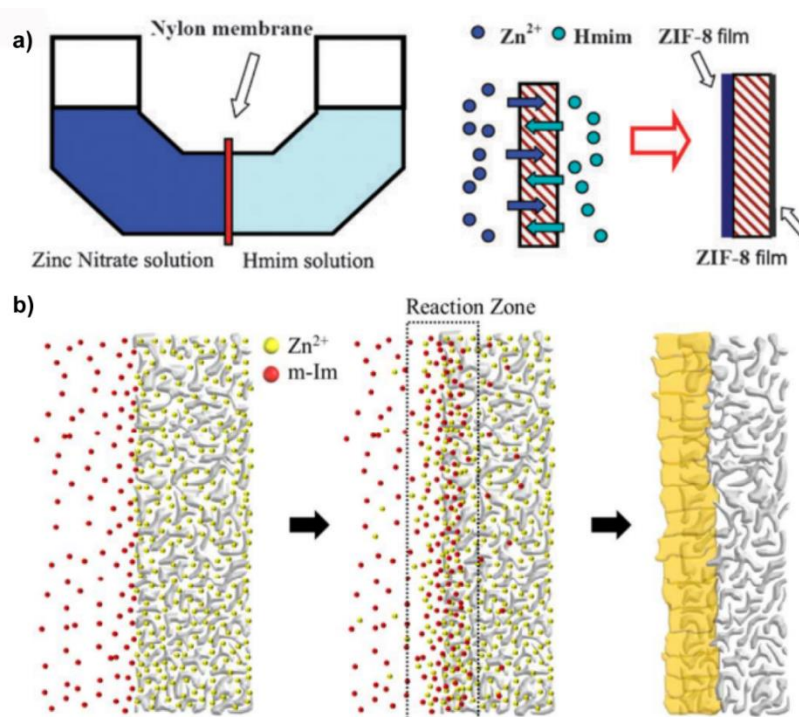


Figure 1.10 (a) Diffusion cell for ZIF-8 film preparation and the schematic of ZIF-8 film formation on nylon support, (b) schematic illustration of the membrane synthesis using the counter-diffusion-based in situ method (*Reproduced with permission from Ref 92, Copyright 2011 Royal Society of Chemistry and Ref 94 Copyright 2013 American Chemical Society*).

He's group [93] further studied the membrane formation in an aqueous solution using a stoichiometric amount of Zn^{2+} and 2-methylimidazole (2-mim) with the addition of sodium hydroxide. It resulted in a thin well-intergrown membrane on the 2-mim side with a thickness of 2.5 μm . Jeong's group [94] improved this technique by the predisposition of Zn^{2+} in alumina disc

followed by counter diffusion of 2-mim under solvothermal synthesis for 4h at 120 ° (Figure 1.10b).

Pienemann et al. have studied the effect of polymer substrate modification on MOF growth. They have modified the polymer support using poly-thiosemicarbazide (PTSC) polymer that can interact with the Zn metal, which favors the formation of ZIF-8 crystals on the polymer substrate. Using the counter diffusion method, an ultrathin and compact ZIF-8 layer grown on the metal-chelating polymer substrate was demonstrated [95].

1.5.4.5 Interfacial microfluid processing

Despite the excellent separation performance of ZIF membranes, the ceramic substrate has obstructed the industrial application of ZIF membranes. This problem can be solved by replacing ceramic membranes with cost-effective polymeric membranes. However, using conventional techniques, it could be very difficult to attain a good membrane on a polymeric substrate. To overcome this challenge, Nair and coworkers [96] come out with a new approach of interfacial microfluid membrane processing (IMMP). In this work, they fabricated a membrane by passing dilute zinc nitrate hexahydrate/*l*-octanol solution at a typical rate of 10 ml/hr through the bore of a horizontally mounted Torlon fibre. A concentrated aqueous 2-methylimidazole solution was present in the reactor chamber on the shell side. They controlled the membrane growth by the use of continuous bore solution flow conditions, static bore solution conditions, or intermittent conditions. They achieved continuous molecular sieving ZIF-8 membranes in single and multiple poly(amide-imide) hollow fibre membrane, with H₂/C₃H₈ and C₃H₆/C₃H₈ separation factors as high as 370 and 12, respectively. In addition, they successfully demonstrated positional control of the ZIF-8 film formation and characterized the contributions of membrane defects and lumen bypass. In our group, we have conducted a similar study on PBI-based hollow fiber membrane and encountered a similar issue of the presence of defects [97] (Figure 1.11).

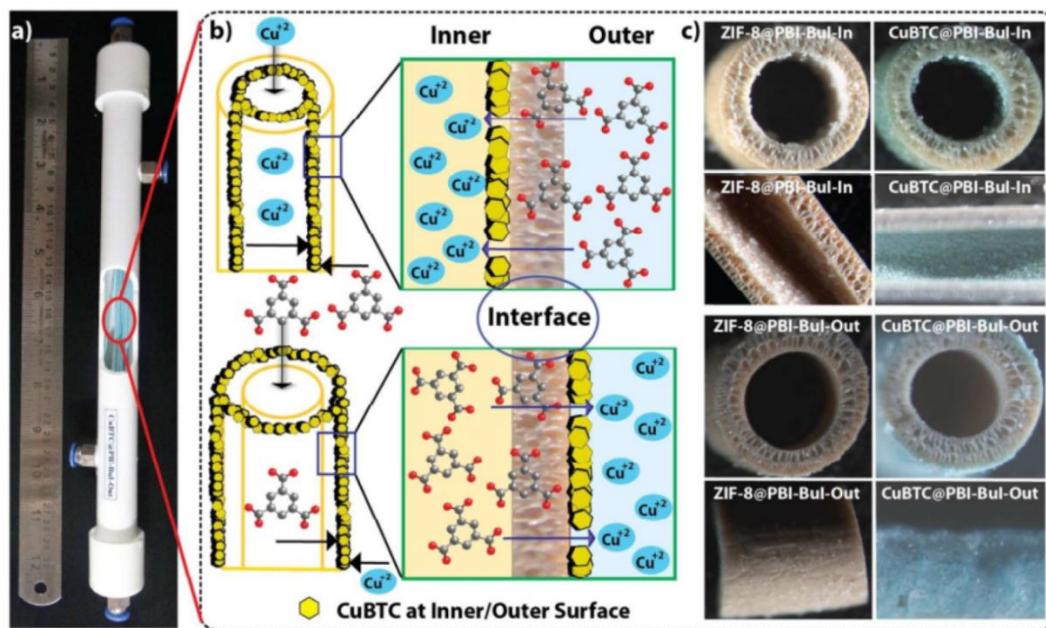


Figure 1.11 (a) Photographic image of hollow fiber module (b) Schematics of interfacial synthesis of CuBTC MOF membrane on PBI HF substrate (c) microscopic image of fabricated membrane. (Reprinted with permission from Ref 97, Copyright 2015 Royal Society of Chemistry)

1.5.4.6 Vapor phase synthesis

The synthetic protocol discussed above involved a solution-based processing step, which might create practical difficulties in scale-up. In addition, the use of solvents like DMF and methanol would create environmental problems [98]. Therefore, solvent-free based fabrications have advantages in cost, addressing environmental issues and scale-up. The vapor phase separation is an effective alternative, well established in zeolite membranes [99]. Several research groups used this method for ZIF membrane fabrication in a porous substrate for separation application. Kwon et al. [100] reported for the first time that ZIF-8 crystals undergo an Ostwald-ripening like process without degradation in the presence of a ligand vapor. The ripening process is dependent on the defect density of the crystals (the more defective, the more amenable to the ripening). The process was adapted to synthesize ultrathin ZIF-8 membranes by vapor phase secondary growth. The membrane prepared by this method showed a propane/propylene separation factor ~ 120 . Zhang and coworkers [101] showed a scalable synthesis of ZIF-8 molecular sieving membrane via gel-vapor deposition (Figure 1.12a). They could reduce the membrane thickness to 17 μm and it showed $\text{C}_3\text{H}_6/\text{C}_3\text{H}_8$ selectivity of 70. Tsapatsis's group [98] has demonstrated the fabrication of ZIF-8 nanocomposite membrane by

all-vapor-phase processing method based on atomic layer deposition (ALD) of ZnO on a porous support, followed by ligand vapor deposition (Figure 1.12b). The ZnO-deposited membrane did not show any selectivity. After the ALD membrane subjected to ligand vapor treatment, it turned the ZnO layer partially to ZIF and showed high mixed gas C_3H_6/C_3H_8 selectivity as well as C_3H_6 permeability. The authors called this transition (impermeable to highly permeable and selective transition) as ligand-induced permselectivation (LIPS).

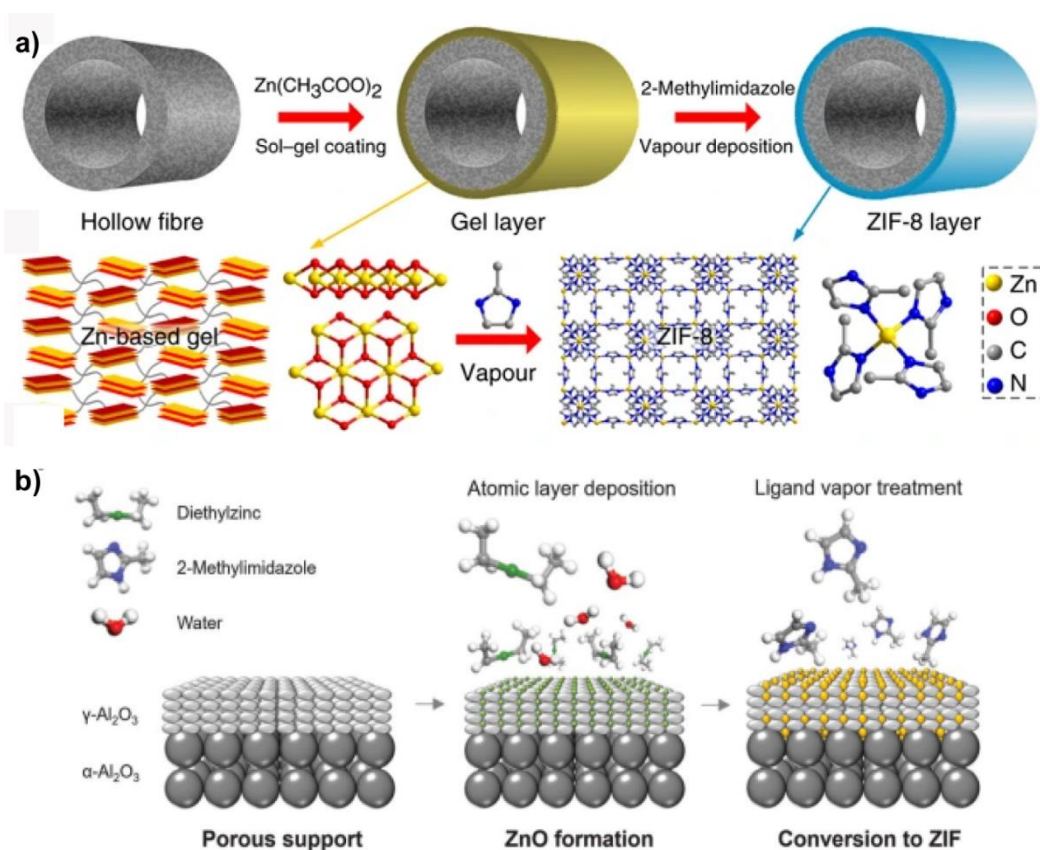


Figure 1.12 Schematic of the (a) ZIF-8 membrane formation by gel vapor deposition and (b) all-vapor phase LIPS membrane fabrication process. (Reprinted with permission from 101 Copyright 2017 authors and Ref 98 Copyright 2018 Science)

1.5.4.7 Current-driven synthesis

The membrane synthesized by conventional hydrothermal methods shows high flexibility due to linker mobility. Zhang et al. [102] proposed that the membrane performance can be improved by arresting the linker motion. Later Knebel et al. [103] demonstrated the switching of ZIF-8 into another structurally rigid polymorph by the application of an external electric field. The ZIF-8 lattice was transformed from cubic (I-43m space group) to monoclinic (Cm space

group) and triclinic (R3m space group) polymorphs, which led to marked changes in the gas permeation performance. The change in gas permeation was attributed to the change of ZIF-8 pore diameter from 3.4 to 3.6 and 3.1 Å in cubic, monoclinic and triclinic, respectively. Among the three polymorphs, Cm phase is stiffer and showed better selectivity of propylene/propane. Recently Wang's group [104] showed an electrochemical method named "fast current-driven synthesis" (FCDS) for the fabrication of ZIF-8 membranes on porous conductive supports (Figure 1.13a,b). The fabricated membrane consisted of 60 to 70% ZIF-8 Cm polymorph with suppressed linker mobility. Therefore the membrane showed an excellent propylene/propane separation factor ~300 with propylene permeance of $1.74 \times 10^{-8} \text{ mol} \cdot \text{Pa}^{-1} \cdot \text{m}^{-2} \cdot \text{s}^{-1}$.

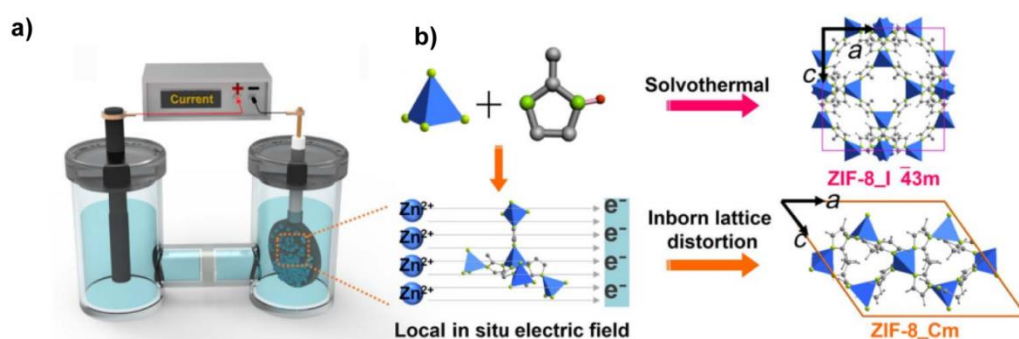


Figure 1.13 (a) The electrochemical cell for membrane growth by FCDS. The substrate served as a cathode in the electrochemical system, (b) schematic illustration of the ZIF-8 membrane growth via FCDS in comparison with solvothermal growth (*Reprinted with permission of Ref 104 copyright 2018 The Authors*)

1.5.4.8 MOF films on polymer support

Polymeric supports are economical as compared to inorganic supports such as titania and alumina. In spite of this, most of the MOF membranes were fabricated on expensive inorganic support rather than the organic support. The hybrid nature of the MOFs opens up the opportunity to fabrication on a polymeric support. Hatton's group fabricated MOF membranes on polymeric support for the first time [105]. The MIL-47 membrane was fabricated on a carboxyl functionalized polyacrylonitrile surface using in situ microwave irradiation. In another report, Yao et al. demonstrated continuous growth of ZIF-8 crystals on nylon support by counter diffusion method [106]. As similar to an inorganic substrate, the interaction of the MOF particle with the substrate surface is necessary for organic substrate also. The achievement of interfacial interaction on MOF/polymer interface is quite easy due to the affinity of organic linkers with polymers.

1.5.4.9 Mixed matrix membrane

The MOF inorganic membranes are an ideal candidate for gas separation application due to their excellent selectivity and good permeability, along with thermal and chemical stability. However, their use at the industrial level is restricted due to high fabrication costs and mechanical brittleness. The highly crystalline nature limits the processibility of these materials. The mixed matrix membrane (MMM) [107] concept was chosen as an effective alternative to mitigate these issues, which is the technique being persuaded over the last decades. This method combines the advantage of both polymer and MOF. The MMM is composed of a polymer and a dispersed additive (MOF) and has great potential to achieve excellent separation properties and scalability on an industrial scale [108]. MMMs based on zeolites are widely studied [72]. They face difficulties such as poor interfacial interaction between polymer and zeolites, challenges in the synthesis of crystals, limited structural diversity, and little tailorability. The synthesis of MOFs is relatively easy and due to the hybrid nature, a favorable interaction exists at MOF/polymer interface. Polymers selected for MMM construction should be capable of withstanding aggressive feed conditions such as temperature, pressure, and corrosive gas mixture. Polymers should also exhibit high gas permeability and selectivity to attain the targeted industrial application. Till date, there have been many MOF-based MMMs reported, which include MOF-5 in Matrimid [109], ZIF-90 in 6FDA-DAM [110], $\text{Cu}_3(\text{BTC})_2$, ZIF-8, and MIL-53 (Al) in Matricide [111], HKUST-1 in polyimide hollow fibre mixed matrix membrane [112], and HKUST-1, MIL-53, MIL-47, and ZIF-8 in PDMS [113]. The critical challenge in the fabrication of MMMs is the compatibility of the polymer with the MOF. Later, our group has reported MMM based on polybenzimidazole (PBI) and ZIF-8 and the membrane showed good performance at 30% ZIF loading [114]. The rationale behind the selection of the PBI for MMMs is that the presence of imidazole moiety similar to ZIF-8 can impart interaction between the ZIF and the polymer. MOF-Mixed matrix membranes are an alternative solution for industrial gas separation applications. Nonetheless, some of these membranes still face issues such as plasticization and poor thermochemical stability and limit their industrial viability.

1.5.5 MOF-based membranes: Gas separation performance

MOF membranes are an attractive candidate for gas separation application, and it attained wide attention in the recent past. Lai and Jeong reported the first MOF-based gas separation membrane on porous support by an in-situ method [75]. The membrane showed lower flux

attributed to the randomly oriented MOF crystals, restricting the diffusion of the gas molecule. The next section discusses some reports on MOF membranes focusing on a specific application.

1.5.5.1 Hydrogen purification

The demand for hydrogen is increased due to its viability, clean energy nature and high energy density as compared to fossil fuels. However, industrially produced hydrogen exists with other gases, such as N₂, CO₂, CH₄, etc. In order to get the desired purity for fuel production, the separation of hydrogen from these gases is required [115]. Membrane technology is an effective energy-efficient alternative over cryogenic distillation, provided optimum membranes are available [83]. MOF-based membranes are widely studied for H₂ separation [116]. In 2009 Liu et al. reported the MOF-based membrane for H₂ separation. The MOF-5 membrane was fabricated on alumina support by using the solvothermal method. The single gas analysis showed that the membranes were following Knudsen diffusion. Hydrogen has the least molecular weight among other gas molecules studied (CO₂, CH₄, N₂, and SF₆). The H₂ gas separation performance of some of the MOF membranes is summarized in Table 1.3.

Table 1.3 Summary of H₂ separation performance of some of the reported MOF-based membranes

MOFs	Pore size (Å)	Substrate	Separation factor (α)	H ₂ permeance (mol m ⁻² s ⁻¹ Pa ⁻¹)	Ref.
Cu ₂ (bza) ₄ (pyz)	2	α -Al ₂ O ₃ sheet	H ₂ /N ₂ (10*) H ₂ /CH ₄ (19*)	6.88×10^{-9}	[117]
ZIF-7	3	α -Al ₂ O ₃ disks	H ₂ /CO ₂ (13.6) H ₂ /N ₂ (18) H ₂ /CH ₄ (14)	4.55×10^{-8}	[61]
ZIF-7	3	α -Al ₂ O ₃ disks	H ₂ /CO ₂ (8.4)	9.00×10^{-9}	[77]
ZIF-22	3	TiO ₂ disks	H ₂ /CO ₂ (7.2) H ₂ /N ₂ (6.4) H ₂ /O ₂ (6.4)	1.60×10^{-7}	[78]
ZIF-8	3.4	TiO ₂ disks	H ₂ /CH ₄ (11.2)	6.70×10^{-8}	[87]
ZIF-8	3.4	Nylon support	H ₂ /N ₂ (4.3)	1.97×10^{-6}	[92]
ZIF-8	3.4	α -Al ₂ O ₃ tube	H ₂ /N ₂ (10.3) H ₂ /CH ₄ (10.4)	2.00×10^{-7}	[80]
ZIF-8	3.4	α -Al ₂ O ₃ disks	H ₂ /N ₂ (11.6) H ₂ /CH ₄ (13)	1.70×10^{-7}	[118]
Zn ₂ (cam) ₂ dabco	3 × 3.5	Porous ZnO	H ₂ /N ₂ (19.1) H ₂ /CH ₄ (14.7)	2.70×10^{-8}	[119]
IF-90	3.5	α -Al ₂ O ₃ disks	H ₂ /CO ₂ (11.7) H ₂ /N ₂ (7.3) H ₂ /CH ₄ (15.3)	2.50×10^{-7}	[118]

Continued Table 1.3

ZIF-90 (post)	3.5	α -Al ₂ O ₃ disks	H ₂ /CO ₂ (15.3) H ₂ /N ₂ (15.8) H ₂ /CH ₄ (18.9)	$1.9\text{--}2.1 \times 10^{-7}$	[120]
Cuhfipbb	3.5	α -Al ₂ O ₃ disk	H ₂ /N ₂ (22a) H ₂ /CO ₂ (4a) CO ₂ /N ₂ (5a)	1.50×10^{-8}	[87]
ZIF-95	3.7	α -Al ₂ O ₃ disks	H ₂ /CO ₂ (25.7)	1.95×10^{-6}	[121]
ZIF-78	3.8	Porous ZnO	H ₂ /CO ₂ (9.5) H ₂ /N ₂ (5.7) H ₂ /CH ₄ (6.4)	1.00×10^{-7}	[122]
CAU-1	3.8	α -Al ₂ O ₃ tube	H ₂ /CO ₂ (12.3) H ₂ /N ₂ (10.33) H ₂ /CH ₄ (10.4)	1.00×10^{-7}	[123]
Zn ₂ (bdc) ₂ dabco	7.5	α -Al ₂ O ₃ disk	H ₂ /CO ₂ (12.1)	2.70×10^{-6}	[124]
NH ₂ -MIL-53(Al)	7.5	Porous SiO ₂	H ₂ /CO ₂ (30.9) H ₂ /N ₂ (23.9) H ₂ /CH ₄ (20.7)	2.00×10^{-6}	[125]
MIL-53(Al)	7.3 × 7.7	α -Al ₂ O ₃ disks	H ₂ /CO ₂ (4*) H ₂ /N ₂ (2.5*) H ₂ /CH ₄ (2.2*)	5.00×10^{-7}	[91]
MOF-5	7.8	α -Al ₂ O ₃ discs	H ₂ , CH ₄ , N ₂ , CO ₂ , SF ₆ (Knudsen diffusion)	3.00×10^{-6}	[76]
MOF-5	7.8	α -Al ₂ O ₃ discs	H ₂ /CO ₂ (2.5) H ₂ /N ₂ (2.7) H ₂ /CH ₄ (2) H ₂ /CO ₂ (4.1*)	8.00×10^{-7}	[126]
HKUST-1	9	Copper net	H ₂ /N ₂ (7) H ₂ /CO ₂ (6.8) H ₂ /CH ₄ (5.9)	1.50×10^{-6}	[83]
HKUST-1	9	PSF	H ₂ /CO ₂ (7.2) H ₂ /C ₃ H ₆ (5.7)	7.90×10^{-8}	[127]
HKUST-1	9	Porous SiO ₂ metal nets	H ₂ /CO ₂ (9.24) H ₂ /N ₂ (8.91) H ₂ /CH ₄ (11.2)	1.00×10^{-6}	[128]
HKUST-1	9	α -Al ₂ O ₃ disks	H ₂ /CO ₂ (4.6) H ₂ /N ₂ (3.7) H ₂ /CH ₄ (3)	$4.00\text{--}6.00 \times 10^{-7}$	[129]
HKUST-1	9	α -Al ₂ O ₃ tube	H ₂ /CO ₂ (13.6) H ₂ /N ₂ (8.66) H ₂ /CH ₄ (6.19)	4.00×10^{-8}	[130]

*: Ideal separation factor; others are mixed gas separation factor

1.5.5.2 CO₂ Separation

Carbon dioxide is the major candidate among greenhouse gases, the emission of which leads to global warming. In addition, CO₂ is one of the major impurities in natural gas, and it needs to be removed to address corrosion issues. Among the conventional separation techniques for CO₂ separation, membranes are highly promising due to their energy-efficient and reliable nature. Several materials have been studied as membrane materials, including zeolites and polymers. However, zeolites suffer low permeation properties, while polymers suffer plasticization [131,132]. MOFs and ZIFs are widely studied as membrane materials for CO₂ separation. In addition to the excellent thermochemical stability, ZIFs are stable to water and other hydrocarbons in the petrochemical stream, making them potential materials for CH₄/CO₂ separation [88,133,134].

1.5.5.3 Hydrocarbon separation

The separation of different hydrocarbons is an energy-consuming process in industries such as petroleum refining, petrochemical and natural gas production. Among the hydrocarbon separations, olefin and paraffin separation is highly energy-intensive [31]. Currently, the olefins are separated from their close-boiling paraffin by cryogenic distillation, which is highly energy intensive. Membrane-based separation is reported to be an attractive alternative to olefin/paraffin separation [135,136]. Polymeric membranes are widely studied due to their low cost and ease of processing [135,136]. However, polymeric membranes lack stability against plasticization and have a trade-off relationship between permeability and selectivity [136]. Facilitated transport membranes, though look superior in terms of selectivity, face instability issues with the carrier agent. [137]. Later, membranes consisting of molecular sieves such as zeolites [14], carbon molecular sieves [138] and metal-organic frameworks emerged as potential candidates for olefin-paraffin separation [139]. Among them, MOFs exhibit superiority because of the abundance of a wide variety and tuneable pore size. Specifically, ZIF frameworks are widely studied for olefin/paraffin separation due to their pore aperture size being close to the size of these gases [140,141]. ZIF-8 is one of the significant members of this family, synthesized from Zn(II) metal and 2-methylimidazole ligand. From X-ray diffraction, it is confirmed that the ZIF-8 has 13 Å pore cavity with 3.4 Å pore window [102]. In 2009, Li et al. [140] have studied the adsorption behavior of propane and propylene in ZIF-8. They found that even though the kinetic diameter of both the gas molecule exceeded 3.4 Å, ZIF-8 can adsorb both the gases and attains same

adsorption equilibrium. The adsorption study at 30 °C reveals that the ratio of the diffusion coefficients is 125 ($P_{\text{propylene}}/P_{\text{propane}}$) [140]. This proves that the ZIF-8 is a potential material for the kinetic separation of these gases. Lai's group reported the ZIF-8 based membrane for propylene/propane separation in 2012 [142]. They could attain a separation factor of 30 and the membrane surpassed the polymeric and carbon molecular sieve (CMS) upper bound limit. Later, ZIF based membranes attracted a wide attention for C3-based separations. Table 1.4 summaries the propylene/propane separation performance of some the ZIF-8 based membranes fabricated by different synthetic method.

Table 1.4 Propylene/propane separation performance of some of the ZIF-8 based membranes [143]

Method of membrane fabrication	Support	Thickness	Permeance of C_3H_6 ($\text{mol}\cdot\text{m}^{-2}\cdot\text{s}^{-1}\cdot\text{Pa}^{-1}$)	Separation factor	Ref.
seeded growth	α - Al_2O_3 support	$\sim 2.2\mu\text{m}$	2.06×10^{-8}	45	[142]
			2.77×10^{-8}	35	
	α - Al_2O_3 support	$\sim 0.5\text{-}1.5\mu\text{m}$	7.8×10^{-9}	89	[143]
			1.56×10^{-8}	50	
α - Al_2O_3 support	$\sim 1.5\mu\text{m}$	2.08×10^{-8}	40	[144]	
	Commercial ceramic	$\sim 1.2\mu\text{m}$	1.90×10^{-8}	80	[145]
Counter diffusion	α - Al_2O_3 support	$\sim 1.5\mu\text{m}$	2.13×10^{-8}	50	[94]
	α - Al_2O_3 support	$1\mu\text{m}$	2.68×10^{-8}	70.6	[146]
	α - Al_2O_3 hollow capillary substrate	$20\mu\text{m}$	1.2×10^{-8}	20	[147]
	α - Al_2O_3 hollow capillary substrate	$40\text{-}50\mu\text{m}$	2.2×10^{-9}	10	[148]
Interfacial microfluidic processing	Polymer hollow fiber	$\sim 8.8\mu\text{m}$	9×10^{-9}	12	[96]
	Polymer hollow fiber	$\sim 8\mu\text{m}$	1.51×10^{-8}	184.4	[149]
	Polymer hollow fiber	$\sim 5\mu\text{m}$	2.21×10^{-8}	65	[150]
Vapor-phase ripening	α - Al_2O_3 hollow capillary substrate	$300\text{-}400\text{nm}$	1.25×10^{-8}	120	[100]
Gel-vapor deposition	PVDF-hollow fiber	$<20\text{nm}$	2.8×10^{-7}	67.2	[101]

Continued Table 1.4

All-vapor ligand-induced permselectivation	γ -Al ₂ O ₃ coated α -Al ₂ O ₃ support	<500 nm	8.8×10^{-8}	71	[98]
			1.6×10^{-7}	74	
Current-driven synthesis	Pt coated AAO support	~200 nm	1.74×10^{-8}	300	[104]

1.6 Covalent Organic Framework (COF)

These types of porous materials are crystalline, porous and are constructed from organic building block which follows reticular synthesis. The tuneable, pre-designable, and easily functionalisable framework structure made these materials as potential candidates for several applications such as gas adsorption, catalysis, separation and sensors. COFs are completely organic in nature and the building block consists of lighter elements such as C, N, and O [151–154]. The building blocks with precise symmetry linked together by strong covalent bond leads to a framework with specific geometry. Due to the pure covalent bond, COFs show good thermal stability and the presence of light elements in the framework displays low density. Based on the symmetric combination of the building block used for the COF synthesis, they can be designed into two or three dimensions. The porosity of the COFs can be tuned by varying the length of the building block (Figure 1.14) [153,154]. Generally, COFs are synthesized by reversible covalent formation reaction, which imparts error checking and proofreading to the system [153]. It results in the formation of thermodynamically stable COF at the end. The most commonly used reversible reaction for the synthesis of COF formation are boronic acid trimerization [155], boronate ester formation [155,156], nitrile group trimerization [152,157,158] and Schiff reaction [159,160].

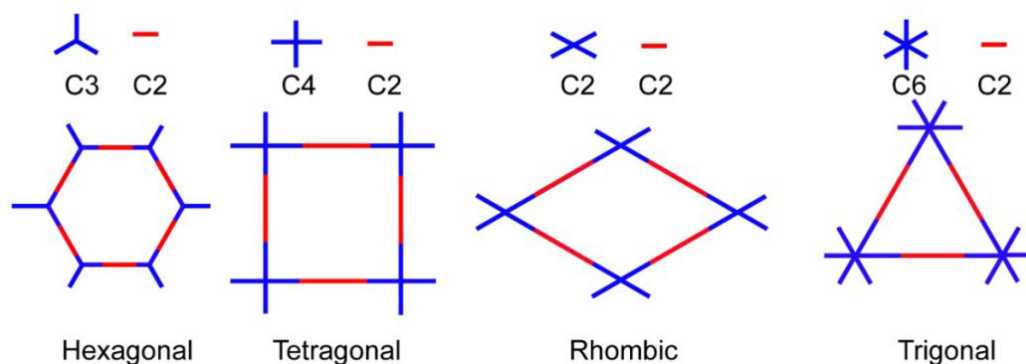


Figure 1.14 Schematic representation of different organic symmetric combination used in COF framework construction

1.6.1 Synthesis of COFs

It is generally carried out by thermodynamically controlled reversible organic reactions. The reversibility in bond formation helps to attain a thermodynamically stable product by bond breaking and reformation. The parameters like reaction media, solvent and experimental conditions like temperature and pressure play a vital role in attaining thermodynamically stable, crystalline and porous covalent organic framework. Following are some of the synthesis methods reported in the literature.

1.6.1.1 Solvothermal synthesis

It is the widely used method for COF synthesis. The monomers are poured into a pyrex tube along with the solvent, followed by degassing the tube by freeze-pump-thaw cycles [152]. Finally, the tube is sealed and kept inside the oven (temperature generally set between 90-120°C) for 2-7 days. The low pressure inside the pyrex tube helps to escape the byproduct (water) from the reaction mixture and helps the formation of the COF crystallites.

1.6.1.2 Microwave synthesis

Cooper and coworkers showcased the microwave-based protocol for COF synthesis [161]. This method has advantages over the solvothermal method, such as the rapid formation of the product and limited impurities generated during the reaction. The COF synthesized by the microwave method shows comparable crystallinity and surface area as that of the solvothermal method.

1.6.1.3 Ionothermal synthesis

This protocol is generally used for the synthesis of covalent triazine framework (CTFs) [152,157]. It was first introduced by Thomas and coworkers [152]. The solid reactant and $ZnCl_2$ are heated at 400°C inside a closed quartz tube. At this temperature, the $ZnCl_2$ melts and act as a solvent. Nonetheless, this method is not studied widely due to the harsh conditions and the less crystallinity of obtained COF.

1.6.1.4 Synthesis of monolayers on a surface

Various COFs are synthesized on the metal surface and on the top of two-dimensional supports. COF-monolayer fabrication is important for photochemical and electrochemical applications. Zwaneveld et al. developed the fabrication of COF on the surface [162]. They demonstrated the first surface-COF (SCOF) based on COF-1 and COF-5 on a clean Ag(III) surface [162]. Ditchel's group fabricated SCOF on the surface of Ag(III) using a sublimation

reaction [163]. In another report, Ditchel and coworkers developed a new method of COF synthesis on single-layered graphene attached to SiO₂ by solvothermal conditions [163]. The thickness of the thin layer is adjusted by varying the reaction time. Li-Jun Wan and coworkers developed an alternative method of fabricating COF on 2D layer [164]. The attained COF growth on highly ordered pyrolytic graphite (HOPG) by drop casting the building units on the surface followed by heating in a closed container in the presence of copper sulfate pentahydrate (CuSO₄ · 5H₂O) [164]. CuSO₄ · 5H₂O is said to maintain the humidity, thereby improving the crystallinity.

1.6.1.5 Mechano-chemical synthesis

Several harsh reaction conditions, such as a sealed pyrex tube, choice of different solvents, and inert atmosphere, are crucial for attaining crystalline porous COF [165]. The aforementioned challenges in COF synthesis reduce the practicability of COFs in real applications. Biswal et al. introduced solvent-free mechano-chemical room temperature synthesis of Schiff base COFs [166]. The crystallinity of the mechanochemically synthesized COFs was moderate as compared to the solvothermal synthesized one. Further, they found that the mechanochemically synthesized COFs show a delaminated layer (more graphene-like morphology) than that of solvothermal synthesized COFs.

1.6.1.6 Organic terracotta process

S. Kark et al. presented a new synthetic strategy wherein they achieved a rapid synthesis of ultraporous crystalline COFs in seconds by salted mediated crystallization approach [167]. They achieved it by introducing a Bronstead acid, P-toluenesulfonic acid (PTSA) as a molecular organizer. The PTSA induces reversibility in reaction, which leads to an ordered network with high porosity and crystallinity by minimizing the framework defect. They showcased the synthesis of twelve different COFs with high surface area (highest 3109 m²/g) in 60 seconds.

1.6.2 Application of COFs

The crystallinity, high porosity and easily functionalisable nature of COFs made them useful for a wide variety of applications such as separation, storage, photoconducting material, sensors and catalysis. The pre-designable and ordered nature of the COF pores is employed for storage applications such as gas storage, doping of catalyst sites, drug and biomolecule storage. The π -conjugated nature of 2-D COF makes them a suitable candidate for charge storage and photoconductive applications. In the recent past, COFs attained wide attention as membrane

material. The next section summarizes the key properties of COFs for membrane separation, fabrication methods, and some widely studied separation applications.

1.6.3 COFs for membrane application

The characteristics COFs, such as high pore density, ordered pore structure and uniform pores, makes them a potential candidate for constructing improved separation membrane. In addition, the size and symmetry of the organic linker decide the tropology of the framework. This enables the fine-tuning of COF pore size for different challenging separation applications. Moreover, COFs having provision for functionalization can further be utilized for attaining the desired separation by host-guest interactions. These superior characteristics of COFs attracted enormous attention and membrane separation became a key application of COFs [168]. COF-based membranes are studied for gas separation, water purification and organic solvent nanofiltration. Key features of COFs in membrane separation are as follows.

a) Pore size

Most of the membranes are based on size exclusion. Thus, the pore size of the COFs plays a major role in deciding the membrane performance. The pore size of the COFs generally depends on the symmetry and size of the linker molecules. Different COFs are reported in the literature, with pore sizes ranging from 0.5 nm to 4.5 nm. This pore-size region covers wide applications such as desalination, nanofiltration and ultrafiltration.

b) Stability

The COF formation reactions are reversible in nature, leading to poor chemical stability. This limits the use of COFs as membrane material for applications involving harsh conditions such as strong acidity, drastic humidity and organic solvents. Therefore, researchers come up with different approaches for synthesizing thermochemical stable COFs. Banerjee et al. reported hydroxyl functionalized imine-based COF by Schiff base reaction (TpPa-1 and TpPa-2)[169]. These COFs displayed excellent stability towards water, acids (9M HCl) and bases (9M NaOH). Their exceptional chemical stability arises due to the keto-enamine tautomerization of imine nitrogen and hydroxyl functional groups. The enol prefers over the keto form due to the more aromaticity, which leads to this transformation is irreversible. Thus this COF exist in enol form only (Figure 1.15) [169].

c) Hydrophilicity or hydrophobicity

Membranes possessing either hydrophobicity or hydrophilicity play a crucial role in membrane separations, such as solvent separation and water separation. This property also plays a crucial role in the control of membrane fouling.

d) Surface charge

In organic solvent nanofiltration and desalination application, the charge present on the membrane surface play a crucial role in governing membrane rejection performance and imparting antifouling property.

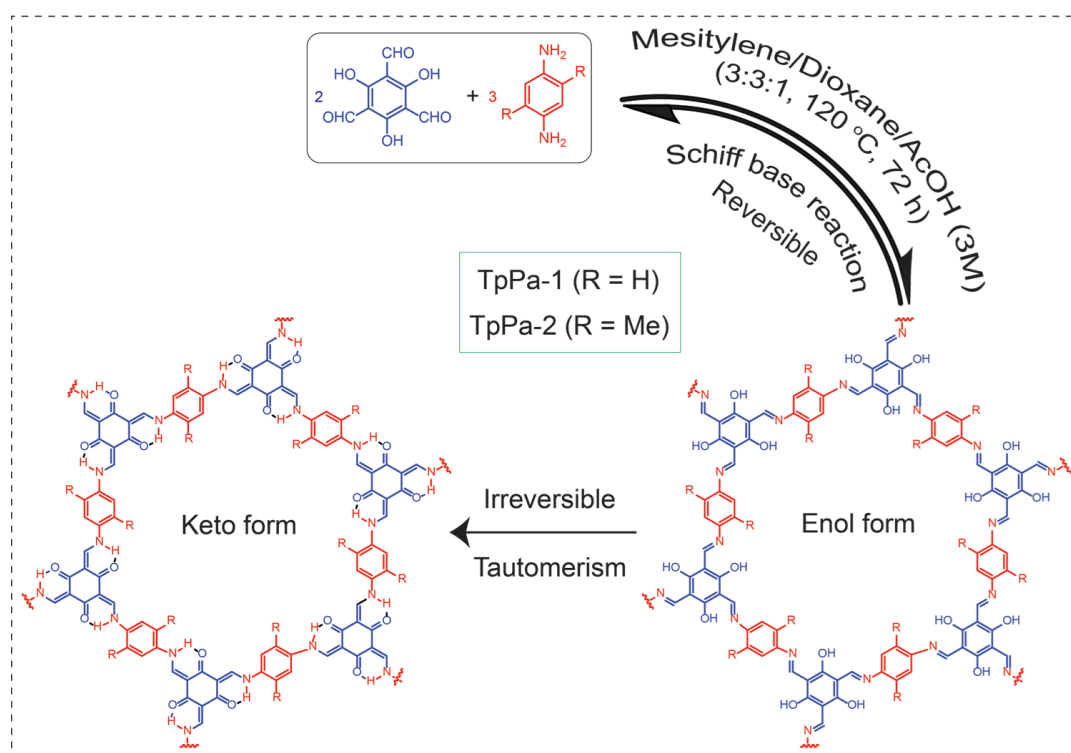


Figure 1.15 Synthesis scheme of stable COF by Schiff base reaction (*Reprinted with permission from Ref 169, Copyright 2012 American chemical society*)

1.6.4 Fabrication of COF membranes

The fabrication of defect-free membrane is a challenging task because of the poor processibility of COF material as compared to polymers. The fabrication technology which can synthesize COF membrane with the full potential of order pores for separation obtained wide attention in the recent past. Initially, COF membranes were synthesized by blending with suitable polymers (MMMs). However, the full potential of the COF material could not achieve in this method due to the contribution of the polymer part. With advanced membrane technology,

pristine COF membranes were synthesized, wherein the pore structure of COF gained increasing significance in membrane separation. The continuous and pristine COF membranes were obtained by in situ growth, layer-by-layer stacking, interfacial polymerization (IP), and Langmuir Blodgett method. The detailed procedure is discussed in the following section.

1.6.4.1 In situ growth

Banerjee and coworkers synthesized self-standing scalable covalent organic framework-based membranes (COMs) using ketoenamine COFs for the first time [170]. Briefly, the procedure consists of knife casting the previous dough by mixing organic linkers and p-toluene sulfonic acid (co-reagent) on a glass plate [170]. Further, the COF membrane is obtained by baking the film at 60-120°C using an oven for 12-24 hours [170]. The membrane exhibited excellent molecular sieving properties as compared to the polyamide-based membrane reported in the literature. Later the same group extended these procedures for fabricating proton exchange membranes [171]

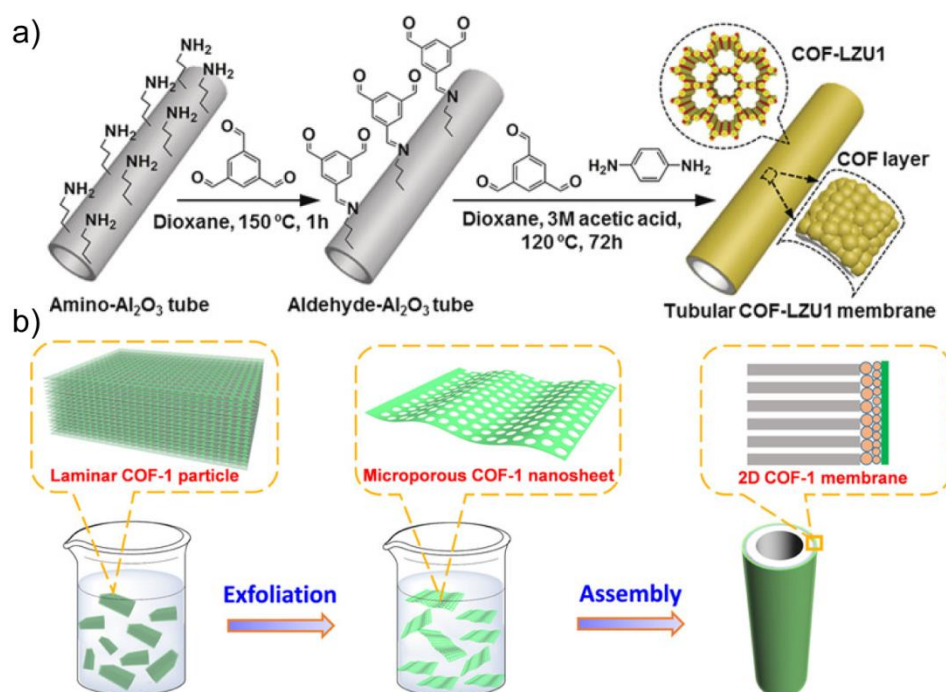


Figure 1.16 (a) Synthesis of tubular COF-LZU1 membranes. First, the surface of the alumina tubes is modified by APTES, followed by a grafting reaction with TFB. Finally, the COF layers are grown onto the support by imine condensation of TFB and PDA (b) Schematic representation of the preparation of a COF-1 membrane via the assembly of exfoliated COF-1 nanosheets (Reproduced with permission from Ref 172, Copyright 2016, John Wiley and Sons and Ref 173, Copyright © 2017, American Chemical Society)

In situ synthesis of COF on inorganic or organic porous support can overcome the mechanical stability issue of the self-standing COF membranes. Caro and coworkers fabricated a continuous membrane using COF-LZU1 on commercially available alumina support modified with 3-amino propyltriethoxysilane (APTS) [172] (Figure 1.16a). These membranes were demonstrated for dye separation application.

1.6.4.2 Layer-by-layer method

In this approach, the COF 2D nanosheets were deposited on various substrates [173,174]. This method is very widely used for the fabrication of graphene or grapheneoxide membrane. In this method, the nanosheet dispersion in water or any other solvent is stacked on porous substrate by pressure, dip coating, or vacuum-assisted filtration to attain a continuous membrane. The main advantage of this method is good control over the thickness of the membrane, thereby attaining a low flow resistance for water or gas or any solvent when it passes through the membrane. Tsuru and coworkers reported ultra-thin COF membrane on α -Al₂O₃ support by dip coating (Figure 1.16b) [173]. They have used SiO₂-ZrO₂ as an intermediate layer to attain a crack-free membrane with high permeance. The fabricated membrane exhibited H₂ permeance of 1×10^{-6} mol m² Pa⁻¹ s⁻¹. Zhong and coworkers fabricated a covalent triazine framework-based membrane using graphene oxide assisted layer-by-layer method [174]. Further, the membrane is demonstrated for H₂/CO₂ application.

1.6.4.3 Interfacial synthesis

Interfacial polymerization (IP) is widely used for the fabrication of polyamide thin film composite membranes due to its scalability and capability to tune the thickness of the membrane. A thin COF membrane is necessary to obtain the full potential of the COF nanochannel. In this regard, the IP can be adapted for COF membrane fabrication. Banerjee and coworkers reported the pioneering fabrication of continuous freestanding imine-based COF membrane using IP (Figure 1.17) [175]. In this study the aldehyde Tp was dissolved in dichloromethane and amine was dissolved in water. Instead of free amine, they have used p-toluensulfonic acid salt of amine to reduce the diffusion rate, thereby avoiding the formation of an amorphous polymer. Ditchel and coworkers reported the fabrication of free-standing film via interfacial polymerization catalyzed by Sc(OTf)₃ [176]. They could vary the thickness of the film by changing the monomer concentration and the organic phase. The films were easily transferred onto polysulfone substrate and they exhibited enhanced rejection of Rhodamine WT. Wang and coworkers reported a

simple strategy for COF membrane synthesis on a polysulfone substrate [177]. This approach eliminates the transfer of the thin film layer to the substrate.

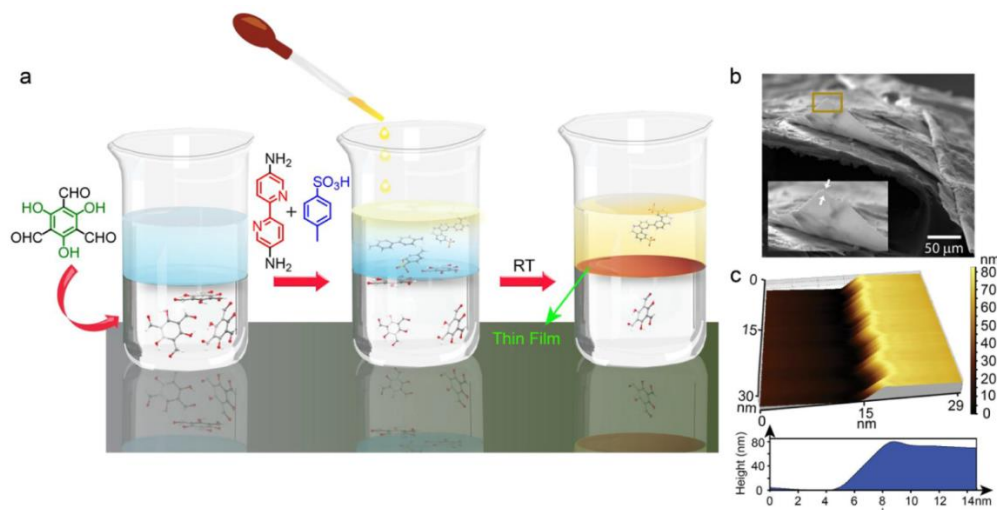


Figure 1.17 Synthesis scheme of COF thin films. (a) Schematic representation of the interfacial crystallization process used to synthesize the Tp-Bpy thin film. (b, c) SEM and AFM images respectively, of the Tp-Bpy thin film. (Redrawn with permission from Ref 175, Copyright © 2017, American Chemical Society)

1.6.4.4 Langmuir-Blodgett (LB) Method

This method has potential to synthesize membranes with large dimensions than can be easily transferred to support and good control over membrane thickness. Lai and coworkers reported the synthesis of crystalline 2D COF membrane using this method; this was the pioneering synthesis of the membrane using LB method [178]. A single layer of COF membrane prepared by this method four four unit cells thick and the thickness can be precisely adjusted by layer-by-layer stacking. The fabricated TFP-DHF2D COF showed excellent solvent flux and sharp molecular sieving properties.

1.6.5 Various separations of COF membranes

COFs have been demonstrated for various separation applications and can be broadly classified in to two, that is, liquid phase and gas phase separations, based on the application point of view. This section highlights and summarizes the significant application of COF membranes

1.6.5.1 Gas separation

Polymer-based membranes are very widely used for gas separation applications. However, the disordered nature and inconsistent pores make it difficult to achieve better perm selectivity in polymeric membranes. In this regard, COFs have the advantage of high porosity and long-range order, which helps the gas molecules to easily pass through the membrane in an

ultrafast manner. Some of the prominent gas separation applications of COF membranes are hydrogen separation, CO₂ separation and hydrocarbon recovery. Hydrogen is a better replacement for conventional fossil fuel, nonetheless, the production of pure hydrogen fuel is challenging due to the presence of unwanted gases in the product. COF membranes were demonstrated for H₂ separation from other gases. Zhong and coworkers introduced graphene oxide-assisted fabrication of a covalent triazine-based framework for H₂ separation from CO₂ [174]. The fabricated membrane exhibited H₂ permeability of 1.7×10^{-6} mol m⁻²s⁻¹Pa⁻¹ and surpassed the 2008 Robeson's upper bound for H₂/CO₂. The large pore size present in the COF limits the usage of COF membrane for gas separation. Caro and coworkers demonstrated the fabrication of a two-dimensional layer stacking COF-COF composite membrane with bilayer geometry on an amino-functionalized alumina substrate [179]. The imine-based bilayer COF-LZU-1/ACOF-1 membrane showed better separation performance than the individual COF membranes (COF-LZU-1 and ACOF-1) due to the interlaced pore network.

Carbon dioxide is one of the major components released by industries along with other gases. In order to prevent the global warming the CO₂ needs to separate from other gases before emitting to atmosphere. In addition, CO₂ separation from CH₄ is important to avoid the pipeline corrosion issue. Polymeric membranes are widely studied for CO₂ separation. However, the plasticization issue of polymeric membrane limits its industrial usage. In this regard, the excellent thermo chemical stability and provision to incorporate functional groups which is having an affinity towards CO₂ makes COFs as a suitable candidate for CO₂ separation. Caro and coworkers developed a 2-D COF membrane based on ACOF-1 on alumina support by solvothermal method [180]. The membranes showed excellent CO₂/CH₄ selectivity and surpassed the 2008 Robeson's upper bound. COFs are also studied for Hydrocarbon recovery. Biswal et al. are pioneers of Tp-pa-1@SBR (Styrene butadiene rubber) thin film composite membrane on polyacrylonitrile substrate for propylene recovery from air [181]. They could achieve a 70% loading of Tp-Pa-1 COF inside the SBR matrix without any defect [181].

1.6.5.2 Liquid separation

Covalent organic frameworks are also employed for liquid-based separations such as water treatment, organic solvent nanofiltration and pervaporation. The stability of the membrane under operating conditions is important for liquid-based separations. The poor

stability of COFs limits the applicability of COFs as membrane material for various liquid-based separations. In this section, we have discussed on COF membrane employed for liquid separation

1.6.5.3 Water separation

There is greater interest in technologies that can purify wastewater and desalination of seawater due to the fast increase in population and industrial development [182,183]. Some of the major components that need to be removed from wastewater or seawater are salts, dyes and organic compounds. COFs have a pore size in the range of 0.5-5 nm, which is ideal for ultrafiltration and nanofiltration. Wang and coworkers developed a COF membrane based on Schiff base reaction on polysulfone ultrafiltration membrane by interfacial polymerization [177]. The membrane shows 99.5% rejection of Congo red coupled with water permeance of $50 \text{ L m}^{-2} \text{ h}^{-1} \text{ bar}^{-1}$. Later Caro and coworkers prepared imine linked COF-LZU1 on alumina tubes by solvothermal synthesis [172]. Ma and coworkers have developed a cationic COF membrane based on ethidium bromide COF using bottom-up interfacial crystallization [184]. The ionic COF membrane exhibited high permeability and rejection for dye molecules/ions due to the presence of a positive charge on the pore wall. Jiang and coworkers studied the performance of 2D COF membrane based on Tp-Pa COF with various functional group for desalination [185]. They found out that the NaCl rejection is more than 95%, along with the water permeance ranging from 1216 to 3375 $\text{kg m}^{-2} \text{ h}^{-1} \text{ bar}^{-1}$. In addition to nanofiltration, COFs are studied for ultrafiltration for removing organics from wastewater. Gao and coworkers are the pioneers of COF-based membranes for ultrafiltration [186]. They constructed a mixed matrix membrane by blending Tp-Pa-2 with polysulfone. The fabricated membrane displayed 90% rejection of humic acid with a water permeance of $377.5 \text{ L m}^{-2} \text{ h}^{-1} \text{ bar}^{-1}$.

1.6.5.4 Organic solvent nanofiltration

Organic solvent nanofiltration (OSN) is an emerging technique in the pharmaceutical and fine chemical industries. Typical OSN membrane consists of pore size in the range of 1-2 nm and the membrane allows the separation, purification and recycling of organic molecules and catalysts from organic solvents [187,188]. The major concern while fabricating an OSN membrane is its robustness towards organic solvents because the membranes are exposed to different solvents for a long duration. Moreover, the membrane should exhibit high solvent permeance and rejection. COFs are chemically robust and consist of well-defined pores, these characteristics make them a potential candidate for OSN to obtain excellent permeability and

selectivity. Banerjee and coworkers reported continuous self-standing stable COF membranes (M-TpTD and M-TpBD) and demonstrated for separation of solutes such as dyes, active pharmaceutical ingredients and organic pollutants [170]. In addition, the membranes showed high permeance for polar organic solvents and the TpTD membranes had acetonitrile permeance of $278 \text{ Lm}^{-2}\text{h}^{-2}\text{bar}^{-1}$ which is 2.5 times higher than the polyamide nanofiltration membrane. Further, they have demonstrated the fabrication of thin film COF membranes using interfacial polymerization [175]. The membrane exhibited excellent solvent permeance towards organic protic and aprotic solvents along with high solute rejection. Lai and coworkers synthesized 2D COF membranes using Langmuir-Blodgett method for the first time [178]. They could be able to transfer the single layer COF with the thickness of a four-unit cell to different support layer by layer. The COF membrane supported on anodic aluminum oxide (AAO) exhibited solvent permeability 100 times higher than the amorphous membrane fabricated by a similar method.

1.7 Reference

- [1] D.S. Sholl, R.P. Lively, Comment, *Nature*. 532 (2016) 6–9.
- [2] R.P. Lively, D.S. Sholl, From water to organics in membrane separations: Membrane materials provide economical means to achieve various separation processes - And their capabilities for processing organic fluids look set to expand significantly., *Nat. Mater.* 16 (2017) 276–279. <https://doi.org/10.1038/nmat4860>.
- [3] P. Angelini, T. Armstrong, R. Counce, W. Griffith, T. Klasson, G. Muralidharan, G. Closset, G. Keller, J. Watson Disclaimer, *Materials for Separation Technologies: Energy and Emission Reduction Opportunities* and Vinod Sikka from ORNL, and the industrial experts working under subcontracts with ORNL, (2005).
- [4] C. Castel, E. Favre, Membrane separations and energy efficiency, *J. Memb. Sci.* 548 (2018) 345–357. <https://doi.org/10.1016/j.memsci.2017.11.035>.
- [5] B. Liang, H. Wang, X. Shi, B. Shen, X. He, Z.A. Ghazi, N.A. Khan, H. Sin, A.M. Khattak, L. Li, Z. Tang, Microporous membranes comprising conjugated polymers with rigid backbones enable ultrafast organic-solvent nanofiltration, *Nat. Chem.* 10 (2018) 961–967. <https://doi.org/10.1038/s41557-018-0093-9>.
- [6] W.J. Koros, R.P. Lively, Water and Beyond: Expanding the Spectrum of Large-Scale Energy Efficient Separation Processes, *AIChE J.* 58 (2012) 2624–2633. <https://doi.org/10.1002/aic>.
- [7] A.G.T. Fane, R. Wang, Y. Jia, *Membrane and Desalination Technologies*, 2011. <https://doi.org/10.1007/978-1-59745-278-6>.
- [8] H. Strathmann, *Membranes and Membrane Separation Processes*, *Ullmann's Encycl. Ind. Chem.* (2005). https://doi.org/10.1002/14356007.a16_187.pub2.
- [9] H.K. Lonsdale, The growth of membrane technology, *J. Memb. Sci.* 10 (1982) 81–181.

- [https://doi.org/10.1016/S0376-7388\(00\)81408-8](https://doi.org/10.1016/S0376-7388(00)81408-8).
- [10] M. Fang, C. Montoro, M. Semsarilar, Metal and covalent organic frameworks for membrane applications, *Membranes* (Basel). 10 (2020). <https://doi.org/10.3390/membranes10050107>.
- [11] P. Bernardo, E. Drioli, G. Golemme, Membrane gas separation: A review/state of the art, *Ind. Eng. Chem. Res.* 48 (2009) 4638–4663. <https://doi.org/10.1021/ie8019032>.
- [12] Z. Kang, H. Guo, L. Fan, G. Yang, Y. Feng, D. Sun, S. Mintova, Scalable crystalline porous membranes: Current state and perspectives, *Chem. Soc. Rev.* 50 (2021) 1913–1944. <https://doi.org/10.1039/d0cs00786b>.
- [13] C. Zhang, B.H. Wu, M.Q. Ma, Z. Wang, Z.K. Xu, Ultrathin metal/covalent-organic framework membranes towards ultimate separation, *Chem. Soc. Rev.* 48 (2019) 3811–3841. <https://doi.org/10.1039/c9cs00322c>.
- [14] N. Rangnekar, N. Mittal, B. Elyassi, J. Caro, M. Tsapatsis, Zeolite membranes - a review and comparison with MOFs, *Chem. Soc. Rev.* 44 (2015) 7128–7154. <https://doi.org/10.1039/c5cs00292c>.
- [15] T. Uemura, N. Yanai, S. Kitagawa, Polymerization reactions in porous coordination polymers, *Chem. Soc. Rev.* 38 (2009) 1228–1236. <https://doi.org/10.1039/b802583p>.
- [16] S. Qiu, M. Xue, G. Zhu, Metal-organic framework membranes: From synthesis to separation application, *Chem. Soc. Rev.* 43 (2014) 6116–6140. <https://doi.org/10.1039/c4cs00159a>.
- [17] K. Geng, T. He, R. Liu, S. Dalapati, K.T. Tan, Z. Li, S. Tao, Y. Gong, Q. Jiang, D. Jiang, Covalent Organic Frameworks: Design, Synthesis, and Functions, *Chem. Rev.* 120 (2020) 8814–8933. <https://doi.org/10.1021/acs.chemrev.9b00550>.
- [18] Z. Wang, S. Zhang, Y. Chen, Z. Zhang, S. Ma, Covalent organic frameworks for separation applications, *Chem. Soc. Rev.* 49 (2020) 708–735. <https://doi.org/10.1039/c9cs00827f>.
- [19] M.A. Little, A.I. Cooper, The Chemistry of Porous Organic Molecular Materials, *Adv. Funct. Mater.* 30 (2020). <https://doi.org/10.1002/adfm.201909842>.
- [20] D. Wu, F. Xu, B. Sun, R. Fu, H. He, K. Matyjaszewski, Design and preparation of porous polymers, *Chem. Rev.* 112 (2012) 3959–4015. <https://doi.org/10.1021/cr200440z>.
- [21] J.M. Zayed, N. Nouvel, U. Rauwald, O.A. Scherman, Chemical complexity—supramolecular self-assembly of synthetic and biological building blocks in water, *Chem. Soc. Rev.* 39 (2010) 2806–2816. <https://doi.org/10.1039/b922348g>.
- [22] S.J. Rowan, S.J. Cantrill, G.R.L. Cousins, J.K.M. Sanders, J.F. Stoddart, Dynamic covalent chemistry, 2002. [https://doi.org/10.1002/1521-3773\(20020315\)41:6<898::aid-anie898>3.0.co;2-e](https://doi.org/10.1002/1521-3773(20020315)41:6<898::aid-anie898>3.0.co;2-e).
- [23] M. Eddaoudi, D.B. Moler, H. Li, B. Chen, T.M. Reineke, M. O’Keeffe, O.M. Yaghi, Modular chemistry: Secondary building units as a basis for the design of highly porous and robust metal-organic carboxylate frameworks, *Acc. Chem. Res.* 34 (2001) 319–330. <https://doi.org/10.1021/ar000034b>.

- [24] L. Li, Z. Ren, X. Lü, H. Wang, Y. Chang, H. Li, B. Wu, J. Lang, Construction of [CuIn]-based coordination polymers via flexible benzimidazolyl-based ligands, *Sci. China Chem.* 53 (2010) 2083–2090. <https://doi.org/10.1007/s11426-010-4044-6>.
- [25] G. Férey, Hybrid porous solids: Past, present, future, *Chem. Soc. Rev.* 37 (2008) 191–214. <https://doi.org/10.1039/b618320b>.
- [26] J. Yu, R. Xu, Rational approaches toward the design and synthesis of zeolitic inorganic open-framework materials, *Acc. Chem. Res.* 43 (2010) 1195–1204. <https://doi.org/10.1021/ar900293m>.
- [27] B. Kesanli, Y. Cui, M.R. Smith, E.W. Bittner, B.C. Bockrath, W. Lin, Highly interpenetrated metal-organic frameworks for hydrogen storage, *Angew. Chemie - Int. Ed.* 44 (2004) 72–75. <https://doi.org/10.1002/anie.200461214>.
- [28] S. Kitagawa, R. Kitaura, S.I. Noro, Functional porous coordination polymers, *Angew. Chemie - Int. Ed.* 43 (2004) 2334–2375. <https://doi.org/10.1002/anie.200300610>.
- [29] M.E. Davis, Ordered porous materials for emerging applications review, *Nature.* 417 (2002) 813–821.
- [30] T. Sawaki, T. Dewa, Y. Aoyama, Immobilization of soluble metal complexes with a hydrogen-bonded organic network as a supporter. A simple route to microporous solid Lewis acid catalysts [12], *J. Am. Chem. Soc.* 120 (1998) 8539–8540. <https://doi.org/10.1021/ja9743351>.
- [31] R. Dawson, E. Stöckel, J.R. Holst, D.J. Adams, A.I. Cooper, Microporous organic polymers for carbon dioxide capture, *Energy Environ. Sci.* 4 (2011) 4239–4245. <https://doi.org/10.1039/c1ee01971f>.
- [32] A. Corma, From microporous to mesoporous molecular sieve materials and their use in catalysis, *Chem. Rev.* 97 (1997) 2373–2419. <https://doi.org/10.1021/cr960406n>.
- [33] Y. Ma, W. Tong, H. Zhou, S.L. Suib, A review of zeolite-like porous materials, *Microporous Mesoporous Mater.* 37 (2000) 243–252. [https://doi.org/10.1016/S1387-1811\(99\)00199-7](https://doi.org/10.1016/S1387-1811(99)00199-7).
- [34] K. Zabielska, T. Aleksandrzak, E. Gabruś, Adsorption equilibrium of carbon dioxide on zeolite 13X at high pressures, *Chem. Process Eng. - Inz. Chem. i Proces.* 39 (2018) 309–321. <https://doi.org/10.24425/122952>.
- [35] C.S. Cundy, P.A. Cox, The hydrothermal synthesis of zeolites: History and development from the earliest days to the present time, *Chem. Rev.* 103 (2003) 663–701. <https://doi.org/10.1021/cr020060i>.
- [36] O.M. Yaghi, G. Li, Li Hailian, Selective binding and removal of guests in a microporous metal-organic framework, *Nature.* 378 (1995) 703–706.
- [37] N.W. Ockwig, A.P. Co, M.O. Keeffe, A.J. Matzger, O.M. Yaghi, Porous , Crystalline , Covalent Organic Frameworks, 310 (2005) 1166–1171.
- [38] T.Q. Wang, Z.G. Yang, RECOMMENDATIONS FOR THE CHARACTERIZATION OF POROUS SOLIDS (Technical Report) Prepared, *Pure Appl. Chem.* 66 (1994) 1739–1758. [https://doi.org/10.1016/S0022-460X\(03\)00515-7](https://doi.org/10.1016/S0022-460X(03)00515-7).

- [39] F. Containing, L. Rectangular, Hydrothermal synthesis of a Metal-Organic Framework Containing Large Rectangular Channels, *J. Am. Chem. Soc.* 117 (1995) 10401–10402.
- [40] R.J. Kuppler, D.J. Timmons, Q.R. Fang, J.R. Li, T.A. Makal, M.D. Young, D. Yuan, D. Zhao, W. Zhuang, H.C. Zhou, Potential applications of metal-organic frameworks, *Coord. Chem. Rev.* 253 (2009) 3042–3066. <https://doi.org/10.1016/j.ccr.2009.05.019>.
- [41] A.U. Czaja, N. Trukhan, U. Müller, Industrial applications of metal–organic frameworks, *Chem. Soc. Rev.* 38 (2009) 1284–1293. <https://doi.org/10.1039/b804680h>.
- [42] K.L. Mulfort, O.K. Farha, C.D. Malliakas, M.G. Kanatzidis, J.T. Hupp, An interpenetrated framework material with hysteretic CO₂ uptake, *Chem. - A Eur. J.* 16 (2010) 276–281. <https://doi.org/10.1002/chem.200902104>.
- [43] X. Gu, Z.H. Lu, Q. Xu, High-connected mesoporous metal-organic framework, *Chem. Commun.* 46 (2010) 7400–7402. <https://doi.org/10.1039/c0cc02808h>.
- [44] S.T. Zheng, J.T. Bu, Y. Li, T. Wu, F. Zuo, P. Feng, X. Bu, Pore space partition and charge separation in cage-within-cage indium-organic frameworks with high CO₂ uptake, *J. Am. Chem. Soc.* 132 (2010) 17062–17064. <https://doi.org/10.1021/ja106903p>.
- [45] J. An, N.L. Rosi, Tuning MOF CO₂ adsorption properties via cation exchange, *J. Am. Chem. Soc.* 132 (2010) 5578–5579. <https://doi.org/10.1021/ja1012992>.
- [46] A.G. Wong-Foy, O. Lebel, A.J. Matzger, Porous crystal derived from a tricarboxylate linker with two distinct binding motifs, *J. Am. Chem. Soc.* 129 (2007) 15740–15741. <https://doi.org/10.1021/ja0753952>.
- [47] H. Chun, D.N. Dybtsev, H. Kim, K. Kim, Synthesis, X-ray crystal structures, and gas sorption properties of pillared square grid nets based on paddle-wheel motifs: Implications for hydrogen storage in porous materials, *Chem. - A Eur. J.* 11 (2005) 3521–3529. <https://doi.org/10.1002/chem.200401201>.
- [48] J.L.C. Rowsell, A.R. Millward, K.S. Park, O.M. Yaghi, Hydrogen Sorption in Functionalized Metal-Organic Frameworks, *J. Am. Chem. Soc.* 126 (2004) 5666–5667. <https://doi.org/10.1021/ja049408c>.
- [49] L. Ma, C. Abney, W. Lin, Enantioselective catalysis with homochiral metal-organic frameworks, *Chem. Soc. Rev.* 38 (2009) 1248–1256. <https://doi.org/10.1039/b807083k>.
- [50] C. Janiak, Functional Organic Analogues of Zeolites Based on Metal-Organic Coordination Frameworks, *Angew. Chemie (International Ed. English)*. 36 (1997) 1431–1434. <https://doi.org/10.1002/anie.199714311>.
- [51] Z.G. Gu, Y.P. Cai, H.C. Fang, Z.Y. Zhou, P.K. Thallapally, J. Tian, J. Liu, G.J. Exarhos, Conversion of nonporous helical cadmium organic framework to a porous form, *Chem. Commun.* 46 (2010) 5373–5375. <https://doi.org/10.1039/c0cc01042a>.
- [52] B. Chen, M. Eddaoudi, S.T. Hyde, M. O’Keeffe, O.M. Yaghi, Interwoven metal-organic framework on a periodic minimal surface with extra-large pores, *Science (80-.)*. 291 (2001) 1021–1023. <https://doi.org/10.1126/science.1056598>.
- [53] P. Pachfule, Y. Chen, J. Jiang, R. Banerjee, Experimental and computational approach of understanding the gas adsorption in amino functionalized interpenetrated metal organic

- frameworks (MOFs), *J. Mater. Chem.* 21 (2011) 17737–17745. <https://doi.org/10.1039/c1jm13762j>.
- [54] J.W. Yoon, S.H. Jung, Y.K. Hwang, S.M. Humphrey, P.T. Wood, J.S. Chang, Gas-sorption selectivity of CUK-1: A porous coordination solid made of cobalt(II) and pyridine-2,4-dicarboxylic acid, *Adv. Mater.* 19 (2007) 1830–1834. <https://doi.org/10.1002/adma.200601983>.
- [55] A. Morozan, F. Jaouen, Metal organic frameworks for electrochemical applications, *Energy Environ. Sci.* 5 (2012) 9269–9290. <https://doi.org/10.1039/c2ee22989g>.
- [56] U. Mueller, M. Schubert, F. Teich, H. Puetter, K. Schierle-Arndt, J. Pastré, Metal-organic frameworks - Prospective industrial applications, *J. Mater. Chem.* 16 (2006) 626–636. <https://doi.org/10.1039/b511962f>.
- [57] H. Hayashi, A.P. Côté, H. Furukawa, M. O’Keeffe, O.M. Yaghi, Zeolite A imidazolate frameworks, *Nat. Mater.* 6 (2007) 501–506. <https://doi.org/10.1038/nmat1927>.
- [58] B. Chen, N.W. Ockwig, A.R. Millward, D.S. Contreras, O.M. Yaghi, High H₂ adsorption in a microporous metal-organic framework with open metal sites, *Angew. Chemie - Int. Ed.* 44 (2005) 4745–4749. <https://doi.org/10.1002/anie.200462787>.
- [59] R. Banerjee, H. Furukawa, D. Britt, C. Knobler, M. O’Keeffe, O.M. Yaghi, Control of pore size and functionality in isorecticular zeolitic imidazolate frameworks and their carbon dioxide selective capture properties, *J. Am. Chem. Soc.* 131 (2009) 3875–3877. <https://doi.org/10.1021/ja809459e>.
- [60] O.M.Y. Rahul Banerjee, Anh Phan, Bo Wang, Carolyn Knobler, Hiroyasu Furukawa, Michael O Keeffe, High-Throughput Synthesis of Zeolitic Imidazolate Frameworks and Application to CO₂ Capture, *Science* (80-.). 319 (2008) 939–944. <https://doi.org/10.1126/science.1152516>.
- [61] K.S. Park, Z. Ni, A.P. Côté, J.Y. Choi, R. Huang, F.J. Uribe-Romo, H.K. Chae, M. O’Keeffe, O.M. Yaghi, Exceptional chemical and thermal stability of zeolitic imidazolate frameworks, *Proc. Natl. Acad. Sci. U. S. A.* 103 (2006) 10186–10191. <https://doi.org/10.1073/pnas.0602439103>.
- [62] C. Ying-Bo, Z. Lin-Fei, W. Biao, H. Xiao-Yu, L. Dong-Qing, Z. Feng-Xiao, Z. Yu-Feng, Structural evolution of zeolitic imidazolate framework-8(ZIF-8), *J. Tianjin Polytech. Univ.* 35 (2016) 1–4. <https://doi.org/10.3969/j.issn.1671-024x.2016.05.001>.
- [63] B. Chen, Z. Yang, Y. Zhu, Y. Xia, Zeolitic imidazolate framework materials: Recent progress in synthesis and applications, *J. Mater. Chem. A.* 2 (2014) 16811–16831. <https://doi.org/10.1039/c4ta02984d>.
- [64] M.O.F. Topologies, N. Stock, S. Biswas, Synthesis of Metal-Organic Frameworks (MOFs): Routes to Various, (2012) 933–969.
- [65] J. Kim, S.T. Yang, S.B. Choi, J. Sim, J. Kim, W.S. Ahn, Control of catenation in CuTATB-n metal-organic frameworks by sonochemical synthesis and its effect on CO₂ adsorption, *J. Mater. Chem.* 21 (2011) 3070–3076. <https://doi.org/10.1039/c0jm03318a>.
- [66] T. Friščić, I. Halasz, P.J. Beldon, A.M. Belenguer, F. Adams, S.A.J. Kimber, V. Honkimäki, R.E. Dinnebier, Real-time and in situ monitoring of mechanochemical milling

- reactions, *Nat. Chem.* 5 (2013) 66–73. <https://doi.org/10.1038/nchem.1505>.
- [67] A. Martinez Joaristi, J. Juan-Alcañiz, P. Serra-Crespo, F. Kapteijn, J. Gascon, Electrochemical synthesis of some archetypical Zn²⁺, Cu²⁺, and Al³⁺ metal organic frameworks, *Cryst. Growth Des.* 12 (2012) 3489–3498. <https://doi.org/10.1021/cg300552w>.
- [68] A. Lagashetty, V. Havanoor, S. Basavaraja, S.D. Balaji, A. Venkataraman, Microwave-assisted route for synthesis of nanosized metal oxides, *Sci. Technol. Adv. Mater.* 8 (2007) 484–493. <https://doi.org/10.1016/j.stam.2007.07.001>.
- [69] P.M. Forster, P.M. Thomas, A.K. Cheetham, Biphasic solvothermal synthesis: A new approach for hybrid inorganic-organic materials, *Chem. Mater.* 14 (2002) 17–20. <https://doi.org/10.1021/cm010820q>.
- [70] M. Shah, M.C. McCarthy, S. Sachdeva, A.K. Lee, H.K. Jeong, Current status of metal-organic framework membranes for gas separations: Promises and challenges, *Ind. Eng. Chem. Res.* 51 (2012) 2179–2199. <https://doi.org/10.1021/ie202038m>.
- [71] O. Shekhah, V. Chernikova, Y. Belmabkhout, M. Eddaoudi, Metal–Organic framework membranes: From fabrication to gas separation, *Crystals.* 8 (2018). <https://doi.org/10.3390/cryst8110412>.
- [72] P. Gorgojo, S. Uriel, C. Téllez, J. Coronas, Development of mixed matrix membranes based on zeolite Nu-6(2) for gas separation, *Microporous Mesoporous Mater.* 115 (2008) 85–92. <https://doi.org/10.1016/j.micromeso.2007.11.046>.
- [73] D. Bradshaw, A. Garai, J. Huo, Metal–organic framework growth at functional interfaces: Thin films and composites for diverse applications, *Chem. Soc. Rev.* 41 (2012) 2344–2381. <https://doi.org/10.1039/c1cs15276a>.
- [74] X. Zhao, Y. Wang, D.S. Li, X. Bu, P. Feng, Metal–Organic Frameworks for Separation, *Adv. Mater.* 30 (2018) 1–34. <https://doi.org/10.1002/adma.201705189>.
- [75] Y. Liu, Z. Ng, E.A. Khan, H.K. Jeong, C. bun Ching, Z. Lai, Synthesis of continuous MOF-5 membranes on porous α -alumina substrates, *Microporous Mesoporous Mater.* 118 (2009) 296–301. <https://doi.org/10.1016/j.micromeso.2008.08.054>.
- [76] Y. Liu, E. Hu, E.A. Khan, Z. Lai, Synthesis and characterization of ZIF-69 membranes and separation for CO₂/CO mixture, *J. Memb. Sci.* 353 (2010) 36–40. <https://doi.org/10.1016/j.memsci.2010.02.023>.
- [77] and J.C. H. Bux, F. Liang, Y. Li, J. Cravillon, M. Wiebcke, Zeolitic Imidazolate Framework Membrane with Molecular Sieving Properties by Microwave-Assisted Solvothermal Synthesis, *JACS.* 131 (2009) 16000–16001. <https://doi.org/10.1021/cm902032y>.
- [78] A. Huang, H. Bux, F. Steinbach, J. Caro, Molecular-sieve membrane with hydrogen permselectivity: ZIF-22 in LTA topology prepared with 3-aminopropyltriethoxysilane as covalent linker, *Angew. Chemie - Int. Ed.* 49 (2010) 4958–4961. <https://doi.org/10.1002/anie.201001919>.
- [79] A. Huang, W. Dou, J. Caro, Steam-stable zeolitic imidazolate framework ZIF-90 membrane with hydrogen selectivity through covalent functionalization, *J. Am. Chem.*

- Soc. 132 (2010) 15562–15564. <https://doi.org/10.1021/ja108774v>.
- [80] M.C. McCarthy, V. Varela-Guerrero, G. V. Barnett, H.K. Jeong, Synthesis of zeolitic imidazolate framework films and membranes with controlled microstructures, *Langmuir*. 26 (2010) 14636–14641. <https://doi.org/10.1021/la102409e>.
- [81] Q. Liu, N. Wang, J. Caro, A. Huang, Bio-inspired polydopamine: A versatile and powerful platform for covalent synthesis of molecular sieve membranes, *J. Am. Chem. Soc.* 135 (2013) 17679–17682. <https://doi.org/10.1021/ja4080562>.
- [82] A. Huang, Q. Liu, N. Wang, J. Caro, Highly hydrogen permselective ZIF-8 membranes supported on polydopamine functionalized macroporous stainless-steel-nets, *J. Mater. Chem. A*. 2 (2014) 8246–8251. <https://doi.org/10.1039/c4ta00299g>.
- [83] H. Guo, G. Zhu, I.J. Hewitt, S. Qiu, Twin copper source" growth of metal-organic framework membrane: Cu₃(BTC)₂ with high permeability and selectivity for recycling H₂, *J. Am. Chem. Soc.* 131 (2009) 1646–1647. <https://doi.org/10.1021/ja8074874>.
- [84] Z. Lai, M. Tsapatsis, J.P. Nicolich, Siliceous ZSM-5 membranes by secondary growth of b-oriented seed layers, *Adv. Funct. Mater.* 14 (2004) 716–729. <https://doi.org/10.1002/adfm.200400040>.
- [85] I. Lee, J.L. Buday, H.K. Jeong, μ -Tiles and mortar approach: A simple technique for the facile fabrication of continuous b-oriented MFI silicalite-1 thin films, *Microporous Mesoporous Mater.* 122 (2009) 288–293. <https://doi.org/10.1016/j.micromeso.2009.03.017>.
- [86] M.A. Snyder, M. Tsapatsis, Hierarchical nanomanufacturing: From shaped zeolite nanoparticles to high-performance separation membranes, *Angew. Chemie - Int. Ed.* 46 (2007) 7560–7573. <https://doi.org/10.1002/anie.200604910>.
- [87] R. Ranjan, M. Tsapatsis, Microporous metal organic framework membrane on porous support using the seeded growth method, *Chem. Mater.* 21 (2009) 4920–4924. <https://doi.org/10.1021/cm902032y>.
- [88] S.R. Venna, M.A. Carreon, Highly permeable zeolite imidazolate framework-8 membranes for CO₂/CH₄ separation, *J. Am. Chem. Soc.* 132 (2010) 76–78. <https://doi.org/10.1021/ja909263x>.
- [89] V.V. Guerrero, Y. Yoo, M.C. McCarthy, H.K. Jeong, HKUST-1 membranes on porous supports using secondary growth, *J. Mater. Chem.* 20 (2010) 3938–3943. <https://doi.org/10.1039/b924536g>.
- [90] J. Nan, X. Dong, W. Wang, W. Jin, N. Xu, Step-by-step seeding procedure for preparing HKUST-1 membrane on porous α -alumina support, *Langmuir*. 27 (2011) 4309–4312. <https://doi.org/10.1021/la200103w>.
- [91] Y. Hu, X. Dong, J. Nan, W. Jin, X. Ren, N. Xu, Y.M. Lee, Metal-organic framework membranes fabricated via reactive seeding, *Chem. Commun.* 47 (2011) 737–739. <https://doi.org/10.1039/c0cc03927f>.
- [92] J. Yao, D. Dong, D. Li, L. He, G. Xu, H. Wang, Contra-diffusion synthesis of ZIF-8 films on a polymer substrate, *Chem. Commun.* 47 (2011) 2559–2561. <https://doi.org/10.1039/c0cc04734a>.

- [93] M. He, J. Yao, L. Li, Z. Zhong, F. Chen, H. Wang, Aqueous solution synthesis of ZIF-8 films on a porous nylon substrate by contra-diffusion method, *Microporous Mesoporous Mater.* 179 (2013) 10–16. <https://doi.org/10.1016/j.micromeso.2013.05.015>.
- [94] H.T. Kwon, H.K. Jeong, In situ synthesis of thin zeolitic-imidazolate framework ZIF-8 membranes exhibiting exceptionally high propylene/propane separation, *J. Am. Chem. Soc.* 135 (2013) 10763–10768. <https://doi.org/10.1021/ja403849c>.
- [95] E. Barankova, X. Tan, L.F. Villalobos, E. Litwiller, K.V. Peinemann, A Metal Chelating Porous Polymeric Support: The Missing Link for a Defect-Free Metal–Organic Framework Composite Membrane, *Angew. Chemie - Int. Ed.* 56 (2017) 2965–2968. <https://doi.org/10.1002/anie.201611927>.
- [96] A.J. Brown, N.A. Brunelli, K. Eum, F. Rashidi, J.R. Johnson, W.J. Koros, C.W. Jones, S. Nair, Interfacial microfluidic processing of metal-organic framework hollow fiber membranes, *Science* (80-.). 345 (2014) 72–75. <https://doi.org/10.1126/science.1251181>.
- [97] B.P. Biswal, A. Bhaskar, R. Banerjee, U.K. Kharul, Selective interfacial synthesis of metal-organic frameworks on a polybenzimidazole hollow fiber membrane for gas separation, *Nanoscale.* 7 (2015) 7291–7298. <https://doi.org/10.1039/c5nr00299k>.
- [98] X. Ma, P. Kumar, N. Mittal, A. Khlyustova, P. Daoutidis, K. Andre Mkhoyan, M. Tsapatsis, Zeolitic imidazolate framework membranes made by ligand-induced permselectivation, *Science* (80-.). 361 (2018) 1008–1011. <https://doi.org/10.1126/science.aat4123>.
- [99] M.Y. Jeon, D. Kim, P. Kumar, P.S. Lee, N. Rangnekar, P. Bai, M. Shete, B. Elyassi, H.S. Lee, K. Narasimharao, S.N. Basahel, S. Al-Thabaiti, W. Xu, H.J. Cho, E.O. Fetisov, R. Thyagarajan, R.F. DeJaco, W. Fan, K.A. Mkhoyan, J.I. Siepmann, M. Tsapatsis, Ultra-selective high-flux membranes from directly synthesized zeolite nanosheets, *Nature.* 543 (2017) 690–694. <https://doi.org/10.1038/nature21421>.
- [100] H.T. Kwon, H.K. Jeong, A.S. Lee, H.S. An, T. Lee, E. Jang, J.S. Lee, J. Choi, Defect-induced ripening of zeolitic-imidazolate framework ZIF-8 and its implication to vapor-phase membrane synthesis, *Chem. Commun.* 52 (2016) 11669–11672. <https://doi.org/10.1039/c6cc05433a>.
- [101] W. Li, P. Su, Z. Li, Z. Xu, F. Wang, H. Ou, J. Zhang, G. Zhang, E. Zeng, Ultrathin metal-organic framework membrane production by gel-vapour deposition, *Nat. Commun.* 8 (2017) 1–8. <https://doi.org/10.1038/s41467-017-00544-1>.
- [102] C. Zhang, W.J. Koros, Zeolitic Imidazolate Framework-Enabled Membranes: Challenges and Opportunities, *J. Phys. Chem. Lett.* 6 (2015) 3841–3849. <https://doi.org/10.1021/acs.jpcclett.5b01602>.
- [103] A. Knebel, B. Geppert, K. Volgmann, D.I. Kolokolov, A.G. Stepanov, J. Twiefel, P. Heitjans, D. Volkmer, J. Caro, Defibrillation of soft porous metal-organic frameworks with electric fields, *Science* (80-.). 358 (2017) 347–351. <https://doi.org/10.1126/science.aal2456>.
- [104] S. Zhou, Y. Wei, L. Li, Y. Duan, Q. Hou, L. Zhang, L.X. Ding, J. Xue, H. Wang, J. Caro, Paralyzed membrane: Current-driven synthesis of a metal-organic framework with sharpened propene/propane separation, *Sci. Adv.* 4 (2018) 1–9.

- <https://doi.org/10.1126/sciadv.aau1393>.
- [105] A. Centrone, Y. Yang, S. Speakman, L. Bromberg, G.C. Rutledge, T.A. Hatton, Growth of metal-organic frameworks on polymer surfaces, *J. Am. Chem. Soc.* 132 (2010) 15687–15691. <https://doi.org/10.1021/ja106381x>.
- [106] J. Yao, D. Dong, D. Li, L. He, G. Xu, H. Wang, Contra-diffusion synthesis of ZIF-8 films on a polymer substrate, *Chem. Commun.* 47 (2011) 2559–2561. <https://doi.org/10.1039/c0cc04734a>.
- [107] M.J.C. Ordoñez, K.J. Balkus, J.P. Ferraris, I.H. Musselman, Molecular sieving realized with ZIF-8/Matrimid® mixed-matrix membranes, *J. Memb. Sci.* 361 (2010) 28–37. <https://doi.org/10.1016/j.memsci.2010.06.017>.
- [108] C. Zhang, Y. Dai, J.R. Johnson, O. Karvan, W.J. Koros, High performance ZIF-8/6FDA-DAM mixed matrix membrane for propylene/propane separations, *J. Memb. Sci.* 389 (2012) 34–42. <https://doi.org/10.1016/j.memsci.2011.10.003>.
- [109] E. V. Perez, K.J. Balkus, J.P. Ferraris, I.H. Musselman, Mixed-matrix membranes containing MOF-5 for gas separations, *J. Memb. Sci.* 328 (2009) 165–173. <https://doi.org/10.1016/j.memsci.2008.12.006>.
- [110] T.-H. Bae, J.S. Lee, W. Qiu, W.J. Koros, C.W. Jones, S. Nair, A High-Performance Gas-Separation Membrane Containing Submicrometer-Sized Metal-Organic Framework Crystals, *Angew. Chemie.* 122 (2010) 10059–10062. <https://doi.org/10.1002/ange.201006141>.
- [111] S. Basu, A. Cano-Odena, I.F.J. Vankelecom, MOF-containing mixed-matrix membranes for CO₂/CH₄ and CO₂/N₂ binary gas mixture separations, *Sep. Purif. Technol.* 81 (2011) 31–40. <https://doi.org/10.1016/j.seppur.2011.06.037>.
- [112] J. Hu, H. Cai, H. Ren, Y. Wei, Z. Xu, H. Liu, Y. Hu, Mixed-matrix membrane hollow fibers of Cu₃(BTC)₂ MOF and polyimide for gas separation and adsorption, *Ind. Eng. Chem. Res.* 49 (2010) 12605–12612. <https://doi.org/10.1021/ie1014958>.
- [113] S. Basu, M. Maes, A. Cano-Odena, L. Alaerts, D.E. De Vos, I.F.J. Vankelecom, Solvent resistant nanofiltration (SRNF) membranes based on metal-organic frameworks, *J. Memb. Sci.* 344 (2009) 190–198. <https://doi.org/10.1016/j.memsci.2009.07.051>.
- [114] A. Bhaskar, R. Banerjee, U. Kharul, ZIF-8@PBI-BuI composite membranes: Elegant effects of PBI structural variations on gas permeation performance, *J. Mater. Chem. A.* 2 (2014) 12962–12967. <https://doi.org/10.1039/c4ta00611a>.
- [115] M. Hong, S. Li, J.L. Falconer, R.D. Noble, Hydrogen purification using a SAPO-34 membrane, *J. Memb. Sci.* 307 (2008) 277–283. <https://doi.org/10.1016/j.memsci.2007.09.031>.
- [116] T.M. Nenoff, MOF membranes put to the test, *Nat. Chem.* 7 (2015) 377–378. <https://doi.org/10.1038/nchem.2218>.
- [117] S. Takamizawa, Y. Takasaki, R. Miyake, Single-crystal membrane for anisotropic and efficient gas permeation, *J. Am. Chem. Soc.* 132 (2010) 2862–2863. <https://doi.org/10.1021/ja910492d>.

- [118] H. Bux, A. Feldhoff, J. Cravillon, M. Wiebcke, Y.S. Li, J. Caro, Oriented zeolitic imidazolate framework-8 membrane with sharp H₂/C₃H₈ molecular sieve separation, *Chem. Mater.* 23 (2011) 2262–2269. <https://doi.org/10.1021/cm200555s>.
- [119] K. Huang, S. Liu, Q. Li, W. Jin, Preparation of novel metal-carboxylate system MOF membrane for gas separation, *Sep. Purif. Technol.* 119 (2013) 94–101. <https://doi.org/10.1016/j.seppur.2013.09.008>.
- [120] A. Huang, J. Caro, Covalent post-functionalization of Zeolitic imidazolate framework ZIF-90 membrane for enhanced hydrogen selectivity, *Angew. Chemie - Int. Ed.* 50 (2011) 4979–4982. <https://doi.org/10.1002/anie.201007861>.
- [121] A. Huang, Y. Chen, N. Wang, Z. Hu, J. Jiang, J. Caro, A highly permeable and selective zeolitic imidazolate framework ZIF-95 membrane for H₂/CO₂ separation, *Chem. Commun.* 48 (2012) 10981–10983. <https://doi.org/10.1039/c2cc35691k>.
- [122] X. Dong, K. Huang, S. Liu, R. Ren, W. Jin, Y.S. Lin, Synthesis of zeolitic imidazolate framework-78 molecular-sieve membrane: Defect formation and elimination, *J. Mater. Chem.* 22 (2012) 19222–19227. <https://doi.org/10.1039/c2jm34102f>.
- [123] S. Zhou, X. Zou, F. Sun, H. Ren, J. Liu, F. Zhang, N. Zhao, G. Zhu, Development of hydrogen-selective CAU-1 MOF membranes for hydrogen purification by “dual-metal-source” approach, *Int. J. Hydrogen Energy.* 38 (2013) 5338–5347. <https://doi.org/10.1016/j.ijhydene.2013.02.074>.
- [124] A. Huang, Y. Chen, Q. Liu, N. Wang, J. Jiang, J. Caro, Synthesis of highly hydrophobic and permselective metal-organic framework Zn(BDC)(TED)_{0.5} membranes for H₂/CO₂ separation, *J. Memb. Sci.* 454 (2014) 126–132. <https://doi.org/10.1016/j.memsci.2013.12.018>.
- [125] F. Zhang, X. Zou, X. Gao, S. Fan, F. Sun, H. Ren, G. Zhu, Hydrogen selective NH₂-MIL-53(Al) MOF membranes with high permeability, *Adv. Funct. Mater.* 22 (2012) 3583–3590. <https://doi.org/10.1002/adfm.201200084>.
- [126] Y. Yoo, Z. Lai, H.K. Jeong, Fabrication of MOF-5 membranes using microwave-induced rapid seeding and solvothermal secondary growth, *Microporous Mesoporous Mater.* 123 (2009) 100–106. <https://doi.org/10.1016/j.micromeso.2009.03.036>.
- [127] D. Nagaraju, D.G. Bhagat, R. Banerjee, U.K. Kharul, In situ growth of metal-organic frameworks on a porous ultrafiltration membrane for gas separation, *J. Mater. Chem. A.* 1 (2013) 8828–8835. <https://doi.org/10.1039/c3ta10438a>.
- [128] M.N. Shah, M.A. Gonzalez, M.C. McCarthy, H.K. Jeong, An unconventional rapid synthesis of high performance metal-organic framework membranes, *Langmuir.* 29 (2013) 7896–7902. <https://doi.org/10.1021/la4014637>.
- [129] T. Ben, C. Lu, C. Pei, S. Xu, S. Qiu, Polymer-supported and free-standing metal-organic framework membrane, *Chem. - A Eur. J.* 18 (2012) 10250–10253. <https://doi.org/10.1002/chem.201201574>.
- [130] S. Zhou, X. Zou, F. Sun, F. Zhang, S. Fan, H. Zhao, T. Schiestel, G. Zhu, Challenging fabrication of hollow ceramic fiber supported Cu₃(BTC)₂ membrane for hydrogen separation, *J. Mater. Chem.* 22 (2012) 10322–10328. <https://doi.org/10.1039/c2jm16371c>.

- [131] D.M. D'Alessandro, B. Smit, J.R. Long, Carbon dioxide capture: Prospects for new materials, *Angew. Chemie - Int. Ed.* 49 (2010) 6058–6082. <https://doi.org/10.1002/anie.201000431>.
- [132] W.J. Koros, R. Mahajan, Pushing the limits on possibilities for large scale gas separation: Which strategies?, *J. Memb. Sci.* 181 (2001) 141. [https://doi.org/10.1016/S0376-7388\(00\)00676-1](https://doi.org/10.1016/S0376-7388(00)00676-1).
- [133] C.J.D. ANH PHAN, A.O.M.Y. FERNANDO J. URIBE-ROMO, CAROLYN B. KNOBLER, MICHAEL O'KEEFFE, Synthesis, Structure, and Carbon Dioxide Capture Properties of Zeolitic Imidazolate Frameworks, *Acc. Chem. Res.* 43 (2010) 58–67. <http://www.ncbi.nlm.nih.gov/pubmed/19877580>.
- [134] X. Gong, Y. Wang, T. Kuang, ZIF-8-Based Membranes for Carbon Dioxide Capture and Separation, *ACS Sustain. Chem. Eng.* 5 (2017) 11204–11214. <https://doi.org/10.1021/acssuschemeng.7b03613>.
- [135] R.W. Baker, Future directions of membrane gas separation technology, *Ind. Eng. Chem. Res.* 41 (2002) 1393–1411. <https://doi.org/10.1021/ie0108088>.
- [136] D.F. Sanders, Z.P. Smith, R. Guo, L.M. Robeson, J.E. McGrath, D.R. Paul, B.D. Freeman, Energy-efficient polymeric gas separation membranes for a sustainable future: A review, *Polymer (Guildf)*. 54 (2013) 4729–4761. <https://doi.org/10.1016/j.polymer.2013.05.075>.
- [137] A.C.C. Campos, R.A. Dos Reis, A. Ortiz, D. Gorri, I. Ortiz, A Perspective of Solutions for Membrane Instabilities in Olefin/Paraffin Separations: A Review, *Ind. Eng. Chem. Res.* 57 (2018) 10071–10085. <https://doi.org/10.1021/acs.iecr.8b02013>.
- [138] W.J. Koros, C. Zhang, Materials for next-generation molecularly selective synthetic membranes, *Nat. Mater.* 16 (2017) 289–297. <https://doi.org/10.1038/nmat4805>.
- [139] G. Liu, V. Chernikova, Y. Liu, K. Zhang, Y. Belmabkhout, O. Shekhah, C. Zhang, S. Yi, M. Eddaoudi, W.J. Koros, Mixed matrix formulations with MOF molecular sieving for key energy-intensive separations, *Nat. Mater.* 17 (2018) 283–289. <https://doi.org/10.1038/s41563-017-0013-1>.
- [140] K. Li, D.H. Olson, J. Seidel, T.J. Emge, H. Gong, H. Zeng, J. Li, Zeolitic imidazolate frameworks for kinetic separation of propane and propene, *J. Am. Chem. Soc.* 131 (2009) 10368–10369. <https://doi.org/10.1021/ja9039983>.
- [141] C. Zhang, R.P. Lively, K. Zhang, J.R. Johnson, O. Karvan, W.J. Koros, Unexpected molecular sieving properties of zeolitic imidazolate framework-8, *J. Phys. Chem. Lett.* 3 (2012) 2130–2134. <https://doi.org/10.1021/jz300855a>.
- [142] Y. Pan, T. Li, G. Lestari, Z. Lai, Effective separation of propylene/propane binary mixtures by ZIF-8 membranes, *J. Memb. Sci.* 390–391 (2012) 93–98. <https://doi.org/10.1016/j.memsci.2011.11.024>.
- [143] Y. Pan, W. Liu, Y. Zhao, C. Wang, Z. Lai, Improved ZIF-8 membrane: Effect of activation procedure and determination of diffusivities of light hydrocarbons, *J. Memb. Sci.* 493 (2015) 88–96. <https://doi.org/10.1016/j.memsci.2015.06.019>.
- [144] H.T. Kwon, H.K. Jeong, Highly propylene-selective supported zeolite-imidazolate framework (ZIF-8) membranes synthesized by rapid microwave-assisted seeding and

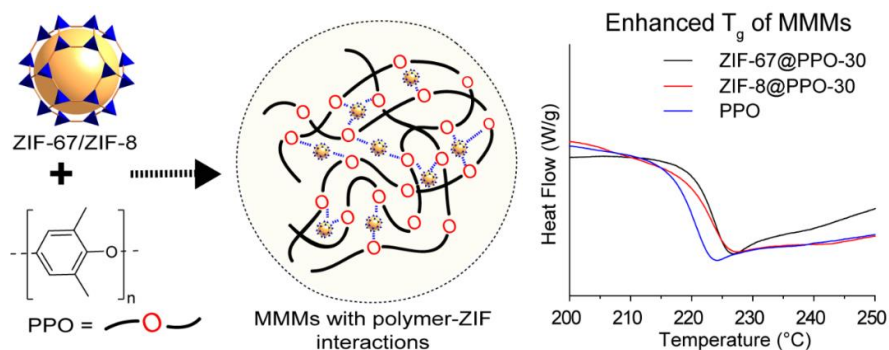
- secondary growth, *Chem. Commun.* 49 (2013) 3854–3856. <https://doi.org/10.1039/c3cc41039k>.
- [145] J. Sun, C. Yu, H.K. Jeong, Propylene-selective thin zeolitic imidazolate framework membranes on ceramic tubes by microwave seeding and solvothermal secondary growth, *Crystals*. 8 (2018). <https://doi.org/10.3390/cryst8100373>.
- [146] H.T. Kwon, H.K. Jeong, Improving propylene/propane separation performance of Zeolitic-imidazolate framework ZIF-8 membranes, *Chem. Eng. Sci.* 124 (2015) 20–26. <https://doi.org/10.1016/j.ces.2014.06.021>.
- [147] N. Hara, M. Yoshimune, H. Negishi, K. Haraya, S. Hara, T. Yamaguchi, ZIF-8 membranes prepared at miscible and immiscible liquid-liquid interfaces, *Microporous Mesoporous Mater.* 206 (2015) 75–80. <https://doi.org/10.1016/j.micromeso.2014.12.018>.
- [148] N. Hara, M. Yoshimune, H. Negishi, K. Haraya, S. Hara, T. Yamaguchi, Effect of temperature on synthesis of ZIF-8 membranes for propylene/propane separation by counter diffusion method, *J. Japan Pet. Inst.* 58 (2015) 237–244. <https://doi.org/10.1627/jpi.58.237>.
- [149] K. Eum, C. Ma, A. Rownaghi, C.W. Jones, S. Nair, ZIF-8 Membranes via Interfacial Microfluidic Processing in Polymeric Hollow Fibers: Efficient Propylene Separation at Elevated Pressures, *ACS Appl. Mater. Interfaces*. 8 (2016) 25337–25342. <https://doi.org/10.1021/acsami.6b08801>.
- [150] K. Eum, A. Rownaghi, D. Choi, R.R. Bhave, C.W. Jones, S. Nair, Fluidic Processing of High-Performance ZIF-8 Membranes on Polymeric Hollow Fibers: Mechanistic Insights and Microstructure Control, *Adv. Funct. Mater.* 26 (2016) 5011–5018. <https://doi.org/10.1002/adfm.201601550>.
- [151] X. Feng, X. Ding, D. Jiang, Covalent organic frameworks, *Chem. Soc. Rev.* 41 (2012) 6010–6022. <https://doi.org/10.1039/c2cs35157a>.
- [152] P. Kuhn, M. Antonietti, A. Thomas, Porous, covalent triazine-based frameworks prepared by ionothermal synthesis, *Angew. Chemie - Int. Ed.* 47 (2008) 3450–3453. <https://doi.org/10.1002/anie.200705710>.
- [153] E.L. Spitler, W.R. Dichtel, Lewis acid-catalysed formation of two-dimensional phthalocyanine covalent organic frameworks, *Nat. Chem.* 2 (2010) 672–677. <https://doi.org/10.1038/nchem.695>.
- [154] P.J. Waller, F. Gándara, O.M. Yaghi, Chemistry of Covalent Organic Frameworks, *Acc. Chem. Res.* 48 (2015) 3053–3063. <https://doi.org/10.1021/acs.accounts.5b00369>.
- [155] A.P. Côté, H.M. El-Kaderi, H. Furukawa, J.R. Hunt, O.M. Yaghi, Reticular synthesis of microporous and mesoporous 2D covalent organic frameworks, *J. Am. Chem. Soc.* 129 (2007) 12914–12915. <https://doi.org/10.1021/ja0751781>.
- [156] A. Nagai, Z. Guo, X. Feng, S. Jin, X. Chen, X. Ding, D. Jiang, Pore surface engineering in covalent organic frameworks, *Nat. Commun.* 2 (2011). <https://doi.org/10.1038/ncomms1542>.
- [157] M.J. Bojdys, J. Jeromenok, A. Thomas, M. Antonietti, Rational extension of the family of layered, covalent, triazine-based frameworks with regular porosity, *Adv. Mater.* 22 (2010)

- 2202–2205. <https://doi.org/10.1002/adma.200903436>.
- [158] R. Palkovits, M. Antonietti, P. Kuhn, A. Thomas, F. Schüth, Solid catalysts for the selective low-temperature oxidation of methane to methanol, *Angew. Chemie - Int. Ed.* 48 (2009) 6909–6912. <https://doi.org/10.1002/anie.200902009>.
- [159] F.J. Uribe-Romo, C.J. Doonan, H. Furukawa, K. Oisaki, O.M. Yaghi, Crystalline covalent organic frameworks with hydrazone linkages, *J. Am. Chem. Soc.* 133 (2011) 11478–11481. <https://doi.org/10.1021/ja204728y>.
- [160] S.Y. Ding, J. Gao, Q. Wang, Y. Zhang, W.G. Song, C.Y. Su, W. Wang, Construction of covalent organic framework for catalysis: Pd/COF-LZU1 in Suzuki-Miyaura coupling reaction, *J. Am. Chem. Soc.* 133 (2011) 19816–19822. <https://doi.org/10.1021/ja206846p>.
- [161] and A.I.C. Neil L. Campbell, Rob Clowes, Lyndsey K. Ritchie, Rapid Microwave Synthesis and Purification of Porous Covalent Organic Frameworks, *Chem. Mater.* (2009) 4342–4344. <https://doi.org/10.1039/b805656k>.
- [162] N.A.A. Zwaneveld, R. Pawlak, M. Abel, D. Catalin, D. Gigmes, D. Bertin, L. Porte, Organized formation of 2D extended covalent organic frameworks at surfaces, *J. Am. Chem. Soc.* 130 (2008) 6678–6679. <https://doi.org/10.1021/ja800906f>.
- [163] J.W. Colson, A.R. Woll, A. Mukherjee, M.P. Levendorf, E.L. Spitler, V.B. Shields, M.G. Spencer, J. Park, W.R. Dichtel, Oriented 2D Covalent Organic Framework Thin Films on Single-Layer Graphene, 332 (2011) 228–232.
- [164] X.H. Liu, C.Z. Guan, S.Y. Ding, W. Wang, H.J. Yan, D. Wang, L.J. Wan, On-surface synthesis of single-layered two-dimensional covalent organic frameworks via solid-vapor interface reactions, *J. Am. Chem. Soc.* 135 (2013) 10470–10474. <https://doi.org/10.1021/ja403464h>.
- [165] J.W. Colson, W.R. Dichtel, Rationally synthesized two-dimensional polymers, *Nat. Chem.* 5 (2013) 453–465. <https://doi.org/10.1038/nchem.1628>.
- [166] B.P. Biswal, S. Chandra, S. Kandambeth, B. Lukose, T. Heine, R. Banerjee, Mechanochemical synthesis of chemically stable isorecticular covalent organic frameworks, *J. Am. Chem. Soc.* 135 (2013) 5328–5331. <https://doi.org/10.1021/ja4017842>.
- [167] S. Karak, S. Kandambeth, B.P. Biswal, H.S. Sasmal, S. Kumar, P. Pachfule, R. Banerjee, Constructing ultraporos covalent organic frameworks in seconds via an organic terracotta process, *J. Am. Chem. Soc.* 139 (2017) 1856–1862. <https://doi.org/10.1021/jacs.6b08815>.
- [168] H.S. Sasmal, A. Halder, S.H. Kunjattu, K. Dey, A. Nadol, T.G. Ajithkumar, P. Ravindra Bedadur, R. Banerjee, Covalent Self-Assembly in Two Dimensions: Connecting Covalent Organic Framework Nanospheres into Crystalline and Porous Thin Films, *J. Am. Chem. Soc.* 141 (2019) 20371–20379. <https://doi.org/10.1021/jacs.9b10788>.
- [169] S. Kandambeth, A. Mallick, B. Lukose, M. V. Mane, T. Heine, R. Banerjee, Construction of crystalline 2D covalent organic frameworks with remarkable chemical (Acid/Base) stability via a combined reversible and irreversible route, *J. Am. Chem. Soc.* 134 (2012) 19524–19527. <https://doi.org/10.1021/ja308278w>.
- [170] S. Kandambeth, B.P. Biswal, H.D. Chaudhari, K.C. Rout, S. Kunjattu H., S. Mitra, S.

- Karak, A. Das, R. Mukherjee, U.K. Kharul, R. Banerjee, Selective Molecular Sieving in Self-Standing Porous Covalent-Organic-Framework Membranes, *Adv. Mater.* 29 (2017). <https://doi.org/10.1002/adma.201603945>.
- [171] H.S. Sasmal, H.B. Aiyappa, S.N. Bhange, S. Karak, A. Halder, S. Kurungot, R. Banerjee, Superprotonic Conductivity in Flexible Porous Covalent Organic Framework Membranes, *Angew. Chemie.* 130 (2018) 11060–11064. <https://doi.org/10.1002/ange.201804753>.
- [172] H. Fan, J. Gu, H. Meng, A. Knebel, J. Caro, High-Flux Membranes Based on the Covalent Organic Framework COF-LZU1 for Selective Dye Separation by Nanofiltration, *Angew. Chemie - Int. Ed.* 57 (2018) 4083–4087. <https://doi.org/10.1002/anie.201712816>.
- [173] G. Li, K. Zhang, T. Tsuru, Two-Dimensional Covalent Organic Framework (COF) Membranes Fabricated via the Assembly of Exfoliated COF Nanosheets, *ACS Appl. Mater. Interfaces.* 9 (2017) 8433–8436. <https://doi.org/10.1021/acsmi.6b15752>.
- [174] Y. Ying, D. Liu, J. Ma, M. Tong, W. Zhang, H. Huang, Q. Yang, C. Zhong, A GO-assisted method for the preparation of ultrathin covalent organic framework membranes for gas separation, *J. Mater. Chem. A.* 4 (2016) 13444–13449. <https://doi.org/10.1039/c6ta04579k>.
- [175] K. Dey, M. Pal, K.C. Rout, S.S. Kunjattu, A. Das, R. Mukherjee, U.K. Kharul, R. Banerjee, Selective Molecular Separation by Interfacially Crystallized Covalent Organic Framework Thin Films, *J. Am. Chem. Soc.* 139 (2017) 13083–13091. <https://doi.org/10.1021/jacs.7b06640>.
- [176] L. Valentino, M. Matsumoto, W.R. Dichtel, B.J. Marinas, Development and Performance Characterization of a Polyimine Covalent Organic Framework Thin-Film Composite Nanofiltration Membrane, *Environ. Sci. Technol.* 51 (2017) 14352–14359. <https://doi.org/10.1021/acs.est.7b04056>.
- [177] R. Wang, X. Shi, A. Xiao, W. Zhou, Y. Wang, Interfacial polymerization of covalent organic frameworks (COFs) on polymeric substrates for molecular separations, *J. Memb. Sci.* 566 (2018) 197–204. <https://doi.org/10.1016/j.memsci.2018.08.044>.
- [178] D.B. Shinde, G. Sheng, X. Li, M. Ostwal, A.H. Emwas, K.W. Huang, Z. Lai, Crystalline 2D Covalent Organic Framework Membranes for High-Flux Organic Solvent Nanofiltration, *J. Am. Chem. Soc.* 140 (2018) 14342–14349. <https://doi.org/10.1021/jacs.8b08788>.
- [179] H. Fan, A. Mundstock, A. Feldhoff, A. Knebel, J. Gu, H. Meng, J. Caro, Covalent Organic Framework-Covalent Organic Framework Bilayer Membranes for Highly Selective Gas Separation, *J. Am. Chem. Soc.* 140 (2018) 10094–10098. <https://doi.org/10.1021/jacs.8b05136>.
- [180] H. Fan, A. Mundstock, J. Gu, H. Meng, J. Caro, An azine-linked covalent organic framework ACOF-1 membrane for highly selective CO₂/CH₄ separation, *J. Mater. Chem. A.* 6 (2018) 16849–16853. <https://doi.org/10.1039/c8ta05641b>.
- [181] B.P. Biswal, S.H. Kunjattu, T. Kaur, R. Banerjee, U.K. Kharul, Transforming covalent organic framework into thin-film composite membranes for hydrocarbon recovery, *Sep. Sci. Technol.* 53 (2018) 1752–1759. <https://doi.org/10.1080/01496395.2018.1443136>.

- [182] S. De Gisi, G. Lofrano, M. Grassi, M. Notarnicola, Characteristics and adsorption capacities of low-cost sorbents for wastewater treatment: A review, *Sustain. Mater. Technol.* 9 (2016) 10–40. <https://doi.org/10.1016/j.susmat.2016.06.002>.
- [183] Z. Wang, A. Wu, L.C. Ciacchi, G. Wei, Recent advances in Nanoporous Membranes for Water Purification, *Nanomaterials*. 8 (2018). <https://doi.org/10.3390/nano8020065>.
- [184] W. Zhang, L. Zhang, H. Zhao, B. Li, H. Ma, A two-dimensional cationic covalent organic framework membrane for selective molecular sieving, *J. Mater. Chem. A*. 6 (2018) 13331–13339. <https://doi.org/10.1039/c8ta04178d>.
- [185] K. Zhang, Z. He, K.M. Gupta, J. Jiang, Computational design of 2D functional covalent-organic framework membranes for water desalination, *Environ. Sci. Water Res. Technol.* 3 (2017) 735–743. <https://doi.org/10.1039/c7ew00074j>.
- [186] L. Xu, J. Xu, B. Shan, X. Wang, C. Gao, TpPa-2-incorporated mixed matrix membranes for efficient water purification, *J. Memb. Sci.* 526 (2017) 355–366. <https://doi.org/10.1016/j.memsci.2016.12.039>.
- [187] S. Sorribas, P. Gorgojo, C. Téllez, J. Coronas, A.G. Livingston, High flux thin film nanocomposite membranes based on metal-organic frameworks for organic solvent nanofiltration, *J. Am. Chem. Soc.* 135 (2013) 15201–15208. <https://doi.org/10.1021/ja407665w>.
- [188] L. Huang, J. Chen, T. Gao, M. Zhang, Y. Li, L. Dai, L. Qu, G. Shi, Reduced Graphene Oxide Membranes for Ultrafast Organic Solvent Nanofiltration, *Adv. Mater.* 28 (2016) 8669–8674. <https://doi.org/10.1002/adma.201601606>.

Investigations of PPO-ZIF Mixed Matrix Membranes (MMMs) for Olefin/Paraffin Separation



Abstract

An assertive formation of ZIF-based mixed matrix membranes (MMMs) with polyphenylene oxide (PPO), a high permeability polymer as a host, is presented. The interfacial interactions between the filler particles and polymer matrix are established by DSC and XPS analyses. The ZIF loading could be achieved up to 40% without hampering the stability of the resulting MMMs. These membranes were evaluated for pure gas permeability, specifically aiming at C₃H₆/C₃H₈ separation, a highly desired application in the industry. The ZIF-PPO hybrids display promising pure gas as well as mixed gas permeation performance. The 40% ZIF-8 and ZIF-67 loaded membrane display promising C₃H₆/C₃H₈ selectivity of 27.5 and 25, with a permeability of 12 and 13 barrer, respectively. The enhanced selectivity is attributed to the absence of defects eliminated due to metal-polymer interactions. The permeation study of a 30% ZIF-8 loaded membrane while varying transmembrane pressure and long-time exposure (150 h) of propylene at 60 psi indicated the excellent stability of the membrane. The sorption analysis further confirmed the molecular sieving characteristics of the ZIF@PPO MMMs. The mixed gas permeation performance showed promising results of high permeability as well as maintaining selectivity over a wide range of compositions.

2.1 Introduction

Olefins are a desired class of chemicals used as raw material in various chemical manufacturing, such as acrylonitrile, propylene oxide, isopropanol, allylchloride, acrolein, acrylic acid and its esters, cumene and different kind of polymers [1]. The annual production of propylene was approximately 100 million tons worldwide in 2016 and is expected to grow at a rate of 3.6% by 2025 [2]. During their production, the separation of olefin and paraffin is one of the crucial steps. Due to the close physicochemical properties of propylene and propane (boiling point: $-47.6\text{ }^{\circ}\text{C}$ and $-42.1\text{ }^{\circ}\text{C}$ and Lennard-Jones diameter: 4.68 \AA and 5.06 \AA , respectively), their separation is known to be highly energy-intensive[3,4]. It is usually done by cryogenic distillation at $-25\text{ }^{\circ}\text{C}$ with 75 m tall columns consisting of >200 trays needing 10-15 reflux ratios and high pressure of 16-20 bar [3,5]. This energy-intensive nature is well quantified in the literature. It is said that the purification of propylene and ethylene alone accounts for 0.3% (120Tbtu/year) of global energy use, roughly equivalent to Singapore's annual energy consumption [6,7]. Various methods, such as extractive distillation, membrane separation, absorption, physical adsorption, and chemical complexation are proposed for olefin-paraffin separation [8,9]. Membrane technology has aroused great attention as an effective alternative for propane propylene separation due to its advantages, including low energy consumption, environmental friendliness, easy operation, and no need for phase change [10–13]. Several materials are studied as a membrane for $\text{C}_3\text{H}_6/\text{C}_3\text{H}_8$ separation, such as polymers [4,14,15], carbon molecular sieves [16,17] and Zeolites [18]. Among these, polymeric membranes have the advantage of easy processibility and scalability. However, some fundamental issues persist in polymeric membranes, such as plasticization and the trade-off relationship between permeability and selectivity, persist in this method [4,19]. Mixed Matrix Membranes (MMMs) are emerging as a new type of membrane material to overcome these issues. In this approach, highly selective and permeable filler particles are dispersed in a polymer matrix. Some such membranes are well placed over the limiting upper bound [20]. In addition, the flexibility and solubility offered by the polymer retain the processability similar to the polymeric membrane[20,21].

Different fillers, such as silica, zeolites, carbon molecular sieves, and porous organic cages have been demonstrated as filler materials [20]. The selection of filler plays a vital role in the performance of Mixed Matrix Membranes (MMMs). For example, due to the inorganic nature of zeolites, surface modification is needed to attain better compatibility with the polymer

[13]. Metal-Organic Frameworks (MOFs) are porous crystalline materials composed of metal atoms linked together by organic linkers [22,23]. The organic and inorganic nature offers better compatibility with the polymer and tunable pore aperture, making them promising filler materials [24]. The Zeolitic Imidazole Frameworks (ZIFs), a subclass of MOF, have been of interest in preparing gas separation membranes due to their similar pore size as that of smaller gas molecules. In addition, they show high chemical and thermal stability [25,26]. The ZIF-8 is one of the widely studied ZIFs. It is composed of Zn metal and 2-methyl imidazole as the ligand. It has a sodalite (SOD) topology possessing a large pore cavity (11.6 Å) and narrow pore aperture (3.4 Å)[26]. A single component diffusion study by Li et al. reveals 125 as the diffusion selectivity of propylene/propane in ZIF-8 [27]. Several strategies are developed to fabricate ZIF-8-based membranes for C₃H₆/C₃H₈, which include pristine ZIF-8 membrane on a substrate [28–31] and MMMs [32]. Jeong's group found that ZIF-67, a cobalt-substituted equivalent of ZIF-8, is also an excellent material for propylene/propane separation [33]. The submicron-thick ZIF-67 membrane resulted in an average propylene/propane separation factor of 85 and propylene permeance of $\sim 460 \times 10^{-10}$ mol Pa⁻¹m⁻²s⁻¹ [33].

Although the incorporation of MOF as a filler in MMMs looks impressive, one of the deterring factors behind this crucial issue is the poor interfacial compatibility of a filler with the polymer, leading to voids at the interface [3]. Several protocols are reported to improve MOF-polymer compatibility. One approach is selecting a polymer matrix that can chemically or physically interact with the MOF [34,35]. The enhancement of interfacial compatibility can also be achieved through non-covalent interactions such as hydrophobicity, [36] hydrophilicity [37], and hydrogen bonding[38]. Various modification strategies to achieve interfacial interactions between MOF and polymer are well reported [39–41]. Li's group has demonstrated covalently grafted polyimide brushes on MOF surfaces to engineer the MOF/polymer interface [42]. Zhong and co-workers demonstrated a bilayer-based strategy to construct MOF-based MMMs for efficient propylene-propane separation [43].

In addition to the MOF-polymer interactions, the intrinsic permeation property of the host polymer is also crucial since the permeated molecule from the MOF has to diffuse through the polymer matrix seamlessly. The polymer with lower permeability would offer resistance to the diffusion of the molecule 'chosen' by the MOF to permeate selectively through MMM. Conversely, if the polymer has high permeability (e.g., PDMS), the permeating molecule would

permeate through the polymer matrix rather than through the MOF particles. Thus, the intrinsic permeation property of the host polymer has to be appropriate, avoiding both above possibilities. In this direction, we have reported ZIF-8-based MMM with N-substituted PBI, possessing a fairly good combination of permeability and selectivity [44]. The reason behind the PBI selection was to enhance the filler matrix compatibility by the metal-polymer interaction (Zn in ZIF-8 and N in the polymer backbone). We could achieve fairly good separation performance for propylene/propane with 30% ZIF loading, outperforming almost all the previously reported MMM in terms of selectivity (~ 32). Despite this, the polymer availability for the scale-up could be an additional issue. To address this, the present work describes a new type of MMM with a common, commercially better feasible polymer host, viz., poly(2,6-dimethyl-1,4-phenylene oxide), commonly called polyphenylene oxide or PPO. The two widely investigated ZIFs, viz., ZIF-8, and ZIF-67, were chosen as fillers (Figure 2.1). The PPO possesses fairly good permeability and moderate selectivity [45,46]. The 'O' atom present in the polymer backbone exhibiting interactions with the metal present in ZIFs (Zn and Co), which in turn enable ZIF-polymer interfacial compatibility is the focus of the present work. The formed MMMs showed enhancement in selectivity and permeability of C_3H_6/C_3H_8 than the host PPO matrix and can fulfill the commercial approach.

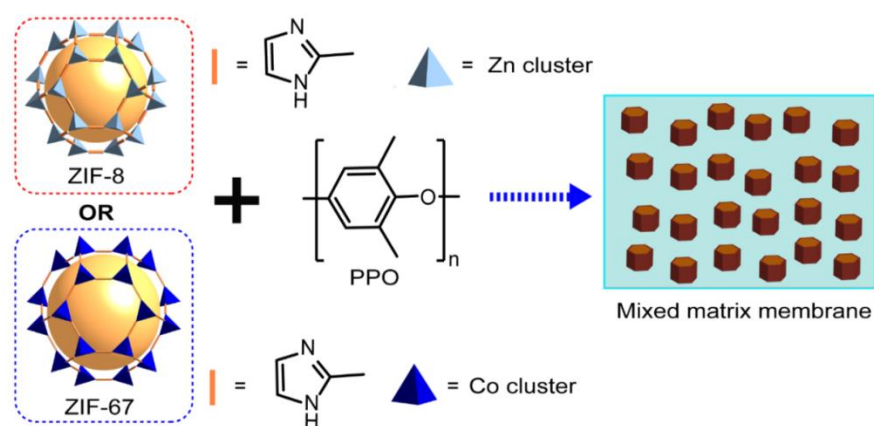


Figure 2.1 Designing MMM by incorporating ZIF into PPO polymer matrix

2.1.1 Scope and objectives

This work will present the fabrication of MMMs by loading ZIF particles in the PPO matrix. The ZIF-8 and ZIF-67 particle will impart better separation performance, and PPO will act as a matrix to hold the ZIF particle without hampering the separation performance in a significant way. Owing to the inherent permeation properties of PPO, and the ability of ZIF

(ZIF-8 and ZIF-67) pore window to discriminate propylene over propane, the objective was to examine the separation performance of resulting MMMs. The polymer ZIF interaction delimits the challenges faced in the MMMs, such as interfacial defect and plasticization. Another objective of this study was to investigate the interfacial interaction using different characterization techniques, correlate them with the separation performance and examine industrial viability.

2.2 Results and discussion

2.2.1 Physical characterizations

2.2.1.1 Formation of MMMs

The synthesized ZIF particles showed uniform particle size (Figure 2.2, 2.3). The average particle size for ZIF-8 was 50 nm, while that of ZIF-67 was 500 nm, which was confirmed by both transmission electron microscopy (TEM) (Figure 2.2) and scanning electron microscopy (SEM) (Figure 2.3). These values were further supported by the DLS analysis (Figure 2.4). The PXRD pattern of both ZIF-8 and ZIF-67 matched well with the respective simulated one (Figure 2.7). For casting MMMs, PPO, a high permeability polymer, was selected as a host for incorporating ZIF particles. The schematic representation of MMM fabrication is shown in Figure 2.1. The stable membranes with 40% ZIF-loading in both types of MMMs (ZIF-8@PPO and ZIF-67@PPO) could be attained easily. Beyond 40%, both types of MMMs were brittle. In our earlier effort [44], the ZIF loading was limited to 30%, wherein the host polymer belonged to the benzimidazole family. The obtained higher loading in the present case can be attributed to the higher molecular weight of the polymer, as depicted by the high intrinsic viscosity of the synthesized PPO ($[\eta] = 0.92$ dL/g).

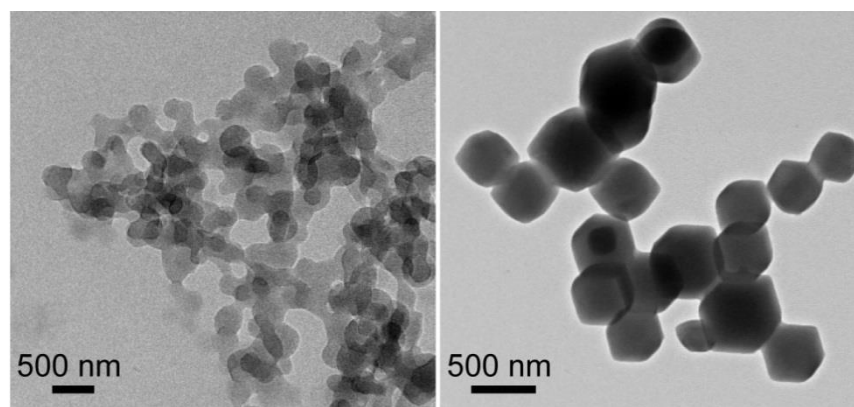


Figure 2.2 TEM images of ZIF-8 (a) and ZIF-67 (b) particles

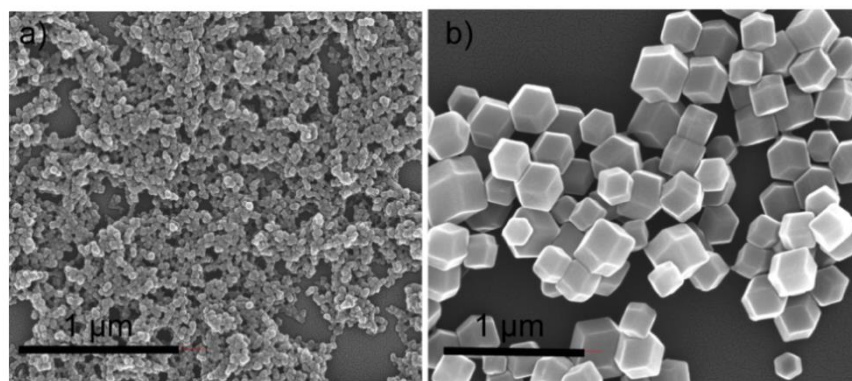


Figure 2.3 SEM images of ZIF-8 (a) and ZIF-67 (b) particles

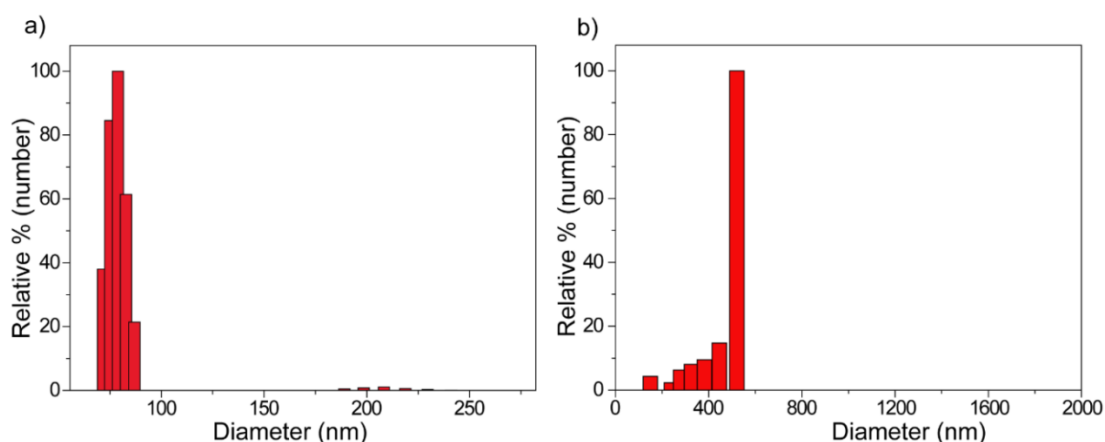


Figure 2.4 The DLS spectra of (a) ZIF-8 and (b) ZIF-67

2.2.1.2 Thermo gravimetric analysis (TGA)

The TGA analyses of PPO and different MMMs were performed in the air to assess the char yield (Figure 2.5). The TGA spectra of PPO (entirely organic) showed no residue at 900°C. With this observation, the char yield of MMMs was ascribed to ZnO and CoO (for ZIF-8 and ZIF-67, respectively). The char yield offered a quantitative estimation of ZIF content in the respective MMM. It was observed that the TGA-estimated value matched well (variation from 0.1-1.5%) with that of the experimental loading taken while casting MMMs (Table 2.1).

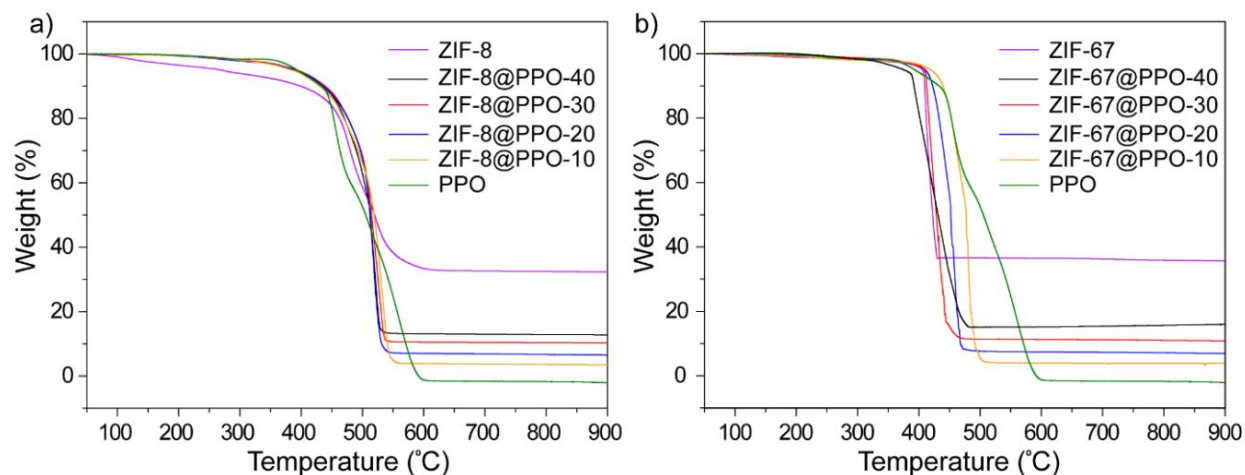


Figure 2.5 The TGA analysis of (a) ZIF-8 and (b) ZIF-67 based MMMs

Table 2.1 Comparison of experimental ZIF loading with that of TGA analysis

ZIF-8 @PPO	ZIF-8 (wt.% in casting solution)	0	10	20	30	40	100
	ZnO (wt.%)*	0	3.5	6.5	10.2	12.8	32.3
	ZIF-8 (wt.% in MMM)**	0	10.7	19.9	31.5	39.5	100
ZIF-67 @PPO	ZIF-67 (wt.% in casting solution)	0	10	20	30	40	100
	CoO (wt.%)*	0	3.8	7.0	10.9	14.5	36.1
	ZIF-67 (wt.% in MMM)**	0	10.6	19.6	30.2	40.1	100

* ZnO/CoO content obtained from TGA in air, ** ZIF content in MMM calculated from the residue (ZnO/CoO) from TGA

2.2.1.3 Structural integrity of ZIF particles in resulting MMMs

The cross-sectional SEM images of ZIF-8@PPO-40 and ZIF-67@PPO-40 are shown in Figure 2.6. The distribution of both types of ZIF particles was found to be uniform in the host PPO matrix. Any sign of particle agglomeration was absent. Similarly, the 20% and 30% ZIF-loaded MMMs showed homogeneous distribution of the ZIF particles. These SEM images also reveal that the morphology and particle size of ZIF particles in the MMMs were comparable with that of as-synthesized ZIF particles. This observation confirms that the structural identity of ZIF particles was retained in the resulting MMM matrix. This highly significant observation (absence of agglomeration) indicates preferred interactions of ZIF particles with the PPO polymer chains possessing oxygen.

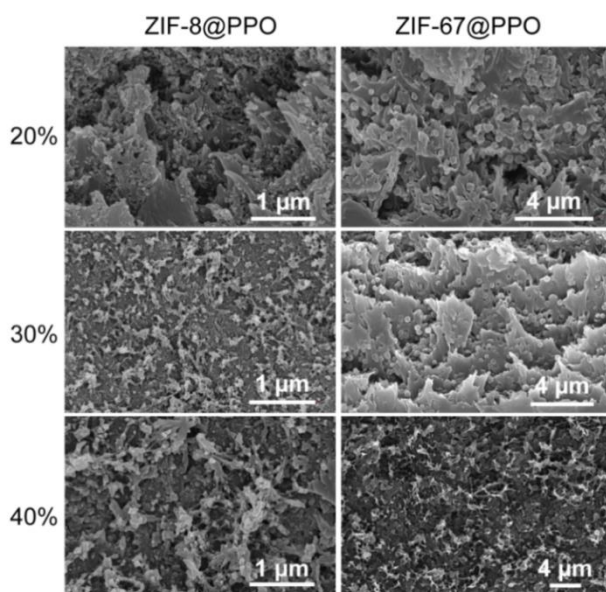


Figure 2.6 Cross-sectional SEM images of ZIF-8 and ZIF-67-based MMMs

The x-ray diffraction patterns of ZIF@PPO MMMs (Figure 2.7) showed the characteristic diffraction peaks of the corresponding ZIF particles. It further substantiates that the structural integrity of the ZIF particle was maintained in the MMMs. The X-ray diffraction spectra of PPO showed a broad, amorphous hump at 14.1° , leading to a d-spacing of 6.2 \AA . The d-spacing of PPO matched well with that of the reported data [47],[48]. In the X-ray diffraction spectra of MMMs, the amorphous peak of PPO was masked by the intense peaks of ZIF particles. This was observed in both ZIF-8 and ZIF-67-based MMMs.

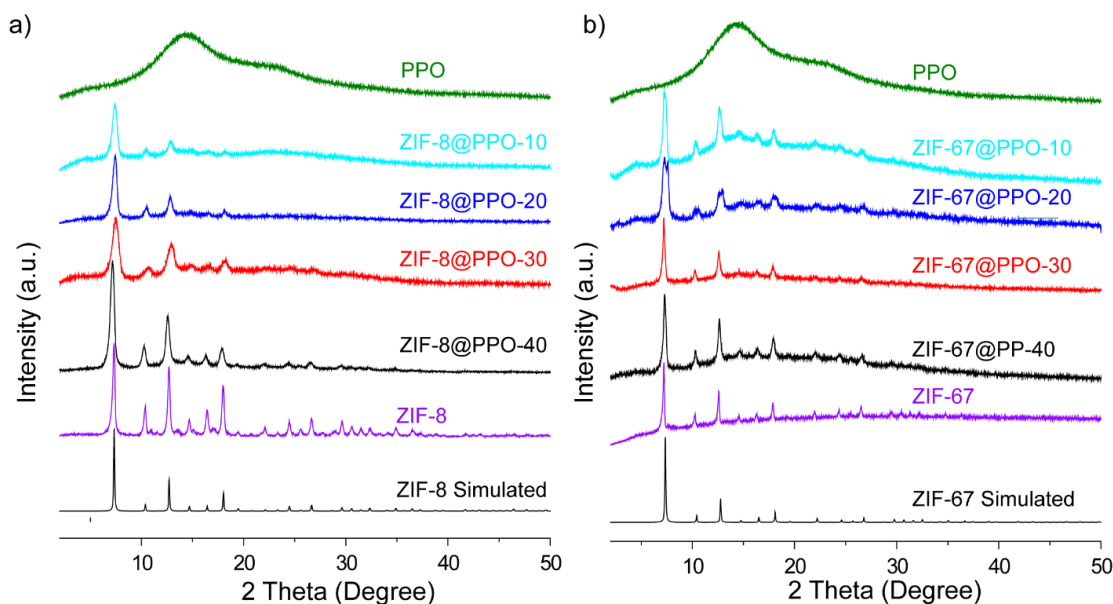


Figure 2.7 The WAXD patterns of (a) ZIF-8 and (b) ZIF-67 based MMMs

2.2.1.4 Interaction between ZIF particles and host PPO

The DSC spectra of ZIF-8 and ZIF-67-based MMMs is shown in Figure 2.8a and b. It is evident from these thermograms that the T_g of all MMMs shifted to a higher temperature than that of pristine PPO, even after a small 10 % ZIF loading. This enhancement in T_g indicated that the ZIF particles restricted the polymer chain mobility due to their interactions with the host PPO. Even though an enhancement in T_g could be small, obtained rigidification is advantageous in tackling the plasticization issue of polymeric membranes.

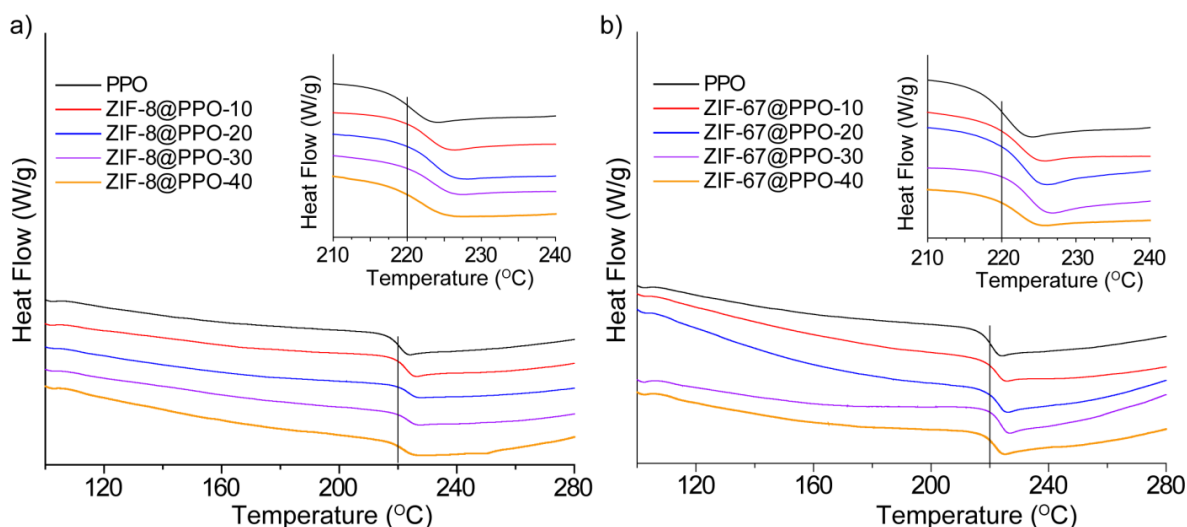


Figure 2.8 DSC thermograms of (a) ZIF-8@PPO and (b) ZIF-67@PPO MMMs

The XPS analysis was performed to investigate the ZIF-polymer interactions further (Figures 2.9, 2.10). The high-resolution O1s spectra of MMMs showed a peak shift vis-à-vis O1s spectra of pristine PPO (Figure 2.9). This observation is highly prominent in the case of 40% loaded MMMs. The O1s peak of MMMs was deconvoluted into two different peaks (Figure 2.9). The one at higher binding energy accounts for the interaction of the 'O' atoms of PPO with the metal atom of the ZIF particle. It could be assigned to the electronegative nature of oxygen belonging to PPO and positively charged metal atom from the ZIF moiety (Zn and Co in ZIF-8 and ZIF-67, respectively). The other peak with lower binding energy is the characteristic peak of PPO-'O' (Figure 2.9). Such a peak shift indicates the polymer-filler interactions. The metal region in XPS spectra (Zn 2p and Co 2p in ZIF-8@PPO and ZIF-67@PPO MMMs, respectively) was also analyzed (Figure 2.10). Two different peaks in the Zn 2p region attributed to Zn 2p 3/2 (lower binding energy) and 2p 1/2 (higher binding energy). A shift in binding energy implies that the Zn atom participated in the interactions. Similarly, the Co atom present in the ZIF-67 shows four

different peaks, including 2p 3/2, 2p 1/2, and two satellite peaks. This shift in binding energy is attributed to the cobalt-oxygen interactions. The XPS analysis confirming PPO-ZIF interactions led to the elevation of T_g of PPO (Figure 2.11). This might also assist in achieving higher ZIF-loading in PPO, providing a compatible interface between the ZIF particles and PPO matrix and suppressing the polymer plasticization/physical aging.

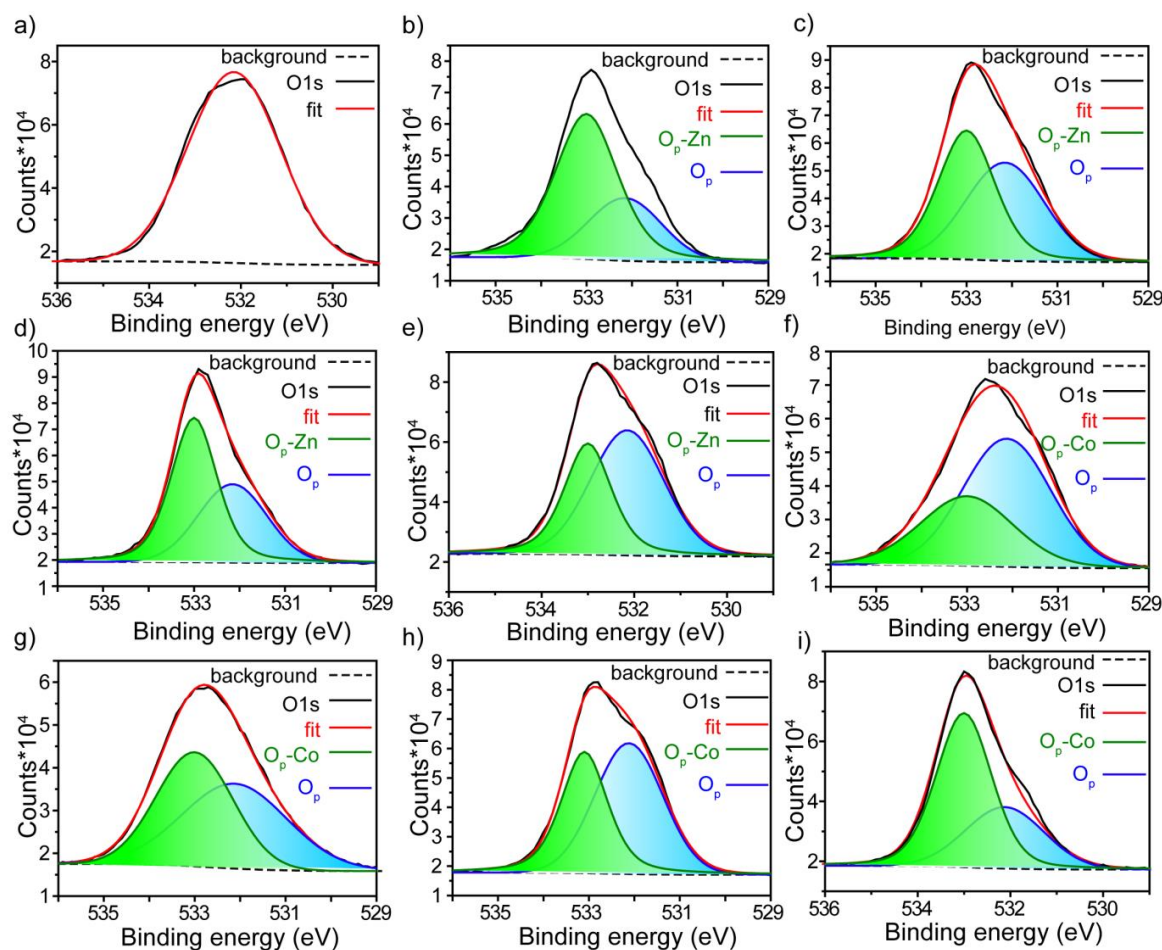


Figure 2.9 High resolution ‘O1s’ XPS spectra of (a) PPO, ZIF-8@PPO (b-e) and ZIF-67@PPO (f-i) MMMs with ZIF loading 10, 20, 30 and 40%, respectively

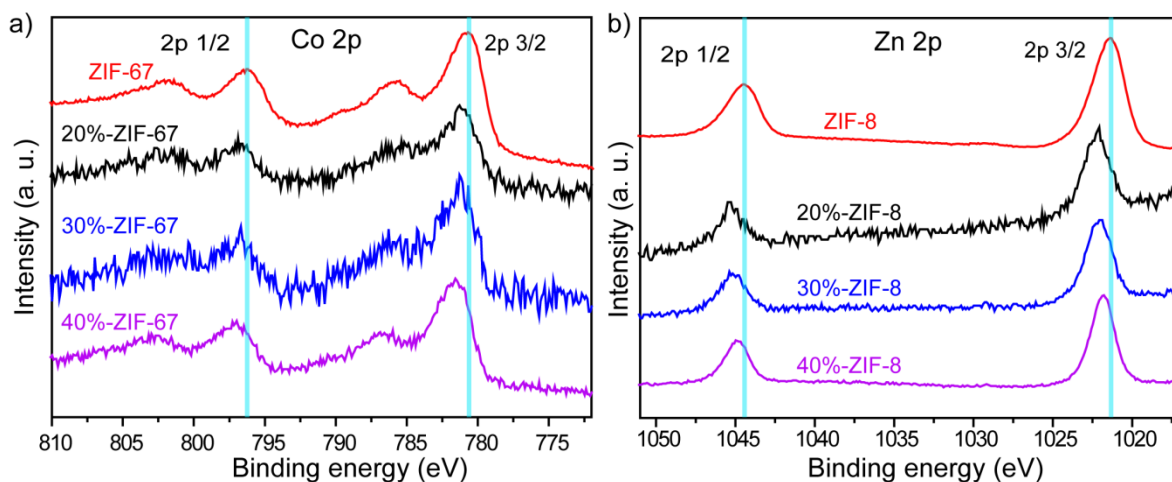


Figure 2.10 (a) Zn 2p and (b) Co 2p XPS spectra of ZIF-8@PPO and ZIF-67@PPO MMMs, respectively

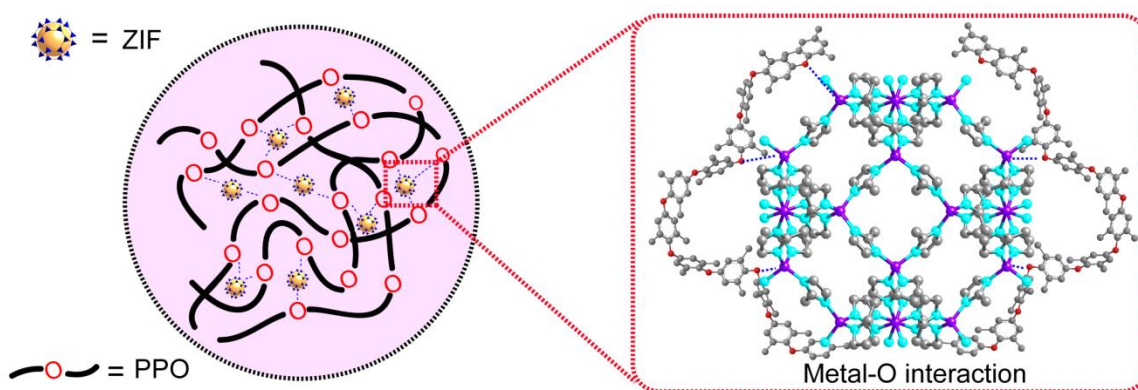


Figure 2.11 Schematic representation of the metal-oxygen interaction present in the MMMs

2.2.2 Gas permeation properties

2.2.2.1 Pure gas analysis

The gas permeability analysis was performed using pure gases of varying kinetic diameters (He, O₂, N₂, CH₄, C₂H₄, C₂H₆, C₃H₆, and C₃H₈). Obtained permeation properties are plotted in Figure 2.12 a,b (Table 2.2). The permeability of all gases, except propane, increased after incorporating ZIF-8 or ZIF-67 in the PPO matrix. This was followed for all the amount of ZIF-loading, as anticipated. It is also evident that for a particular MMM, the permeability of various gases generally increased with the lowering of permeant size. A prominent exception was seen for ethylene as a permeant. Figure 2.12a (ZIF-8 based MMMs) and Figure 2.12b (ZIF-67 based MMMs) showed a prominent hump for the permeability coefficient of ethylene (~4.2

Å), which is higher than that of permeability of N_2 and CH_4 . This permeability elevation (than that of N_2 and CH_4) was seen for all percent loadings in both families of MMMs. This shows not only the role of ZIFs in discriminating permeants but also the shape of the permeant is also vital in determining the permeability. Although the C_2H_4 molecule has a higher kinetic diameter and molecular weight than that of N_2 and CH_4 , the unsaturated dumbbell shape of C_2H_4 might pass it easily through the pore window of ZIF (3.4 Å). Thus, the higher ethylene permeability could be attributed to its shape rather than just its kinetic diameter.

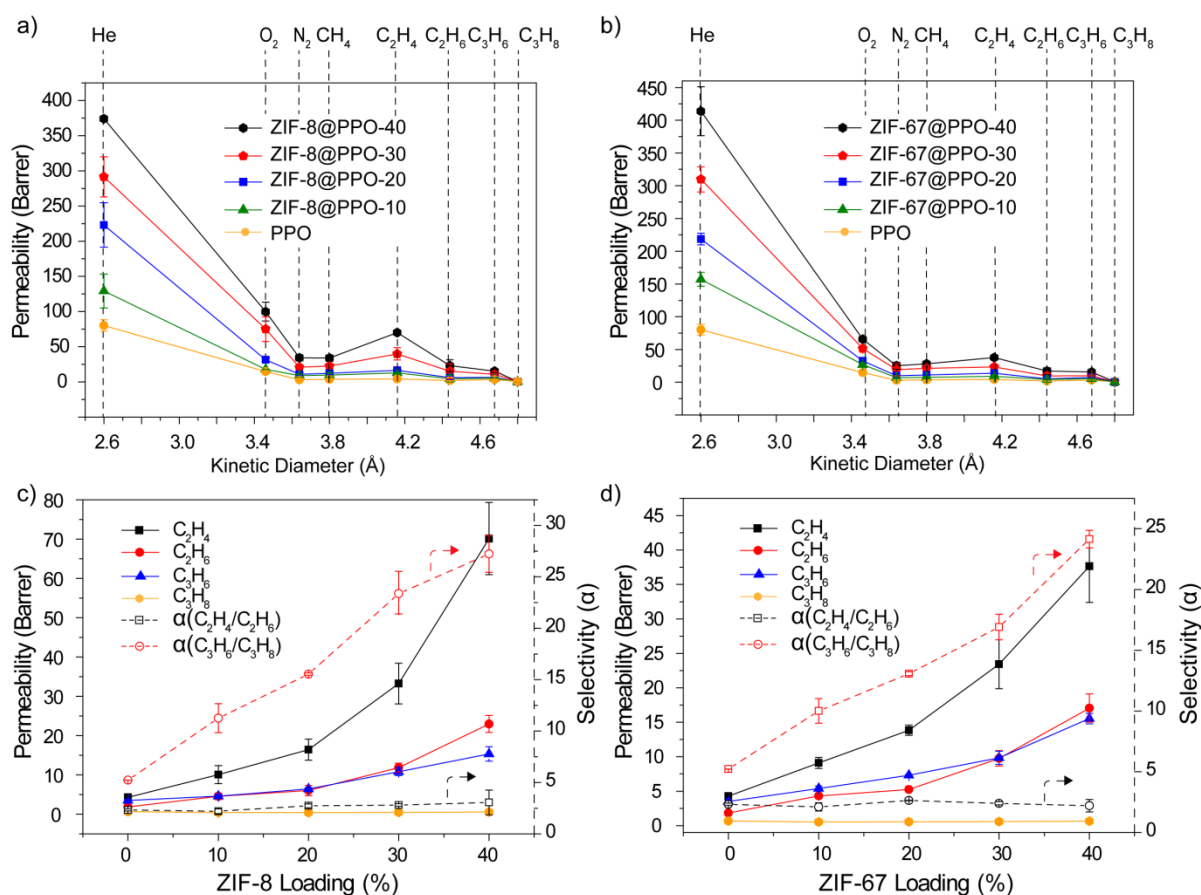


Figure 2.12: Variation of gas permeability with kinetic diameter of penetrants in (a) ZIF-8@PPO and (b) ZIF-67@PPO MMM; pure gas permeability of C_2H_4 , C_2H_6 , C_3H_6 and C_3H_8 , and selectivity of C_2H_4/C_2H_6 and C_3H_6/C_3H_8 in (c) ZIF-8@PPO and (d) ZIF-67@PPO MMMs

Table 2.2 Pure gas permeability of MMMs and pristine PPO

	ZIF-8@PPO				ZIF-67@PPO				PPO
	40%	30%	20%	10%	40%	30%	20%	10%	
He	374.17	291.50	223.07	129.19	413.68	309.76	218.67	157.22	80.17
N ₂	34.17	20.82	10.91	8.84	25.20	19.28	9.85	6.96	3.10
O ₂	99.94	75.17	31.53	17.84	65.90	51.58	32.66	26.99	14.64
CH ₄	33.91	22.48	12.35	9.83	28.13	21.20	11.12	7.55	3.61
C ₂ H ₆	22.97	11.87	6.02	4.56	17.06	9.76	5.24	4.31	1.85
C ₂ H ₄	70.12	33.23	16.45	10.07	37.65	23.43	13.84	9.10	4.28
C ₃ H ₈	0.56	0.46	0.42	0.41	0.64	0.58	0.56	0.54	0.67
C ₃ H ₆	15.35	10.84	6.45	4.61	15.53	9.84	7.31	5.37	3.50

The pure gas C₃H₆ and C₃H₈ separation performance of ZIF-8@PPO and ZIF-67@PPO membranes are plotted in Figures 2.12c and 2.12d, respectively. The incorporation of ZIF particles in the PPO matrix showed a remarkable increase in the permeability of the C₃H₆. Compared to the pristine PPO, there is a 3.7 and 3.4 fold enhancement of the permeability of C₃H₆ observed for ZIF-8@PPO-40 and ZIF-67@PPO-40. The C₃H₈ permeability did not exhibit any substantial difference with the ZIF loading. From this observation, it can be said that for the permeation of propane, the highly permeable nature of PPO nullifies the effect of the tortuous path created by ZIF particles. The increase in propylene permeability and maintaining similar propane permeability led to improved C₃H₆/C₃H₈ selectivity. The 40% loaded ZIF-8@PPO and ZIF-67@PPO membranes showed an ideal selectivity of 27 and 25, respectively. It attributes that the pore window (3.4 Å) present in the ZIF-8 and ZIF-67 could exclude propane but passes propylene through it. However, the C₂H₄/C₂H₆ selectivity of MMMs did not significantly improve. This indicates the inability of ZIF-8 and ZIF-67 to discriminate this pair of gases. Both the ZIF-8@PPO and ZIF-67@PPO exhibited appreciable separation performance for propane-propylene. In view of the highly permeable and commercial availability of PPO, it might serve as an effective membrane for industrially demanding propane-propylene separation.

To elucidate the contribution of interfacial interaction resisting plasticization, we have evaluated the propylene permeability of the ZIF-8@PPO-30 membrane at different pressure and time. With variation in transmembrane pressure of 20-80 psi, the permeability varied in a range

of 11.6-8.8 barrer (Figure 2.13a). In another study, a long-term permeability analysis (150 h) of this membrane at a transmembrane pressure of 60 psi revealed that the permeability varied marginally from 9.4-11.1 barrer (Figure 2.13b). The permeability values observed in both these studies are significantly different than that of the permeability of pristine PPO (3.5 barrer). These studies indicated the stability of the membrane towards time and long-time exposure to propylene. Both these studies may also indicate the positive role of metal-oxygen interaction in protecting the membrane from plasticization or aging.

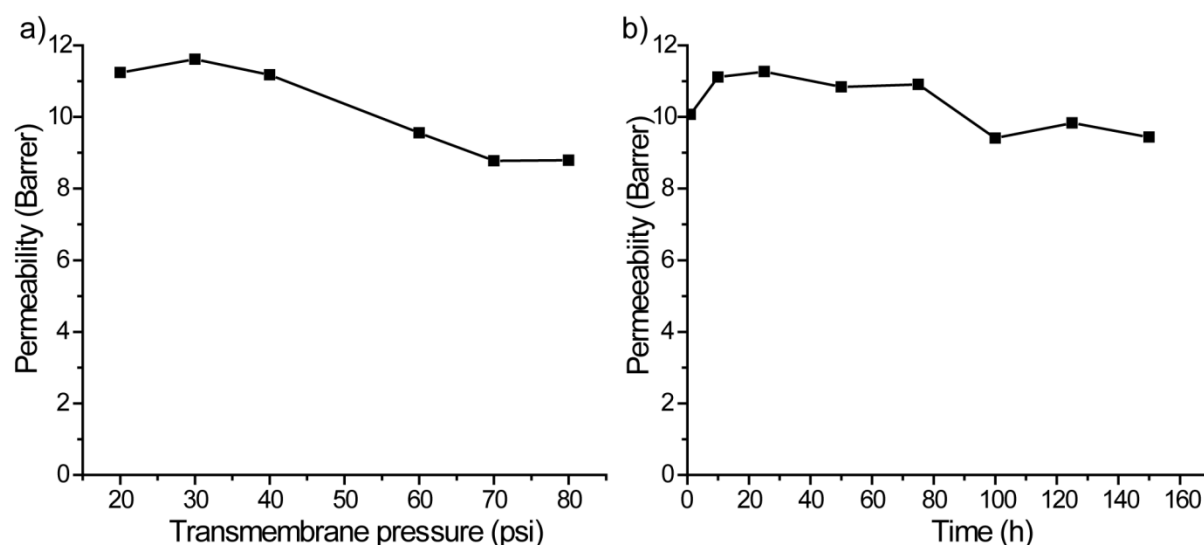


Figure 2.13 Variation in C₃H₆ permeability of ZIF-8@PPO-30 MMM with (a) upstream gas pressure (a) long-term exposure at 60 psi upstream

2.2.2.2 Sorption analysis

A sorption analysis of MMMs possessing 40% ZIF loading was performed in order to understand the contribution of sorption in governing the permeability (Figure 2.14a). The data points fit the Langmuir model well [21].

$$c_i = \frac{C'_{H,i} b_i P_i}{1 + b_i P_i} \quad (1)$$

where, c_i is the sorption uptake, $C_{H,i}$ is the capacity constant, and b_i is the affinity constant for component i . Table S1 shows the Langmuir parameter and calculated sorption coefficient of the 40% loaded ZIF-8 and ZIF-67-based MMMs. For the given membrane, both C₃H₆ and C₃H₈ show a similar sorption uptake and a similar C₃H₆/C₃H₈ sorption selectivity (~1) at 4.8 atm (Table 2.3). This indicates that the addition of ZIF particles into the PPO matrix has not affected the C₃H₆/C₃H₈ solubility selectivity. The permeability coefficient is the product of the sorption

and diffusion coefficients. The sorption analysis at different pressure (0-5 atm) enabled us to calculate the diffusion coefficient. The MMMs with 40% loading showed an enhancement in the diffusivity coefficient of C_3H_6 in contrast to the pristine PPO membrane. This revealed the fast diffusion of propylene gas through the MMMs. In the case of propane, there was a slight decrease in the diffusivity coefficient; it may be due to the inability of ZIFs to permeate propane, which in turn causes a tortuous path for the propane to permeate through the PPO matrix while avoiding ZIF particles. It results in a five-fold increase in the diffusion selectivity of 40% (both ZIF-8 and ZIF-67) loaded MMMs compared to the pristine PPO membrane (Figure 2.14b). It confirms that diffusion dominates in attaining the C_3H_6/C_3H_8 selectivity for both ZIF-8@PPO-40 and ZIF-67@PPO-40 MMMs.

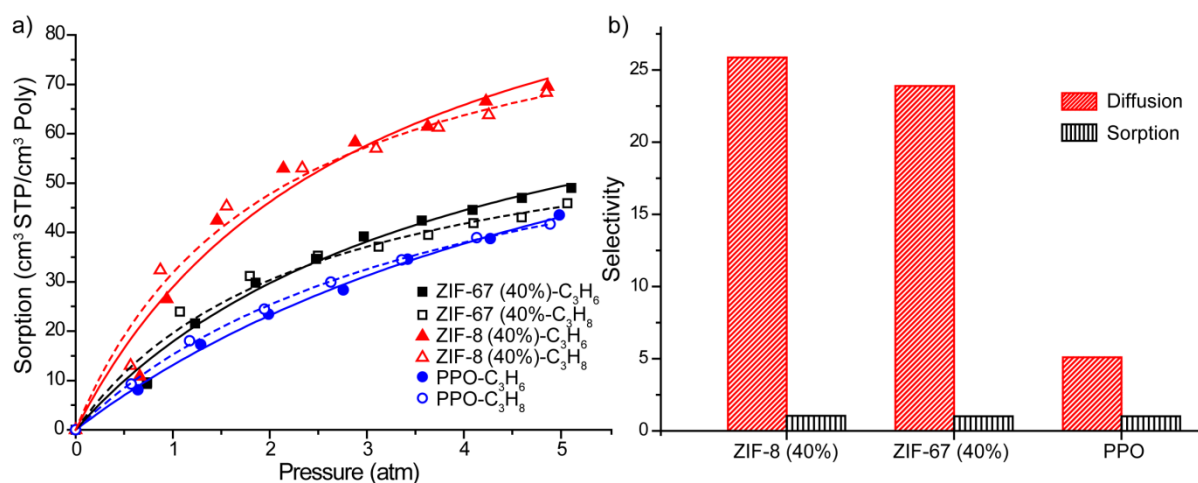


Figure 2.14 (a) Sorption isotherm, and (b) diffusion and sorption selectivity of PPO, ZIF-8@PPO-40 and ZIF-67@PPO MMMs

Table 2.3 Langmuir sorption parameter, sorption and diffusion coefficient of ZIF membrane

		C'_H	b	S	D
PPO	C_3H_6	100.97	0.149	8.732	0.400
	C_3H_8	75.35	0.252	8.528	0.078
ZIF-8@PPO-40	C_3H_6	88.16	0.254	9.59	1.599
	C_3H_8	67.08	0.412	9.05	0.061
ZIF-67@PPO-40	C_3H_6	111.5	0.353	14.30	1.085
	C_3H_8	95.78	0.496	14.08	0.045

2.2.2.3 Mixed gas performance

A single gas permeation analysis proved that ZIF-8 and ZIF-67-based MMMs are potential candidates for propane-propylene separation. A mixed gas analysis of 40% loaded MMMs was performed to investigate their viability for industrial application. Different feed compositions of propane and propylene were used, and the results are summarized in Figure 2.15. The separation factor is lesser than the ideal selectivity. It could be attributed to the competitive nature of the gas molecules and is a well-known phenomenon [49]. The separation factor was almost constant when the concentration of propylene in the feed was increased [21,44]. The maximum separation factor of ZIF-8@PPO and ZIF-67@PPO was 17.5 and 16.2, respectively. However, the permeability was enhanced when the propylene concentration in the feed was increased. At 70:30 (C_2H_6/C_3H_8) feed composition, the 40% loaded ZIF-8@PPO and ZIF-67@PPO showed permeability of propylene as ~ 11 barrer.

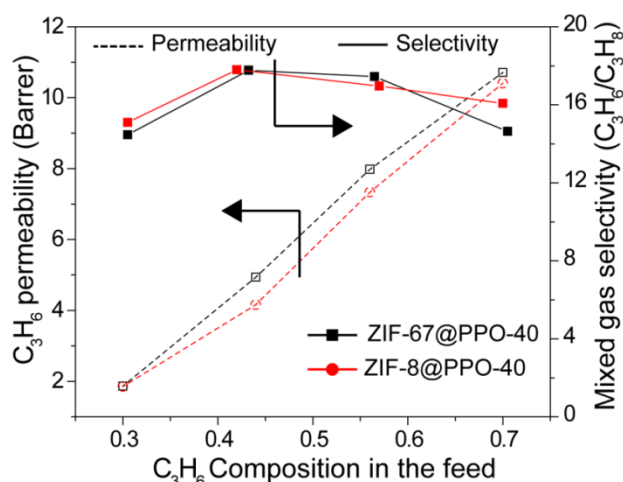


Figure 2.15 Mixed gas permeability and selectivity of ZIF-8@PPO-40 and ZIF-67@PPO-40 membranes at the different composition of C_3H_6 in feed

The performance of ZIF-8@PPO and ZIF-67@PPO MMMs was compared with the literature data (Robeson upper bound, Figure 2.16). The performance of the present ZIF@PPO-30/40 MMMs exceeded the 2008-upper bound, which is highly promising.

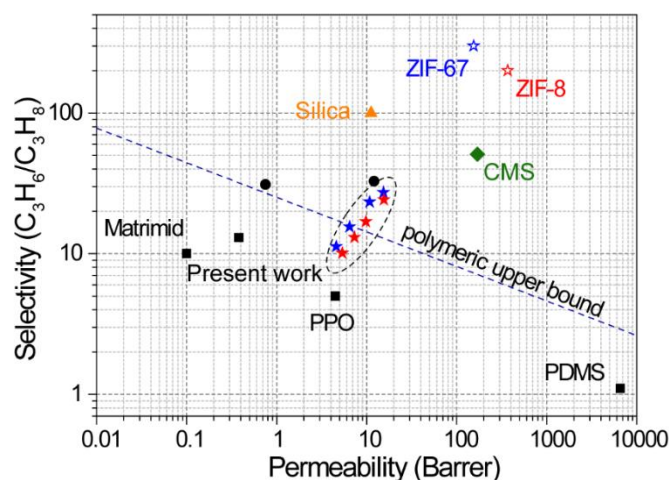


Figure 2.16 Appearance of present and reported membranes on empirical C_3H_6/C_3H_8 Robeson's upper bound; ★: ZIF-8@PPO, ★: ZIF-67@PPO and reported membranes (■: [4], ●: [44][49], ▲: [2], ◆: [50], ☆: [51] and ☆: [33])

2.3 Conclusions

This study successfully demonstrated that the interfacial compatibility of the polymer and ZIFs could be achieved by the selection of an appropriate functional polymer capable of providing ZIF-polymer interactions. The ZIF loading up to 40% in the PPO matrix was successfully achieved. The existence of polymer filler interactions was established by DSC thermogram and XPS analyses. The polymer-filler interactions led to uniform distribution of ZIF particles without agglomeration, even at higher (40%) loading. The gas sorption analysis revealed that the MMMs did not exhibit propylene and propane sorption selectivity. Thus, the gas permeation selectivity (ideal selectivity) is attributable only to the discriminating character of ZIFs between propylene and propane. The mixed gas analysis showed that the ZIF-8 and ZIF-67-based MMMs are potential candidates for propene-propane separation.

This study demonstrated that polymer filler compatibility plays a vital role in achieving the performance of MMMs. The present methodology of using ZIFs and host (PPO) as such does not need any filler or polymer modification. The gas permeation data reveals that the ZIF@PPO membrane possessed significant gas separation performance for C_3H_6/C_3H_8 , surpassing the Robeson upper bound and could be of commercial interest.

2.4 Experimental

2.4.1 Materials

The zinc nitrate hexahydrate ($\text{Zn}(\text{NO}_3)_2 \cdot 6\text{H}_2\text{O}$), cobalt nitrate hexahydrate ($\text{Co}(\text{NO}_3)_2 \cdot 6\text{H}_2\text{O}$), 2-Methylimidazole, chloroform, tetrachloroethane, methanol and toluene were purchased from Merck. Cupric chloride (CuCl_2), morpholine, and 2,6-dimethylphenol were procured from Sigma-Aldrich. The gases, viz., He, N_2 , O_2 were purchased from Ms. Vadilal Gases, while C_2H_4 , C_2H_6 , C_3H_6 , and C_3H_8 were procured from Delux Gas. All the chemicals were used without further purification.

2.4.2 Synthesis of polymer and ZIF nanoparticles

The ZIF-8 and ZIF-67 were synthesized by the reported method [44][52][53]. The synthesized nanoparticles were dispersed in chloroform and used to prepare mixed matrix membranes (MMMs).

2.4.2.1 Synthesis of polyphenylenoxide (poly(2,6-dimethyl-1,4-phenylene oxide), PPO)

The reported procedure of oxidative coupling was followed for the synthesis of PPO [54]. In a 500 ml three-necked round-bottomed flask, 20 g of 2,6-dimethylphenol (0.164 mol) and 10 ml of morpholine were added. To this mixture, 0.34 gm of CuCl_2 (0.00253 mol) and a toluene-ethanol mixture (160 ml+40 ml) were added. Oxygen gas was bubbled continuously into the stirred reaction mixture. After 6 hours, the reaction mixture was precipitated into methanol while stirring, filtered and washed thrice with methanol. The obtained polymer was air dried, followed by vacuum drying at 60 °C for 12 hours. It was further purified by dissolving in chloroform (4% w/v), filtering and reprecipitation in methanol. The precipitate was washed with methanol, oven dried at 60 °C for 8 hours, followed by vacuum drying at 60 °C for 3 days. The intrinsic viscosity $[\eta]$ of the obtained polymer, using tetrachloroethane as a solvent was determined using a Ubbelohde viscometer and was found to be 0.92 dL.g⁻¹.

2.4.2.2 Synthesis of ZIF-8

The ZIF-8 nanoparticles were synthesized by following the literature method [55]. A solution of 2-methylimidazole (16.22 g, 0.197 mol) was prepared in 500 ml of methanol. A separate solution of $\text{Zn}(\text{NO}_3)_2 \cdot 6\text{H}_2\text{O}$ (7.33 g, 0.024 mol) was prepared in 500 ml of methanol. The two solutions were mixed together and stirred for an hour. Thus obtained suspension was centrifuged and the sediment was collected. It was washed twice with 200 ml of methanol followed by once with 200 ml of chloroform. It was dispersed in 200 ml of chloroform while

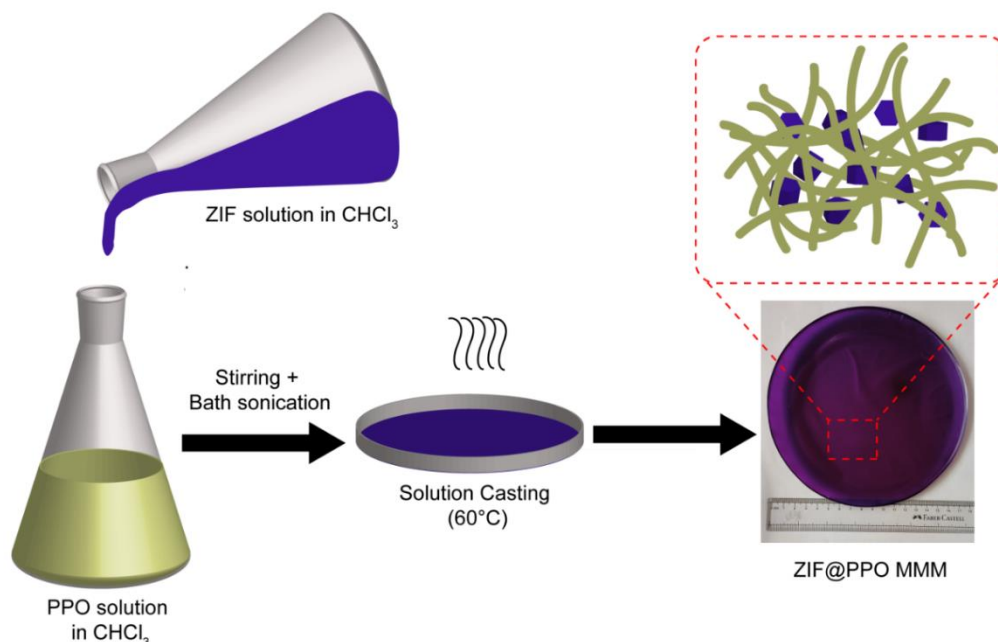
stirring; bath sonicated four times (10 min for each cycle, with an interval of 1 h, while stirring). The obtained suspension was stable for a minimum of 10 days. It was used as a stock suspension for making composite membranes.

2.4.2.3 Synthesis of ZIF-67

ZIF-67 was prepared according to the reported procedure [53]. A solution of cobalt nitrate hexahydrate ($\text{Co}(\text{NO}_3)_2 \cdot 6\text{H}_2\text{O}$, 16.25g) in methanol (500 ml) was added to a solution of 2-methylimidazole ($\text{C}_4\text{H}_6\text{N}_2$, 7.2 g) in 500 ml of methanol. The solution was stirred vigorously for 10 min, and purple crystals appeared immediately. This solution was centrifuged and washed with methanol two times, then washed with chloroform and dispersed in chloroform, as above. For the preparation of the composite membranes, this chloroform suspension of the respective ZIF was used.

2.4.3 Membrane fabrication

The dense membranes based on PPO were prepared by the solution casting method using 3% (w/v) chloroform solution at 40 °C for 12 h in a pre-leveled petri-dish placed in an oven. After 12 h, the membrane was peeled off from the petri dish. It was kept in a vacuum oven at 60 °C for seven days and then used for further characterization. The mixed matrix membranes (MMMs) were prepared by mixing an appropriate amount of ZIF dispersion in a prepared PPO chloroform solution, as schematically represented in Figure 2.1. It was stirred for 24 h with one-hour bath sonication and a six-hour interval. The homogeneously dispersed solution was poured into a petri dish at 40 °C for 12 h to make a membrane by solution casting method (Scheme 2.1). The PPO mixed matrix membranes (MMMs) were prepared with 10, 20, 30, and 40% loading of ZIFs (ZIF-8 and ZIF-67). In addition, 50% ZIF-loaded membranes were also fabricated by a similar method; however, the mechanical stability of the membranes was insufficient to carry out the permeation study. The membranes were designated as ‘ZIF@PPO-%ZIF’ (for example, ZIF-67@PPO-40 has a 40% loading of ZIF-67 in the PPO matrix). The membranes were dried in a vacuum oven at 60 °C for a week before using for further analysis.



Scheme 2.1 Solution casting of ZIF@PPO MMMs

2.4.4 Gas permeation and sorption analysis

The pure gas permeation analysis was conducted using a variable pressure method at a constant temperature of 35 °C [44] (Figure 2.17). The membranes used were dried in a vacuum oven at 60 °C for 7 days and samples of 12.5 cm² active area were used for permeation analysis (Figure 2.18). The vacuum on the permeate side was measured using an MKS vacuum transmitter, and the online data was collected with the help of LabVIEW software. The permeability coefficient, P_i of a given gas, is determined following Eq. 2.

$$P_i = \frac{dp}{dt} \frac{lV}{ART\Delta p} 10^{10} \quad (2)$$

where, 'dp/dt' is the slop of permeate pressure versus time, 'l' is the membrane thickness, 'Δp' is the transmembrane pressure, 'V' is the downstream volume, 'T' is the temperature, and 'A' is the membrane area. The ideal selectivity (α_{ij}) was calculated by calculating the ratio of pure gas permeability of the fast permeating component (P_i) to the slow permeating one (P_j).

$$\alpha_{ij} = \frac{P_i}{P_j} \quad (3)$$

The gas sorption isotherms were collected at 35 °C using the pressure decay method [44]. The data were collected using LabVIEW software, and the pressure was measured using WIKA pressure transmitter P-30. The sorption coefficient S_i is calculated using the following Eq. 4.

$$S_i = \frac{c_i}{p_i} \quad (4)$$

where, ' c_i ' is the gas uptake obtained from the sorption isotherm at pressure ' p_i '. The diffusion coefficient (D) of MMMs was calculated from the sorption (S) and permeability (P) coefficients.

$$D_i = \frac{P_i}{S_i} \quad (5)$$

The mixed-gas permeation experiments were performed for different feed compositions of propane and propylene at 50 psi as the feed pressure. The feed and permeate compositions were determined using gas chromatography equipped with an FID detector. The mixed gas permeability was calculated using the following Eq. 6.

$$P_i = \frac{y_i \frac{dy}{dx} IV}{x_i ART \Delta p} 10^{10} \quad (6)$$

where, x and y represent the mole fraction of a gas in the feed and permeate stream, respectively. The separation factor while feeding the gas mixture to the membrane was calculated using Eq. 7.

$$\alpha_{(i/j)} = \frac{y_i/y_j}{x_i/x_j} \quad (7)$$

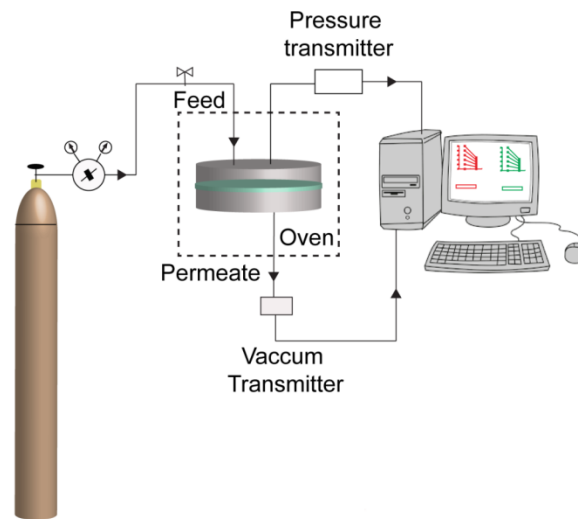


Figure 2.17 Variable pressure gas separation set-up

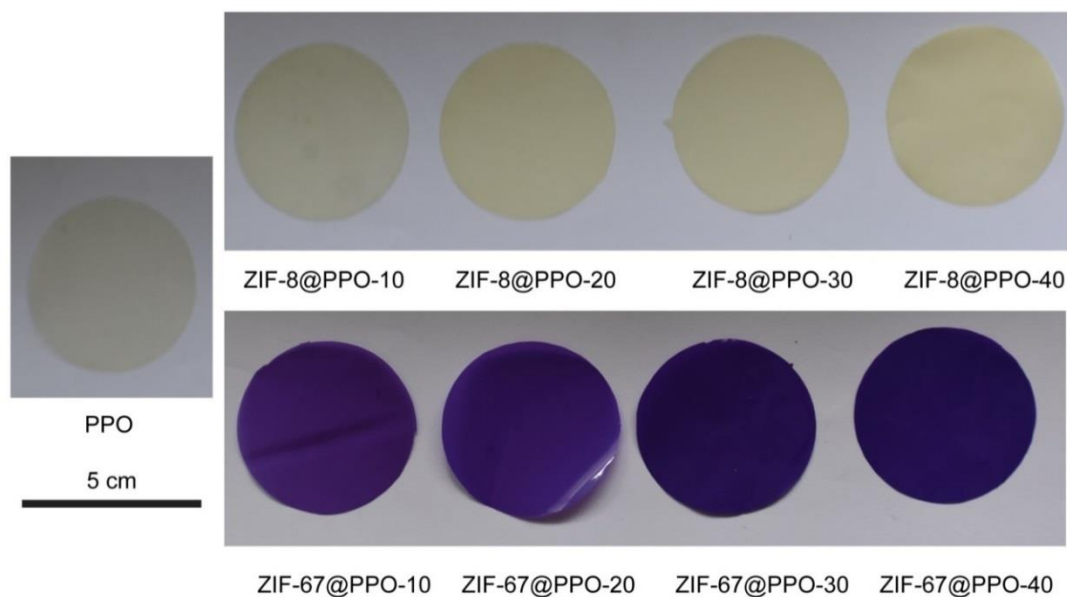


Figure 2.18 Digital photographic images of MMMs

2.4.5 Characterization methods

SEM images were obtained with an FEI, QUANTA 200 3D SEM. The ZIF samples for SEM analyses were prepared by the drop-cast method using methanol emulsion on a silicon wafer, while membrane cross-sectional samples were prepared by cryogenic fracturing in LN₂. The samples were sputtered with Au (nano-sized film) prior to imaging by an SCD 040 Balzers Union.

The TEM images were recorded using FEI Tecnai G2 F20 X-TWIN TEM at an accelerating voltage of 200 kV. The ZIF samples were prepared by the drop-cast sampling of methanol emulsion on a copper grid.

The X-ray photoelectron spectroscopy (XPS) measurements were performed on a Thermo K-alpha X-ray photoelectron spectrometer with an exciting source of Al-K- α with energy of 1486.6 eV. The electron flood gun was used for charge compensation. The binding energies obtained in the XPS analysis were corrected for specimen charging by referencing the C 1s to 284.60 eV.

The wide angle X-ray diffraction spectra were recorded on Rigaku Smart Lab Instrument with Cu-K α radiation at wavelength of 1.54 Å, in the 2 θ range of 2-50°.

The differential scanning calorimetry (DSC) thermograms were recorded by TA Q-100 analyzer at the heating rate of $10\text{ }^{\circ}\text{C min}^{-1}$ within a temperature range $50\text{--}300\text{ }^{\circ}\text{C}$ under N_2 atmosphere. These analyses were performed after preheating the samples at $250\text{ }^{\circ}\text{C}$.

The thermogravimetric analysis (TGA) was done on a PerkinElmer STA-6000 analyzer at a heating rate of $10\text{ }^{\circ}\text{C min}^{-1}$ under air atmosphere till $900\text{ }^{\circ}\text{C}$. The samples were preheated at $200\text{ }^{\circ}\text{C}$ before the analysis. The percentage of ZIF loading was calculated from the residual weight.

The density measurement of ZIFs and MMMs was done using Kruss Force Tensiometer K100 by the buoyancy of the sample immersed in the decaline. The density of 5 different samples was measured, and the average value is given in Table S3.

The dynamic light scattering (DLS) analysis was done using Brookhaven Zeta Potential analyzer using the dilute methanol suspension of ZIF samples.

2.5 References

- [1] R. Faiz, K. Li, Olefin/paraffin separation using membrane based facilitated transport/chemical absorption techniques, *Chem. Eng. Sci.* 73 (2012) 261–284. <https://doi.org/10.1016/j.ces.2012.01.037>.
- [2] M. Guo, M. Kanazashi, Recent progress in a membrane-based technique for propylene/propane separation, *Membranes* (Basel). 11 (2021). <https://doi.org/10.3390/membranes11050310>.
- [3] T.H. Lee, J.G. Jung, Y.J. Kim, J.S. Roh, H.W. Yoon, B.S. Ghanem, H.W. Kim, Y.H. Cho, I. Pinnau, H.B. Park, Defect Engineering in Metal-Organic Frameworks Towards Advanced Mixed Matrix Membranes for Efficient Propylene/Propane Separation, *Angew. Chemie.* (2021). <https://doi.org/10.1002/ange.202100841>.
- [4] R.L. Burns, W.J. Koros, Defining the challenges for $\text{C}_3\text{H}_6 / \text{C}_3\text{H}_8$ separation using polymeric membranes, 211 (2003) 299–309.
- [5] H.R. Amedi, M. Aghajani, Economic Estimation of Various Membranes and Distillation for Propylene and Propane Separation, *Ind. Eng. Chem. Res.* 57 (2018) 4366–4376. <https://doi.org/10.1021/acs.iecr.7b04169>.
- [6] A. Cadiou, K. Adil, P.M. Bhatt, Y. Belmabkhout, M. Eddaoudi, A metal-organic framework-based splitter for separating propylene from propane, *Science* (80-.). 353 (2016) 137–140. <https://doi.org/10.1126/science.aaf6323>.
- [7] D.S. Sholl, R.P. Lively, Comment, *Nature.* 532 (2016) 6–9.
- [8] J. Padin, R.T. Yang, New sorbents for olefin/paraffin separations by adsorption via π -complexation: Synthesis and effects of substrates, *Chem. Eng. Sci.* 55 (2000) 2607–2616. [https://doi.org/10.1016/S0009-2509\(99\)00537-0](https://doi.org/10.1016/S0009-2509(99)00537-0).

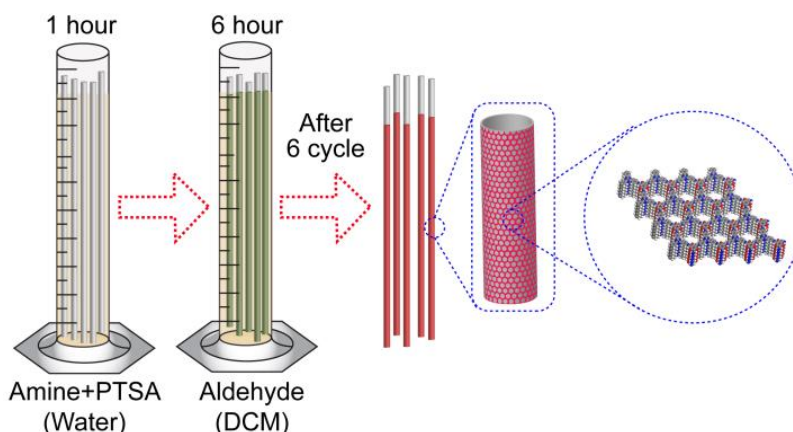
- [9] Z. Bao, S. Alnemrat, L. Yu, I. Vasiliev, Q. Ren, X. Lu, S. Deng, Adsorption of ethane, ethylene, propane, and propylene on a magnesium-based metal-organic framework, *Langmuir*. 27 (2011) 13554–13562. <https://doi.org/10.1021/la2030473>.
- [10] K. Tanaka, A. Taguchi, J. Hao, H. Kita, K. Okamoto, Permeation and separation properties of polyimide membranes to olefins and paraffins, *J. Memb. Sci.* 121 (1996) 197–207. [https://doi.org/10.1016/S0376-7388\(97\)00128-2](https://doi.org/10.1016/S0376-7388(97)00128-2).
- [11] R.W. Baker, Future directions of membrane gas separation technology, *Ind. Eng. Chem. Res.* 41 (2002) 1393–1411. <https://doi.org/10.1021/ie0108088>.
- [12] P. Bernardo, E. Drioli, G. Golemme, Membrane Gas Separation : A Review / State of the Art, (2009) 4638–4663.
- [13] G. Liu, V. Chernikova, Y. Liu, K. Zhang, Y. Belmabkhout, O. Shekhah, C. Zhang, S. Yi, M. Eddaoudi, W.J. Koros, Mixed matrix formulations with MOF molecular sieving for key energy-intensive separations, *Nat. Mater.* 17 (2018) 283–289. <https://doi.org/10.1038/s41563-017-0013-1>.
- [14] C. Staudt-bickel, W.J. Koros, Olefin / paraffin gas separations with 6FDA-based polyimide membranes, 170 (2000) 205–214.
- [15] T.H. Lee, M.G. Shin, J.G. Jung, E.H. Suh, J.G. Oh, J.H. Kang, B.S. Ghanem, J. Jang, J.H. Lee, I. Pinnau, H.B. Park, Facile suppression of intensified plasticization in glassy polymer thin films towards scalable composite membranes for propylene/propane separation, *J. Memb. Sci.* 645 (2022) 120215. <https://doi.org/10.1016/j.memsci.2021.120215>.
- [16] X. Ma, S. Williams, X. Wei, J. Kniep, Y.S. Lin, Propylene/Propane Mixture Separation Characteristics and Stability of Carbon Molecular Sieve Membranes, *Ind. Eng. Chem. Res.* 54 (2015) 9824–9831. <https://doi.org/10.1021/acs.iecr.5b02721>.
- [17] S.J. Kim, J.F. Kim, Y.H. Cho, S.E. Nam, H. Park, Y.I. Park, Aging-resistant carbon molecular sieve membrane derived from pre-crosslinked Matrimid® for propylene/propane separation, *J. Memb. Sci.* 636 (2021) 119555. <https://doi.org/10.1016/j.memsci.2021.119555>.
- [18] I.G. Giannakopoulos, V. Nikolakis, Separation of Propylene / Propane Mixtures Using Faujasite-Type Zeolite Membranes, (2005) 226–230.
- [19] Lloyd M. Robeson, Robeson.pdf, (2008) 390–400. <https://doi.org/10.1016/j.memsci.2008.04.030>.
- [20] H.B. Park, J. Kamcev, L.M. Robeson, M. Elimelech, B.D. Freeman, Maximizing the right stuff: The trade-off between membrane permeability and selectivity, *Science* (80-.). 356 (2017) 1138–1148. <https://doi.org/10.1126/science.aab0530>.
- [21] C. Zhang, Y. Dai, J.R. Johnson, O. Karvan, W.J. Koros, High performance ZIF-8/6FDA-DAM mixed matrix membrane for propylene/propane separations, *J. Memb. Sci.* 389 (2012) 34–42. <https://doi.org/10.1016/j.memsci.2011.10.003>.
- [22] H. Furukawa, K.E. Cordova, M. O’Keeffe, O.M. Yaghi, The chemistry and applications of metal-organic frameworks, *Science* (80-.). 341 (2013). <https://doi.org/10.1126/science.1230444>.

- [23] H. Hayashi, A.P. Côté, H. Furukawa, M. O’Keeffe, O.M. Yaghi, Zeolite A imidazolate frameworks, *Nat. Mater.* 6 (2007) 501–506. <https://doi.org/10.1038/nmat1927>.
- [24] M. O’Keeffe, O.M. Yaghi, Deconstructing the crystal structures of metal-organic frameworks and related materials into their underlying nets, *Chem. Rev.* 112 (2012) 675–702. <https://doi.org/10.1021/cr200205j>.
- [25] K.S. Park, Z. Ni, A.P. Côté, J.Y. Choi, R. Huang, F.J. Uribe-Romo, H.K. Chae, M. O’Keeffe, O.M. Yaghi, Exceptional chemical and thermal stability of zeolitic imidazolate frameworks, *Proc. Natl. Acad. Sci. U. S. A.* 103 (2006) 10186–10191. <https://doi.org/10.1073/pnas.0602439103>.
- [26] Rahul Banerjee, 1 Bo Wang Anh Phan, C. Knobler, H. Furukawa, M. O’Keeffe, O.M. Yaghi, High-Throughput Synthesis of Zeolitic, *ReVision.* 939 (2008) 939–944. <https://doi.org/10.1126/science.1152516>.
- [27] K. Li, D.H. Olson, J. Seidel, T.J. Emge, H. Gong, H. Zeng, J. Li, Zeolitic imidazolate frameworks for kinetic separation of propane and propene, *J. Am. Chem. Soc.* 131 (2009) 10368–10369. <https://doi.org/10.1021/ja9039983>.
- [28] S. Dangwal, A. Ronte, H. Lin, R. Liu, J. Zhu, J. Suk, H. Gappa-fahlenkamp, S. Kim, ZIF-8 membranes supported on silicalite-seeded substrates for propylene / propane separation, *J. Memb. Sci.* 626 (2021) 119165. <https://doi.org/10.1016/j.memsci.2021.119165>.
- [29] J. Hua, C. Li, H. Tao, L. Wang, E. Song, H. Lian, C. Wang, J. Jiang, Y. Pan, W. Xing, Improved C₃H₆/C₃H₈ separation performance on ZIF-8 membranes through enhancing PDMS contact-dependent confinement effect, *J. Memb. Sci.* 636 (2021) 119613. <https://doi.org/10.1016/j.memsci.2021.119613>.
- [30] H. Lian, Y. Yang, J. Chen, B. Bao, W. Yang, R. Hou, S. Ju, Y. Pan, Highly durable ZIF-8 tubular membranes via precursor-assisted processing for propylene/propane separation, *J. Memb. Sci.* 660 (2022) 120813. <https://doi.org/10.1016/j.memsci.2022.120813>.
- [31] E. Song, K. Wei, H. Lian, J. Hua, H. Tao, T. Wu, Y. Pan, W. Xing, Improved propylene / propane separation performance under high temperature and pressures on in-situ ligand-doped ZIF-8 membranes, *J. Memb. Sci.* 617 (2021) 118655. <https://doi.org/10.1016/j.memsci.2020.118655>.
- [32] S. Song, H. Jiang, H. Wu, M. Zhao, Z. Guo, B. Li, Y. Ren, Y. Wang, C. Ye, M.D. Guiver, G. He, Z. Jiang, Weakly pressure-dependent molecular sieving of propylene/propane mixtures through mixed matrix membrane with ZIF-8 direct-through channels, *J. Memb. Sci.* 648 (2022) 120366. <https://doi.org/10.1016/j.memsci.2022.120366>.
- [33] H.T. Kwon, H.K. Jeong, A.S. Lee, H.S. An, J.S. Lee, Heteroepitaxially Grown Zeolitic Imidazolate Framework Membranes with Unprecedented Propylene/Propane Separation Performances, *J. Am. Chem. Soc.* 137 (2015) 12304–12311. <https://doi.org/10.1021/jacs.5b06730>.
- [34] L. Xiang, L. Sheng, C. Wang, L. Zhang, Y. Pan, Y. Li, Amino-Functionalized ZIF-7 Nanocrystals: Improved Intrinsic Separation Ability and Interfacial Compatibility in Mixed-Matrix Membranes for CO₂/CH₄ Separation, *Adv. Mater.* 29 (2017) 1–8. <https://doi.org/10.1002/adma.201606999>.

- [35] L. Ma, F. Svec, Y. Lv, T. Tan, Engineering of the Filler/Polymer Interface in Metal–Organic Framework-Based Mixed-Matrix Membranes to Enhance Gas Separation, *Chem. - An Asian J.* 14 (2019) 3502–3514. <https://doi.org/10.1002/asia.201900843>.
- [36] Q. Xin, T. Liu, Z. Li, S. Wang, Y. Li, Z. Li, J. Ouyang, Z. Jiang, H. Wu, Mixed matrix membranes composed of sulfonated poly(ether ether ketone) and a sulfonated metal-organic framework for gas separation, *J. Memb. Sci.* 488 (2015) 67–78. <https://doi.org/10.1016/j.memsci.2015.03.060>.
- [37] N. Tien-Binh, H. Vinh-Thang, X.Y. Chen, D. Rodrigue, S. Kaliaguine, Crosslinked MOF-polymer to enhance gas separation of mixed matrix membranes, *J. Memb. Sci.* 520 (2016) 941–950. <https://doi.org/10.1016/j.memsci.2016.08.045>.
- [38] V.C. Putu Doddy Sutisna, Jingwei Hou, Hongyu Li, Yatao Zhang, Sutrisna.pdf, (2016) 266–279.
- [39] Z. Wang, D. Wang, S. Zhang, L. Hu, J. Jin, Interfacial Design of Mixed Matrix Membranes for Improved Gas Separation Performance, *Adv. Mater.* 28 (2016) 3399–3405. <https://doi.org/10.1002/adma.201504982>.
- [40] H. Li, L. Tuo, K. Yang, H.K. Jeong, Y. Dai, G. He, W. Zhao, Simultaneous enhancement of mechanical properties and CO₂ selectivity of ZIF-8 mixed matrix membranes: Interfacial toughening effect of ionic liquid, *J. Memb. Sci.* 511 (2016) 130–142. <https://doi.org/10.1016/j.memsci.2016.03.050>.
- [41] G. Yu, X. Zou, L. Sun, B. Liu, Z. Wang, P. Zhang, G. Zhu, Constructing Connected Paths between UiO-66 and PIM-1 to Improve Membrane CO₂ Separation with Crystal-Like Gas Selectivity, *Adv. Mater.* 31 (2019) 1–9. <https://doi.org/10.1002/adma.201806853>.
- [42] H. Wang, S. He, X. Qin, C. Li, T. Li, Interfacial Engineering in Metal-Organic Framework-Based Mixed Matrix Membranes Using Covalently Grafted Polyimide Brushes, *J. Am. Chem. Soc.* 140 (2018) 17203–17210. <https://doi.org/10.1021/jacs.8b10138>.
- [43] Y. Sun, L. Tian, Z. Qiao, C. Geng, X. Guo, C. Zhong, Surface modification of bilayer structure on metal-organic frameworks towards mixed matrix membranes for efficient propylene/propane separation, *J. Memb. Sci.* 648 (2022) 120350. <https://doi.org/10.1016/j.memsci.2022.120350>.
- [44] S.H. Kunjattu, V. Ashok, A. Bhaskar, K. Pandare, R. Banerjee, U.K. Kharul, ZIF-8@DBzPBI-BuI composite membranes for olefin/paraffin separation, *J. Memb. Sci.* 549 (2018) 38–45. <https://doi.org/10.1016/j.memsci.2017.11.069>.
- [45] K. Toi, G. Morel, D.R. Paul, Gas sorption and transport in poly(phenylene oxide) and comparisons with other glassy polymers, *J. Appl. Polym. Sci.* 27 (1982) 2997–3005. <https://doi.org/10.1002/app.1982.070270823>.
- [46] Y.S. Bhole, U.K. Kharul, S.P. Somani, S.C. Kumbharkar, Benzoylation of polyphenylene oxide: Characterization and gas permeability investigations, *Eur. Polym. J.* 41 (2005) 2461–2471. <https://doi.org/10.1016/j.eurpolymj.2005.03.026>.
- [47] B. Nagendra, A. Cozzolino, C. Daniel, P. Rizzo, G. Guerra, F. Auriemma, C. De Rosa, M.C. D’Alterio, O. Tarallo, A. Nuzzo, Two Nanoporous Crystalline Forms of Poly(2,6-

- dimethyl-1,4-phenylene)oxide and Related Co-Crystalline Forms, *Macromolecules*. 52 (2019) 9646–9656. <https://doi.org/10.1021/acs.macromol.9b01911>.
- [48] B.J. Story, W.J. Koros, Sorption and transport of CO₂ and CH₄ in chemically modified poly(phenylene oxide), *J. Memb. Sci.* 67 (1992) 191–210. [https://doi.org/10.1016/0376-7388\(92\)80025-F](https://doi.org/10.1016/0376-7388(92)80025-F).
- [49] X. Ma, R.J. Swaidan, Y. Wang, C. en Hsiung, Y. Han, I. Pinnau, Highly compatible hydroxyl-functionalized microporous polyimide-zif-8 mixed matrix membranes for energy efficient propylene/propane separation, *ACS Appl. Nano Mater.* 1 (2018) 3541–3547. <https://doi.org/10.1021/acsanm.8b00682>.
- [50] K.M. Steel, W.J. Koros, An investigation of the effects of pyrolysis parameters on gas separation properties of carbon materials, *Carbon N. Y.* 43 (2005) 1843–1856. <https://doi.org/10.1016/j.carbon.2005.02.028>.
- [51] S. Zhou, Y. Wei, L. Li, Y. Duan, Q. Hou, L. Zhang, L.X. Ding, J. Xue, H. Wang, J. Caro, Paralyzed membrane: Current-driven synthesis of a metal-organic framework with sharpened propene/propane separation, *Sci. Adv.* 4 (2018) 1–9. <https://doi.org/10.1126/sciadv.aau1393>.
- [52] J. Cravillon, S. Münzer, S.J. Lohmeier, A. Feldhoff, K. Huber, M. Wiebcke, Rapid room-temperature synthesis and characterization of nanocrystals of a prototypical zeolitic imidazolate framework, *Chem. Mater.* 21 (2009) 1410–1412. <https://doi.org/10.1021/cm900166h>.
- [53] X. Feng, M.A. Carreon, Kinetics of transformation on ZIF-67 crystals, *J. Cryst. Growth*. 418 (2015) 158–162. <https://doi.org/10.1016/j.jcrysgro.2015.02.064>.
- [54] Y.S. Bhole, P.B. Karadkar, U.K. Kharul, Nitration and amination of polyphenylene oxide: Synthesis, gas sorption and permeation analysis, *Eur. Polym. J.* 43 (2007) 1450–1459. <https://doi.org/10.1016/j.eurpolymj.2007.01.017>.
- [55] J. Cravillon, R. Nayuk, S. Springer, A. Feldhoff, K. Huber, M. Wiebcke, Controlling zeolitic imidazolate framework nano- and microcrystal formation: Insight into crystal growth by time-resolved in situ static light scattering, *Chem. Mater.* 23 (2011) 2130–2141. <https://doi.org/10.1021/cm103571y>.

In-situ, Interfacially synthesized, Scalable Covalent Organic Framework (COF) Hollow Fibre Membranes for Organic Solvent Nano-filtration



Abstract

Covalent organic frameworks have great potential for energy-efficient size-exclusion-based separations. However, it is challenging to implement COFs as an alternative membrane material because of the lack of a scalable and cost-effective fabrication methodology. Here we developed a new method for the fabrication of scalable, in situ COF hollow fiber membrane (HFM) by interfacial polymerization (IP) approach at ambient temperature. The 2D COF film constructed on polyacrylonitrile HF substrate from an aldehyde, 1,3,5-trimethylphloroglucinol (Tp) and two amines precursors, viz., 4,4'-azodianiline (Azo) and 4,4',4''-(1,3,5-triazine-2,4,6-triyl) trianiline (Tta). The resulting COF membrane on PAN HFM substrate exhibited 99% rejection of direct red-80 dye and remarkable solvent permeance. The precursor concentrations were optimized, and the performance of the resulting membranes was analyzed for permeation and solute rejection. The durability study reveals the stability of the membrane towards organic solvents. We also demonstrated the scalability feature of our new membrane fabrication approach. Finally, this method can facilitate industrially challenging molecular sieving applications using COF-based membranes.

3.1 Introduction

A substantial portion of the energy consumed in industry accounts for separating chemicals into pure form. Distillation accounts for 10-15 percent of the annual energy consumption [1–3]. Membrane-based separation can reduce energy consumption by replacing conventional heat-energy-based separations such as distillation, evaporation, and drying [1–4]. Organic solvent nanofiltration (OSN) is a rapidly growing technology in the chemical industry for organic solvent concentration, exchange, purification, and recovery [2,5,6]. Like other membrane processes, the viability of OSN in the industry is decided by permeability and selectivity. However, most of the OSN membrane reports are based on amorphous polymers such as polyimide, polyacrylonitrile (PAN) and poly(amide-imide), which lacks ordered pore channels; thus, it leads to limited permeance and selectivity[7]. The permeance of OSN membranes is generally enhanced by employing the thin-film composite (TFC)[2,6,8,9] membrane concept or by enhancing the free volume of the polymer [10–12]. Still, achieving a better permeability in the polymeric membrane without compromising the selectivity is challenging due to the permeability-selectivity trade-off relationship. In this regard, membranes based on porous crystalline materials, viz. zeolite, metal-organic frameworks (MOFs), and covalent organic frameworks (COF), have attained wide attention due to the precise sieving nature and high permeance [12–14]. Among these, covalent organic frameworks (COFs) can better function as a material for OSN membranes than the other two. COFs have nanometre (1-2 nm) range porosity, which is easily tailorable size. This aspect is lacking in zeolite, while chemical robustness is insufficient for MOFs [5].

COFs are crystalline porous polymers with periodically long-range order composed of rigid organic building units using covalent linkage [15–17]. Their tunable pore size, functionality, and thermochemical stability towards organic solvents acquired a particular interest in membrane fabrication [18–20]. Several 2D COFs are reported with pore sizes ranging from 1-2 nm, which are highly desired in fabricating OSN membranes [18,21]. Nonetheless, unlike polymers, the processability of COF materials is very poor. Poor processability restricts the fabrication of COF into self-standing film with desired mechanical stability and thin film composite film formation on porous support [22,23]. Self-standing COFs films are highly desired to achieve the advantage of COFs as a molecular sieving membrane. In an early report, Kanambeth et al. demonstrated for the first time a COF-based self-standing membrane by the

support method [19]. Later Dey et al. demonstrated a liquid-liquid interfacial way to fabricate COF thin film [20]. However, fabricating such crystalline material to a defect-free self-standing film with required mechanical stability is challenging while considering large-scale production. Remarkable attempts were made to make continuous COF films on different substrate surfaces, including inorganic and polymeric supports [24] by interfacial polymerization [2,8], solid-vapor interfacial polymerization [14] and polydopamine modulated synthesis [25,26] to overcome the mechanical stability issues.

Polymers can be built into hollow fiber morphology due to their excellent processability and mechanical strength [27]. Unlike polymers, the processability of porous crystalline materials is very poor, and engineering such material into morphologies, such as hollow fiber is complicated. Hollow fiber membranes can achieve a higher membrane area with low module volume [28]. The limited processability of crystalline porous polymers (COFs and MOFs) makes the fabrication of such material into hollow fiber (HF) membrane morphology challenging. Nair's group has reported a new methodology to fabricate molecular sieving MOF membranes on polymer hollow fiber support, referring to interfacial microfluid processing [27]. This study addresses the challenge of fabricating a thin film COF membrane on a polymeric HFM substrate. We report a methodology for achieving a 2D COF (Tp-Azo and Tp-Tta) on Polyacrylonitrile (PAN) HFM substrate through interfacial synthesis. We demonstrated the protocol with two different imine-based COFs, viz., Tp-Azo and Tp-Tta, having pore sizes of 26 and 14 Å, respectively (Figure 3.1). The rationale behind selecting PAN substrate was their overall organic solvent stability and the compatibility of COFs with polymer substrate [29]. The key features of our methods are i) In-situ synthesis of COF film ii) two solvent-based interfacial room temperature fabrication by dip-coating iii) the concentration of the monomer solution can vary the thickness of the membrane iv) at a time large-scale production is possible.

3.1.1 Scope and Objectives

This work introduced a new methodology to fabricate COF thin film membranes for organic solvent nano filtration. Compared to the polymeric membrane, the COF thin film membrane has the advantage of better solvent stability, pore size modification by linker size and functionality, and a better trade-off between selectivity and permeability. Two different imine based COFs were chosen, while PAN was selected as a substrate to offer better compatibility with COFs.

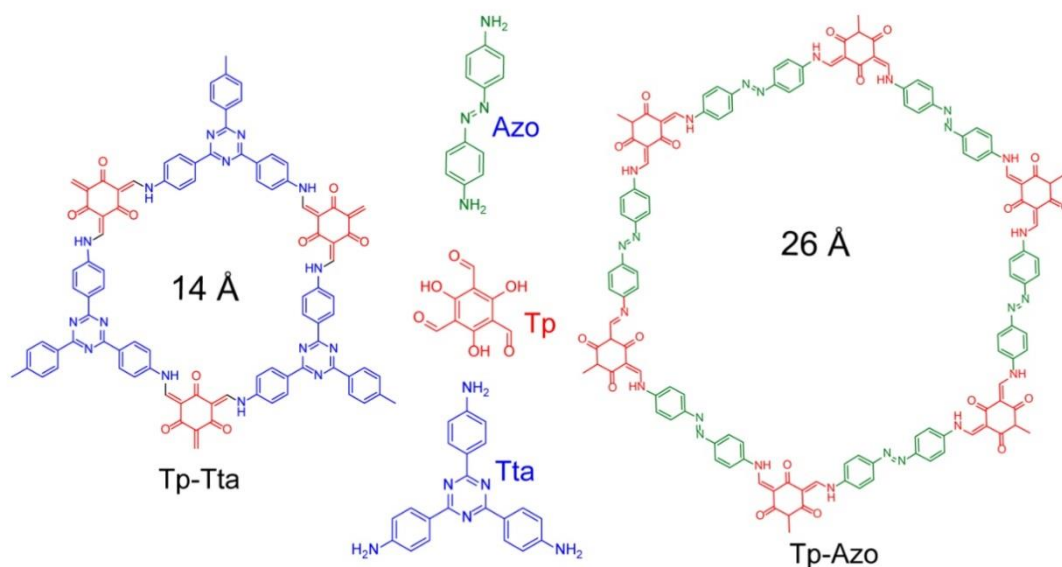


Figure 3.1 Structures of COFs: Tp-Tta and Tp-Azo

The critical objectives of the present work are as follows

- ❖ Fabrication of imine-based COF thin film composite membrane on PAN-HFM substrate by interfacial synthesis
- ❖ Optimization of the precursor concentration for the interfacial synthesis of COF on PAN surface
- ❖ Characterizations of the COF membranes
- ❖ OSN performance evaluation and durability study of resulting membranes.

3.2 Results and Discussion

3.2.1 Membrane fabrication and characterizations

The membranes (Tp-Tta and Tp-Azo) were fabricated on the substrate surface by an in-situ IP process. The Schiff base reaction starts on the PAN substrate surface while dipping in the Tp solution after soaking the Amine+PTSA solution (Figure 3.2). The interaction of amine with the PAN helps to initiate the nucleation on the substrate surface. To understand the interaction between protonate amine and PAN surface, we have carried out Fourier Transform Infrared (FTIR) spectroscopy of PAN-HF and dipping in amine+PTSA solution. The absence of OH stretching frequency in the spectra of amine-dipped fiber indicates that the free acid moiety present in the PAN substrate surface reacts with the amine-PTSA salt (Figure 3.3). PTSA, a co-reagent that binds with amine reversibility, helped attain crystallinity. The Tp-Tta and Tp-Azo

membranes showed yellow and red color, respectively. The color intensity enhanced with the precursor solution concentration (Figure 3.2).

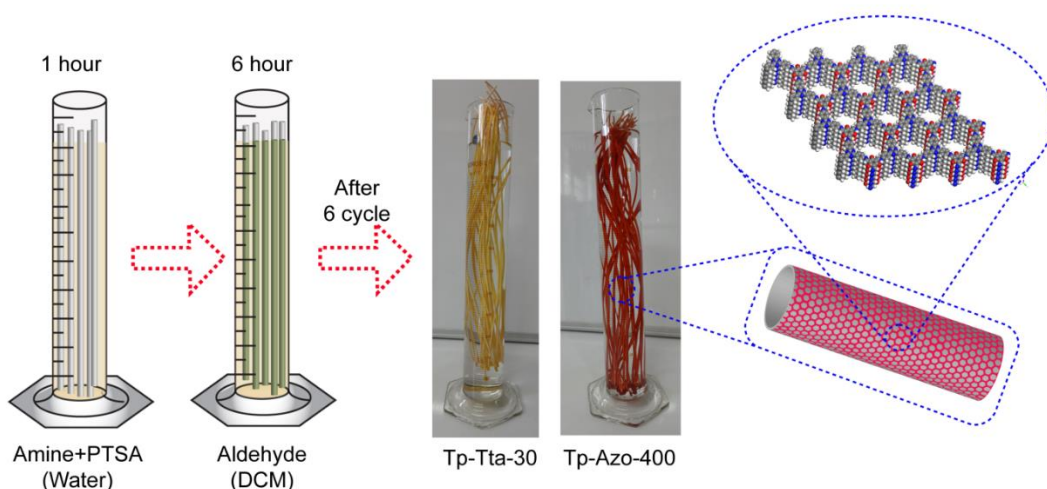


Figure 3.2. Schematics of interfacially synthesized COF thin film layer on HFM

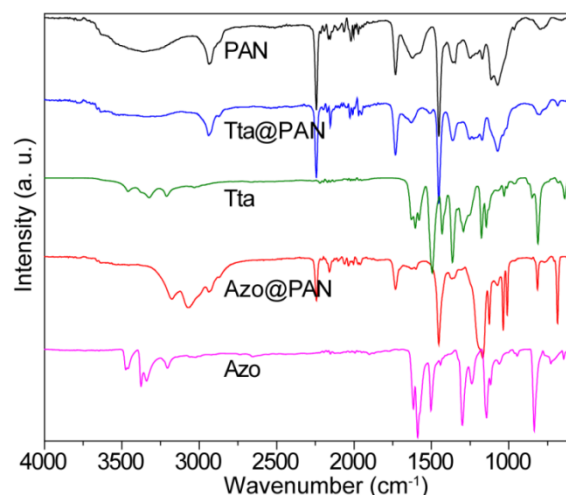


Figure 3.3 IR spectra showing the PAN-amine interactions

In addition to color change, the thin-film membrane showed a significant morphological difference with precursor solution concentration. The scanning microscopic images reveal that the COF particle on the substrate showed bead-like morphology up to Tp-Tta-60. Beyond that, for Tp-Tta-120 and Tp-Tta-480, rod morphology could be observed (Figure 3.4 and 3.5). The higher magnification SEM images showed that rods were formed by aggregation of small COF particles. The cross-sectional microscopic images revealed that the COF layer was continuous on the outer surface of the PAN-HFM (Figure 3.6). The intensity of color varied with the concentration of precursor solution. This stipulated that the membrane thickness can be

controlled by varying the thickness. In the case of the Tp-Azo membrane, slight growth was observed inside the polymer layer on the outer edge of the HFM. It could have happened in the initial stages of the synthesis, as the COF layer formed on the HFM surface would restrict the percolation of monomer further inside the bulk of the HFM. The cross-sectional SEM imaging of the COF-HF membrane was carried out to determine the thickness of the thin film. The images revealed that though there was a thin film formation on the outer surface of the HFM, a clear boundary to separate the COF layer from the PAN substrate was nondetectable (Figure 3.6). Further, atomic force microscopy (AFM) was carried out using COF thin film separated from the PAN substrate (by dissolving the PAN layer in *N,N*-dimethylformamide). The height analysis of the thin-film was cast on a silicon wafer showed a thickness of ~ 120 and 20 nm for Tp-Azo-800 and Tp-Tta-120, respectively (Figure 3.7). A separate thin film could not be recovered after dissolving substrate in DMF for the membranes fabricated using lower precursor concentrations (less than $800 \mu\text{M}$ and $120 \mu\text{M}$ for Tp-Azo and Tp-Tta, respectively).

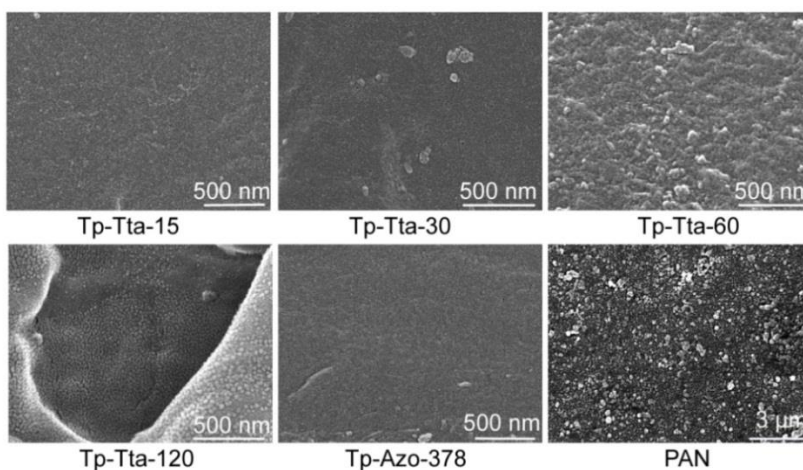


Figure 3.4 Surface SEM images of COF thin-film HFM

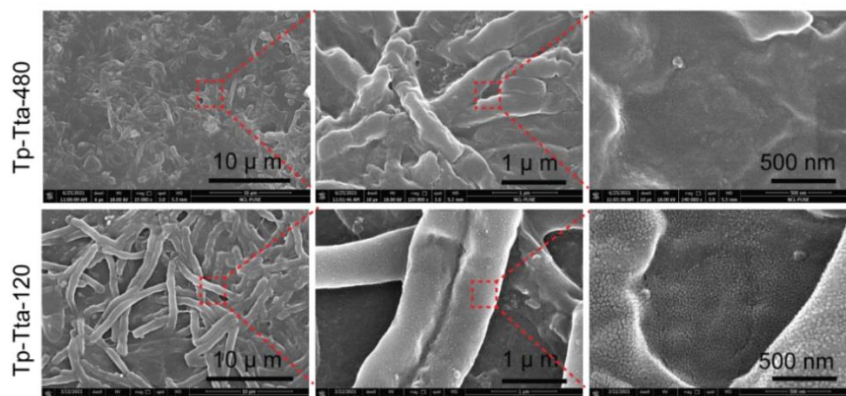


Figure 3.5 SEM images of Tp-Tta-120 and Tp-Tta-240 showing rod-like morphology

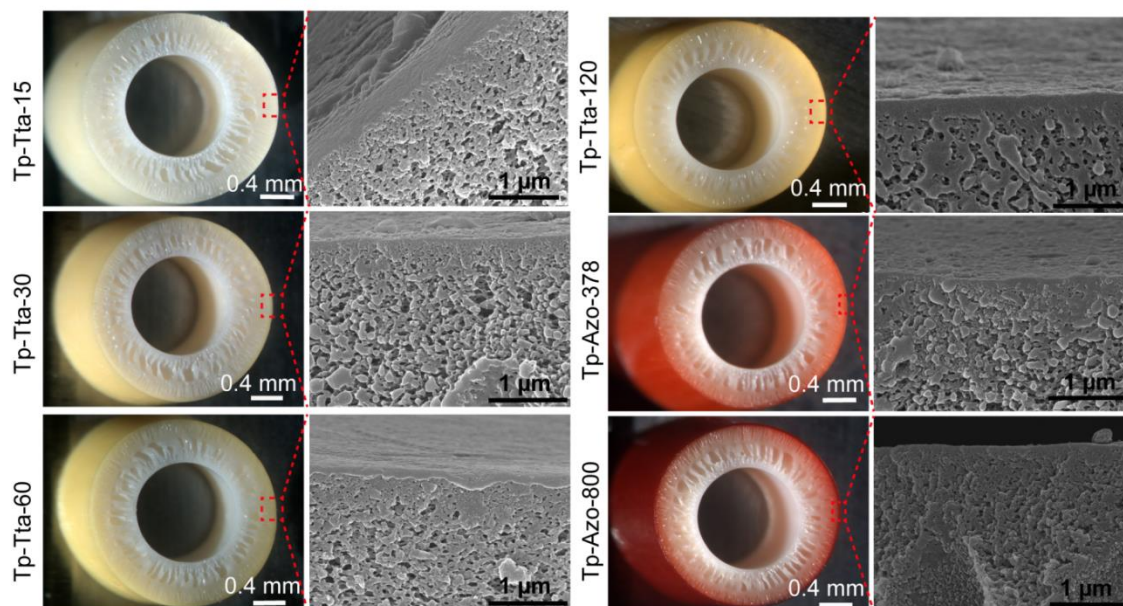


Figure 3.6 Stereomicroscopic images and SEM images of COF thin-film HFM

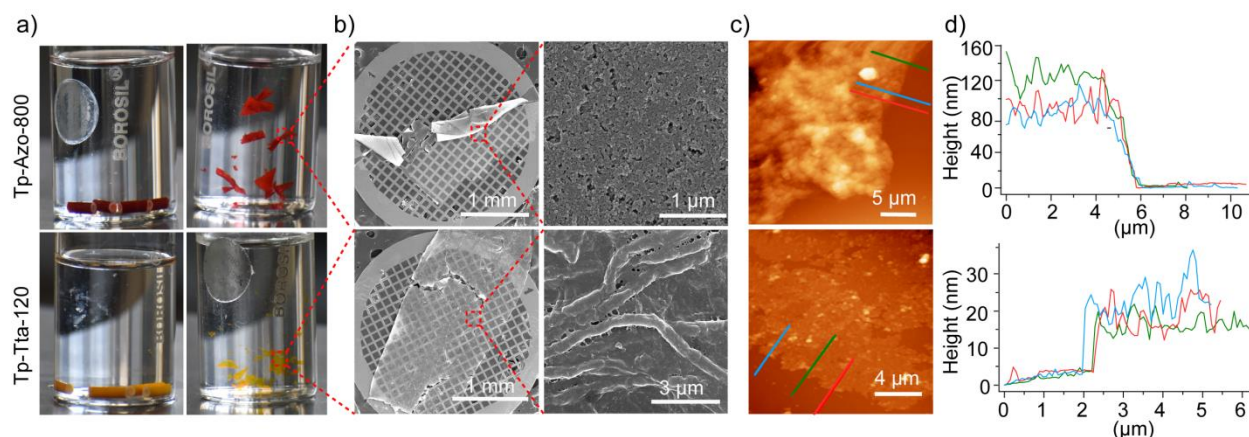


Figure 3.7 a) photographic images of COF thin-film HFM before and after removing the PAN substrate, b) SEM images, c) AFM images of COF thin films after removing the PAN substrate, d) height profile of COF thin films

The crystalline nature of COF membranes was investigated using powder X-ray diffraction (PXRD). The thin film HFM did not show any characteristic peak of COFs even at a higher precursor concentration (Tp-Tta 480 and Tp-Azo-800) (Figure 3.8). It is due to the low COF to PAN ratio. The PAN layer was removed by dissolving it in *N,N*-dimethylformamide (DMF) to get a sufficient COF sample. The undissolved COF thin films were separated using centrifugation and washed twice with DMF, followed by acetone. These separated COF films showed an intense high peak at 2θ value of 3.2° for Tp-Azo and a distinct peak 2θ value of 5.8° for Tp-Tta. They correspond to the 100 planes of the COF. The peaks at 2θ values of 17° and 26°

were attributed to the PAN and 001 planes of the COF, respectively (Figure 3.9). The presence of PAN peak, even after three-time washing using the DMF confirms that COF interacts strongly with the PAN substrate.

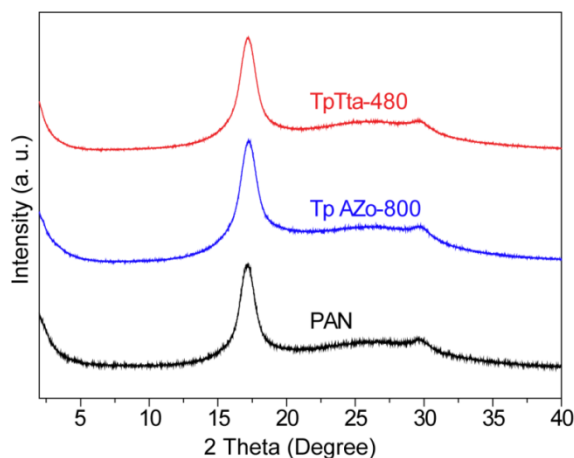


Figure 3.8 PXRD pattern of COF thin film HF membrane

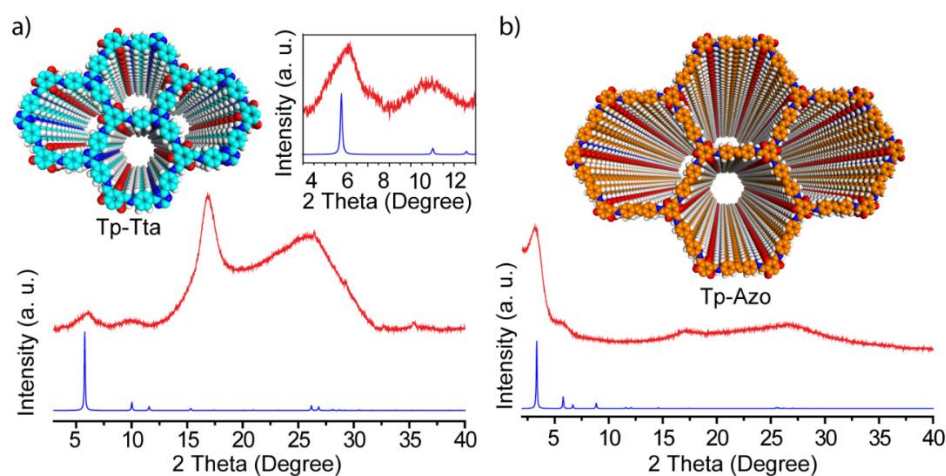


Figure 3.9 PXRD pattern of Tp-Azo (a) and Tp-Tta (b) thin-film membrane

The formation of COF membrane over PAN HFM substrate was further characterized by FTIR (Figure 3.10,3.11) and C^{13} NMR spectroscopy (Figure 3.12). The FTIR spectra of COF membrane showed characteristic peaks of PAN and the COF. The COF peaks matched well with the previously reported data. The characteristic stretching bands of $-C-N-$, $-C=C-$ and $-C=O$ were visible at 1279, 1516 and 1579 cm^{-1} for Tp-Tta. For Tp-Azo, these bands were observed at 1252, 1577 and 1619 cm^{-1} . This indicates the β -ketoenamine nature of the framework structure (Figure 3.10 and 3.11). The solid-state C^{13} NMR of the COF was carried out using the sample after removing the PAN layer, as explained above. The characteristic peak at ~ 183 ppm and 107

ppm reveals the presence of carbonyl (-C=O) and exocyclic (-C=C) carbon atoms. The spectra of Tp-Tta showed a peak at 169 ppm corresponding to the carbon atom present in the triazine ring (Figure 3.12).

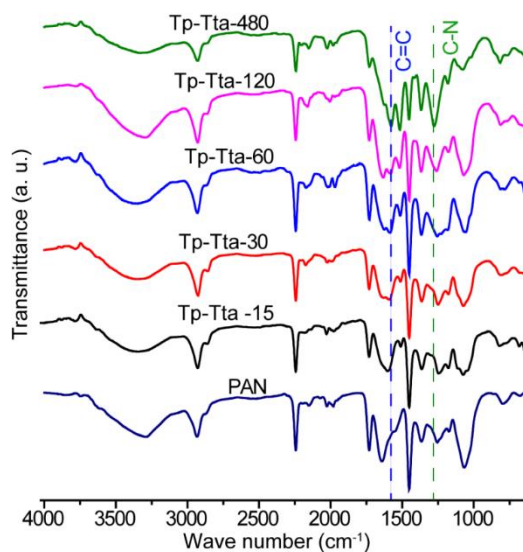


Figure 3.10 FTIR spectra of Tp-Tta thin-film HF membrane

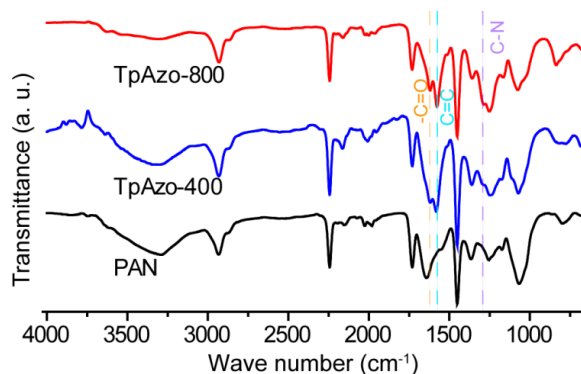


Figure 3.11 FTIR spectra of Tp-Azo thin-film HF membrane

The X-ray photoelectron spectroscopy reveals the surface elemental composition of the thin film HFM. Compared to the PAN substrate, the thin film membranes showed a lower C/N ratio, confirming the COF layer formation on the PAN substrate (Figure 3.13). As compared to the PAN, both the COFs have a higher C/N percentage. The C/N ratio is inversely related to the precursor concentration. It indicates that the thickness of the membrane varies with the concentration of the precursor solution used for the membrane fabrication. The deconvoluted C1s spectra showed three different peaks corresponding to C=O , C=N and C=C carbon (Figure 1.14). The thermal stability of the COF membrane was evaluated using thermo-gravimetric

analysis under N₂ atmosphere. The PAN and COF thin film membranes started degradation at ~ 300 °C (Figure 1.15). The membranes were immersed in different solvents viz., methanol, *n*-propanol, isopropanol, acetone, ethanol, tetrahydrofuran, and toluene for seven days at room temperature to assess solvent resistance. The membranes were found to be stable since there was no coloration of the solvent. Further, the FTIR spectra of membranes kept for seven days in solvent matched well with the fabricated membrane, indicating the solvent stability of COF@PAN HFMs (Figure 1.16).

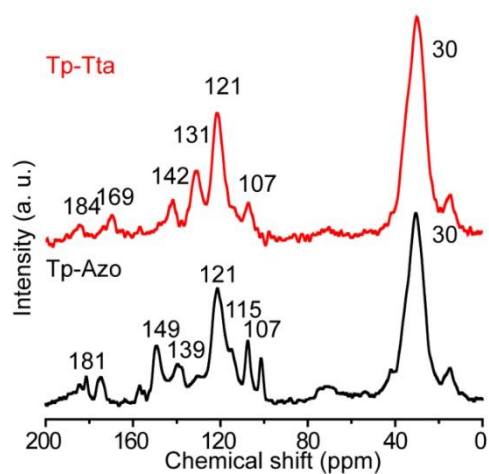


Figure 3.12 C¹³ NMR spectra of thin-film membrane

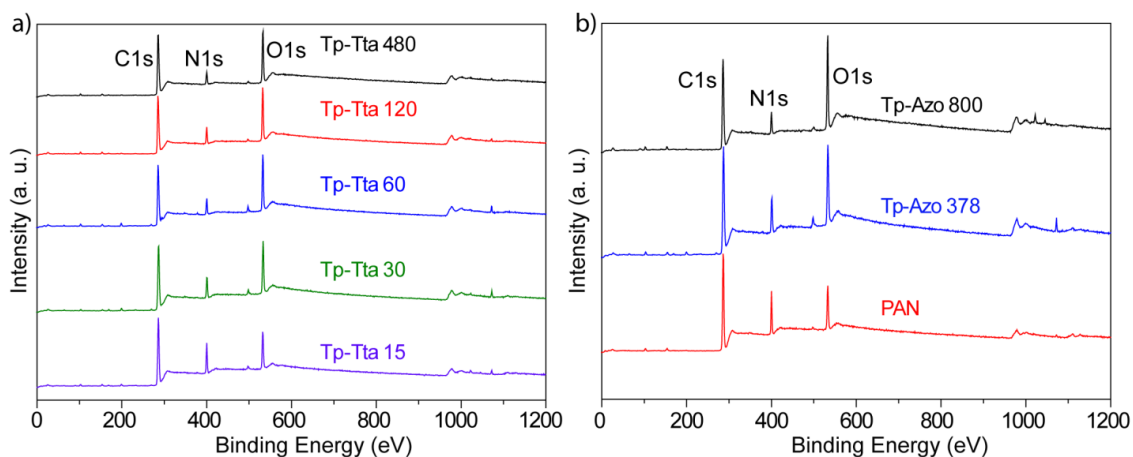


Figure 3.13 XPS survey of (a) Tp-Tta and (b) Tp-Azo thin film HF membrane

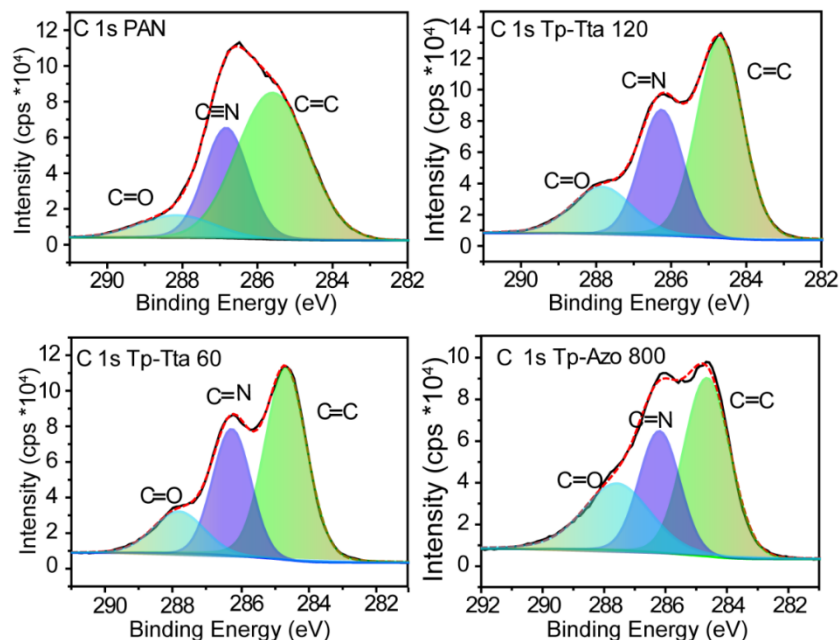


Figure 3.14 High-resolution C1s XPS pattern of COF thin-film HF membrane

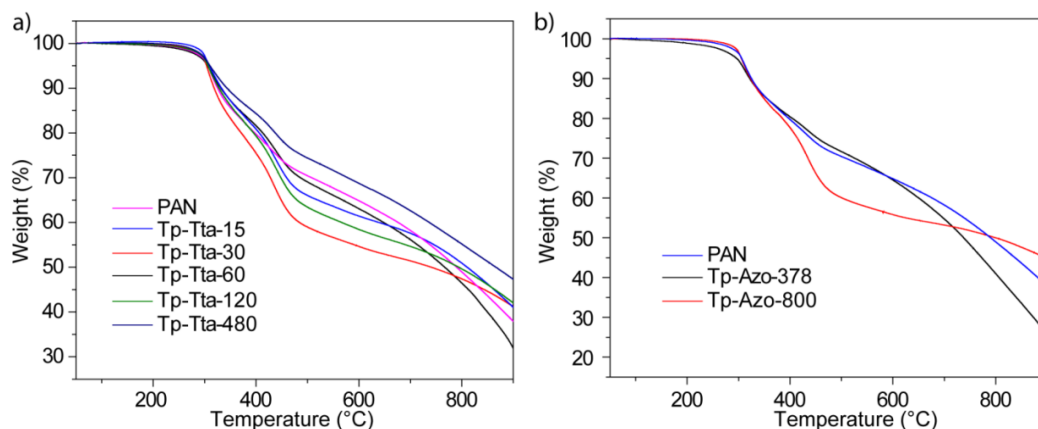


Figure 3.15 TGA thermogram of Tp-Tta (a) and Tp-Azo (b) thin film HF membrane

The wettability of the PAN substrate and COF membranes was obtained using the sessile drop method and Wilhelmy plate method (Figure 3.17,3.18). The data obtained from both methods do not match each other but follow the same trend. The water contact angle of COF thin-film membranes showed hydrophobic nature as compared to the PAN substrate. It is due to the presence of a benzene ring in the COF structure. The increment in the water contact angle with respect to precursor concentration used for IP further substantiates the thickness variation. The Tp-Tta-480 membrane showed water contact angles of 73° and 95° by sessile drop and Wilhelmy plate method, respectively. The Tp-Tta showed a higher contact angle than that of Tp-Azo, which might be due to its higher benzene ring density.

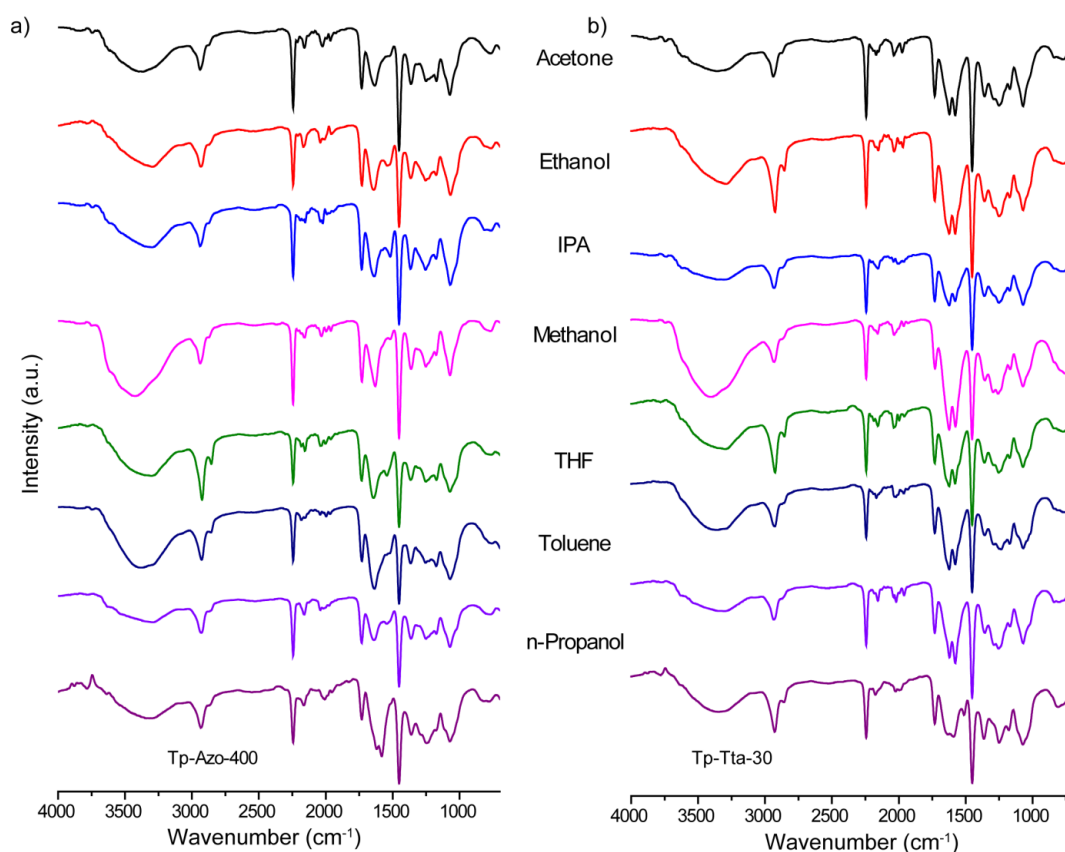


Figure 3.16 IR spectroscopy of Tp-Azo-400 (a) and Tp-Tta-30 (b) membranes after keeping them in the corresponding solvent for seven days.

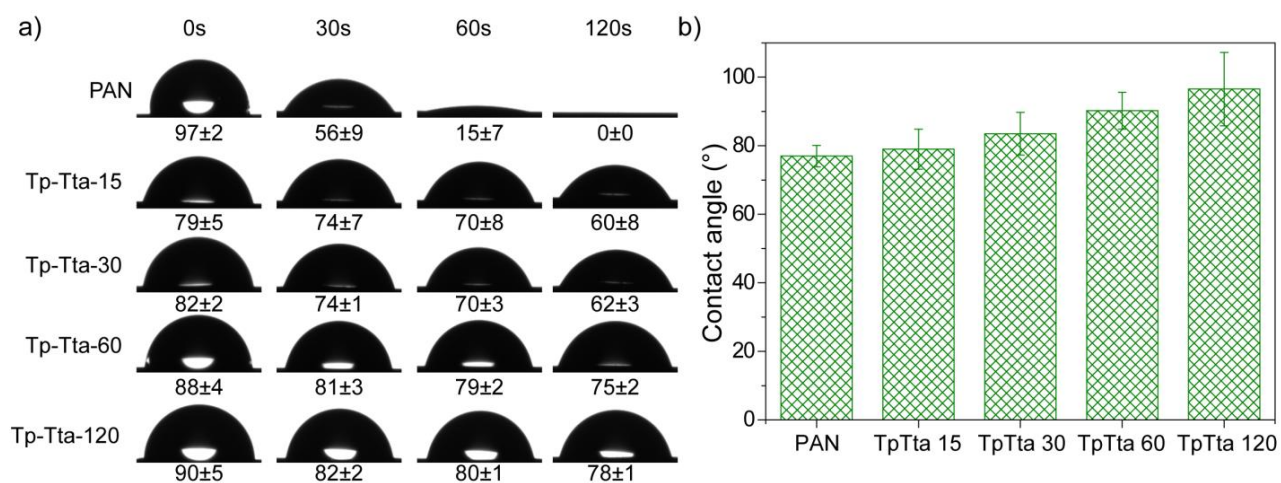


Figure 3.17 Contact angle of Tp-Tta thin film HFM by a) sessile drop method and b) wilhelmy plate method

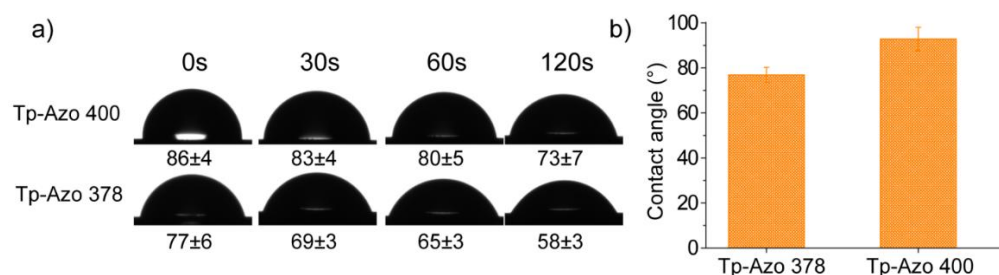


Figure 3.18 Contact angle of Tp-Azo thin film HF membrane by a) sessile drop method and b) wilhelmy plate method

3.2.2 Nanofiltration performance analysis

The hollow fiber membrane modules were prepared to study the separation performance. The housing was PVC or stainless steel pipe. The potting was done using epoxy resin. The permeation study of pure organic solvent and water was conducted at 1.5 bar pressure. A total of six solvents were selected for the permeation study, viz., tetrahydrofuran (THF), methanol, acetone, isopropanol and *n*-propanol. The Tp-Tta-15, Tp-Tta-30 and Tp-Azo-400 membranes were chosen for the permeation analysis (Figure 3.18, Table 3.1). For a given membrane, THF showed the highest permeance. The permeance was found to decrease with the solvent viscosity. A relation between the molecular size of the solvent and its permeance was not seen. To study the effect of precursor concentration on the permeation, the methanol and acetone permeation of Tp-Tta membranes was carried out (Figure 3.19). The Tp-Tta membrane fabricated at a lower precursor concentration (Tp-Tta-15) showed the highest solvent permeance. As the precursor concentration increased, the permeance decreased as anticipated. It validated the control of membrane thickness by varying the precursor concentration.

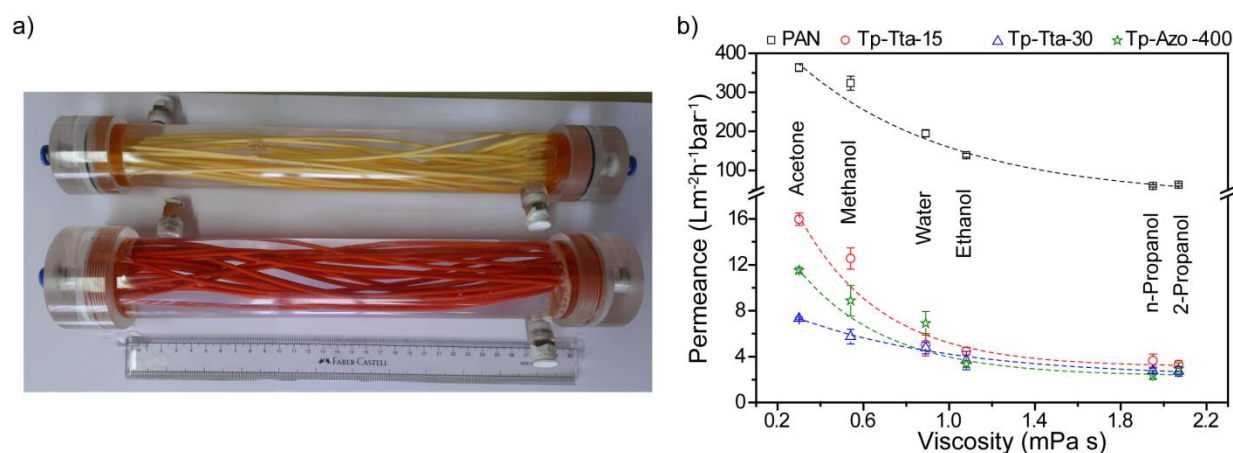


Figure 3.19 a) Photograph of HF module, b) pure solvent permeance of COF thin film HFMs

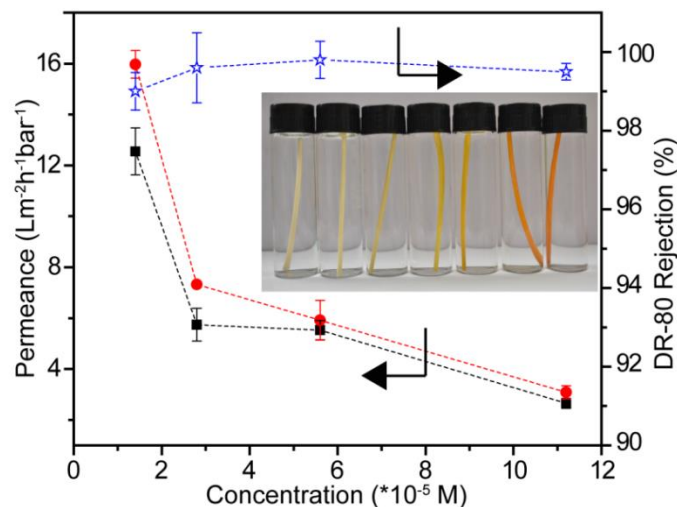


Figure 3.20 Acetone and methanol presence and direct-80 rejection of Tp-Tta thin film HFM as a function of the concentration of precursor solution. Inset: photograph showing the color intensity variation with precursor concentration

Table 3.1 Pure solvent permeance ($\text{Lm}^{-2}\text{h}^{-1}\text{bar}^{-1}$) of Tp-Tta and Tp-Azo thin film HFM

Solvent	Solvent permeance ($\text{Lm}^{-2}\text{h}^{-1}\text{bar}^{-1}$)			
	Tp-Tta-15	Tp-Tta-30	Tp-Azo-400	PAN
Tetrahydrofuran	16.5		10.5	411
Acetone	16	7.3	11.5	363
Methanol	12.5	5.7	8.8	323
Water	5	4.7	6.9	195
Ethanol	4.4	3.6	3.35	139
n-propanol	3.6	2.7	2.36	60
Isopropanol	3.3	2.7	2.92	63

We characterized the rejection performance of the membrane by using different dye molecules. The dye molecules used in this study for rejection analysis were Brilliant Blue (BB), Congo red (CR), direct red-23(DR-23) and direct red-80 (DR-80) (Figure 3.21, Table 3.2) (Figure 3.22, 3.23, 3.24). As compared to the PAN substrate, the COF membrane showed excellent rejection performance. The DR-80 showed 99% rejection for both Tp-Azo and Tp-Tta membranes. This is due to the large size of the dye as compared to the pore size of COFs. For a given membrane, the percentage rejection decreased in the order: DR-80>DR-23>CR>BB. The rejection performance of the Tp-Tta membranes improved with the precursor solution concentration. The Tp-Tta-120 membrane showed >90% rejection for CR, DR-23 and DR-80, which is attributed to the staggering pores resulting from the aggregation of COF particles. It further showed the advantage of the current fabrication methodology, i.e., reasonable control

over the membrane thickness by the membrane performance. To substantiate the relationship between the percentage rejection and molecular size of the dye molecule used for rejection analysis, the molecular diameter using Density Functional Theory (DFT) was calculated (Figure 3.25, Table 3.3). The results showed a good agreement between the experimental rejection performance and the molecular diameter calculated from the DFT calculation.

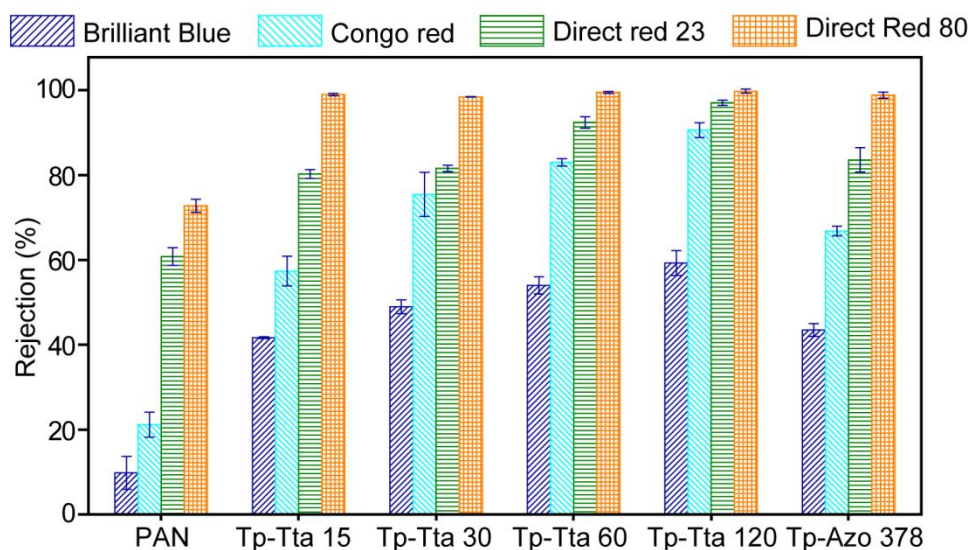


Figure 3.21 Organic solvent nanofiltration performance of COF thin film HFM

Table 3.2 Nanofiltration performance of Tp-Tta and Tp-Azo thin film HFM in comparison to the PAN substrate

Dye	Brilliant Blue (BB)	Congored (CR)	Directred-23 (DR-23)	Directred-80 (DR-80)
Molecular mass (g/mol)	854	697	814	1379
Solvent	Methanol	Methanol	Methanol	Methanol
% Rejection for Tp-Tta-15	41.6	57.3	80.2	98.5
% Rejection for Tp-Tta-30	48.9	75.4	81.9	98.46
% Rejection for Tp-Tta-60	54.5	83	92.4	99.5
% Rejection for Tp-Tta-120	59.2	90.6	97	99.8
% Rejection for Tp-Azo-400	43.4	66.8	83	98.8
% Rejection for PAN	9.8	21.1	60.1	72.8

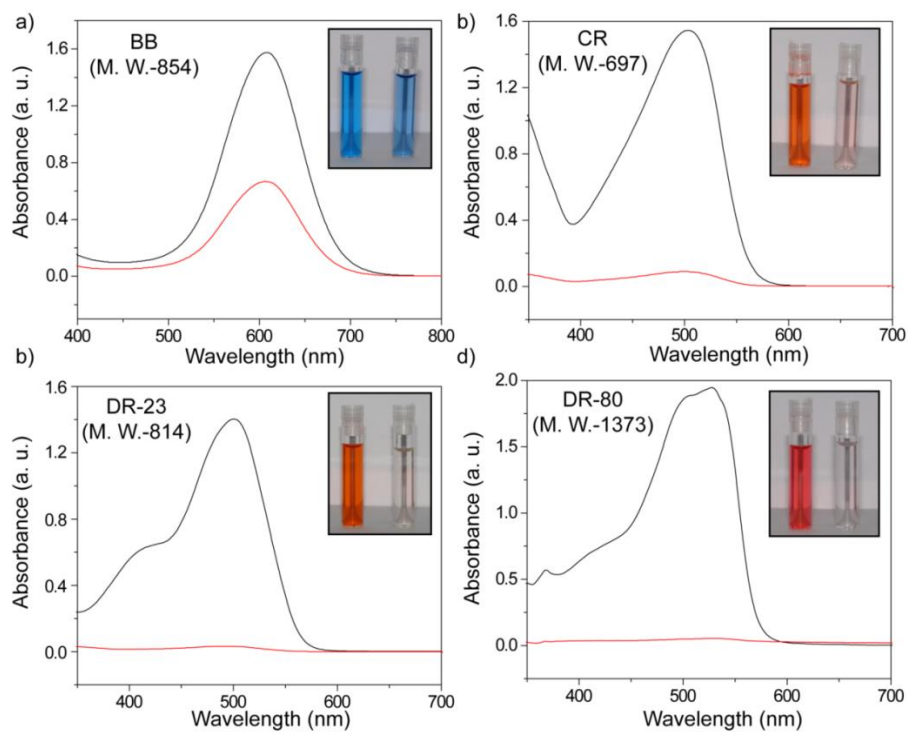


Figure 3.22 UV-visible spectra showing the concentration of dye molecule a)BB b) CR c) DR-23 and d) DR-80 in the feed and permeate after passing through Tp-Tta-120 membrane

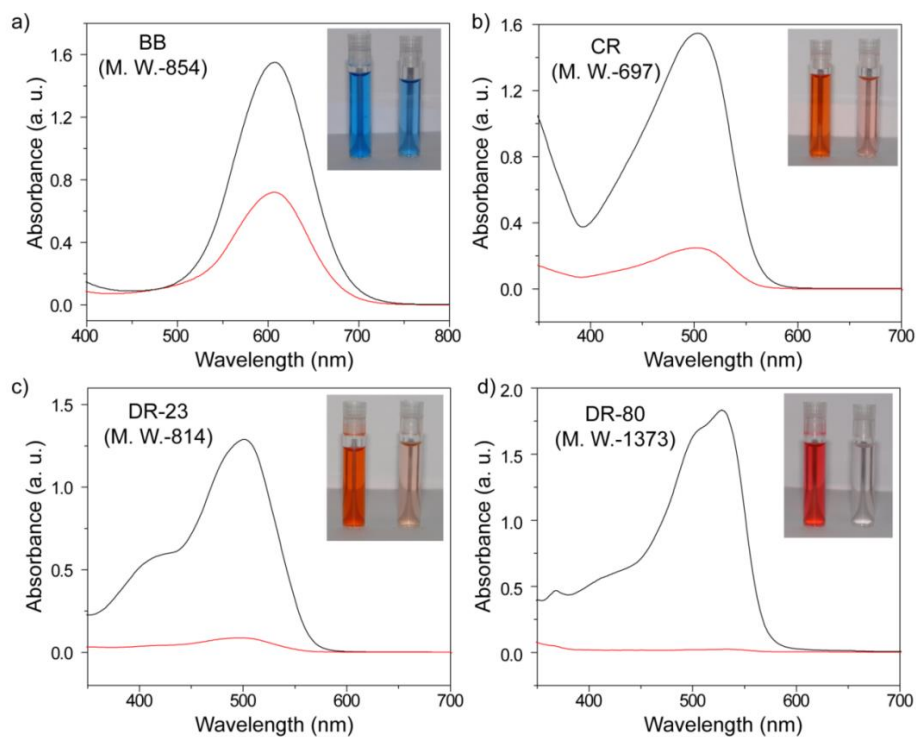


Figure 3.23 UV-visible spectra showing the concentration of dye: a) BB, b) congo red, c) DR-23 and d) DR-80 in the feed and permeate after passing through Tp-Tta-60 membrane

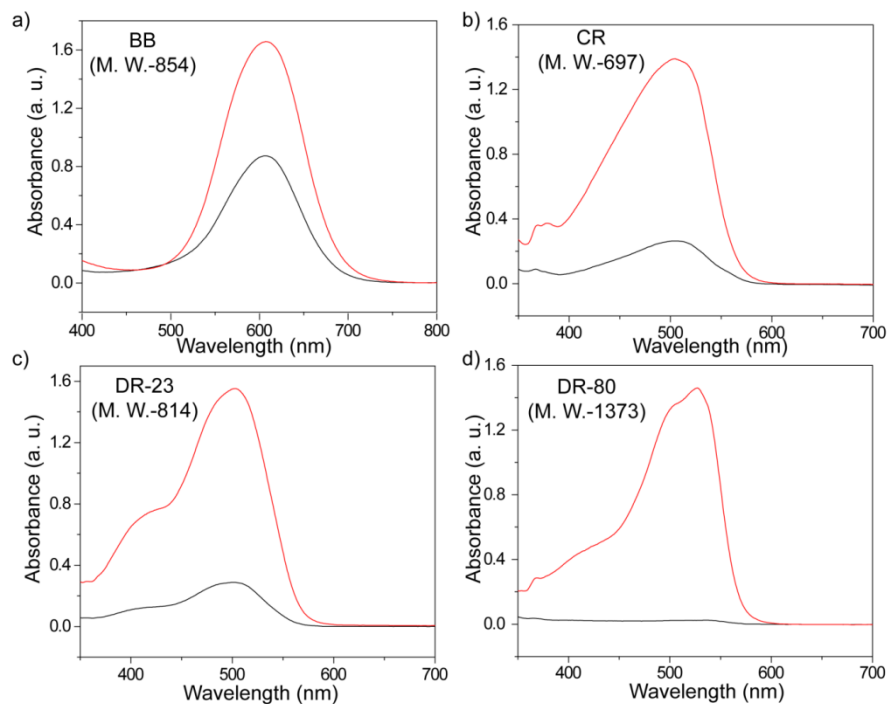


Figure 3.24 UV-visible spectra showing the concentration of dye molecule, a) BB, b) congo red c) DR-23 and d) DR-80 in the feed and permeate after passing through

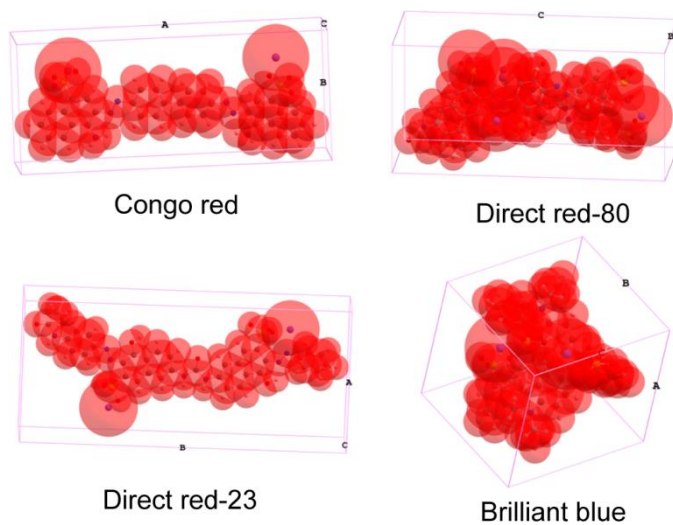


Figure 3.25 Structure of dye molecule used for OSN study

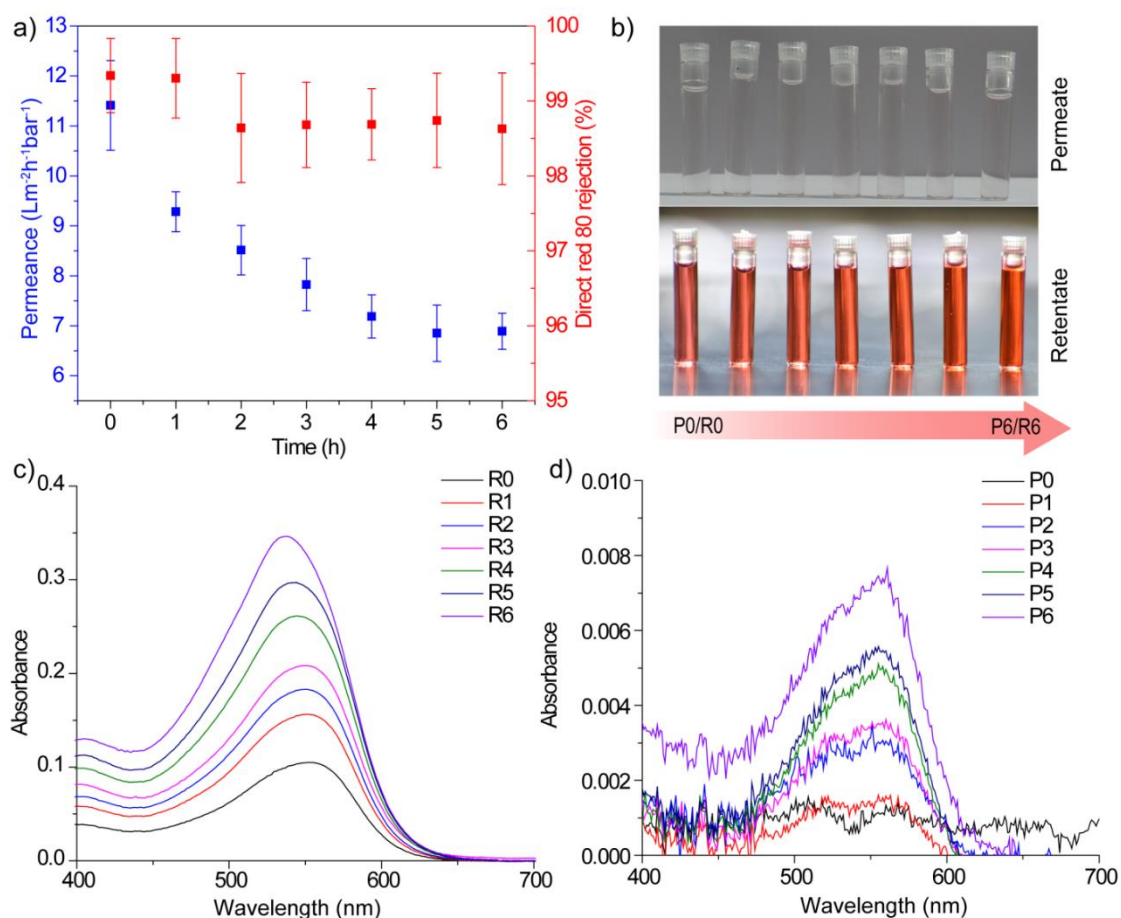


Figure 3.26 Adsorption study: a) Rejection performance of Tp-Tta-15 carried out using 100mg/l direct red-80 in methanol solution, b) photographic images of permeate and retentate collected in each interval c,d) UV-absorption spectra of retentate and permeate respectively

Table 3.3 Dimension of dye molecule obtained from DFT study

Dye	Dimension (Å)			Collision diameter(Å)
	A	B	C	
Brilliant Blue	12.9	13.1	14.3	13.4
Congo red	28.5	12	8.1	14
Direct red-23	15.2	33.9	7.2	15.4
Direct red-80	13.1	11.9	26.9	16.1

The DR-80 dye solution (100 mg/L) was passed through the Tp-Tta-30 membrane module to study the membrane's adsorption behavior. The experiment showed that even after six hours, the membrane showed 99 % rejection (Figure 2.26a). The gradual increase in the dye concentration on the retentate side revealed that the DR-80 dye molecule is not adsorbing on the membrane surface, instead, it gets retained on the reject stream. This can be seen from the

photographic image of retentate solutions collected at regular intervals (Figure 2.26b). Further, we tested the long-term performance of the Tp-Tta-15 membrane using acetone and methanol for 150 hours. Both the solvents showed constant permeance after an initial decrement (Figure 2.27a). The rejection performance was evaluated after 150 h using DR-80 and the membrane showed 99% rejection (Figure 3.27a). In addition, the permeance and DR-80 rejection was analysed after six months, and it was found that the membrane retains the separation performance. Finally, the effect of pressure on solvent permeance was evaluated on both Tp-Azo-400 and Tp-Tta-15. The membrane exhibited linear performance in the pressure range 0.5-2.5 bar (Figure 3.27b)

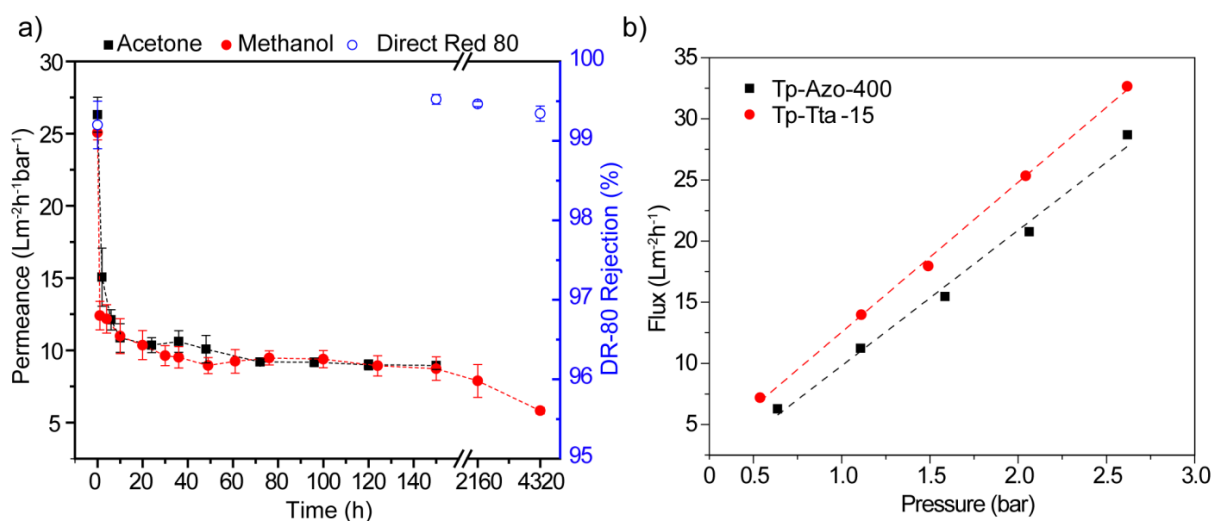


Figure 3.27 Durability study of Tp-Tta-15 membrane (b) Pressure v/s flux of COF thin film HF membrane

3.3 Conclusions

A simple and facile method was developed for fabricating imine-based COF membranes on HF substrate using interfacial polymerization. The current approach enables to overcome the processibility and scalability issues. The synthesized COF thin films on PAN substrate showed excellent adhesion with the substrate. The fabricated membrane exhibited appreciable permeance in broad solvent range and rejection of different dye molecules. The in-situ interfacial polymerization (IP) allowed fine controlling of the COF layer thickness, thereby achieving precise control over the performance of permeance and rejection. The low cost of polymeric substrate and straightforward IP method capacitate the scalable fabrication of COF membranes. Moreover, the durability study showed the applicability of COF membranes for industrially challenging practical applications. Considering the highly reproducible, scalable, mechanically

stable membranes and simple fabrication method, our approach can address challenging problems in the separation field, such as organic solvent recovery and wastewater treatment.

3.4 Experimental section

3.4.1 Materials and Methods

Starting material, viz., 1,3,5-triformylphloroglucinol (Tp), 4',4''-(1,3,5-triazine-2,4,6-triyl) trianiline (Tta) were synthesized by following the previously reported procedure [30,31]. A 4,4'-diaminoazobenzene was purchased from Thermo Fischer. All other chemicals used in this study were purchased from Sigma Aldrich, TCI Chemicals, Loba chemicals and Thomas Baker. All solvents and chemicals were used as received. The PAN powder was purchased from Technorbital India Pvt. Ltd.

3.4.2 Polyacrylonitrile (PAN) hollow fibre membrane (HFM) spinning

The PAN was vacuum dried at 60°C for 24 hr prior to dope solution preparation. The dope solution comprised of PAN (polymer), citric acid (as a pore-forming agent) and *N,N*-dimethylformamide (solvent). HFMs were fabricated by passing the dope solution through a spinneret with water as a bore fluid. The fabricated HFMs were treated with distilled water for 48 hours to ensure the complete removal of the solvent. The details about the dope solution and spinning parameter are given in Table 3.4.

Table 3.4 Spinning parameters for making PAN based HFMs

Dope solution composition	
PAN	11 %
Citric acid	4%
<i>N,N</i> -Dimethylformamide	85%
Conditions followed for hollow fiber membrane spinning	
Take-up	5 m/sec
Air gap	4 cm
Coagulation bath temperature	27 °C

3.4.3 COF thin-film HF membrane fabrication

PAN hollow fibre membranes showed water permeance of 200 Lm⁻²h⁻¹ and BSA rejection of 95%. The interfacial synthesis was attained by dipping the HF membrane in amine solution in water, followed by an aldehyde solution in dichloromethane. To prevent the entry of

precursor solution inside the HF bore, one side of the HFM was blocked with epoxy resin. The precursor solution for IP was made separately by dissolving amine and aldehyde in water and DCM, respectively. The *p*-toluenesulfonic acid (PTSA) was added along with the amine solution as a catalyst. The PAN hollow-fibre substrate was first dipped in amine+PTSA solution for an hour. After 1 hour, the substrate was removed gently and the water on the surface was removed by wiping it with absorbent paper. Further, the substrate was dipped in an aldehyde solution for six-hour. This procedure was repeated for six cycles with the same solution and was finally washed with water. For each synthesis, the membrane area used was kept constant, and the ratio of solution to the area was 13 ml/cm². After each cycle, the color intensity of the membrane was changed to yellow and red, respectively for Tp-Tta and Tp-Azo. The membrane is denoted as Tp-Tta/Azo(X), where X represents the amine and aldehyde solution concentration in mM (Table 3.5).

Table 3.5 Concentration of precursor solution used for thin film HF fabrication

Membrane Identification	Concentration of amine (mM)	Concentration of Aldehyde (mM)
Tp-Azo-400	400	400
Tp-Azo-800	800	800
Tp-Tta-15	15	15
Tp-Tta-30	30	30
Tp-Tta-60	60	60
Tp-Tta-120	120	120

3.4.4 Hollow fibre member module making

Each module consisted 10 HFMs with 20 cm active length and average active area of 150 cm². Two-component epoxy resin was used for potting. To modules were made using acrylate pipe with an effective surface area of 0.05 m², while those for analysis were made using SS housing.

3.4.5 Solvent permeation analysis

The permeation analysis was performed in out-to-in mode (shell to bore) (Figure 2.28). The upstream pressure was maintained at 1.5 bar, while the permeate side was maintained at ambient. The permeate was collected from one end of the bore side after 15 minutes from the beginning of the experiment to ensure a steady state. Three consecutive readings were taken for the permeance and calculated from the permeate volume collected (V) per unit time (t) through

membrane area (A) under pressure (p) using equation 1. At least three modules were tested for each COF thin film membrane and averaged.

$$p = \frac{V(l)}{A(m^2)t(h)p(bar)} \quad 1$$

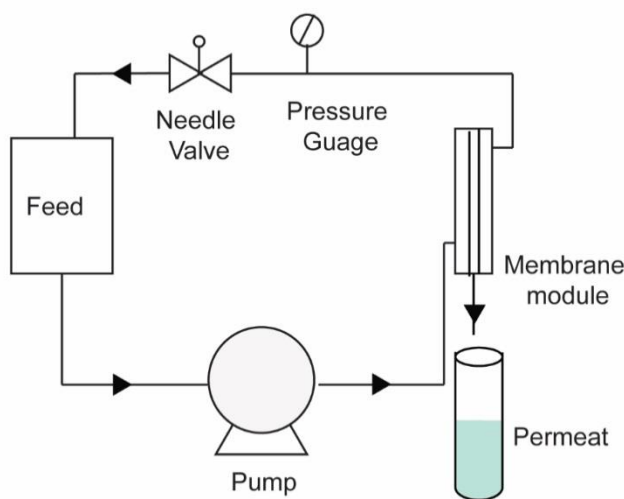


Figure 3.28 Schematic representation of permeation setup

3.4.6 Rejection analysis

The rejection performance of the membranes was evaluated by using a 50 mg/l methanol solution of chosen dyes (direct red-80, direct red-23, congo red and brilliant blue). The analysis was carried out at 1.5 bar pressure using the same setup used for the permeation analysis. The dye concentration in the feed and permeate was measured after 15 minutes from the start of the experiment using UV visible spectroscopy. The percentage rejection is calculated by Equation 2.

$$R(\%) = \left(1 - \frac{C_p}{C_f}\right) \times 100 \quad 2$$

where, C_p and C_f are the concentration of dye concentration in the feed and permeate, respectively.

3.4.7 Adsorption Study

A continuous rejection analysis of Tp-Tta-15 membrane was carried out using 100 mg/l methanol solution of direct red-80 to assess the molecular sieving nature. The effective membrane area of the membrane used for the study was $\sim 0.015 \text{ m}^2$. The rejection analysis was carried out using a similar setup. The transmembrane pressure was maintained at 1.5 bars throughout the experiment. The permeate and retentate were collected at a regular interval of 1

hour and dye concentration was analysed using UV-Vis spectroscopy. Approximately 1L of permeate was collected after six hr experiment. The experiment was repeated for three different membrane modules; the data presented is an average of three.

3.4.8 Characterisation method

a) Powder X-ray Diffraction (PXRD)

Wide-angle X-ray diffraction (WAXD) patterns were recorded on a Rigaku Smart Lab Instrument with PhotonMax high-flux 9 kW rotating anode X-ray source. The samples were recorded in the 2θ range of 2–40 ° and the radiation used was CuK with wavelength 1.54 Å.

b) Solid-state NMR spectra

Solid state NMR spectra were recorded on Bruker 300 MHz NMR spectrometer, where carbon chemical shifts are expressed in parts per million.

c) Fourier-transform infrared spectroscopy (IR)

The Fourier transform infrared (FTIR) spectroscopy was carried out on PerkinElmer spectrum one FTIR instrument using Universal ATR (Attenuated total internal reflection) accessory. The analysis was done in the range of 600-4000 cm^{-1} .

d) Contact angle

The static contact angle analysis was done using Kruss drop shape analyser, DSA 25S. The measurements were taken with the help of Advance software using the sessile drop method. The hollow fiber membrane samples were horizontally mounted on the sample holder and 1 μl of water was dropped on the surface. The angles were measured up to 2 min in a regular intervals of 30 s. The water contact angle measurement was also carried out using Wilhelmy plate method on Kruss force tensiometer K100. The HF samples with one end blocked with epoxy resin were used for the analysis.

e) Scanning electron microscope (SEM)

The scanning electron microscope images were obtained using FEI, QUANTA 200 3D SEM instrument operating at 10, 15 and 20 kV, using tungsten filament as electron source and before imaging, the samples were sputtered with gold by using SCD 040 Balzers Union. The cross-sectional samples were made by freeze cracking in liquid nitrogen.

f) Atomic Force Microscopy (AFM)

ASYLUM RESEARCH, USA, Mode- MFP-3D_BIO was used for the surface morphology analysis of the COF thin film membrane. The images were scanned in tapping mode

using a silicon cantilever (Asyelec-02) with a frequency 300 kHz. The nominal radius of the silicon tip is 25 nm and the shape of the tip is three-sided.

g) Thermo gravimetric analysis (TGA)

Thermo gravimetric analysis (TGA) was performed using PerkinElmer STA-6000 analyzer under N₂ atmosphere at a heating rate of 10 °C/min. The analysis was done in a temperature range of 50-900 °C.

h) X-ray photoelectron spectroscopy (XPS)

X-ray photoelectron spectroscopy (XPS) analyses were performed on a Thermo Fisher Scientific Instruments UK, Sr.No.-KAS2020 with an exciting source of Al-K- α with the energy of 1486.6 eV

i) Stereo microscope

The optical images of the COF thin-film hollow fiber membrane were captured using Zeiss (model SteREO Discovery.V20) microscope.

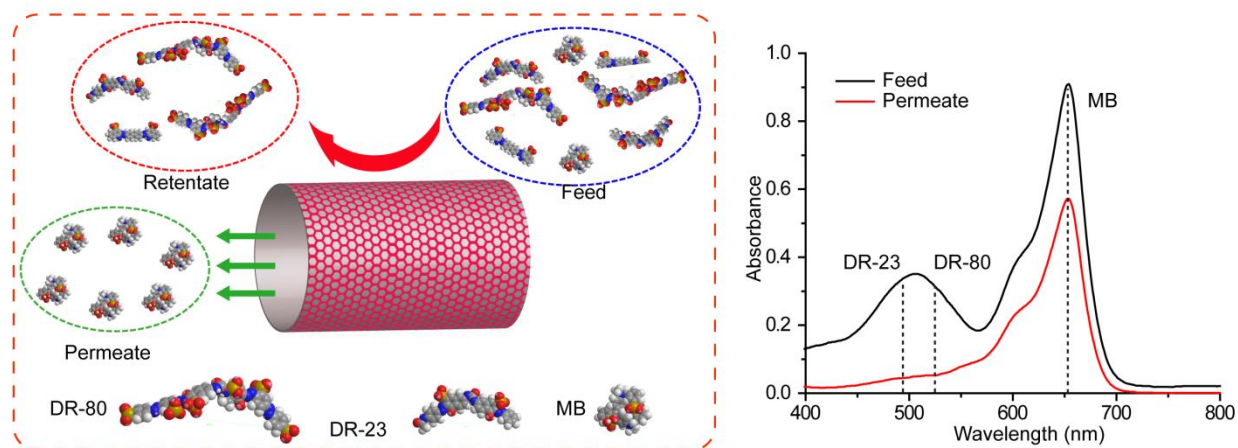
3.5 References

- [1] D.S. Sholl, R.P. Lively, Comment, *Nature*. 532 (2016) 6–9.
- [2] Y. Zhang, H. Ye, D. Chen, N. Li, Q. Xu, H. Li, J. He, J. Lu, In situ assembly of a covalent organic framework composite membrane for dye separation, *J. Memb. Sci.* 628 (2021). <https://doi.org/10.1016/j.memsci.2021.119216>.
- [3] C. Castel, E. Favre, Membrane separations and energy efficiency, *J. Memb. Sci.* 548 (2018) 345–357. <https://doi.org/10.1016/j.memsci.2017.11.035>.
- [4] Y. Yin, M.D. Guiver, Microporous polymers: Ultrapermeable membranes, *Nat. Mater.* 16 (2017) 880–881. <https://doi.org/10.1038/nmat4961>.
- [5] D.B. Shinde, G. Sheng, X. Li, M. Ostwal, A.H. Emwas, K.W. Huang, Z. Lai, Crystalline 2D Covalent Organic Framework Membranes for High-Flux Organic Solvent Nanofiltration, *J. Am. Chem. Soc.* 140 (2018) 14342–14349. <https://doi.org/10.1021/jacs.8b08788>.
- [6] P. Marchetti, M.F. Jimenez Solomon, G. Szekely, A.G. Livingston, Molecular separation with organic solvent nanofiltration: A critical review, *Chem. Rev.* 114 (2014) 10735–10806. <https://doi.org/10.1021/cr500006j>.
- [7] N. Manoranjan, F. Zhang, Z. Wang, Y. Dong, W. Fang, Y. Zhang, Y. Zhu, J. Jin, A Single-Walled Carbon Nanotube/Covalent Organic Framework Nanocomposite Ultrathin Membrane with High Organic Solvent Resistance for Molecule Separation, *ACS Appl. Mater. Interfaces.* 12 (2020) 53096–53103. <https://doi.org/10.1021/acsami.0c14825>.
- [8] L. Valentino, M. Matsumoto, W.R. Dichtel, B.J. Marinas, Development and Performance

- Characterization of a Polyimine Covalent Organic Framework Thin-Film Composite Nanofiltration Membrane, *Environ. Sci. Technol.* 51 (2017) 14352–14359. <https://doi.org/10.1021/acs.est.7b04056>.
- [9] D.B. Shinde, L. Cao, A.D.D. Wananke, X. Li, S. Kumar, X. Liu, M.N. Hedhili, A.H. Emwas, M. Addicoat, K.W. Huang, Z. Lai, Pore engineering of ultrathin covalent organic framework membranes for organic solvent nanofiltration and molecular sieving, *Chem. Sci.* 11 (2020) 5434–5440. <https://doi.org/10.1039/d0sc01679a>.
- [10] M.F. Jimenez-Solomon, Q. Song, K.E. Jelfs, M. Munoz-Ibanez, A.G. Livingston, Polymer nanofilms with enhanced microporosity by interfacial polymerization, *Nat. Mater.* 15 (2016) 760–767. <https://doi.org/10.1038/nmat4638>.
- [11] B. Liang, H. Wang, X. Shi, B. Shen, X. He, Z.A. Ghazi, N.A. Khan, H. Sin, A.M. Khattak, L. Li, Z. Tang, Microporous membranes comprising conjugated polymers with rigid backbones enable ultrafast organic-solvent nanofiltration, *Nat. Chem.* 10 (2018) 961–967. <https://doi.org/10.1038/s41557-018-0093-9>.
- [12] J. Hou, H. Zhang, G.P. Simon, H. Wang, Polycrystalline Advanced Microporous Framework Membranes for Efficient Separation of Small Molecules and Ions, *Adv. Mater.* 32 (2020) 1–13. <https://doi.org/10.1002/adma.201902009>.
- [13] H. Fan, J. Gu, H. Meng, A. Knebel, J. Caro, High-Flux Membranes Based on the Covalent Organic Framework COF-LZU1 for Selective Dye Separation by Nanofiltration, *Angew. Chemie - Int. Ed.* 57 (2018) 4083–4087. <https://doi.org/10.1002/anie.201712816>.
- [14] N.A. Khan, R. Zhang, H. Wu, J. Shen, J. Yuan, C. Fan, L. Cao, M.A. Olson, Z. Jiang, Solid-Vapor Interface Engineered Covalent Organic Framework Membranes for Molecular Separation, *J. Am. Chem. Soc.* 142 (2020) 13450–13458. <https://doi.org/10.1021/jacs.0c04589>.
- [15] X. Chen, K. Geng, R. Liu, K.T. Tan, Y. Gong, Z. Li, S. Tao, Q. Jiang, D. Jiang, Covalent Organic Frameworks: Chemical Approaches to Designer Structures and Built-In Functions, *Angew. Chemie - Int. Ed.* 59 (2020) 5050–5091. <https://doi.org/10.1002/anie.201904291>.
- [16] C.S. Diercks, O.M. Yaghi, The atom, the molecule, and the covalent organic framework, *Science* (80-.). 355 (2017). <https://doi.org/10.1126/science.aal1585>.
- [17] N. Huang, P. Wang, D. Jiang, Covalent organic frameworks: A materials platform for structural and functional designs, *Nat. Rev. Mater.* 1 (2016). <https://doi.org/10.1038/natrevmats.2016.68>.
- [18] S. Yuan, X. Li, J. Zhu, G. Zhang, P. Van Puyvelde, B. Van Der Bruggen, Covalent organic frameworks for membrane separation, *Chem. Soc. Rev.* 48 (2019) 2665–2681. <https://doi.org/10.1039/c8cs00919h>.
- [19] S. Kandambeth, B.P. Biswal, H.D. Chaudhari, K.C. Rout, S. Kunjattu H., S. Mitra, S. Karak, A. Das, R. Mukherjee, U.K. Kharul, R. Banerjee, Selective Molecular Sieving in Self-Standing Porous Covalent-Organic-Framework Membranes, *Adv. Mater.* 29 (2017). <https://doi.org/10.1002/adma.201603945>.
- [20] K. Dey, M. Pal, K.C. Rout, S.S. Kunjattu, A. Das, R. Mukherjee, U.K. Kharul, R.

- Banerjee, Selective Molecular Separation by Interfacially Crystallized Covalent Organic Framework Thin Films, *J. Am. Chem. Soc.* 139 (2017) 13083–13091. <https://doi.org/10.1021/jacs.7b06640>.
- [21] Z. Wang, S. Zhang, Y. Chen, Z. Zhang, S. Ma, Covalent organic frameworks for separation applications, *Chem. Soc. Rev.* 49 (2020) 708–735. <https://doi.org/10.1039/c9cs00827f>.
- [22] H.S. Sasmal, H.B. Aiyappa, S.N. Bhange, S. Karak, A. Halder, S. Kurungot, R. Banerjee, Superprotonic Conductivity in Flexible Porous Covalent Organic Framework Membranes, *Angew. Chemie.* 130 (2018) 11060–11064. <https://doi.org/10.1002/ange.201804753>.
- [23] H. Wang, Z. Zeng, P. Xu, L. Li, G. Zeng, R. Xiao, Z. Tang, D. Huang, L. Tang, C. Lai, D. Jiang, Y. Liu, H. Yi, L. Qin, S. Ye, X. Ren, W. Tang, Recent progress in covalent organic framework thin films: fabrications, applications and perspectives, *Chem. Soc. Rev.* 48 (2019) 488–516. <https://doi.org/10.1039/c8cs00376a>.
- [24] D. Liu, K. Li, M. Li, Z. Wang, M. Shan, Y. Zhang, Moderately Crystalline Azine-Linked Covalent Organic Framework Membrane for Ultrafast Molecular Sieving, *ACS Appl. Mater. Interfaces.* 13 (2021) 37775–37784. <https://doi.org/10.1021/acscami.1c06891>.
- [25] J. Shen, R. Zhang, Y. Su, B. Shi, X. You, W. Guo, Y. Ma, J. Yuan, F. Wang, Z. Jiang, Polydopamine-modulated covalent organic framework membranes for molecular separation, *J. Mater. Chem. A.* 7 (2019) 18063–18071. <https://doi.org/10.1039/c9ta05040j>.
- [26] Y. Zhang, J. Guo, G. Han, Y. Bai, Q. Ge, J. Ma, C.H. Lau, L. Shao, Molecularly soldered covalent organic frameworks for ultrafast precision sieving, *Sci. Adv.* 7 (2021) 1–10. <https://doi.org/10.1126/sciadv.abe8706>.
- [27] A.J. Brown, N.A. Brunelli, K. Eum, F. Rashidi, J.R. Johnson, W.J. Koros, C.W. Jones, S. Nair, Interfacial microfluidic processing of metal-organic framework hollow fiber membranes, *Science* (80-.). 345 (2014) 72–75. <https://doi.org/10.1126/science.1251181>.
- [28] K. Eum, A. Rownaghi, D. Choi, R.R. Bhave, C.W. Jones, S. Nair, Fluidic Processing of High-Performance ZIF-8 Membranes on Polymeric Hollow Fibers: Mechanistic Insights and Microstructure Control, *Adv. Funct. Mater.* 26 (2016) 5011–5018. <https://doi.org/10.1002/adfm.201601550>.
- [29] B.P. Biswal, S.H. Kunjattu, T. Kaur, R. Banerjee, U.K. Kharul, Transforming covalent organic framework into thin-film composite membranes for hydrocarbon recovery, *Sep. Sci. Technol.* 53 (2018) 1752–1759. <https://doi.org/10.1080/01496395.2018.1443136>.
- [30] J.H. Chong, M. Sauer, B.O. Patrick, M.J. MacLachlan, Highly Stable Keto-Enamine Salicylideneanilines, (2003) 2–5.
- [31] A. Halder, S. Kandambeth, B.P. Biswal, G. Kaur, N.C. Roy, M. Addicoat, J.K. Salunke, S. Banerjee, K. Vanka, T. Heine, S. Verma, R. Banerjee, Decoding the Morphological Diversity in Two Dimensional Crystalline Porous Polymers by Core Planarity Modulation, *Angew. Chemie - Int. Ed.* 55 (2016) 7806–7810. <https://doi.org/10.1002/anie.201600087>.

Ionic COFs: Thin Film Membrane Preparation and Analysis



Abstract

Covalent organic frameworks are promising candidates for energy-efficient and precise molecular sieving. This chapter unveils a new approach to fabricating thin, charged COF membranes. The hollow fiber membrane (HFM) based on polyacrylonitrile (PAN) was used as the substrate. COFs were synthesized on the surface of PAN-HFM by an interfacial method using cationic 3,8-diamino-5-ethyl-6-phenylphenanthridinium bromide and 1,3,5-triformylphloroglucinol. The halide ion in the building blocks was replaced by the co-reagent (p-toluenesulfonate and trifluoroacetate anion) used while synthesizing COFs. Obtained COF-coated membranes exhibited methanol permeance of ~ 13 and $10 \text{ Lm}^{-2}\text{h}^{-1}\text{bar}^{-1}$ for TpEt-PTSA-0.5 and TpEt-TFA-0.5, respectively. These membranes showed selective retention of the solute molecules based on their charge rather than their size. This peculiarity can offer a new tool to modulate the porosity for organic solvent nanofiltration.

4.1 Introduction

Membranes based on porous materials with a provision to tune their pore size in the nanometer range are an attractive alternative for energy-intensive industrial separation applications. Covalent Organic Frameworks (COFs) are an emerging class of porous organic materials comprised of periodically ordered pore structure, good thermochemical stability, and high permanent porosity [1–6]. The size, symmetry, and connectivity of the building units of COFs decide the pore size and gain the ability of size exclusion-based separations with high efficacy and selectivity [7–10]. Moreover, the functionality can be changed by introducing different groups in the linker molecule and attaining precise control of the host-guest interactions. COFs thus possess unique features over other porous materials [11]. These characteristics of COFs attracted wide attention in the recent past as a membrane material due to their application in organic solvent nanofiltration [12-15], water purification[14][16], and gas separation [17,18] applications.

The previous chapter (Chapter 3) discussed the scalable fabrication of COF membranes on the hollow fiber substrate by following interfacial polymerization. The membrane showed noticeable solvent permeance and rejection performance in organic solvent nanofiltration. To meet the specific separation requirements, fine-tuning the pore size is necessary. Two modification methods were used to construct COFs with the desired pore size [9]. The first method is changing the length of the building block to achieve variable pore size and geometry. Banerjee and coworkers synthesized a series of imine-based COF membranes by interfacial polymerization with pore size varying from 1.4 to 2.6 nm by changing the length of the building unit [19]. The second strategy is to incorporate side chain moiety to the building block either by a bottom-up approach (wherein the premodified building units are used for COF synthesis) [20] or the post-synthetic modification [21,22]. These strategies helped to fine-tune the pore size and imparted host-guest interactions leading to efficient separation. Jiang and coworkers modified the pore size of COF by post-synthetic modification via covalent bond formation [21,22]. In this approach, they have synthesized an azide-functionalized COF using an azide-appended building block. The pore modification was done by the click reaction using a suitable alkyne group containing a reagent. The same group also functionalized the pore structure with different groups such as -COOH, -COOMe, -OH, and -NH₂ [22]. In another study, Shinde et al. fabricated COF

membranes using a bottom-up approach [23]. They used organic linkers with side chains possessing different functional groups to control the pore size.

Incorporating ionic charge into the COF pores plays a significant role in OSN and desalination [24,25]. The charge on the pore wall will control the molecular sieving and also reduce membrane fouling [26]. Zhang et al. reported a cationic COF, viz., EB-COF:Br, obtained by a bottom-up approach. The presence of abundant positive charges led to the selective separation of dye molecules. The previous chapter demonstrated a successful fabrication methodology for developing thin COF membrane over PAN HF substrate. The current chapter presents the fabrication of COF having cationic imine groups on the PAN-HFM substrate by interfacial polymerization. The bromide anion was exchanged with the co-reagent used for interfacial polymerization. This approach eliminates the crystallinity issue associated with the bottom-up strategy [11] and thus reduces an extra step needed in the post-synthetic modification.

4.1.1 Scope and objectives

This work depicts cationic COF fabrication on the outer surface of HF membrane substrate. The charge on the COF pores is anticipated to help the rejection performance of the membrane. Moreover, the anion exchange with the co-reagent would help to achieve in situ pore modification while fabricating the membrane. Further, it can be an effective tool for the selective separation of solute molecules. The key objectives are the fabrication of the cationic COF with in situ anion exchange, characterizing the membrane, study of the separation performance of the membrane. The substrate was kept the same as in the earlier Chapter, i.e. PAN-based hollow fiber membrane.

4.2 Interfacial synthesis of cationic COFs and anion exchange

The TpEt-COF membrane was fabricated by reacting 3,8-diamino-5-ethyl-6-phenylphenanthridinium bromide) amine, commonly known as ethidium bromide (Et), with an aldehyde, viz., 1,3,5-triphenylphlouroglunol (Tp). The interfacial polymerization was carried out in the presence of co-reagent p-toluene sulfonic (PTSA) acid or triflouroacetic acid (TFA) on the surface of PAN-based HFM (Figure 4.1). The membranes were fabricated at different aldehyde and amine precursor concentrations in dichloromethane and water, respectively. The membrane synthesized using PTSA and TFA are denoted as TpEt-PTSA-XX and TpEt-TFA-XX, respectively. The XX represents the concentration of precursor solutions used for the IP in ‘mM.’ The XPS study revealed the anion exchange of the Br⁻ with the corresponding co-reagent anion

(*p*-toluene sulfonate or trifluoroacetate) used for the synthesis. IR and C^{13} NMR spectroscopy confirmed the formation of the COF layer on the PAN substrate. The permeance and rejection properties were evaluated using membranes prepared with 0.5 mM precursor solution. Different dye molecules in methanol were used as solutes.

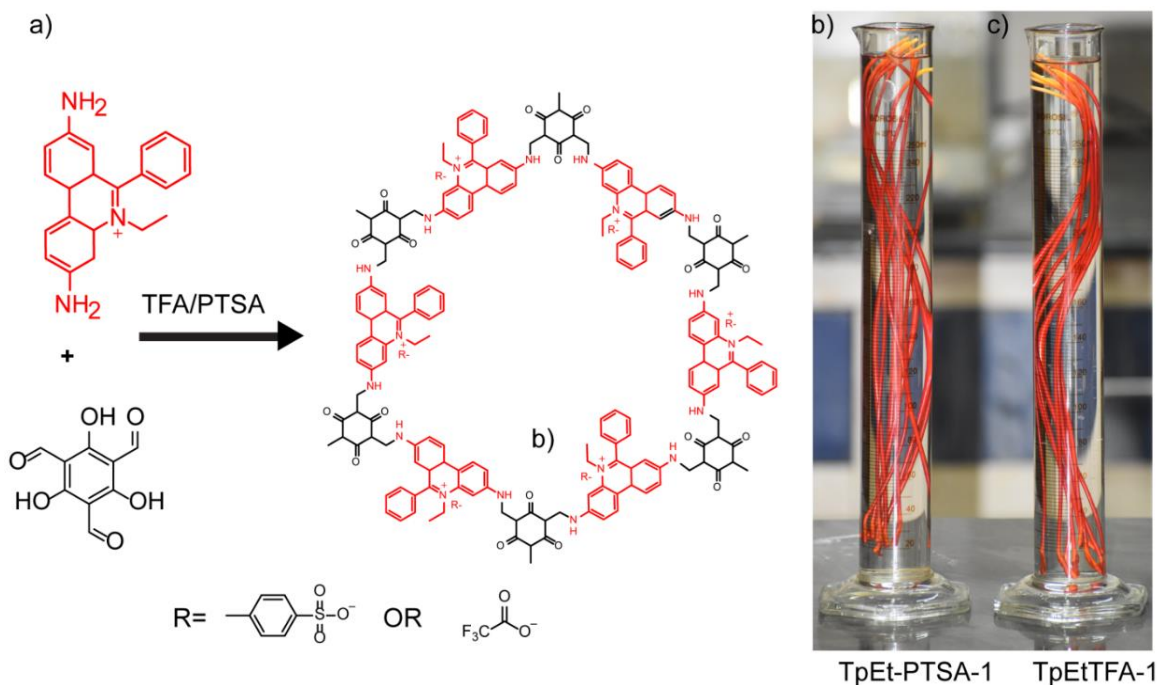


Figure 4.1 The (a) structure of TpEt-COF and photographic images of TpEt-PTSA-1, and (c) TpEt-TFA-1 membranes

4.3 Results and discussion

4.3.1 FTIR and C^{13} NMR analyses

The formation of Tp-Et COF on the surface of polyacrylonitrile (PAN) based hollow fiber membrane (HFM) substrate was confirmed by FTIR spectra (Figure 4.2). In addition to the characteristic peaks of PAN, the COF membranes fabricated using PTSA and TFA exhibited two new peaks at 1583 (attributable to C=C) and 1263 cm^{-1} (attributable to C=N). They represent characteristic peaks of COF formation, and the presence of C=C stretching confirms the existence of COF in the keto form [12].

The formation of the COF membrane on the PAN substrate was confirmed by the C^{13} MAS solid-state nuclear magnetic resonance (NMR) spectroscopy (Figure 4.3). In order to get a sufficient sample for the analysis, the PAN substrate layer was removed by dissolving it in *N,N*-

dimethylformamide (DMF), followed by washing DMF and subsequent drying in the vacuum oven at 80° C for one day. The appearance of a peak at 162 ppm and 184 ppm corresponds to the characteristic imine (-C=N) and the carbonyl (-C=O) functionality of the keto form, respectively. The intense peak at 29 corresponds to the carbon (-C-C-) peak of PAN polymer, which remains associated with the COF even after efforts to remove it by dissolving it in DMF.

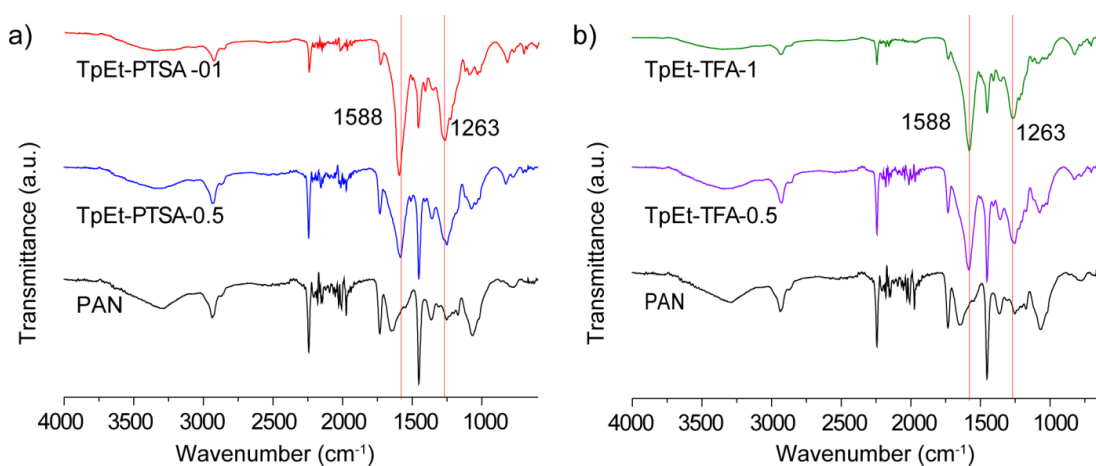


Figure 4.2 FTIR spectra of TpEt-PTSA (a) and TpEt-TFA (b) membrane in comparison to the PAN substrate

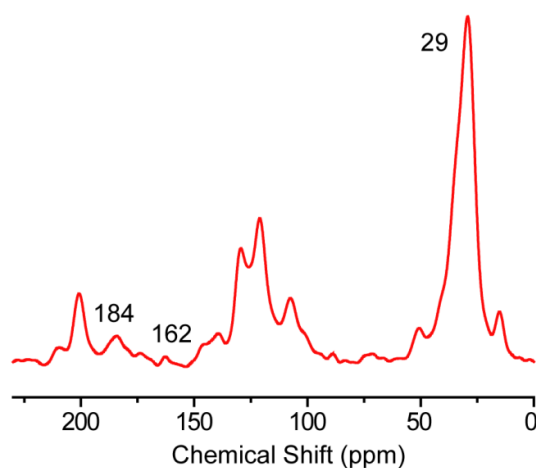


Figure 4.3 C^{13} NMR spectra of TpEt-PTSA membrane

4.3.2 Wide-angle X-ray diffraction

In order to investigate the crystallinity of the COF membrane, wide-angle X-ray diffraction (WAXD) spectra were recorded (Figure 4.4). The PAN membrane showed a peak at 17°. The COF membrane samples were made similarly to that for NMR analysis (by removing

the PAN substrate using DMF solvent). The diffraction patterns indicated that the membranes synthesized using PTSA and TFA were moderately crystalline. The first peak appeared at 3.3° , which corresponds to 100 plane, while the peak at 27° corresponds to the 001 plane. The high intensity of the 001 plane as compared to that of 100 plane is attributable to the presence of a bulky anionic group, which restricts the π - π stacking of the COF 2D layers. The substrate-removed COF membrane still shows a characteristic peak of PAN, indicating the persistence of PAN even after its dissolution in DMF. A similar observation was seen in the case of NMR analysis. It could be attributed to the interactions between the PAN substrate and the COF layer. This is a positive aspect of the COF-PAN pair as far as membrane formation and stability are concerned.

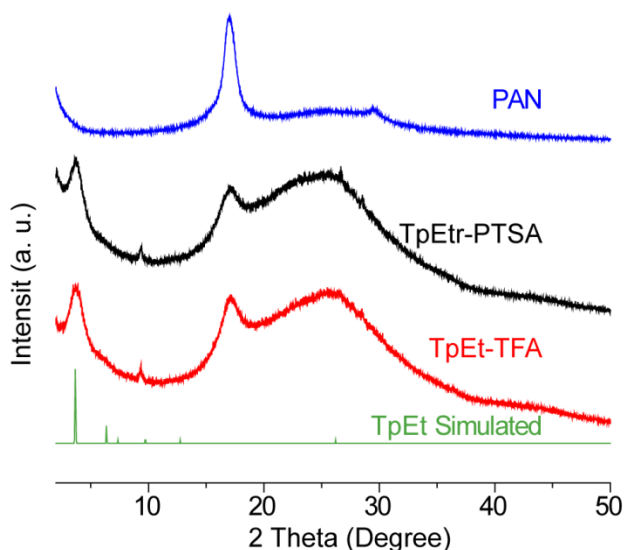


Figure 4.4 Comparison WAXD patterns of as-synthesized TpEt membranes with that of a simulated one

4.3.3 Scanning electron microscopy

The cross-sectional microscopic images of HFMs fabricated using PTSA and TFA (Figure 4.5a,d) show that the COF layer is continuous on the outer surface of the PAN substrate. There is no penetration into the bulk or inside the fiber, conveying the success of the interfacial thin layer formation. The cross-sectional SEM images of the TpEt-PTSA and TpEt-TFA showed a dense layer on the outer surface of the HFM (Figure 4.5b,e) and some porosity after the thickness of a couple of μm . A continuous crystalline structure could be visualized from the surface images (Figure 4.5c,f).

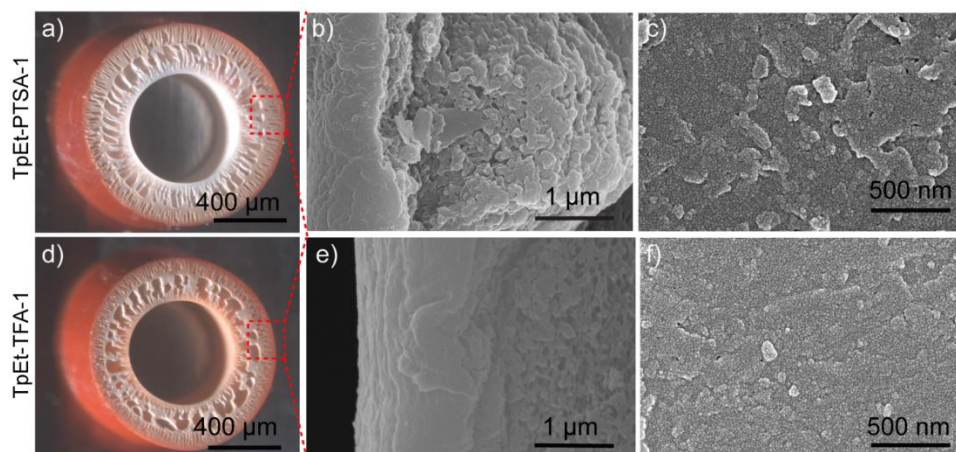


Figure 4.5 Microscope images showing cross-sectional view of (a,d) COF thin film HFM and SEM images showing cross-sectional (b,e) and surface (c,f) view of COF thin film HFM.

4.3.4 Contact angle analysis

The hydrophilicity/hydrophobicity of the COF thin-film HF membrane is determined using the water contact angle. The PAN substrate shows better water wettability, and the water droplet spreads through the membrane surface within 2 minutes. However, in the case of the COF thin-film membrane, the drop was retained on the surface even after 2 minutes. It could be due to the hydrophobic nature of the COF (Figure 4.6).

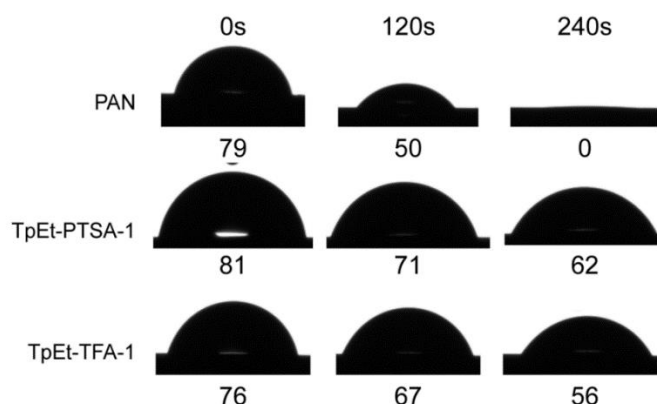


Figure 4.6 Comparison of contact angle of PAN substrate with COF thin film HFM

4.3.5 X-ray photoelectron spectroscopy

The X-ray photoelectron spectroscopy (XPS) was performed to confirm the formation of COF thin film formation and Br^- exchange with anion used as the co-reagent in the interfacial polymerization. The XPS survey of COF thin film showed a higher C/N atomic ratio as

compared to that of PAN HFM substrate. This confirms the COF formation on the surface of the PAN HFM substrate (Figure 4.7a). The high-resolution XPS analysis of Br and S atom in the TpEt-PTSA COF thin-film membrane indicates that there is no Br⁻ present in the membrane; instead found, the presence of the S atom (Figure 4.7 b,d). Simultaneously, the high-resolution survey of Br and F in TpEt-TFA membrane confirms the presence of the F atom instead of Br (Figure 4.7 c,e). Finally, the high-resolution XPS survey substantiates the in-situ anion exchange while fabricating the thin-film membrane.

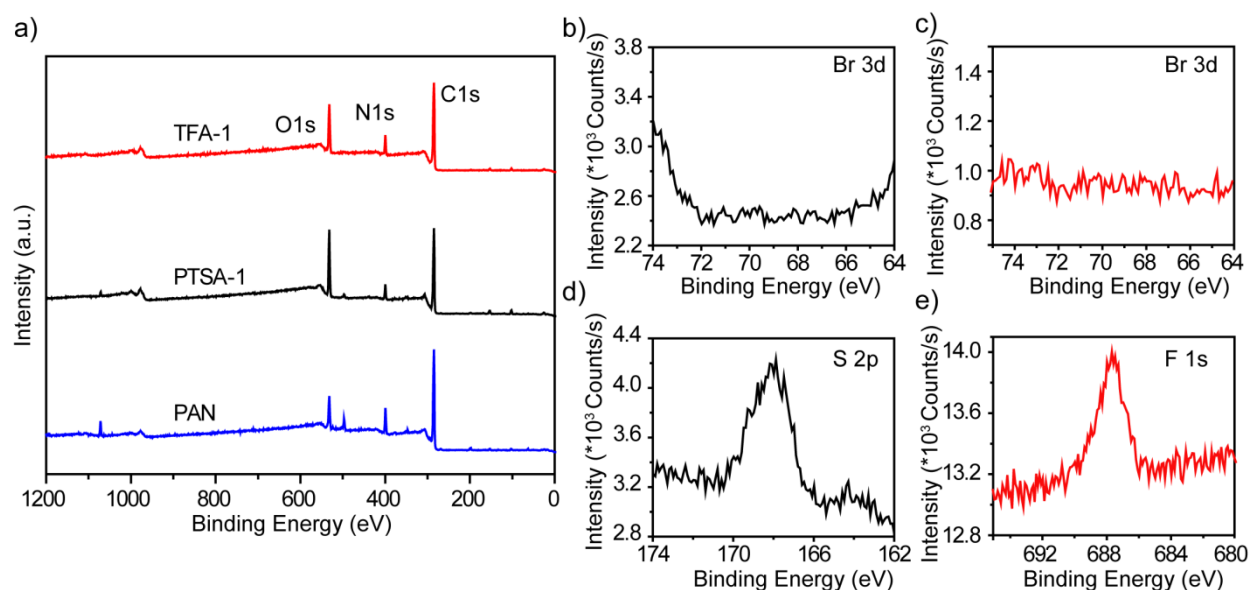


Figure 4.7 The XPS spectra of COF thin film HFM: (a) high-resolution XPS spectra of Br 3d in TpEt-PTSA-1, (b) TpEt-TFA-1 membrane; (d) high-resolution XPS spectra of S 2p in TpEt-PTSA-1, and (e) high-resolution XPS spectra of F 1s in TpEt-TFA-1

4.3.6 Molecular rejection performance

To evaluate the separation performance, we carried out pure methanol permeance study and rejection analysis of membrane fabricated at 50 mM precursor solution (TpEt-PTSA and TpEt-TFA) (Figure 4.8a). The membranes exhibit appreciable pure water and methanol permeance. The TpEt-PTSA-0.5 membranes showed 13.6 and 10.4 $\text{Lm}^{-2}\text{h}^{-1}\text{bar}^{-1}$, respectively for water and methanol. Simultaneously for the same solvents, TpEt-TFA-0.5 membranes exhibited 7.8 and 9 $\text{Lm}^{-2}\text{h}^{-1}\text{bar}^{-1}$. The reason behind the difference between the two membranes fabricated in the presence of different co-reagent (PTSA and TFA) might be a variation in the thickness of the COF membrane formed. In the presence of TFA, the COF formation reaction might be more

favorable, which results in a thicker membrane layer. The thicker layer further reduces the mass transfer, thereby, the permeability.

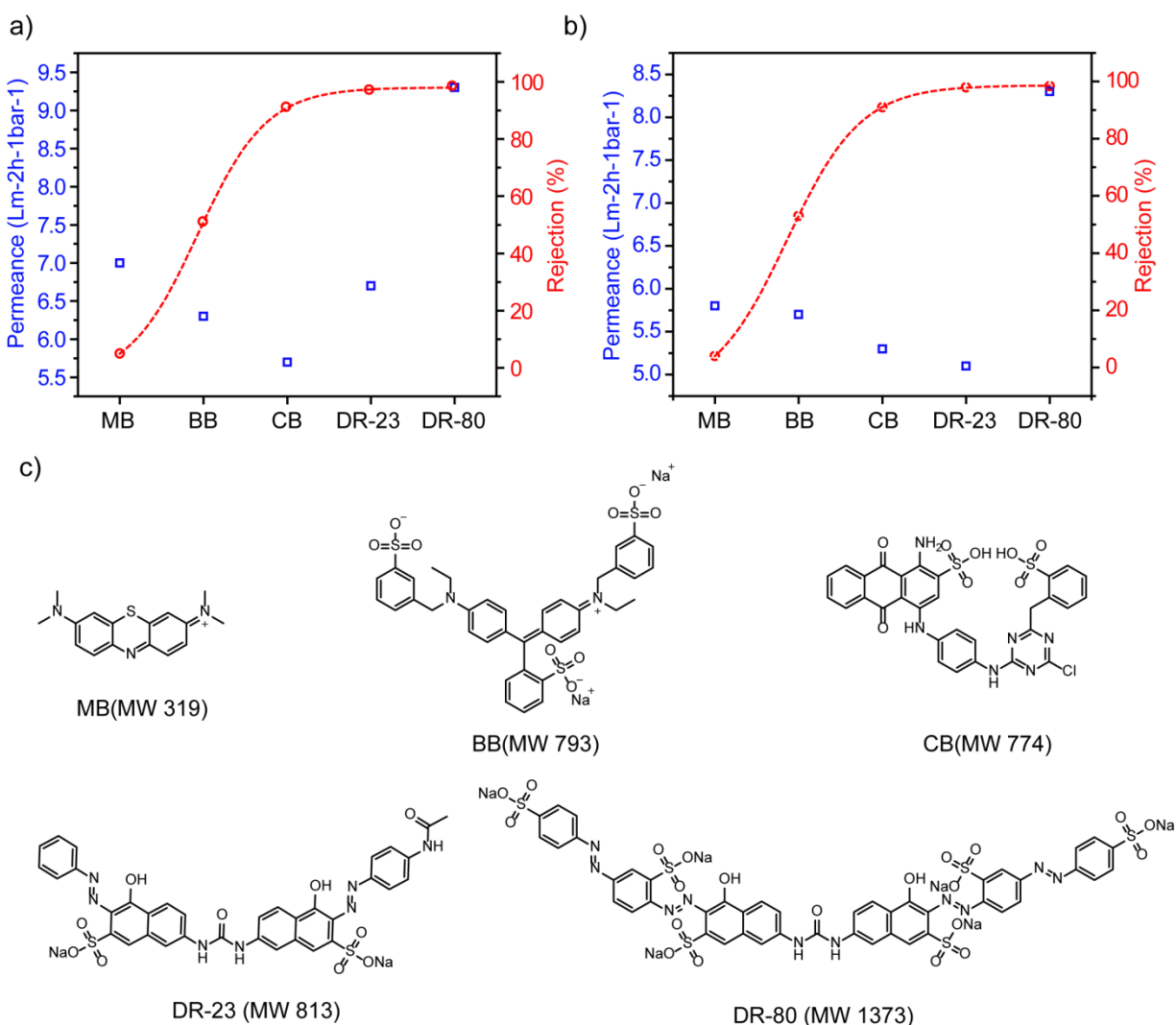


Figure 4.8 Rejection performance of various dyes in methanol through TpEt-PTSA-0.5 (a), and TpEt-TFA-0.5 thin film HF membrane, (b) Molecular structure of methylene blue (MB), brilliant blue (BB), cibacron blue (CB), direct red-23 (DR-80), and direct red-80 dye

To study the influence of anion exchange on the membrane porosity and rejection, we evaluated the membrane rejection using five different dye molecules viz. methylene blue (MB), brilliant blue (BB), cibacron blue (CB), direct red-23 (DR-23) and direct red-80 (DR-80) (Figure 4.8c). Among the dye molecule selected, CB, DR-23, and DR-83 showed more than 90% rejection. The OSN membrane rejection performance depends on the charge and size of the solute molecule. Here the rejection analysis was conducted using an organic solvent, so the

dissociation of dyes in the solution is negligible. The same is visible from the percentage rejection of BB, CB, and DR-23. Even though all three dye molecules possess almost similar molecular weight and charge, CB and DR-23 showed more than 90% rejection. At the same time, BB exhibited ~60% rejection. This fact indicated that in methanol, the rejection performance of the dye molecule depends only on the size exclusion.

We also studied the effectiveness of the membrane for separating mixed dyes (MB, DR-80 and DR-23) in methanol using TpEt-PTSA-0.5. The ultra-violet absorption spectrum shows that direct red-23 and direct red-80 were rejected almost quantitatively by the membrane, while the methylene blue passes through the membrane (36% rejection) (Figure 4.9). This data agrees with the single dye experiment data given in figure 4.7a.

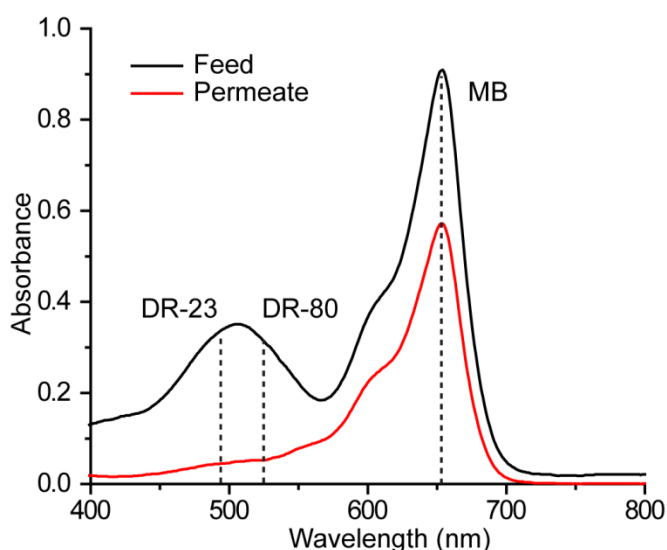


Figure 4.9 Ultra-violet absorption spectra of mixed dye (MB, DR-23, and DR-80) in feed and permeate of TpEt-PTS-0.5 membrane

The permeance of methanol for TpEt-PTSA-0.5 and TpEt-TFA-0.5 membranes was measured before and after the dye rejection. It helped to analyze the membrane fouling (Figure 4.10). The permeance data indicated that there is no significant variation in the methanol permeance. This observation suggested that dye molecules were not deposited on the COF surface or inside the pores of the COF.

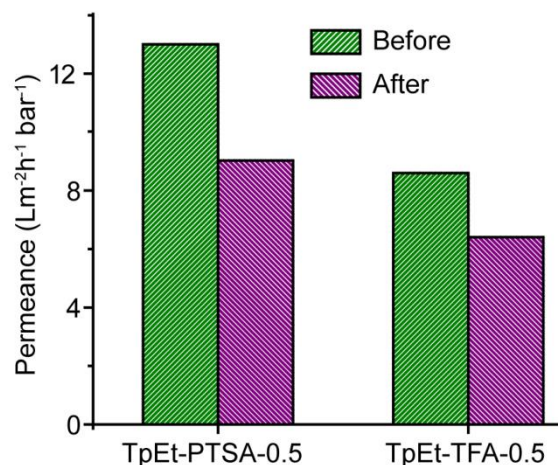


Figure 4.10 Methanol permeance of TpEt-PTSA-0.5 and TpEt-TFA-0.5 membrane before and after dye rejection analysis

4.4 Conclusions

In summary, we developed a scalable method to fabricate cationic COF membranes by employing interfacial synthesis on a porous polymeric substrate. Further, we were able to modify the pore wall by in-situ anion exchange. The pore wall modification could be achieved by changing the co-reagent used for the fabrication process. The membranes were characterized using IR, NMR, and PXRD. The XPS spectra confirm the complete exchange of anion with the co-reagent used for the interfacial synthesis. Due to the well-ordered porous framework structure, the COF thin-film HF membrane shows appreciable methanol permeance and rejection performance. Even though the membranes could not achieve any significant change in the separation process by anion exchange, we believe that this method can address the challenges in many s by precisely controlling pore size, shape, and chemistry.

4.5 Experimental procedures

4.5.1 Materials

1,3,5-triformylphloroglucinol (Tp) was synthesized following a reported method [27]. PAN was procured from Technorbital Advanced Materials Ltd., India. The TFA, ethidium bromide, direct red-80, direct red-23, cibacron blue, brilliant blue, and methylene blue were purchased from Sigma-Aldrich Pvt. Ltd. The PTSA was procured from TCI Chemicals (India) Pvt. Ltd., while *N,N*-dimethylformamide (DMF), and citric acid were procured from Merck.

Other common solvents (methanol, dichloromethane) were obtained from Thomas Baker. All materials purchased from commercial suppliers were used without further purification.

4.5.2 Spinning of polyacrylonitrile (PAN) based HFM and their analysis

The PAN was vacuum dried at 60°C for 24 h. The dope solution comprised PAN, citric acid (as a pore-forming agent), and *N,N*-dimethylformamide as solvent. HFMs were spun by the phase inversion method using a tube-in orifice spinneret (0.8 as needle OD and 2.0 mm as orifice diameter). Water was used as a bore fluid as well as a the coagulation bath. Obtained HFMs were treated with DI water for 48 hours to ensure complete removal of the solvent. The dope composition and spinning parameters are given in following Table 1.

Table 4.1 Dope solution composition and spinning parameters used for making PAN based HFMs

A) Dope solution composition	
PAN (wt %)	11
Citric acid (wt %)	4
<i>N,N</i> -Dimethyl formamide (wt %)	85
B) Spinning conditions	
Take-up (m.sec)	5
Air gap (cm)	4
Coagulation bath temperature (°C)	27

The water permeance analysis of PAN HFMs was performed using a membrane module with an active area of 150 cm², in triplicate. The average water permeance was 300 Lm⁻²h⁻¹bar⁻¹. The rejection analysis of BSA (0.1% concentration in the feed) was performed at pH 7.5 using McIlvaine buffer in cross-flow mode. The protein concentration in the feed and permeate was analyzed at 280 and 260 nm wavelength by the double beam UV spectrophotometer (Chemito, Spectrascan UV 2700) using Equation 1.

$$[C] = (1.55 \times A_{280} - 0.76 \times A_{260}) \quad 1$$

The percent rejection (%R) was calculated by using Equation 2.

$$R(\%) = \left(1 - \frac{c_p}{c_f}\right) \times 100 \quad 2$$

where, C_p is the concentration of permeate, while C_f is the feed concentration. The membranes showed > 90% rejection for BSA.

4.5.3 TpEt-based membrane preparation

The precursor solutions were prepared by dissolving the appropriate quantity of ethidiumbromide (Et) and 1,3,5-triformylphloroglucinol (Tp) in water and DCM, respectively (Table 2). A 6 molar equivalent of co-reagent, PTSA, or TFA (for TpEt-PTSA and TpEt-TFA, respectively) was added along with the amine solution. A 500 ml measuring cylinder was used for dipping HFMs into the precursor solution. The bottom side of each HFM was blocked using epoxy resin to prevent the entry of precursor solution inside the bore. The interfacial synthesis of COF on the surface of HFMs was performed by dipping them first in an aqueous solution for 1 hr. It was followed by air drying for 5 min, while holding HFMs vertically to drain the excess aqueous solution. The HFMs were then dipped in dichloromethane (DCM) solution for 6 hr to allow COF formation on the surface of HFM. This procedure was repeated for six cycles with the same solution and washed with sufficient water at the end. For each synthesis, the membrane area used was kept constant, and the ratio of solution to the area was 13 ml/cm².

Table4. 2 Concentration of precursor solution used for membrane fabrication

Membrane Identification	Concentration of amine (mM)	Concentration of Aldehyde (mM)	Concentration of Co-reagent (mM)*
TpEt-PTSA-1	1	1	6
TpEt-PTSA-0.5	0.5	0.5	3
TpEt-TFA-1	1	1	6
TpEt-TFA-0.5	0.5	0.5	3

*The co-reagent is PTSA and TFA, respectively, for TpEt-PTSA and TpEt-TFA

4.5.4 Characterization methods

a) FTIR-ATR

The Fourier transform infrared (FTIR) spectroscopy was carried out using PerkinElmer spectrum one FTIR instrument using Universal ATR (Attenuated total internal reflection) accessory. The analysis was done in the range of 600-4000 cm⁻¹.

b) Solid-state NMR

Solid state C¹³ NMR spectra were recorded on Bruker 300 MHz NMR spectrometer, where carbon chemical shifts are expressed in parts per million.

c) Wide-angle X-ray diffraction (WAXD)

The WAXD pattern was recorded on a Rigaku Smart Lab Instrument with PhotonMax high-flux 9 kW rotating anode X-ray source. The 2θ range was $2\text{--}40^\circ$ and the radiation used was $\text{CuK}\alpha$ with wavelength 1.5418 \AA .

d) Contact angle

The static contact angle analysis was measured using a Kruss drop shape analyzer, DSA 25S. The measurements were taken with the help of Advance software using the sessile drop method. The hollow fiber membrane samples were horizontally mounted on the sample holder, and $1 \mu\text{l}$ of water was dropped on the surface. The contact angles were measured up to 2 min with a regular interval of 30 s.

e) Scanning electron microscopy (SEM)

The HFM samples were freeze-fractured in liquid nitrogen and gold-sputtered using SCD 040 Balzers Union. The SEM images were obtained using FEI, QUANTA 200 3D SEM instrument operating at 10, 15 and 20 kV, using tungsten filament as an electron source.

f) X-ray photoelectron spectroscopy (XPS)

The XPS analyses were performed on a Thermo Fisher Scientific Instruments UK, Sr.No.-KAS2020, with an exciting source of $\text{Al-K}\alpha$ with the energy of 1486.6 eV

4.5.5 Preparation of HFM modules

The PVC pipe of $0.5''$ diameter was used as a shell. Each module comprised 10 HFMs with a 20 cm active length and an average active area of 150 cm^2 . Two-component epoxy resin was used for potting.

4.5.6 Solvent permeation analysis

The permeation analysis was performed in out-to-in mode (shell to bore). The upstream pressure was maintained as 1.5 bar, while the permeate side was maintained at the ambient pressure. The permeate was collected from one end of the bore side after 15 minutes from the beginning of the experiment to ensure the steady state. Permeance was calculated from the permeate volume collected (V) per unit time (t) through membrane area (A) under pressure (p) using Eq. 3. At least three modules were tested for each COF thin film membrane and averaged.

$$p = \frac{V(l)}{A(m^2)t(h)p(bar)} \quad 3$$

4.5.7 Rejection analysis

The rejection performance of the membrane module was evaluated using a 50 mg/l methanol solution of a chosen dye (direct red-80, direct red-23, cibacron blue, brilliant blue, or methylene blue). The upstream pressure was maintained at 1.5 bar, while the downstream was maintained at ambient. The dye concentration in the feed and permeate was measured after 15 minutes from the start of the experiment using UV visible spectroscopy. The percent rejection was calculated by Eq 4.

$$R(\%) = \left(1 - \frac{c_p}{c_f}\right) \times 100 \quad 4$$

where, C_p and C_f are the concentration of dye in the feed and permeate, respectively.

4.6 References

- [1] P.J. Waller, F. Gándara, O.M. Yaghi, Chemistry of Covalent Organic Frameworks, *Acc. Chem. Res.* 48 (2015) 3053–3063. <https://doi.org/10.1021/acs.accounts.5b00369>.
- [2] A.P. Côté, H.M. El-Kaderi, H. Furukawa, J.R. Hunt, O.M. Yaghi, Reticular synthesis of microporous and mesoporous 2D covalent organic frameworks, *J. Am. Chem. Soc.* 129 (2007) 12914–12915. <https://doi.org/10.1021/ja0751781>.
- [3] X. Feng, X. Ding, D. Jiang, Covalent organic frameworks, *Chem. Soc. Rev.* 41 (2012) 6010–6022. <https://doi.org/10.1039/c2cs35157a>.
- [4] J.W. Colson, A.R. Woll, A. Mukherjee, M.P. Levendorf, E.L. Spitler, V.B. Shields, M.G. Spencer, J. Park, W.R. Dichtel, Oriented 2D Covalent Organic Framework Thin Films on Single-Layer Graphene, 332 (2011) 228–232.
- [5] N.W. Ockwig, A.P. Co, M.O. Keeffe, A.J. Matzger, O.M. Yaghi, Porous , Crystalline , Covalent Organic Frameworks, 310 (2005) 1166–1171.
- [6] K. Geng, T. He, R. Liu, S. Dalapati, K.T. Tan, Z. Li, S. Tao, Y. Gong, Q. Jiang, D. Jiang, Covalent Organic Frameworks: Design, Synthesis, and Functions, *Chem. Rev.* 120 (2020) 8814–8933. <https://doi.org/10.1021/acs.chemrev.9b00550>.
- [7] Z. Wang, S. Zhang, Y. Chen, Z. Zhang, S. Ma, Covalent organic frameworks for separation applications, *Chem. Soc. Rev.* 49 (2020) 708–735. <https://doi.org/10.1039/c9cs00827f>.
- [8] Z. Kang, H. Guo, L. Fan, G. Yang, Y. Feng, D. Sun, S. Mintova, Scalable crystalline porous membranes: current state and perspectives, *Chem. Soc. Rev.* (2021) 1913–1944. <https://doi.org/10.1039/d0cs00786b>.
- [9] S. Yuan, X. Li, J. Zhu, G. Zhang, P. Van Puyvelde, B. Van Der Bruggen, Covalent organic frameworks for membrane separation, *Chem. Soc. Rev.* 48 (2019) 2665–2681. <https://doi.org/10.1039/c8cs00919h>.
- [10] M. Fang, C. Montoro, M. Semsarilar, Metal and covalent organic frameworks for membrane applications, *Membranes* (Basel). 10 (2020). <https://doi.org/10.3390/membranes10050107>.

- [11] T. Rasheed, S. Khan, T. Ahmad, N. Ullah, Covalent Organic Frameworks-Based Membranes as Promising Modalities from Preparation to Separation Applications: An Overview, 202200062 (2022). <https://doi.org/10.1002/tcr.202200062>.
- [12] S. Kandambeth, B.P. Biswal, H.D. Chaudhari, K.C. Rout, S. Kunjattu H., S. Mitra, S. Karak, A. Das, R. Mukherjee, U.K. Kharul, R. Banerjee, Selective Molecular Sieving in Self-Standing Porous Covalent-Organic-Framework Membranes, *Adv. Mater.* 29 (2017). <https://doi.org/10.1002/adma.201603945>.
- [13] D.B. Shinde, G. Sheng, X. Li, M. Ostwal, A.H. Emwas, K.W. Huang, Z. Lai, Crystalline 2D Covalent Organic Framework Membranes for High-Flux Organic Solvent Nanofiltration, *J. Am. Chem. Soc.* 140 (2018) 14342–14349. <https://doi.org/10.1021/jacs.8b08788>.
- [14] R. Wang, X. Shi, A. Xiao, W. Zhou, Y. Wang, Interfacial polymerization of covalent organic frameworks (COFs) on polymeric substrates for molecular separations, *J. Memb. Sci.* 566 (2018) 197–204. <https://doi.org/10.1016/j.memsci.2018.08.044>.
- [15] H. Fan, M. Peng, I. Strauss, A. Mundstock, H. Meng, J. Caro, High-Flux Vertically Aligned 2D Covalent Organic Framework Membrane with Enhanced Hydrogen Separation, *J. Am. Chem. Soc.* 142 (2020) 6872–6877. <https://doi.org/10.1021/jacs.0c00927>.
- [16] J. Shen, R. Zhang, Y. Su, B. Shi, X. You, W. Guo, Y. Ma, J. Yuan, F. Wang, Z. Jiang, Polydopamine-modulated covalent organic framework membranes for molecular separation, *J. Mater. Chem. A* 7 (2019) 18063–18071. <https://doi.org/10.1039/c9ta05040j>.
- [17] H. Fan, A. Mundstock, A. Feldhoff, A. Knebel, J. Gu, H. Meng, J. Caro, Covalent Organic Framework-Covalent Organic Framework Bilayer Membranes for Highly Selective Gas Separation, *J. Am. Chem. Soc.* 140 (2018) 10094–10098. <https://doi.org/10.1021/jacs.8b05136>.
- [18] H. Fan, A. Mundstock, J. Gu, H. Meng, J. Caro, An azine-linked covalent organic framework ACOF-1 membrane for highly selective CO₂/CH₄ separation, *J. Mater. Chem. A* 6 (2018) 16849–16853. <https://doi.org/10.1039/c8ta05641b>.
- [19] K. Dey, M. Pal, K.C. Rout, S.S. Kunjattu, A. Das, R. Mukherjee, U.K. Kharul, R. Banerjee, Selective Molecular Separation by Interfacially Crystallized Covalent Organic Framework Thin Films, *J. Am. Chem. Soc.* 139 (2017) 13083–13091. <https://doi.org/10.1021/jacs.7b06640>.
- [20] D.B. Shinde, S. Kandambeth, P. Pachfule, R.R. Kumar, R. Banerjee, Bifunctional covalent organic frameworks with two dimensional organocatalytic micropores, *Chem. Commun.* 51 (2015) 310–313. <https://doi.org/10.1039/c4cc07104b>.
- [21] N. Huang, R. Krishna, D. Jiang, Tailor-Made Pore Surface Engineering in Covalent Organic Frameworks: Systematic Functionalization for Performance Screening, *J. Am. Chem. Soc.* 137 (2015) 7079–7082. <https://doi.org/10.1021/jacs.5b04300>.
- [22] A. Nagai, Z. Guo, X. Feng, S. Jin, X. Chen, X. Ding, D. Jiang, Pore surface engineering in covalent organic frameworks, *Nat. Commun.* 2 (2011). <https://doi.org/10.1038/ncomms1542>.

- [23] D.B. Shinde, L. Cao, A.D.D. Wonanke, X. Li, S. Kumar, X. Liu, M.N. Hedhili, A.H. Emwas, M. Addicoat, K.W. Huang, Z. Lai, Pore engineering of ultrathin covalent organic framework membranes for organic solvent nanofiltration and molecular sieving, *Chem. Sci.* 11 (2020) 5434–5440. <https://doi.org/10.1039/d0sc01679a>.
- [24] T. Chen, B. Li, W. Huang, C. Lin, G. Li, H. Ren, Y. Wu, S. Chen, W. Zhang, H. Ma, Highly crystalline ionic covalent organic framework membrane for nanofiltration and charge-controlled organic pollutants removal, *Sep. Purif. Technol.* 256 (2021) 117787. <https://doi.org/10.1016/j.seppur.2020.117787>.
- [25] X. Wang, J. Yang, X. Shi, Z. Zhang, C. Yin, Y. Wang, Electrosynthesis of Ionic Covalent Organic Frameworks for Charge-Selective Separation of Molecules, (n.d.). <https://doi.org/10.1002/sml.202107108>.
- [26] B.L. and H.M. Wenxiang, Zhang Liming, Zhang, Haifeng Zhao, Two-Dimensional Cationic Covalent Organic Framework Membrane for Selective Molecular Sieving, *J. Mater. Chem. A.* 6 (2018) 13331–13339. <https://doi.org/10.1039/C8TA04178D>.
- [27] J.H. Chong, M. Sauer, B.O. Patrick, M.J. MacLachlan, Highly Stable Keto-Enamine Salicylideneanilines, (2003) 2–5.

Conclusions

Membrane processes are being proven as a viable alternative to the conventional methods of separation processes. Newer challenges of industrial separations drive the new membrane development. The Metal-Organic Frameworks (MOF) and Covalent Organic Frameworks (COF) are being projected as promising membrane materials having the capability to address crucial separation challenges for gas separations (specifically olefin-paraffin separation) and solvent-based separations (Organic Solvent Nanofiltration, OSN). The present work investigated critical issues related to MOF and COF-based membranes, specifically scaleable membrane preparation methodologies.

The first chapter introduces the need for membrane-based separations and various membrane aspects (types of membrane processes, materials, configurations, etc.), followed by introducing MOFs and COFs. Their different synthetic methodologies, applications, significance as membrane materials, and potential to address unmet challenges are reviewed. The literature survey conveyed that the performance of crystalline porous material-based membranes could be superior to conventional polymer-based membranes.

Chapter 2 presents the fabrication of Zeolitic Imidazolate Framework (ZIF) based mixed matrix membranes (MMM) for olefin/paraffin separation. As widely documented in the literature, although ZIFs seems to be a highly promising material family for this industrially crucial task, their membrane preparation on a large scale remains a key challenge. These crystalline materials to be blended with adequate polymers could be one solution to address their scalability. The permeation properties and compatibility of the host polymer with ZIFs are essential aspects that need to be addressed. The present work demonstrated good interfacial compatibility between the host polymer, polyphenylene oxide (PPO), and chosen ZIF particles. The interfacial compatibility as a result of the interaction of metal ions in the ZIF (Zn and Co in ZIF-8 and ZIF-67, respectively) with the 'O' atom present in the polymer (PPO) backbone is demonstrated by various characterization tools. The membranes exhibited good propane/propylene separation, coupled with attractive permeability of propylene. The ideal separation factor for propylene/propane was ~27 and 25 for 40% loaded ZIF-8 and ZIF-67

MMMs, respectively. Moreover, the performances of these membranes were appreciable in a mixed gas environment. Their sustainable performance for a longer duration addressed plasticization and aging aspects positively.

The third chapter demonstrates a new methodology for fabricating COF thin films on the surface of polyacrylonitrile (PAN) based hollow fiber membrane (HF) surface by interfacial synthesis. This method is easily scalable and allows good control on the membrane thickness. The membranes showed promising solvent permeance. For example, the Tp-Tta-15 and Tp-Azo-400 membranes exhibited acetone permeance of 16 and 11.5 $\text{Lm}^{-2}\text{h}^{-1}\text{bar}^{-1}$, respectively. Most importantly, the rejection analysis shows that the membranes have high molecular sieving ability. The long-time dye rejection study reveals that the contribution of dye adsorption to rejection is negligible. The membranes exhibited solvent resistance in different organic media and superior long-term stability, conveying their promises for organic solvent nanofiltration (OSN).

The fourth chapter deals with the fabrication of charged ethidium bromide-based COF membranes by interfacial synthesis. The synthetic methodology allowed modification of the COF-pores by in-situ anion exchange. The membrane performance showed a significant aspect of governing membrane permeation properties by the charge present on the COF surface. In this approach, rather than the molecular weight of the solute, the charge present on the COF surface was found to govern membrane selectivity and opens up a new direction to make OSN membranes with good control on charge-based exclusion.

In summary, this thesis revealed a significant understanding of membrane fabrication using ZIFs and COFs for addressing separation challenges of practical significance. The membrane-making methodologies were simple and scalable, addressing unmet needs.

ABSTRACT

Name of the Student: Shebeeb K. H.

Registration No.: 10CC19J26027

Faculty of Study: Chemical Science

Year of Submission: 2022

AcSIR academic centre/CSIR Lab: CSIR-NCL

Name of the Supervisor: Dr. Ulhas K. Kharul

Title of the thesis: Membrane Based on Crystalline Porous Materials: Preparation and Investigation for Gas and Niche Liquid Separations

A substantial portion of the energy consumed in industry accounts for separating chemicals into pure form, including distillation, evaporation, and drying. Membrane-based separation is recognized as a powerful technology that guarantees high selectivity, low energy consumption, and a small footprint for separation applications and fulfils the need for new sustainable industrial process effectiveness. Polymeric materials have been widely studied as membrane materials for separation applications due to their excellent processability and cost-effectiveness. The absence of ordered identical pores in amorphous polymers lacks a trade-off between permeability and selectivity. Crystalline porous materials (CPMs) with ordered pore structures with high selectivity and large pore volumes for high flux are highly attractive for membrane separation. In addition to the ordered porous structure, we can tailor the pore size of the CPMs, which is highly desired for membrane separation to attain critical separations. The CPMs are widely studied for separation applications. However, the real potential of the materials couldn't be fully achieved due to the poor processability and lack of a proper fabrication protocol. In this thesis, we showcased a new methodology to fabricate the membrane based on MOFs and COFs in a scalable way without defects. Further, the membranes were demonstrated for industrially challenging separation applications.

In the second chapter, we fabricated ZIF-8 and ZIF-67-based mixed matrix membranes for olefin/paraffin separation. The 40% ZIF-loaded membranes show propylene permeability of ~ 12 barrer with propylene-propane selectivity of 25 and 27 for ZIF-67 and ZIF-8, respectively. In the third chapter, we could achieve a scalable COF-based thin-film membrane on the outer surface of the PAN hollow fiber substrate. The membranes showcased for the organic solvent nano-filtration. The thin-film membrane exhibits good solvent flux, and appreciable selectivity of solute molecule based on size exclusion. The fourth chapter could achieve pore modification of COF membrane in-situ by anion exchange method. The charged COF membrane exhibited selective molecular sieving based on the size of the solute molecule.

Details of the Publications Emanating from the Thesis Work

1) List of publication(s) in SCI Journal(s) (published & accepted) emanating from the thesis work, with complete bibliographic details.

(i) Shebeeb Kunjattu H., Ulhas K. Kharul, PPO-ZIF MMMs possessing metal-polymer interactions for propane/propylene separation, J. Membr. Sci. 668 (2023),121208

DOI: <https://doi.org/10.1016/j.memsci.2022.121208>

2) List of Papers with abstract presented (oral/poster) at national/international conferences/seminars with complete details.

(i) Presented a poster entitled “*ZIF-8@DBzPBI-BuI composite membranes for olefin/paraffin separation*” during National Science Day Celebrations at CSIR-National Chemical Laboratory, Pune, India, February 2021..

Abstract: ZIF-8 is a member of Zeolitic Imidazole Framework family having high internal surface area, the high thermo-chemical stability and ease of synthesis gained immense attention for its highly selective sieving ability. Transforming it into a membrane form and practical utility remains a challenge. Any success towards this direction would radically reduce the cost of propylene/propane separation. Present study reports use of substituted polybenzimidazole (DBzPBI-BuI) for fabrication of flexible, thus scalable composite membranes with ZIF-8 (ZIF-8@DBzPBI-BuI) possessing host-guest compatibility. The membrane with 30% ZIF-8 loading showed promising propylene-propane separation (ideal selectivity of 32.7), coupled with propylene permeability of 12.13 Barrer. Analysis of sorption shed light on the high contribution of diffusivity on governing permeation properties of the composite membranes. The mixed gas analysis offered highly encouraging results in comparison to known composite membranes of different polymers with ZIF-8. Placement of present data on ‘upper-bound’ showed a rapid enhancement in selectivity by the addition of ZIF-8 in the polymer matrix, which seems to be a result of the elimination of inter-phase defects. It was made possible due to the functionality of host polymer.

(ii) Presented an oral talk entitled “*ZIF-8@DBzPBI-BuI composite membranes for olefin/paraffin separation*” at the International Conference SETEC-18 at BITS Pilani Goa.

Abstract: See the abstract for entry (i)



PPO-ZIF MMMs possessing metal-polymer interactions for propane/propylene separation

Shebeeb Kunjattu H^{a,b}, Ulhas K. Kharul^{a,b,*}

^a Polymer Science and Engineering Division, CSIR-National Chemical Laboratory, Pune, 411008, India

^b Academy of Scientific and Innovative Research (AcSIR), Ghaziabad, 201002, India

ARTICLE INFO

Keywords:

Zeolitic imidazole framework
Olefin-paraffin separation
Mixed matrix membrane
poly(phenyleneoxide)
Interfacial interactions

ABSTRACT

An assertive formation of ZIF-based mixed matrix membranes (MMMs) with polyphenylene oxide (PPO), a high permeability polymer as a host, is presented. The interfacial interactions between the filler particles and polymer matrix are established by DSC and XPS analyses. The ZIF loading could be achieved up to 40% without hampering the stability of the resulting MMMs. These membranes were evaluated for pure gas permeability, specifically aiming at C₃H₆/C₃H₈ separation, a highly desired application in industry. The ZIF-PPO hybrids display promising pure gas as well as mixed gas permeation performance. The 40% ZIF-8 and ZIF-67 loaded membrane display promising C₃H₆/C₃H₈ selectivity of 27.5 and 25, with a permeability of 12 and 13 barrer, respectively. The enhanced selectivity is attributed to the absence of defects eliminated due to metal-polymer interactions. The permeation study of a 30% ZIF-8 loaded membrane while varying transmembrane pressure and long-time exposure (150 h) of propylene at 60 psi indicated the excellent stability of the membrane. The sorption analysis further confirmed the molecular sieving characteristics of the ZIF@PPO MMMs. The mixed gas permeation performance showed promising results of high permeability as well as maintaining selectivity over a wide range of compositions.

1. Introduction

Olefins are a desired class of chemicals used as a raw material in various chemical manufacturing such as acrylonitrile, propylene oxide, iso-propanol, allylchloride, acrolein, acrylic acid and its esters, cumene and different kind of polymers [1]. The annual production of propylene was approximately 100 million tons worldwide in 2016 and is expected to grow at a rate of 3.6% by 2025 [2]. During their production, the separation of olefin and paraffin is one of the crucial steps. Due to the close physicochemical properties of propylene and propane (boiling point: -47.6 °C and -42.1 °C and Lennard-Jones diameter: 4.68 Å vs 5.06 Å, respectively); their separation is known to be highly energy-intensive [3,4]. It is usually done by cryogenic distillation at -25 °C with 75 m tall columns consisting of >200 trays needing 10–15 reflux ratios and high pressure of 16–20 bar [3,5]. This energy-intensive nature is well quantified in the literature. It is said that the purification of propylene and ethylene alone accounts for 0.3% (120TBtu/year) of global energy use, roughly equivalent to Singapore's annual energy consumption [6,7]. Various methods such as extractive distillation, membrane separation, absorption, physical adsorption, and chemical

complexation are proposed for olefin-paraffin separation [8,9]. Membrane technology has aroused great attention as an effective alternative for propane propylene separation due to its advantages, including low energy consumption, environmental friendliness, easy operation, and no need for phase change [10–13]. Several materials are studied as a membrane for C₃H₆/C₃H₈ separation, such as polymers [4,14,15], carbon molecular sieves [16,17] and Zeolites [18]. Among these, polymeric membranes have the advantage of easy processibility and scalability. However, some fundamental issues persist in polymeric membranes, such as plasticization and the trade-off relationship between permeability and selectivity [4,19]. Mixed Matrix Membranes (MMMs) are emerging as a new type of membrane material to overcome these issues. In this approach, highly selective and permeable filler particles are dispersed in a polymer matrix. Some such membranes are well placed over the limiting upper bound [20]. In addition, the flexibility and solubility offered by the polymer retain the processability similar to the polymeric membrane [20,21].

Different fillers such as silica, zeolites, carbon molecular sieves, and porous organic cages have been demonstrated as filler materials [20]. The selection of filler plays a vital role in the performance of Mixed

* Corresponding author. Polymer Science and Engineering Division, CSIR-National Chemical Laboratory, Pune, 411008, India.

E-mail address: uk.kharul@ncl.res.in (U.K. Kharul).

<https://doi.org/10.1016/j.memsci.2022.121208>

Received 28 June 2022; Received in revised form 6 November 2022; Accepted 19 November 2022

Available online 25 November 2022

0376-7388/© 2022 Elsevier B.V. All rights reserved.

Matrix Membranes (MMMs). For example, due to the inorganic nature of zeolites, surface modification is needed to attain better compatibility with the polymer [13]. Metal-Organic Frameworks (MOFs) are porous crystalline materials composed of metal atoms linked together by organic linkers [22]. The organic and inorganic nature offers better compatibility with the polymer and tunable pore aperture, making them promising filler materials [23]. The Zeolitic Imidazole Frameworks (ZIFs), a subclass of MOF, have been of interest in preparing gas separation membranes due to their similar pore size as that of smaller gas molecules. In addition, they show high chemical and thermal stability [24,25]. The ZIF-8 is one of the widely studied ZIFs. It is composed of Zn metal and 2-methyl imidazole as the ligand. It has a sodalite (SOD) topology possessing a large pore cavity (11.6 Å) and narrow pore aperture (3.4 Å) [26]. A single component diffusion study by Li et al. reveals 125 as the diffusion selectivity of propylene/propane in ZIF-8 [27]. Several strategies are developed to fabricate ZIF-8-based membranes for C₃H₆/C₃H₈, which include pristine ZIF-8 membrane on a substrate [28–31] and MMMs [13,32]. Jeong's group found that ZIF-67, a cobalt-substituted equivalent of ZIF-8, is also an excellent material for propylene/propane separation [33]. The submicron-thick ZIF-67 membrane resulted in an average propylene/propane separation factor of 85 and propylene permeance of $\sim 460 \times 10^{-10} \text{ mol Pa}^{-1} \text{ m}^{-2} \text{ s}^{-1}$ [33].

Although the incorporation of MOF as a filler in MMMs looks impressive, one of the deterring factors behind this crucial issue is the poor interfacial compatibility of a filler with the polymer, leading to voids at the interface [3]. Several protocols are reported to improve the MOF-polymer compatibility. One approach is selecting a polymer matrix that can chemically or physically interact with the MOF [34,35]. The enhancement of interfacial compatibility can also be achieved through non-covalent interactions such as hydrophobicity [36], hydrophilicity [37] and hydrogen bonding [38]. Various modification strategies to achieve interfacial interactions between MOF and polymer are well reported [39–41]. Li's group has demonstrated covalently grafted polyimide brushes on MOF surfaces to engineer the MOF/polymer interface [42]. Zhong and co-workers demonstrated a bilayer-based strategy to construct MOF-based MMMs for efficient propylene-propane separation [43].

In addition to the MOF-polymer interactions, the intrinsic permeation property of the host polymer is also crucial since the permeated molecule from the MOF has to diffuse through the polymer matrix seamlessly. The polymer with lower permeability would offer resistance for the diffusion of the molecule 'chosen' by the MOF to permeate selectively through MMM. Conversely, if the polymer has high permeability (e.g., PDMS), the permeating molecule would permeate through the polymer matrix rather than through the MOF particles. Thus, the intrinsic permeation property of the host polymer has to be appropriate, avoiding both above possibilities. In this direction, we have reported ZIF-8-based MMM with N-substituted PBI, possessing a fairly good combination of permeability and selectivity [44]. The reason behind PBI selection was to enhance the filler matrix compatibility by the metal-polymer interaction (Zn in ZIF-8 and N in the polymer backbone). We could achieve fairly good separation performance for propylene/propane with 30% ZIF loading, outperforming almost all the previously reported MMM in terms of selectivity (~ 32). Despite this, the polymer availability for the scale-up could be an additional issue. To address this, the present work describes a new type of MMM with a common, commercially better feasible polymer host, viz., poly(2,6-dimethyl-1,4-phenylene oxide), commonly called polyphenylene oxide or PPO. The two widely investigated ZIFs, viz., ZIF-8, and ZIF-67, were chosen as fillers. The PPO possesses fairly good permeability and moderate selectivity [45,46]. The 'O' atom present in the polymer backbone exhibiting interactions with the metal present in ZIFs (Zn and Co), which in turn enable ZIF-polymer interfacial compatibility is the focus of the present work. The formed MMMs showed enhancement in selectivity and permeability of C₃H₆/C₃H₈ than the host PPO matrix and can fulfil the commercial approach.

2. Experimental

2.1. Materials

The zinc nitrate hexahydrate (Zn(NO₃)₂·6H₂O), cobalt nitrate hexahydrate (Co(NO₃)₂·6H₂O), 2-Methylimidazole, chloroform, tetrachloroethane, methanol and toluene were purchased from Merck. Cupric chloride (CuCl₂), morpholine, and 2,6-dimethylphenol were procured from Sigma-Aldrich. The gases, viz., He, N₂, O₂ were purchased from Ms. Vadilal Gases, while C₂H₄, C₂H₆, C₃H₆, and C₃H₈ were procured from Delux Gas. All the chemicals were used without further purification.

2.2. Synthesis of ZIF nanoparticles

The ZIF-8 and ZIF-67 were synthesized by the reported method [44, 47,48] The details of their synthesis are given in the Supplementary Information. The synthesized nanoparticles were dispersed in chloroform and used to prepare mixed matrix membranes (MMMs).

2.3. Membrane fabrication

The dense membranes based on PPO were prepared by the solution casting method using 3% (w/v) chloroform solution at 40 °C for 12 h in a pre-levelled petri-dish placed in an oven. After 12 h, the membrane was peeled off from the Petri-dish. It was kept in a vacuum oven at 60 °C for seven days and then used for further characterizations. The mixed matrix membranes (MMMs) were prepared by mixing an appropriate amount of ZIF dispersion in a prepared PPO chloroform solution, as schematically represented in Fig. 1. It was stirred for 24 h with 1-h bath sonication and 6-h interval. The homogeneously dispersed solution was poured in a petri dish at 40 °C for 12 h to make a membrane by solution casting method (Scheme S1). The PPO mixed matrix membranes (MMMs) were prepared with 10, 20, 30, and 40% loading of ZIFs (ZIF-8 and ZIF-67). In addition, 50% ZIF-loaded membranes were also fabricated by a similar method, however, the mechanical stability of the membranes was insufficient to carry out the permeation study. The membranes were designated as 'ZIF@PPO-%ZIF' (for example, ZIF-67@PPO-40 has 40% loading of ZIF-67 in the PPO matrix). The membranes were dried in a vacuum oven at 60 °C for a week before using for further analysis.

2.4. Gas permeation and sorption analysis

The pure gas permeation analysis was conducted using a variable pressure method at a constant temperature of 35 °C [44]. The membranes used were dried in a vacuum oven at 60 °C for 7 days and samples of 12.5 cm² active area were used for permeation analysis. The vacuum on the permeate side was measured using an MKS vacuum transmitter, and the online data was collected with the help of LabVIEW software. The permeability coefficient, P_i of a given gas, is determined following Eq. (1).

$$P_i = \frac{dp}{dt} \frac{lV}{ART\Delta p} \times 10^{10} \quad (1)$$

where, 'dp/dt' is the slop of permeate pressure versus time, 'l' is the membrane thickness, 'Δp' is the transmembrane pressure, 'V' is the downstream volume, 'T' is the temperature, and 'A' is the membrane area. The ideal selectivity (α_{ij}) was calculated by calculating the ratio of pure gas permeability of the fast permeating component (P_i) to the slow permeating one (P_j).

$$\alpha_{ij} = \frac{P_i}{P_j} \quad (2)$$

The gas sorption isotherms were collected at 35 °C using the pressure

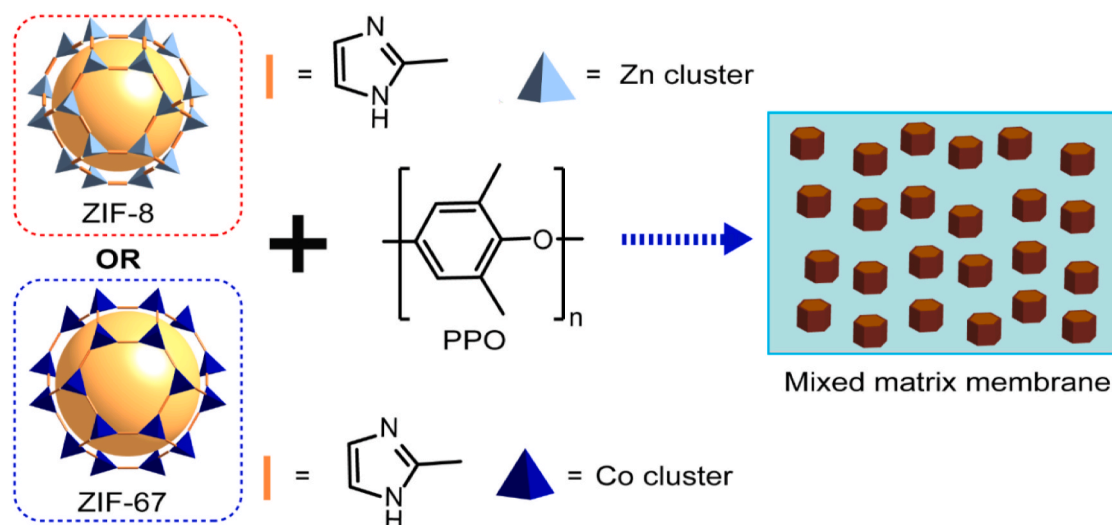


Fig. 1. Designing MMM by incorporating ZIF in to PPO polymer matrix.

decay method [44]. The data were collected using LabVIEW software, and the pressure was measured using WIKA pressure transmitter P-30. The sorption coefficient S_i is calculated using the following Eq. (3).

$$S_i = \frac{c_i}{p_i} \quad (3)$$

where, ' c_i ' is the gas uptake obtained from the sorption isotherm at pressure ' p_i '. The diffusion coefficient (D) of MMMs was calculated from the sorption (S) and permeability (P) coefficients.

$$D_i = \frac{P_i}{S_i} \quad (4)$$

The mixed-gas permeation experiments were performed for different feed compositions of propane and propylene at 50 psi as the feed pressure. The feed and permeate compositions were determined using gas

chromatography equipped with an FID detector. The mixed gas permeability was calculated using the following Eq. (5).

$$P_i = \frac{y_i \frac{dy}{dx} IV}{x_i ART \Delta p} 10^{10} \quad (5)$$

where, x and y represent the mole fraction of a gas in the feed and permeate stream, respectively. The separation factor while feeding the gas mixture to the membrane was calculated using Eq. (6).

$$\alpha_{(ij)} = \frac{y_i/y_j}{x_i/x_j} \quad (6)$$

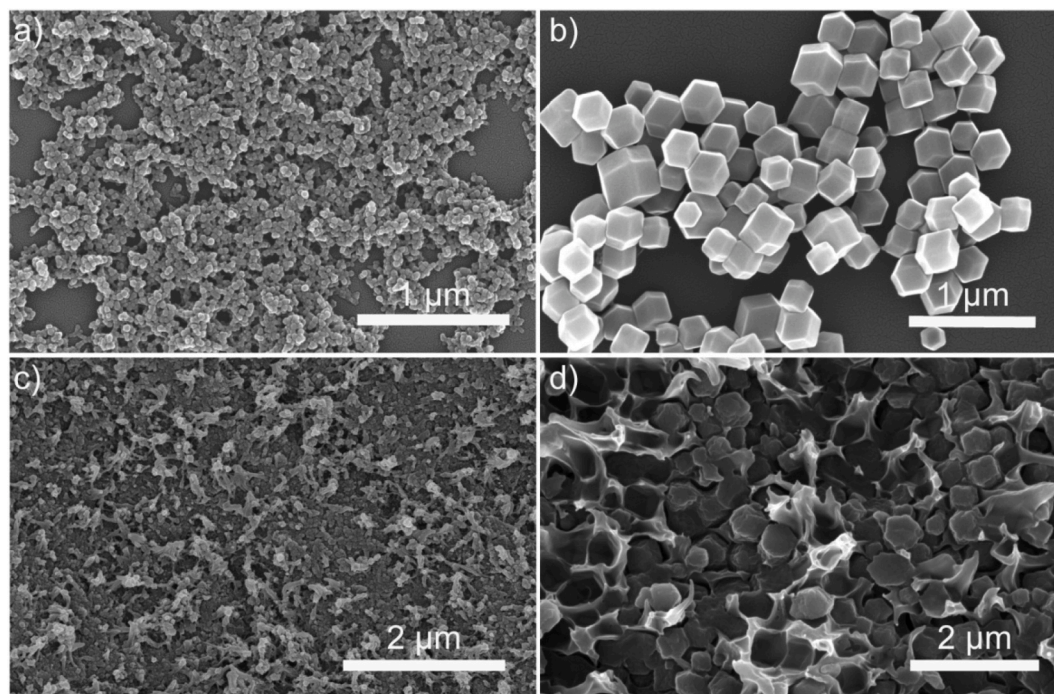


Fig. 2. The (a,b) SEM images of ZIF-8 and ZIF-67 particles, respectively; cross-sectional SEM image of (c) ZIF-8@PPO and (d) ZIF-67@PPO composite membranes having 40% ZIF-loading.

3. Results and discussion

3.1. Physical characterizations

3.1.1. Formation of MMMs

The synthesized ZIF particles showed uniform particle size (Fig. 2 a, b). The average particle size for ZIF-8 was 50 nm, while that of ZIF-67 was 500 nm. These values were further supported by the DLS analysis (Fig. S1). The PXRD pattern of both ZIF-8 and ZIF-67 matched well with the respective simulated one (Fig. S2). For casting MMMs, PPO, a high permeability polymer, was selected as a host for incorporating ZIF particles. The design of MMM fabrication is shown in Fig. 1. The stable membranes with 40% ZIF-loading in both the types of MMMs (ZIF-8@PPO and ZIF-67@PPO) could be attained easily. Beyond 40%, both types of MMMs were brittle. In our earlier effort [44], the ZIF loading was limited to 30%, wherein the host polymer belonged to the benzimidazole family. The obtained higher loading in the present case can be attributed to the higher molecular weight of the polymer, as depicted by the high intrinsic viscosity of the synthesized PPO ($[\eta] = 0.92$ dL/g). The TGA analyses of PPO and different MMMs were performed in the air to assess the char yield (Fig. S3). The TGA spectra of PPO (entirely organic) showed no residue at 900 °C. With this observation, the char yield of MMMs was ascribed to ZnO and CoO (for ZIF-8 and ZIF-67, respectively). The char yield offered a quantitative estimation of ZIF content in the respective MMM. It was observed that the TGA-estimated value matched well (variation from 0.1 to 1.5%) with that of the experimental loading taken while casting MMMs (Table S1).

3.2. Structural integrity of ZIF particles in resulting MMMs

The cross-sectional SEM images of ZIF-8@PPO-40 and ZIF-67@PPO-40 are shown in Fig. 2c and d. The distribution of both types of ZIF particles was found to be uniform in the host PPO matrix. Any sign of particle agglomeration was absent. Similarly, the 20% and 30% ZIF-loaded MMMs showed homogeneous distribution of the ZIF particles (Fig. S4). These SEM images also reveal that the morphology and particle size of ZIF particles in the MMMs were comparable with that of as-synthesized ZIF particles. This observation confirms that the structural identity of ZIF particles was retained in the resulting MMM matrix. This highly significant observation (absence of agglomeration) indicates preferred interactions of ZIF particles with the PPO polymer chains, possessing oxygen.

The x-ray diffraction patterns of ZIF@PPO MMMs (Fig. S2) showed

the characteristic diffraction peaks of the corresponding ZIF particles. It further substantiates that the structural integrity of the ZIF particle was maintained in the MMMs. The X-ray diffraction spectra of PPO showed a broad, amorphous hump at 14.1°, leading to a d-spacing of 6.2 Å. The d-spacing of PPO matched well with that of the reported data [49,50]. In the X-ray diffraction spectra of MMMs, the amorphous peak of PPO was masked by the intense peaks of ZIF particles. This was observed in both ZIF-8 and ZIF-67-based MMMs.

3.2.1. Interaction between ZIF particles and host PPO

The DSC spectra of ZIF-8 and ZIF-67-based MMMs is shown in Fig. 3a and b. It is evident from these thermograms that the T_g of all MMMs shifted to a higher temperature than that of pristine PPO, even after a small, 10% ZIF loading. This enhancement in T_g indicated that the ZIF particles restricted the polymer chain mobility due to their interactions with the host PPO. Even though an enhancement in T_g could be small, obtained rigidification is advantageous in tackling the plasticization issue of polymeric membranes. The XPS analysis was performed to investigate the ZIF-polymer interactions further (Fig. 4a-c and S5). The high-resolution O1s spectra of MMMs showed a peak shift vis-à-vis O1s spectra of pristine PPO (Fig. 4b and c and Fig. S5). This observation is highly prominent in the case of 40% loaded MMMs. The O1s peak of MMMs was deconvoluted into two different peaks (Fig. 4a-c and S5). The one at higher binding energy accounts for the interaction of the 'O' atoms of PPO with the metal atom of the ZIF particle. It could be assigned to the electronegative nature of oxygen belonging to PPO and positively charged metal atom from the ZIF moiety (Zn and Co in ZIF-8 and ZIF-67, respectively). The other peak with lower binding energy is the characteristic peak of PPO-'O' (Fig. 4a). Such a peak shift indicates the polymer-filler interactions. The metal region in XPS spectra (Zn 2p and Co 2p in ZIF-8@PPO and ZIF-67@PPO MMMs, respectively) was also analyzed (Figs. S6a and b). Two different peaks in the Zn 2p region attributed to Zn 2p 3/2 (lower binding energy) and 2p 1/2 (higher binding energy). A shift in binding energy implies that the Zn atom participated in the interactions. Similarly, the Co atom present in the ZIF-67 shows four different peaks, including 2p 3/2, 2p 1/2, and two satellite peaks. This shift in binding energy is attributed to the cobalt-oxygen interactions. The XPS analysis confirming PPO-ZIF interactions led to the elevation of T_g of PPO. This might also assist in achieving higher ZIF-loading in PPO, providing a compatible interface between the ZIF particles and PPO matrix and suppressing the polymer plasticization/physical aging.

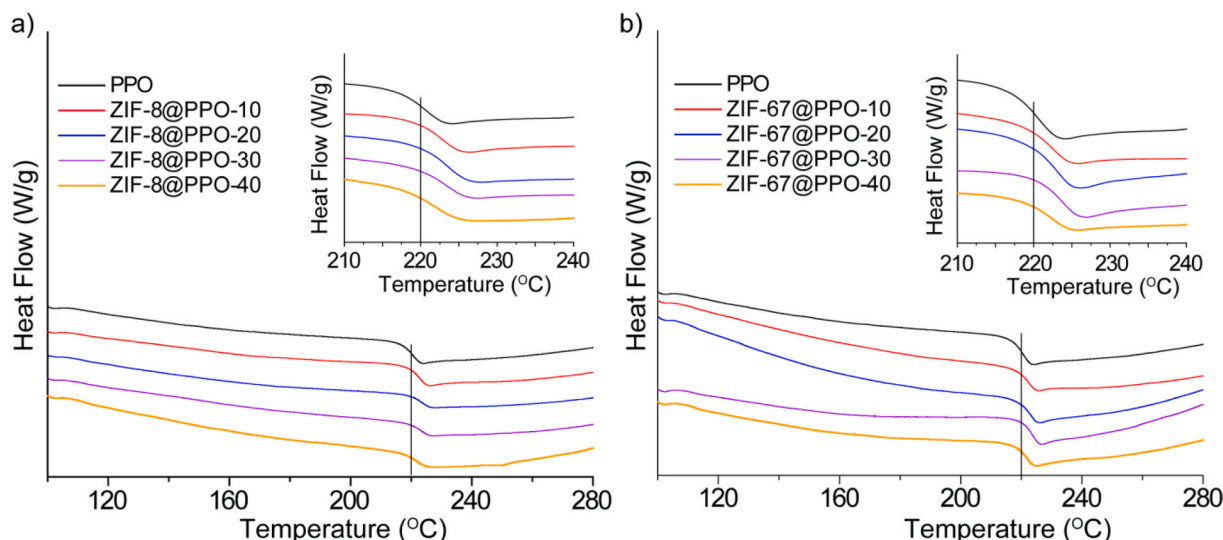


Fig. 3. DSC thermograms of (a) ZIF-8@PPO and (b) ZIF-67@PPO MMMs.

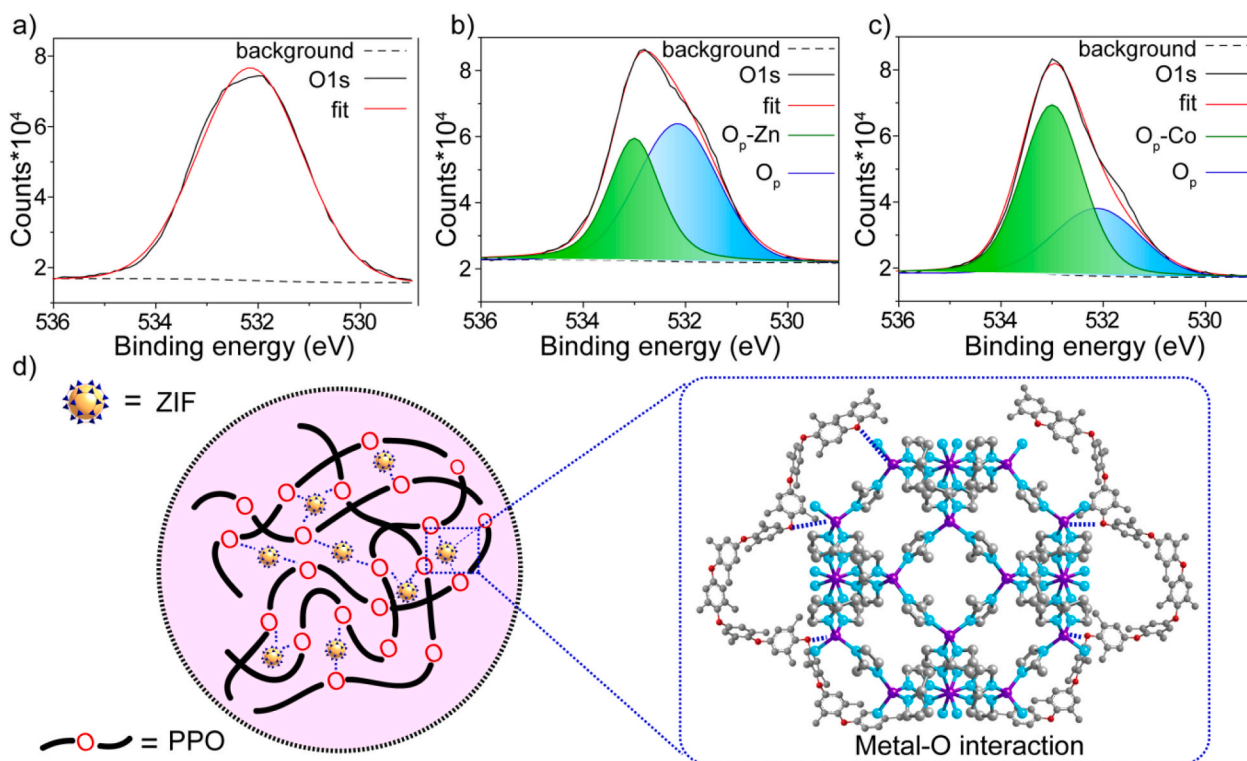


Fig. 4. High resolution 'O1s' XPS spectra of (a) PPO, (b,c) ZIF-8@PPO-40 and ZIF-67@PPO-40, and (d) schematic representation of the metal oxygen interaction present in the MMMs.

3.3. Gas permeation properties

3.3.1. Pure gas analysis

The gas permeability analysis was performed using pure gases of varying kinetic diameters (He, O₂, N₂, CH₄, C₂H₄, C₂H₆, C₃H₆, and C₃H₈). Obtained permeation properties are plotted in Fig. 5a and b (Table S2). The permeability of all gases, except propane, increased after incorporating ZIF-8 or ZIF-67 in the PPO matrix. This was followed for all the amount of ZIF-loading, as anticipated. It is also evident that for a particular MMM, the permeability of various gases generally increased with the lowering of permeant size. A prominent exception was seen for ethylene as a permeant. Fig. 5a (ZIF-8 based MMMs) and Fig. 5b (ZIF-67 based MMMs) showed a prominent hump for the permeability coefficient of ethylene (~4.2 Å), which is higher than that of permeability of N₂ and CH₄. This permeability elevation (than that of N₂ and CH₄) was seen for all percentage-loadings in both families of MMMs. This shows not only the role of ZIFs in discriminating permeants but also the shape of the permeant is also vital in determining the permeability. Although the C₂H₄ molecule has a higher kinetic diameter and molecular weight than that of N₂ and CH₄, the unsaturated dumbbell shape of C₂H₄ might pass it easily through the pore window of ZIF (3.4 Å). Thus, the higher ethylene permeability could be attributed to its shape rather than just its kinetic diameter.

The pure gas C₃H₆ and C₃H₈ separation performance of ZIF-8/PPO and ZIF-67@PPO membranes are plotted in Fig. 5c and d, respectively. The incorporation of ZIF particles in the PPO matrix showed a remarkable increase in the permeability of the C₃H₆. Compared to the pristine PPO, there is a 3.7 and 3.4 fold enhancement of the permeability of C₃H₆ observed for ZIF-8@PPO-40 and ZIF-67@PPO-40. The C₃H₈ permeability did not exhibit any substantial difference with the ZIF loading. From this observation, it can be said that for the permeation of propane, the highly permeable nature of PPO nullifies the effect of the tortuous path created by ZIF particles. The increase in propylene permeability and maintaining the similar propane permeability led to improved C₃H₆/C₃H₈ selectivity. The 40% loaded ZIF-8@PPO and ZIF-

67@PPO membrane showed an ideal selectivity of 27 and 25, respectively. It attributes that the pore window (3.4 Å) present in the ZIF-8 and ZIF-67 could exclude propane but passes propylene through it. However, the C₂H₄/C₂H₆ selectivity of MMMs did not significantly improve. This indicates the inability of ZIF-8 and ZIF-67 to discriminate this pair of gases. Both the ZIF-8@PPO and ZIF-67@PPO exhibited appreciable separation performance for propane-propylene. In view of the highly permeable and commercial availability of PPO, it might serve as an effective membrane for industrially demanding propane-propylene separation.

To elucidate the contribution of interfacial interaction resisting plasticization, we have evaluated the propylene permeability of the ZIF-8@PPO-30 membrane at different pressure and time. With variation in transmembrane pressure of 20–80 psi, the permeability varied in a range of 11.6–8.8 barrer (Fig. 6a). In another study, a long-term permeability analysis (150 h) of this membrane at a transmembrane pressure of 60 psi revealed that the permeability varied marginally from 9.4 to 11.1 barrer (Fig. 6b). The permeability values observed in both these studies are significantly different than that of the permeability of pristine PPO (3.5 barrer). These studies indicated the stability of the membrane towards time and long-time exposure to propylene. Both these studies may also indicate the positive role of metal-oxygen interaction in protecting the membrane from plasticization or aging.

3.4. Sorption analysis

A sorption analysis of MMMs possessing 40% ZIF loading was performed in order to understand the contribution of sorption in governing the permeability (Fig. 7a). The data points fit the Langmuir model well [21].

$$c_i = \frac{C_{H,i} b_i P_i}{1 + b_i P_i} \quad (7)$$

where, c_i is the sorption uptake, $C_{H,i}$ is the capacity constant, and b_i is the

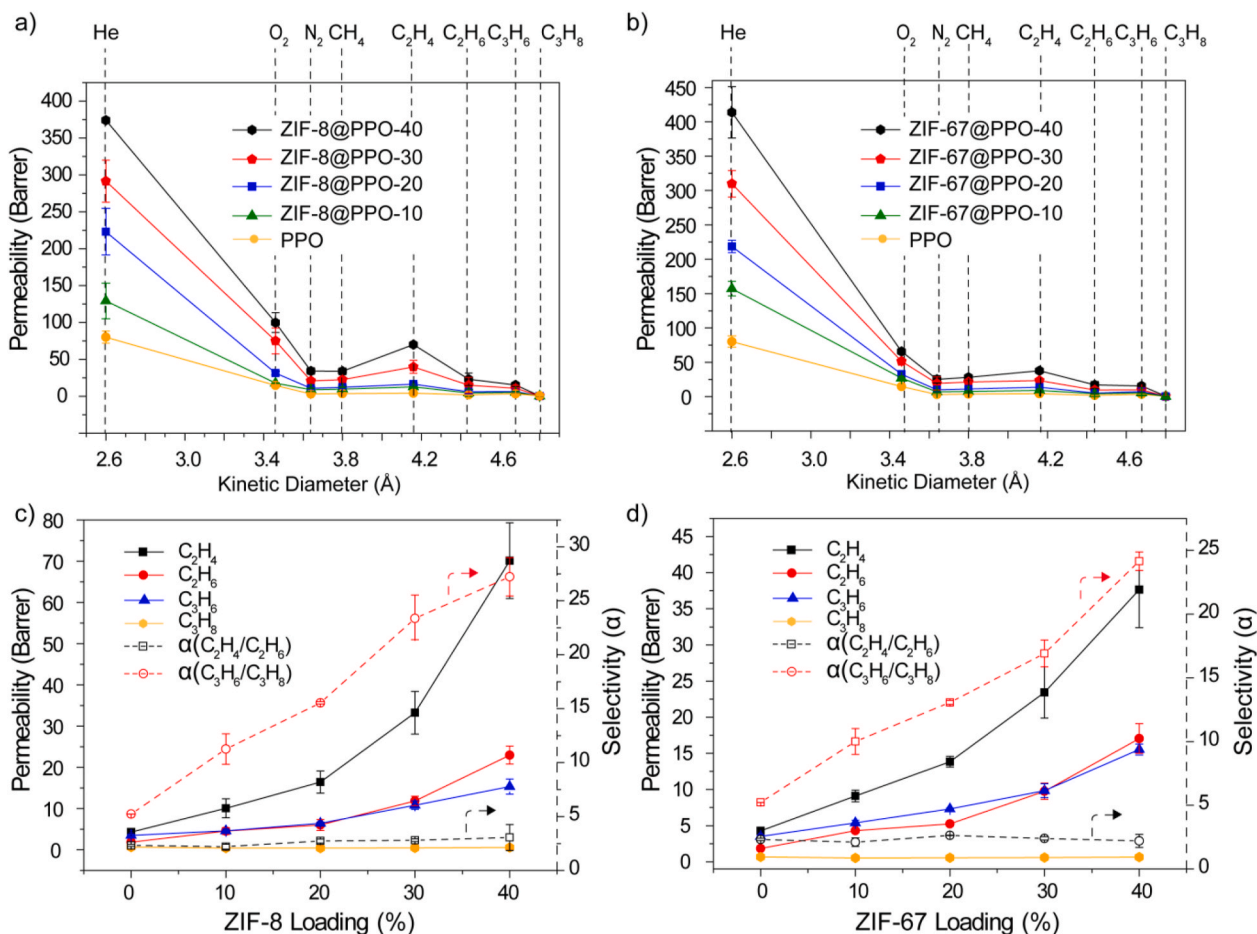


Fig. 5. Permeability coefficient of different gases in (a) ZIF-8@PPO and (b) ZIF-67@PPO MMM, pure gas permeability of C₂H₄, C₂H₆, C₃H₆ and C₃H₈, and selectivity of C₂H₄/C₂H₆ and C₃H₆/C₃H₈ in (c) ZIF-8@PPO and (d) ZIF-67@PPO MMMs.

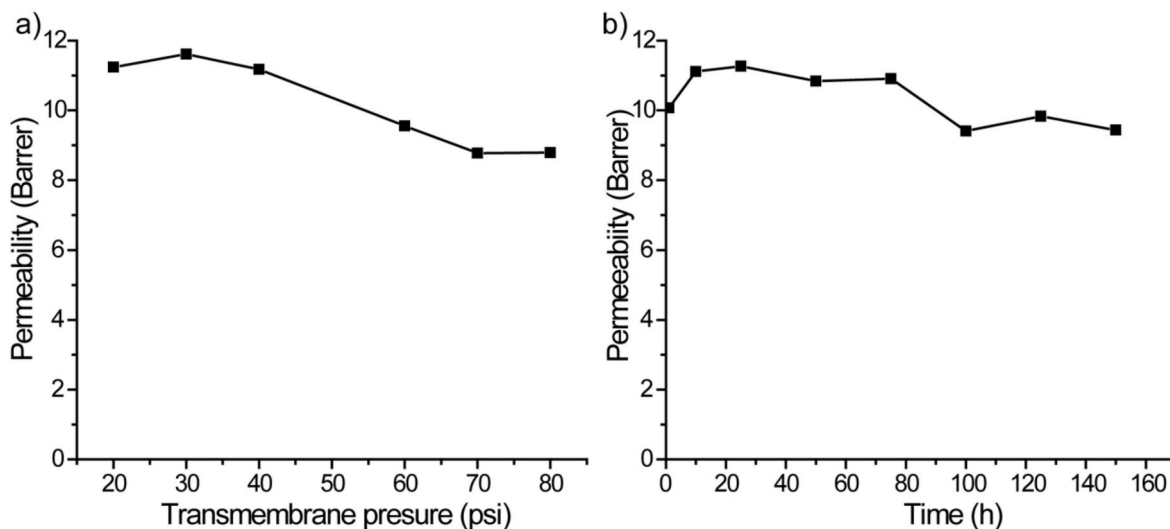


Fig. 6. Variation in C₃H₆ permeability of ZIF-8@PPO-30 membrane with (a) upstream pressure (a) long-term exposure at 60 psi upstream.

affinity constant for component *i*. Table S3 shows the Langmuir parameter and calculated sorption coefficient of the 40% loaded ZIF-8 and ZIF-67-based MMMs. For the given membrane, both C₃H₆ and C₃H₈ show a similar sorption uptake and a similar C₃H₆/C₃H₈ sorption selectivity (~1) at 4.8 atm (Table S3). This indicates that the addition of ZIF particles into the PPO matrix has not affected the C₃H₆/C₃H₈

solubility selectivity. The permeability coefficient is the product of the sorption and diffusion coefficient. The sorption analysis at different pressure (0–5 atm) enabled us to calculate the diffusion coefficient. The MMMs with 40% loading showed an enhancement in the diffusivity coefficient of C₃H₆ in contrast to the pristine PPO membrane. This revealed the fast diffusion of propylene gas through the MMMs. In the

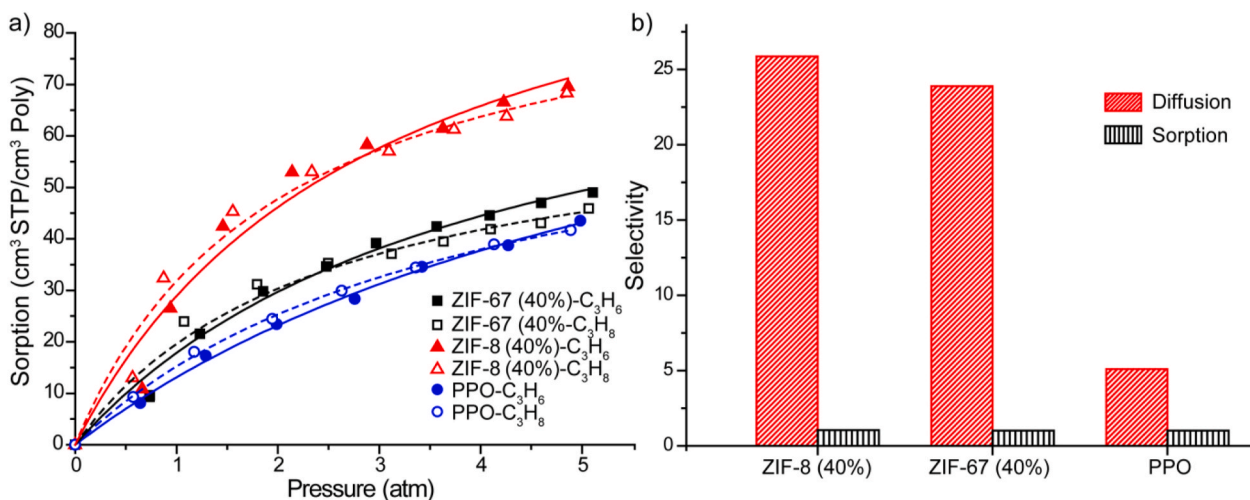


Fig. 7. (a) Sorption isotherm, and (b) diffusion and sorption selectivity of PPO and ZIF-8@PPO-40 and ZIF-67@PPO MMMs.

case of propane, there was a slight decrease in the diffusivity coefficient; it may be due to the inability of ZIFs to permeate propane, which in turn causes a tortuous path for the propane to permeate through the PPO matrix while avoiding ZIF particles. It results in a five-fold increase in the diffusion selectivity of 40% (both ZIF-8 and ZIF-67) loaded MMMs compared to the pristine PPO membrane (Fig. 7b). It confirms that diffusion dominates in attaining the C₃H₆/C₃H₈ selectivity for both ZIF-8@PPO-40 and ZIF-67@PPO-40 MMMs.

3.5. Mixed gas performance

A single gas permeation analysis proved that ZIF-8 and ZIF-67-based MMMs are potential candidates for propane-propylene separation. A mixed gas analysis of 40% loaded MMMs was performed to investigate their viability for industrial application. Different feed compositions of propane and propylene were used, and the results are summarized in Fig. 8. The separation factor is lesser than the ideal selectivity. It could be attributed to the competitive nature of the gas molecules and is a well-known phenomenon [3,51]. The separation factor was almost constant when the concentration of propylene in the feed was increased [21,44]. The maximum separation factor of ZIF-8@PPO and ZIF-67@PPO was 17.5 and 16.2, respectively. However, the permeability was enhanced when the propylene concentration in the feed was

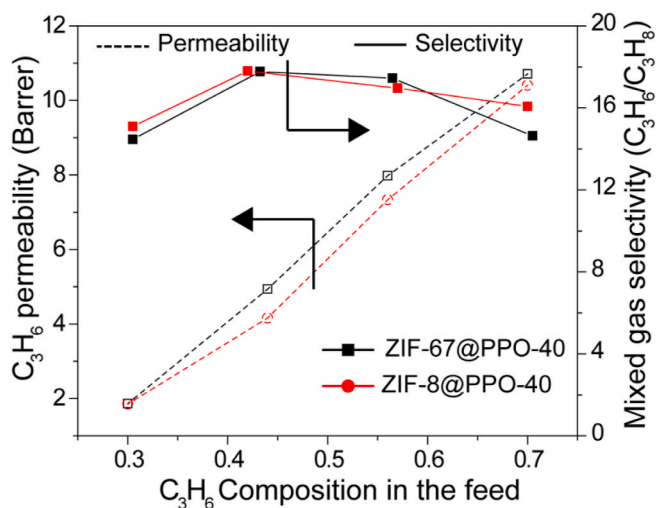


Fig. 8. Mixed gas permeability and selectivity of ZIF-8@PPO-40 and ZIF-67@PPO-40 membranes at different composition of C₃H₆ in feed.

increased. At 70:30 (C₂H₆/C₃H₈) feed composition, the 40% loaded ZIF-8@PPO and ZIF-67@PPO showed permeability of propylene as ~11 barrer.

The performance of ZIF-8@PPO and ZIF-67@PPO MMMs was compared with the literature data (Robeson upper bound, Fig. 9). The performance of the present ZIF@PPO-30/40 MMMs exceeded the 2008- upper bound, which is highly promising.

4. Conclusions

This study successfully demonstrated that the interfacial compatibility of the polymer and ZIFs could be achieved by the selection of an appropriate functional polymer capable of providing ZIF-polymer interactions. The ZIF loading up to 40% in the PPO matrix was successfully achieved. The existence of polymer filler interactions was established by DSC thermogram and XPS analyses. The polymer-filler interactions led to uniform distribution of ZIF particles without agglomeration even at higher (40%) loading. The gas sorption analysis revealed that the MMMs did not exhibit propylene and propane sorption selectivity. Thus, the gas permeation selectivity (ideal selectivity) is attributable only to the discriminating character of ZIFs between propylene and propane. The

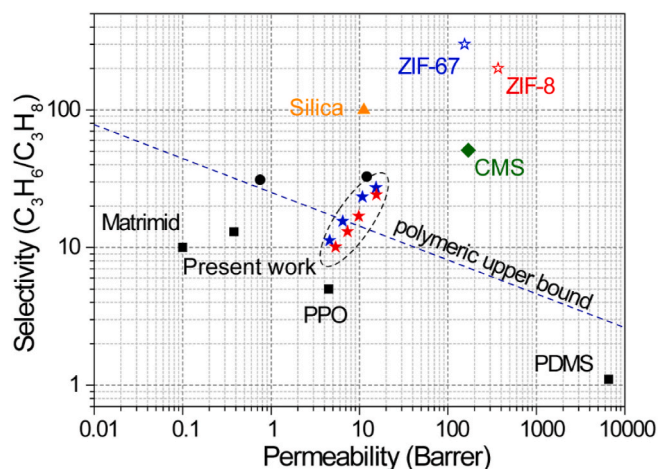


Fig. 9. Appearance of present and reported membranes on empirical C₃H₆/C₃H₈ Robeson's upper bound; ★: ZIF-8@PPO, ★: ZIF-67@PPO and reported membranes (■: [4], ●: [44,51], ▲: [2], ◆: [52], ☆: [53] and ☆: [33]).

mixed gas analysis showed that the ZIF-8 and ZIF-67-based MMMs are potential candidates for propene-propane separation.

This study demonstrated that polymer filler compatibility plays a vital role in achieving the performance of MMMs. The present methodology of using ZIFs and host (PPO) as such does not need any filler or polymer modification. The gas permeation data reveals that the ZIF@PPO membrane possessed significant gas separation performance for C₃H₆/C₃H₈, surpassing the Robeson upper bound and could be of commercial interest.

Author statement

Shebeeb Kunjattu H: Conceptualization, Methodology, Investigation, Validation, Writing - Original Draft, Ulhas K. Kharul: Conceptualization, Methodology, Writing - Review & Editing, Funding acquisition.

Declaration of competing interest

The authors declare that they have no known competing financial interests or personal relationships that could have appeared to influence the work reported in this paper.

Data availability

Data will be made available on request.

Acknowledgement

K. H. Shebeeb acknowledges Council of Scientific and Industrial Research, Ministry of Science and Technology, Government of India for Senior Research fellowship (Grant number 31/011(1102)/2019-EMR-I).

Appendix A. Supplementary data

Supplementary data to this article can be found online at <https://doi.org/10.1016/j.memsci.2022.121208>.

References

- [1] R. Faiz, K. Li, Olefin/paraffin separation using membrane based facilitated transport/chemical absorption techniques, *Chem. Eng. Sci.* 73 (2012) 261–284, <https://doi.org/10.1016/j.ces.2012.01.037>.
- [2] M. Guo, M. Kanezashi, Recent progress in a membrane-based technique for propylene/propane separation, *Membranes* 11 (2021), <https://doi.org/10.3390/membranes11050310>.
- [3] T.H. Lee, J.G. Jung, Y.J. Kim, J.S. Roh, H.W. Yoon, B.S. Ghanem, H.W. Kim, Y. H. Cho, I. Pinnau, H.B. Park, Defect engineering in metal-organic frameworks towards advanced mixed matrix membranes for efficient propylene/propane separation, *Angew. Chem.* (2021), <https://doi.org/10.1002/ange.202100841>.
- [4] R.L. Burns, W.J. Koros, Defining the Challenges for C₃H₆/C₃H₈ Separation Using Polymeric Membranes, vol. 211, 2003, pp. 299–309, [https://doi.org/10.1016/S0376-7388\(02\)00430-1](https://doi.org/10.1016/S0376-7388(02)00430-1).
- [5] H.R. Amedi, M. Aghajani, Economic estimation of various membranes and distillation for propylene and propane separation, *Ind. Eng. Chem. Res.* 57 (2018) 4366–4376, <https://doi.org/10.1021/acs.iecr.7b04169>.
- [6] A. Cadiau, K. Adil, P.M. Bhatt, Y. Belmabkhout, M. Eddaoudi, A metal-organic framework-based splitter for separating propylene from propane, *Science* 353 (2016) 137–140, <https://doi.org/10.1126/science.aaf6323>.
- [7] D.S. Sholl, R.P. Lively, Comment, *Nature* 532 (2016) 6–9.
- [8] J. Padin, R.T. Yang, New sorbents for olefin/paraffin separations by adsorption via π -complexation: synthesis and effects of substrates, *Chem. Eng. Sci.* 55 (2000) 2607–2616, [https://doi.org/10.1016/S0009-2509\(99\)00537-0](https://doi.org/10.1016/S0009-2509(99)00537-0).
- [9] Z. Bao, S. Alnemrat, L. Yu, I. Vasiliev, Q. Ren, X. Lu, S. Deng, Adsorption of ethane, ethylene, propane, and propylene on a magnesium-based metal-organic framework, *Langmuir* 27 (2011) 13554–13562, <https://doi.org/10.1021/la2030473>.
- [10] K. Tanaka, A. Taguchi, J. Hao, H. Kita, K. Okamoto, Permeation and separation properties of polyimide membranes to olefins and paraffins, *J. Membr. Sci.* 121 (1996) 197–207, [https://doi.org/10.1016/S0376-7388\(97\)00128-2](https://doi.org/10.1016/S0376-7388(97)00128-2).
- [11] R.W. Baker, Future directions of membrane gas separation technology, *Ind. Eng. Chem. Res.* 41 (2002) 1393–1411, <https://doi.org/10.1021/ie0108088>.
- [12] P. Bernardo, E. Drioli, G. Golemme, Membrane Gas Separation: A Review/State of the Art, 2009, pp. 4638–4663, <https://doi.org/10.1021/ie801903z>.
- [13] G. Liu, V. Chernikova, Y. Liu, K. Zhang, Y. Belmabkhout, O. Shekhat, C. Zhang, S. Yi, M. Eddaoudi, W.J. Koros, Mixed matrix formulations with MOF molecular sieving for key energy-intensive separations, *Nat. Mater.* 17 (2018) 283–289, <https://doi.org/10.1038/s41563-017-0013-1>.
- [14] C. Staudt-bickel, W.J. Koros, Olefin/Paraffin Gas Separations with 6FDA-Based Polyimide Membranes, vol. 170, 2000, pp. 205–214, [https://doi.org/10.1016/S0376-7388\(99\)00351-8](https://doi.org/10.1016/S0376-7388(99)00351-8).
- [15] T.H. Lee, M.G. Shin, J.G. Jung, E.H. Suh, J.G. Oh, J.H. Kang, B.S. Ghanem, J. Jang, J.H. Lee, I. Pinnau, H.B. Park, Facile suppression of intensified plasticization in glassy polymer thin films towards scalable composite membranes for propylene/propane separation, *J. Membr. Sci.* 645 (2022), 120215, <https://doi.org/10.1016/j.memsci.2021.120215>.
- [16] X. Ma, S. Williams, X. Wei, J. Kniep, Y.S. Lin, Propylene/propane mixture separation characteristics and stability of carbon molecular sieve membranes, *Ind. Eng. Chem. Res.* 54 (2015) 9824–9831, <https://doi.org/10.1021/acs.iecr.5b02721>.
- [17] S.J. Kim, J.F. Kim, Y.H. Cho, S.E. Nam, H. Park, Y.I. Park, Aging-resistant carbon molecular sieve membrane derived from pre-crosslinked Matrimid® for propylene/propane separation, *J. Membr. Sci.* 636 (2021), 119555, <https://doi.org/10.1016/j.memsci.2021.119555>.
- [18] I.G. Giannakopoulos, V. Nikolakis, Separation of propylene/propane mixtures using faujasite-type zeolite membranes, *Ind. Eng. Chem. Res.* 44 (2005) 226–230, <https://doi.org/10.1021/ie049508r>, 2005.
- [19] L.M. Robeson, The upper bound revisited, *J. Membr. Sci.* 320 (2008) 390–400, <https://doi.org/10.1016/j.memsci.2008.04.030>.
- [20] H.B. Park, J. Kamcev, L.M. Robeson, M. Elimelech, B.D. Freeman, Maximizing the right stuff: the trade-off between membrane permeability and selectivity, *Science* 356 (2017) 1138–1148, <https://doi.org/10.1126/science.aab0530>.
- [21] C. Zhang, Y. Dai, J.R. Johnson, O. Karvan, W.J. Koros, High performance ZIF-8/6FDA-DAM mixed matrix membrane for propylene/propane separations, *J. Membr. Sci.* 389 (2012) 34–42, <https://doi.org/10.1016/j.memsci.2011.10.003>.
- [22] H. Furukawa, K.E. Cordova, M. O’Keeffe, O.M. Yaghi, The chemistry and applications of metal-organic frameworks, *Science* 341 (2013), <https://doi.org/10.1126/science.1230444>.
- [23] M. O’Keeffe, O.M. Yaghi, Deconstructing the crystal structures of metal-organic frameworks and related materials into their underlying nets, *Chem. Rev.* 112 (2012) 675–702, <https://doi.org/10.1021/cr200205j>.
- [24] H. Hayashi, A.P. Côté, H. Furukawa, M. O’Keeffe, O.M. Yaghi, Zeolite A imidazolate frameworks, *Nat. Mater.* 6 (2007) 501–506, <https://doi.org/10.1038/nmat1927>.
- [25] K.S. Park, Z. Ni, A.P. Côté, J.Y. Choi, R. Huang, F.J. Uribe-Romo, H.K. Chae, M. O’Keeffe, O.M. Yaghi, Exceptional chemical and thermal stability of zeolitic imidazolate frameworks, *Proc. Natl. Acad. Sci. U. S. A.* 103 (2006) 10186–10191, <https://doi.org/10.1073/pnas.0602439103>.
- [26] R. Banerjee, A. Phan, B. Wang, C. Knobler, H. Furukawa, M. O’Keeffe, O.M. Yaghi, High-throughput synthesis of zeolitic imidazolate frameworks and application to CO₂ capture, *Science* 319 (5865) (2008) 939–943, <https://doi.org/10.1126/science.1152516>.
- [27] K. Li, D.H. Olson, J. Seidel, T.J. Emge, H. Gong, H. Zeng, J. Li, Zeolitic imidazolate frameworks for kinetic separation of propane and propene, *J. Am. Chem. Soc.* 131 (2009) 10368–10369, <https://doi.org/10.1021/ja9039983>.
- [28] S. Dangwal, A. Ronte, H. Lin, R. Liu, J. Zhu, J. Suk, H. Gappa-fahlenkamp, S. Kim, ZIF-8 membranes supported on silicalite-seeded substrates for propylene/propane separation, *J. Membr. Sci.* 626 (2021), 119165, <https://doi.org/10.1016/j.memsci.2021.119165>.
- [29] J. Hua, C. Li, H. Tao, L. Wang, E. Song, H. Lian, C. Wang, J. Jiang, Y. Pan, W. Xing, Improved C₃H₆/C₃H₈ separation performance on ZIF-8 membranes through enhancing PDMS contact-dependent confinement effect, *J. Membr. Sci.* 636 (2021), 119613, <https://doi.org/10.1016/j.memsci.2021.119613>.
- [30] H. Lian, Y. Yang, J. Chen, B. Bao, W. Yang, R. Hou, S. Ju, Y. Pan, Highly durable ZIF-8 tubular membranes via precursor-assisted processing for propylene/propane separation, *J. Membr. Sci.* 660 (2022), 120813, <https://doi.org/10.1016/j.memsci.2022.120813>.
- [31] E. Song, K. Wei, H. Lian, J. Hua, H. Tao, T. Wu, Y. Pan, W. Xing, Improved propylene/propane separation performance under high temperature and pressures on in-situ ligand-doped ZIF-8 membranes, *J. Membr. Sci.* 617 (2021), 118655, <https://doi.org/10.1016/j.memsci.2020.118655>.
- [32] S. Song, H. Jiang, H. Wu, M. Zhao, Z. Guo, B. Li, Y. Ren, Y. Wang, C. Ye, M. D. Guiver, G. He, Z. Jiang, Weakly pressure-dependent molecular sieving of propylene/propane mixtures through mixed matrix membrane with ZIF-8 direct-through channels, *J. Membr. Sci.* 648 (2022), 120366, <https://doi.org/10.1016/j.memsci.2022.120366>.
- [33] H.T. Kwon, H.K. Jeong, A.S. Lee, H.S. An, J.S. Lee, Heteroepitaxially grown zeolitic imidazolate framework membranes with unprecedented propylene/propane separation performances, *J. Am. Chem. Soc.* 137 (2015) 12304–12311, <https://doi.org/10.1021/jacs.5b06730>.
- [34] L. Xiang, L. Sheng, C. Wang, L. Zhang, Y. Pan, Y. Li, Amino-Functionalized ZIF-7 nanocrystals: improved intrinsic separation ability and interfacial compatibility in mixed-matrix membranes for CO₂/CH₄ separation, *Adv. Mater.* 29 (2017) 1–8, <https://doi.org/10.1002/adma.201606999>.
- [35] L. Ma, F. Svec, Y. Lv, T. Tan, Engineering of the filler/polymer interface in metal-organic framework-based mixed-matrix membranes to enhance gas separation, *Chem. Asian J.* 14 (2019) 3502–3514, <https://doi.org/10.1002/asia.201900843>.
- [36] Q. Xin, T. Liu, Z. Li, S. Wang, Y. Li, Z. Li, J. Ouyang, Z. Jiang, H. Wu, Mixed matrix membranes composed of sulfonated poly(ether ether ketone) and a sulfonated

- metal-organic framework for gas separation, *J. Membr. Sci.* 488 (2015) 67–78, <https://doi.org/10.1016/j.memsci.2015.03.060>.
- [37] N. Tien-Binh, H. Vinh-Thang, X.Y. Chen, D. Rodrigue, S. Kaliaguine, Crosslinked MOF-polymer to enhance gas separation of mixed matrix membranes, *J. Membr. Sci.* 520 (2016) 941–950, <https://doi.org/10.1016/j.memsci.2016.08.045>.
- [38] P.D. Sutisna, J. Hou, H. Li, Y. Zhang, V. Chen, Improved operational stability of Pebax-based gas separation membranes with ZIF-8: a comparative study of flat sheet and composite hollow fibre membranes, *J. Membr. Sci.* 524 (2016) 266–279, <https://doi.org/10.1016/j.memsci.2016.11.048>.
- [39] Z. Wang, D. Wang, S. Zhang, L. Hu, J. Jin, Interfacial design of mixed matrix membranes for improved gas separation performance, *Adv. Mater.* 28 (2016) 3399–3405, <https://doi.org/10.1002/adma.201504982>.
- [40] H. Li, L. Tuo, K. Yang, H.K. Jeong, Y. Dai, G. He, W. Zhao, Simultaneous enhancement of mechanical properties and CO₂ selectivity of ZIF-8 mixed matrix membranes: interfacial toughening effect of ionic liquid, *J. Membr. Sci.* 511 (2016) 130–142, <https://doi.org/10.1016/j.memsci.2016.03.050>.
- [41] G. Yu, X. Zou, L. Sun, B. Liu, Z. Wang, P. Zhang, G. Zhu, Constructing connected paths between UiO-66 and PIM-1 to improve membrane CO₂ separation with crystal-like gas selectivity, *Adv. Mater.* 31 (2019) 1–9, <https://doi.org/10.1002/adma.201806853>.
- [42] H. Wang, S. He, X. Qin, C. Li, T. Li, Interfacial engineering in metal-organic framework-based mixed matrix membranes using covalently grafted polyimide brushes, *J. Am. Chem. Soc.* 140 (2018) 17203–17210, <https://doi.org/10.1021/jacs.8b10138>.
- [43] Y. Sun, L. Tian, Z. Qiao, C. Geng, X. Guo, C. Zhong, Surface modification of bilayer structure on metal-organic frameworks towards mixed matrix membranes for efficient propylene/propane separation, *J. Membr. Sci.* 648 (2022), 120350, <https://doi.org/10.1016/j.memsci.2022.120350>.
- [44] S.H. Kunjattu, V. Ashok, A. Bhaskar, K. Pandare, R. Banerjee, U.K. Kharul, ZIF-8@DBzPBI-Bul composite membranes for olefin/paraffin separation, *J. Membr. Sci.* 549 (2018) 38–45, <https://doi.org/10.1016/j.memsci.2017.11.069>.
- [45] K. Toi, G. Morel, D.R. Paul, Gas sorption and transport in poly(phenylene oxide) and comparisons with other glassy polymers, *J. Appl. Polym. Sci.* 27 (1982) 2997–3005, <https://doi.org/10.1002/app.1982.070270823>.
- [46] Y.S. Bhole, U.K. Kharul, S.P. Somani, S.C. Kumbharkar, Benzoylation of polyphenylene oxide: characterization and gas permeability investigations, *Eur. Polym. J.* 41 (2005) 2461–2471, <https://doi.org/10.1016/j.eurpolymj.2005.03.026>.
- [47] J. Cravillon, S. Münzer, S.J. Lohmeier, A. Feldhoff, K. Huber, M. Wiebcke, Rapid room-temperature synthesis and characterization of nanocrystals of a prototypical zeolitic imidazolate framework, *Chem. Mater.* 21 (2009) 1410–1412, <https://doi.org/10.1021/cm900166h>.
- [48] X. Feng, M.A. Carreon, Kinetics of transformation on ZIF-67 crystals, *J. Cryst. Growth* 418 (2015) 158–162, <https://doi.org/10.1016/j.jcrysgro.2015.02.064>.
- [49] B. Nagendra, A. Cozzolino, C. Daniel, P. Rizzo, G. Guerra, F. Auremma, C. De Rosa, M.C. D'Alterio, O. Tarallo, A. Nuzzo, Two nanoporous crystalline forms of poly(2,6-dimethyl-1,4-phenylene)oxide and related Co-crystalline forms, *Macromolecules* 52 (2019) 9646–9656, <https://doi.org/10.1021/acs.macromol.9b01911>.
- [50] B.J. Story, W.J. Koros, Sorption and transport of CO₂ and CH₄ in chemically modified poly(phenylene oxide), *J. Membr. Sci.* 67 (1992) 191–210, [https://doi.org/10.1016/0376-7388\(92\)80025-F](https://doi.org/10.1016/0376-7388(92)80025-F).
- [51] X. Ma, R.J. Swaidan, Y. Wang, C. en Hsiung, Y. Han, I. Pinnau, Highly compatible hydroxyl-functionalized microporous polyimide-zif-8 mixed matrix membranes for energy efficient propylene/propane separation, *ACS Appl. Nano Mater.* 1 (2018) 3541–3547, <https://doi.org/10.1021/acsanm.8b00682>.
- [52] K.M. Steel, W.J. Koros, An investigation of the effects of pyrolysis parameters on gas separation properties of carbon materials, *Carbon N. Y.* 43 (2005) 1843–1856, <https://doi.org/10.1016/j.carbon.2005.02.028>.
- [53] S. Zhou, Y. Wei, L. Li, Y. Duan, Q. Hou, L. Zhang, L.X. Ding, J. Xue, H. Wang, J. Caro, Paralyzed membrane: current-driven synthesis of a metal-organic framework with sharpened propene/propane separation, *Sci. Adv.* 4 (2018) 1–9, <https://doi.org/10.1126/sciadv.aau1393>.